NEURAL CIRCUITRY, BEHAVIORAL CORRELATES AND GENETIC ORGANIZATION OF THE MAMMALIAN CIRCADIAN CLOCK

By

Christopher M. Ciarleglio

Dissertation

Submitted to the Faculty of the

Graduate School of Vanderbilt University

in partial fulfillment of the requirements

for the degree of

DOCTOR OF PHILOSOPHY

in

Neuroscience

May, 2009

Nashville, Tennessee

Approved:

Professor Douglas G. McMahon, Ph.D.

Professor Terry L. Page, Ph.D.

Professor Carl H. Johnson, Ph.D.

Professor Marshall L. Summar, M.D.

For the Nonny and the fambly.

ACKNOWLEDGEMENTS

First and foremost, I would like to thank Doug McMahon for taking me on as a graduate student despite my relatively questionable collegiate success. I could not have asked for a healthier and more nurturing work environment than he provided with his open door and avid interest in his lab members' well-being. I must also acknowledge Karen Gamble, my partner in crime for all four years, who pushed me incessantly to apply for an NRSA and to think critically about the formulation of sound scientific hypotheses and the application of statistical techniques. Without her or my undergraduate mentee and friend, John Axley, I could have never finished this dissertation in so short a time. They have shared equally in my triumphs and failures over these years, and I am eternally grateful. I must acknowledge the fine training I received from Hidenobu Ohta, and I thank Shin Yamazaki and Julie Pendergast (Drs. Doom & Gloom) for so many critical-thinking sessions and tips. I am grateful to my committee members, Carl Johnson and Marshall Summar, for the opportunity to gain experience in human genetics research. Without Sydney Larson, another undergraduate mentee, that project would probably still be sitting in a drawer. She has received little credit for her momentous effort, but I am extremely grateful for her contribution. I'd like to thank former undergraduates Josh Wiedermann for his contribution to this project, and Ben Strauss for his contribution to the seasonality project, and I wish them good luck in their medical futures. Jeremiah "Coach" Cohen saved me literally a year or more of mind-numbing analysis by writing a computer program for me, and so John, Ben and I owe him a huge thanks. Terry Page, my committee chair, has been a great mentor in my time here, and has offered me many opportunities to thrive—I am enormously grateful. I thank Jeanette Norden for giving me the chance to illustrate her lecture series "Understanding the Brain" for The Teaching Company—this was an amazing opportunity.

I gratefully acknowledge the NIMH for the T32 MH64913 NRSA and F31 MH080547 NRSA support, and the supplementary support of the Vanderbilt Brain Institute (Mary Early-Zald, Elaine Sanders-Bush, Randy Blakely and Mark Wallace) and the Vanderbilt Department of Biological Sciences (Roz Johnson, Stacey Johnson and Charles Singleton)—it was immensely appreciated. I'd like to thank Mormon Dan Anderson and Rick Penney for their humor, drama and support—they've made graduate school enjoyable. Lastly, I'd like to thank the rest of the McMahon Lab for a fun and productive four years—they have blessed me with insightful comments, criticisms and assistance without which I would have been lost.

These have been some of the best years of my life, and I am forever a Vanderbilt Commodore.

TABLE OF CONTENTS

Page

LIST OF TABLES

LIST OF FIGURES

LIST OF ABBREVIATIONS

Word or Phrase	Abbreviation
Adenylyl cyclase	AC
[Familial] Advanced Sleep Phase Syndrome	ASPS *or* FASPS
Arginine vasopressin	AVP
Aryl hydrocarbon receptor nuclear translocator-like	*Arntl* (also *Bmal1*)
Brain and Muscle Arnt-like 1	*Bmal1*
Brain and Muscle Arnt-like 2	*Bmal2*
Casein Kinase 1 δ	CK1δ
Casein Kinase 1 ε	CK1ε
Circadian rhythm sleep disorders	CRSD
Circadian Time	CT
Constant darkness	DD
Constant light	LL
Cryptochrome1	*Cry1*
Cryptochrome2	*Cry2*
Cyclic adenine monophosphate	cAMP
Delayed Sleep Phase Syndrome	DSPS
Deoxyribonucleic acid	DNA
Diurnal cycle	LD
Environmental period or day	T
Free-running disorder	FRD
Free-running period	FRP

γ-amino butyric acid ..... GABA

Gastrin-releasing peptide ..... GRP

Global positioning satellite ..... GPS

Green fluorescent protein ..... GFP

Infrared motion detection ..... IR

In situ hybridization ..... ISH

Intergeniculate leaflet ..... IGL

International Classification of Sleep Disorders ..... ICSD

Irregular sleep-wake rhythm/phase ..... ISWR

Long photoperiod ..... LPP *or* LD 16:8

Luciferase ..... Luc

Melanopsin ganglion cell ..... MGC

Million years ago ..... MYA

Mitogen-activated protein kinase ..... MAPK

Monoamine oxidase ..... MAO

Monoamine oxidase inhibitor ..... MAOI

Neonatal intensive care unit ..... NICU

Neuropeptide Y ..... NPY

Non-24 hour sleep-wake disorder N-24

Parachlorophenylalanine ..... pCPA

Peptide histidine isoleucine ..... PHI

Period ..... τ

Period1 ..... *Per1*

Period2 ..... *Per2*

Period3 ..... *Per3*

Phase of master oscillator ..... Φ

Phase of slave oscillator ..... ϕ

Pituitary adenylate cyclase-activating polypeptide ..... PACAP

Protein kinase A ..... PKA

Retinohypothalamic tract ..... RHT

Ribonucleic acid ..... RNA

Seasonal Affective Disorder ..... SAD

Serotonin 5-HT

Short photoperiod ..... SPP *or* LD 8:16

Simple nucleotide polymorphism ..... SNP

Suprachiasmatic nuclei of the hypothalamus ..... SCN

Transcription/Translation Feedback Loop ..... TTFL

Vasoactive intestinal polypeptide ..... *VIP*

VIP heterozygote ..... $VIP^{+/-}$

VIP knockout ..... $VIP^{-/-}$

VIP wildtype ..... $VIP^{+/+}$

VIP receptor 2 ..... *Vipr2 or* $VPAC_2$

VIP receptor heterozygote ..... $Vipr2^{+/-}$ *or* $VPAC_2^{+/-}$

VIP receptor knockout ..... $Vipr2^{-/-}$ *or* $VPAC_2^{-/-}$

VIP receptor wildtype ..... $Vipr2^{+/+}$ *or* $VPAC_2^{+/+}$

Zeitgeber Time ..... ZT

PREFACE

In my junior year at Holy Cross High School, I had the unusual opportunity to take a class on neuroscience under the superb teacher Linda Rinaldini. At the same time, my Godfather was diagnosed with a benign brain tumor and forced to have it surgically removed. I was given the huge opportunity to meet his surgeon, Joe Piepmeier, then Chief of Neuro-Oncology and Professor of Neurosurgery at Yale University. Dr. Piepmeier became my mentor, and altogether, these situations instilled in me a respect and appreciation for neuroscience and neurology that carried me through my studies at Swarthmore College. There, I chose to do research on the development of the hamster hippocampus in the lab of circadian and behavioral biologist Kathleen K. Siwicki. In the fall of 2003, in fulfillment of my Biology major requirements, I took an invited-speaker seminar on "Biology & Time." At the end of the semester, the class received a group assignment to give a presentation on who *should* have been invited to speak in the seminar series. I had become intrigued by Doug McMahon's use of a GFP reporter for the *Period1* gene in a mouse model, and swayed my group to propose Dr. McMahon as a missed opportunity. Doug McMahon had recently moved to Vanderbilt University from the University of Kentucky, and I applied to Vanderbilt on the strength of their Neuroscience program. As luck would have it, I got to interview with Dr. McMahon and he fascinated me with the latest time-series movie of *Per1*::GFP expression results in the SCN. Having trained as an undergraduate under two circadian biologists (Kathy Siwicki and Sara Hiebert-Burch), I was drawn to Doug's lab in my rotations and immediately got involved in learning brain slice culture and upgrading the circadian mouse facilities.

Using this reporter mouse model and a VIP knockout, we sought to characterize the network properties of the SCN in a mouse that lacked neuronal synchrony, and to demonstrate a

correlation between those neuronal properties and the behavioral phenotype of the adult animal. In early 2007, after reading a paper on multi-unit electrophysiology from the laboratory of Johanna Meijer, I had become convinced that our lab's *Per1*::GFP mouse line was the best way to explain how seasonality was encoded by neurons in the SCN. John Axley, Ben Strauss and I went right to work entraining mice to long and short photoperiods. Our results were novel and exciting; until we were scooped by a very nice paper published using similar methods in the lab of Ken-Ichi Honma. Not to be discouraged, Doug and I brainstormed the idea of going back to my root interests in developmental neurobiology and testing to see if photoperiod played any role in hard-wiring—imprinting—the organization of the SCN.

This dissertation is the culmination of essentially four years of research spanning topics from neural network organization to behavior to human genetics. While there are still plenty of unanswered questions in the field, it is my hope that this work has contributed in some way to our understanding of circadian neurobiology, and that it may eventually translate into advances for human health.

C.M.Ciarleglio
27 March 2009

CHAPTER I

INTRODUCTION

In 1975, in response to the successes of the Apollo missions, NASA scientists William K. Hartmann and Donald R. Davis suggested that the formation of the moon was the result of a catastrophic impact between $Earth_{Mark1}$ and a planetoid that shared Earth's orbit in the early solar system's formation[3]. This planetoid, known as Theia[a], is thought to have occupied an orbital position known as the Lagrangian point—a place where the gravitational influence of the Sun and Earth are equal on the planetoid[4]. With the large growth of $Earth_{Mark1}$ outpacing Theia's own growth, the gravitational influence on its orbit is thought to have become unbalanced about 4.5 billion years ago, hurling the Mars-sized planet at Earth for an oblique double-collision with four historic results: 1) the collision sterilized what could have been two life-supporting planets; 2) the mantle and crust ejected from the collision coalesced into our moon; 3) the resulting single planet, our own $Earth_{Mark2}$ was left spinning on its axis with a regular cycle subjecting the planet to periodic day and night; 4) Earth's spin, stabilized by its new moon, is maintained at 23° off-perpendicular, creating the seasons. Over the 4.5 billion years since, the dragging effect of the tide and a slowly enlarging lunar orbit has gradually lengthened the day from a blistering 4 hours to the 24 hours we know today[5]. This key event in Earth's history spawned a conserved genetic program that accounts for the length of the day in almost all life. How the modern mammalian circadian pacemaker uses this set of genes to temporally organize itself into a coherent, responsive neural network will be the focus of this dissertation.

[a] sometimes called "Orpheus" or "Hephæstus"

The day-night cycle has proved a critical environmental factor shaping the evolution of life on Earth. In Earth's tumultuous history, extraterrestrial impacts like the moon-forming event, and geological upheaval and vulcanism were not uncommon. While early life likely evolved in the water, these factors wreaked havoc on the ability of the sun's light to reach the oceans, at times darkening the planet for years. In at least two extreme instances in the young planet's history, the entire globe was covered with a sheet of white ice miles thick in some places—the so-called "Snowball Earths". These deep ice-ages lasted millions of years 800-600 MYA, bouncing most of the sun's light back into space and trapping early life in a dark ocean. Yet we find in the present that the endogenous circadian clock is an almost ubiquitous feature of life on Earth, suggesting that it has offered some increased fitness. How did circadian rhythms become the rule rather than the exception? It is thought that the ability to anticipate day/night transitions and coordinate internal metabolic processes was advantageous for the earliest life on the planet. By tracking these transitions, photosynthetic organisms could capture the sun's light and fix carbon on a regular schedule. Similarly, organisms that fed on these photosynthesizers could avoid the damaging effects of the sun's UV light by sinking to deeper water during the day and feeding at night. An endogenous circadian rhythm allowed an organism to maintain a fairly consistent phase angle, despite changes in the primary zeitgebers[b]. Circadian clocks could be "entrained" rather than purely "driven" or "synchronized", allowing the organism clock to generally keep time despite irregularities in weather—as due to seasonal changes—and/or the absence of light—as due to volcanic ash, asteroid impact or Snowball Earth.

Seminal work by Carl Johnson and colleagues elegantly demonstrated that circadian clocks do offer competitive fitness when the endogenous rhythm is resonant with the external environment[6, 7]. Such a competitive fitness test is difficult to perform in mammals, however,

[b] German for "time-giver." The entraining stimulus such as light.

where pitting two mice of significantly different innate circadian periods against each other in a death-match would have difficulty receiving approval by institutional animal care and use committees. Pat DeCoursey, however, made the fortuitous observation in GPS-tagged ground squirrels that having a functional circadian clock did indeed decrease mortality of ground squirrels both in the wild and in semi[c]-captivity[8-10]. If the implications of these studies are to be believed, the mammalian biological circadian clock, located in the hypothalamus of the brain, is an indispensible component of life in the wild. It would follow, then, that understanding how mutations in circadian genes disrupt the function of behavioral rhythmicity is important not only on the merits of scientific interest, but also for its implications to human health. Further, using these properties as tools to dissect the clock, it may be possible to understand how neurons within the biological clock organize into a network that, in turn, controls daily behavior.

How the neural network of the central mammalian pacemaker is organized to produce a behavioral output has to this point only been addressed by proxy: the brains of neonatal animals were studied as a model whose network properties are thought to reflect the behavior of adult animals, and those results were then, in turn, extrapolated to explain human behavioral phenotypes. In this dissertation research, I have sought to characterize the behavioral, molecular and genetic organization of the mammalian circadian clock by the manipulation of key genetic factors involved in entrainment and neural synchrony, and by further altering zeitgebers that serve to set the phase of the clock. While these studies serve as only a small piece of the puzzle, they provide a snapshot of circadian neural organization in behaviorally characterized mice, and peer into the genetic makeup of human circadian clocks.

[c] While the squirrels could not get out of the pen, a predatory weasel somehow got in, almost ruining the experiment, but at the same time providing invaluable evidence for the importance of a behavioral circadian rhythm in mammals (P. DeCoursey, *personal communication*).

Section 1.1: The Nature of Circadian Rhythms

Circadian rhythms are the physiological processes whereby an organism regulates its activity and coordinates other physiological processes on a self-sustained daily cycle. These processes involve measurable rhythms at both the behavioral and molecular levels. Behavioral rhythms govern several characteristics in animals: eating, drinking, waking/sleeping, attention, torpor, body temperature, *etc.* Molecular circadian rhythms can be found in hormone release and even cell division[11]. Presently[d], a circadian rhythm has three fundamental properties: 1) the rhythm is self-sustained and about 24-hours in length; 2) the rhythm is entrained by external factors such as light; and 3) the rhythm is temperature compensated.

The first of these fundamental properties is the persistence of the circadian rhythm in constant conditions (generally light and temperature) at a near 24-hour period (τ). In rodent models, this endogenous period is most often assessed by behavioral monitoring—such as activity recorded by wheel-running (Fig. I-1, *left*), infrared motion detection (Fig. I-1, *right*), laser beam-break or water-drinking—in constant darkness. Mice, for example, are a nocturnal species that exhibit activity during the dark of night. If placed in a monitored cage in constant darkness, mice will generally exhibit a free-running period (FRP) of slightly less than 24 hours, and continue to run only during what they perceive as "night." The same form of activity monitoring (known as *actigraphy*) may be used to assess rhythms of higher species such as humans, but the FRP of diurnal humans tends to run slightly longer than 24 hours. Even in humans, wakefulness occurs during what they perceive as "day" in the absence of photic or social cues.

The second fundamental property of circadian rhythms is that they can be entrained by external factors such as light. The Earth's rotation yields a day that is clearly demarcated by

[d] Given that the length of the day has not always been 24-hours, this is a modern definition.

light-dark transitions, making for the key environmental stimulus by which the endogenous circadian clock is set. While light is the primary *zeitgeber*, or *time-giver*, other environmental factors can reset the phase of the endogenous clock. Forced exercise during the circadian day, for example, has been shown to phase advance hamster behavioral circadian rhythms independent of light[12]. In humans, societal pressure to stay awake into the very late night is a potent zeitgeber commonly resulting in weekend "social jetlag"[13]. The mechanisms by which light and non-photic stimuli entrain the circadian clock will be discussed in Section 1.2: The Art of Entrainment.

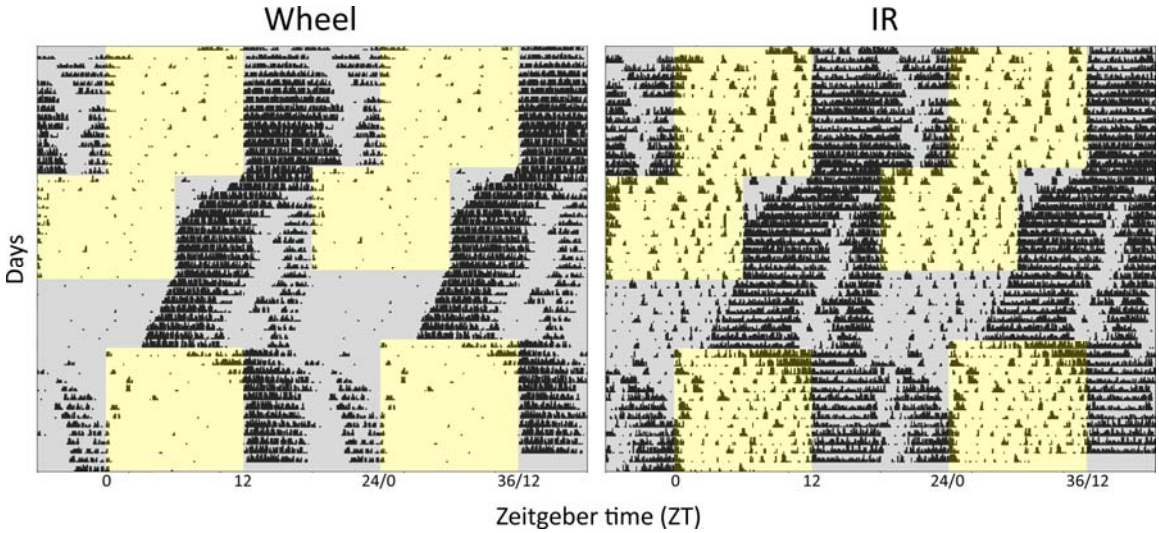

Figure I-1. | **Representative double-plotted actograms illustrate circadian behavior in response to changing lighting conditions.** *Left*, actogram of wheel-running activity; *right*, actogram of the same animal (*left*) as monitored by infrared motion detection. **Black** ticks represent activity in 5-minute bins; **yellow** background denotes lights-on; gray background denotes lights-off.

The third property of a circadian rhythm is the ability of the rhythm to maintain a nearly constant period in changing temperatures. This is an unusual characteristic in biology, in that most other biochemical reactions tend to speed up as temperature increases—or at least until degrative to the protein's structure. While circadian rhythms can entrain or phase shift to changing temperatures, angular velocity, and thus the duration of the cycle stays ~24 hours

regardless. While this property of the biological clock is fascinating, this dissertation will not discuss the characteristic further.

Section 1.2: The Art of Entrainment

The light-dark cycle created by the Earth's rotation is a natural, robust and reliable oscillation. Presently, each day is exactly 24-hours. In circadian biology, the Earth's rotation serves as the master oscillator. The circadian rhythms are themselves physiological oscillations that are not passively driven by the environment, but rather entrained. Zeitgebers such as light adjust the phase of biological clock (ϕ) with the effect that its circadian rhythm is synchronized to the environmental stimulus (Φ). In mice, for example, entrainment manifests as a behavioral period (τ) equal to the period of the entraining stimulus (T) with a stable phase relationship between the circadian rhythm and the environment, and the phase measure persisting even after the absence of the zeitgeber (constant conditions)[14].

As the brilliant fourth paper in the series on mammalian rhythms by Pittendrigh and Daan[15] would suggest, conservation of the phase relationship between the master oscillator (Earth) and its slave oscillator (the circadian biological clock) is the essence of entrainment. This relationship is called phase angle (ψ). ψ is arguably the most important aspect of entrainment. Evolutionarily, this relationship could be the key reason circadian rhythms developed: the ability to predict time of day persistently—even in the absence of rhythmic zeitgebers as caused by bad weather, geological upheaval or severe climate change—offered some fitness that allowed feeding or photosynthesis to occur on a generally regular schedule. Considering that completely divergent species like cyanobacteria and the mouse produce circadian rhythms—despite the fact that their last common ancestor lived some 2-3 billion years ago when the length of the day was far shorter than 24 hours—is a testament to that theory. Circadian rhythms were either so

important to early evolving life that they persist in most species today, or circadian rhythms have become so important that convergent evolution has made them a general property of life on Earth. Either way, adaptive flexibility to the changing geophysical day and the ability to entrain with a stable phase angle was important in evolution.

There are two proposed models of entrainment: the continuous (parametric) model and the discrete (nonparametric) model. Both models have been championed by founders of the field, and both have merit and drawbacks. In the continuous model, Jurgen Aschoff suggested that the intensity of light proportionally changed the speed of the biological clock in a phase-dependent manner, thus squeezing or stretching the circadian period (τ) to fit into the actual environmental day (T). In contrast, Colin Pittendrigh suggested that the discrete model could explain entrainment of the circadian clock by simply shifting ϕ. This model used a Phase Response Curve (PRC) to explain phase-dependent shifts to discrete pulses of light that, alone or in combination, added up to the period of the environmental day (Fig. I-2)[14]. Thus, $\tau = T$ in LD.

The ability to entrain to the geophysical day with a constant phase angle is of paramount importance, especially when considering the seasonal changes in photoperiod that may perturb that relationship between the master and slave oscillators. Further work on mammalian entrainment by Pittendrigh and Daan[16] sought to address how ψ was conserved across changes in photoperiod due to season (for more information, see Section 1.6: Seasonality). The conclusions were and are controversial: they proposed that the circadian clock consists of two coupled oscillators—a morning and an evening oscillator. They suggested that each oscillator is entrained to a light-dark transition (either dusk or dawn), and that the relationship between these oscillators accounts for photoperiodic encoding. While many studies have attempted to find a molecular/cellular correlate for this hypothesis, no convincing evidence exists. In this regard, questions remain about how seasonality/photoperiodism is encoded in mammals, and

whether the rules outlined by Pittendrigh and others concerning the entrainment and the conservation of phase angle persist at the tissue or cellular level.

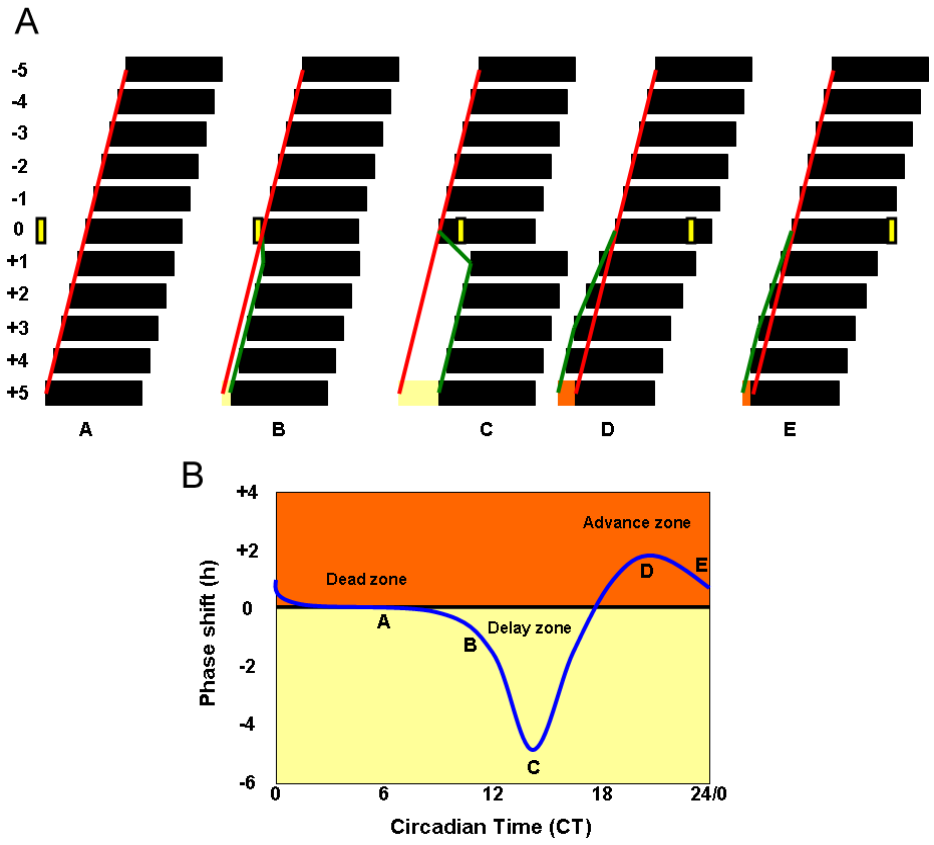

Figure I-2. | **Phase shifts to discrete pulses of light and the PRC of wildtype mice (*Mus musculus*). a** | Idealized DD actograms showing that a 1-hour pulse of light (**yellow**) on day zero shifts the phase of activity onset (black bars are activity) on subsequent days in a phase-dependent manner. **Red** line is activity onset based on FRP; **green** line is the new activity onset after the light pulse, and traces any transients leading to resumption of a stable FRP; **cream** bar represents the total phase delay; and the **orange** bar represents the total phase advance. **b** | Idealized phase response curve (**blue** line) tracing the phase shifts (h) in Fig. I-2a over circadian time (CT). **Cream** area of the graph represents the phase delay zone; and the **orange** area of the graph represents the phase advance zone. Letters A-E in Fig. I-2a represent the shift responsible for the point in the PRC (Fig. I-2b) represented by the same letters. ©2008 by Ciarleglio and Friday.

Section 1.3: SCN – The Central Mammalian Pacemaker

In the latter-half of the 20th century, the nascent field of chronobiology picked-up speed on the mammalian front with the publication of classic and brilliant works by the field's founding

fathers. Colin Pittendrigh and Serge Daan published a masterpiece on the properties of rodent behavioral rhythms[15-19]; Jurgen Aschoff furthered our understanding of human rhythms and the effects of light on the speed of the clock, postulating what Pittendrigh would later call Aschoff's rules[20-28]; and Franz Halberg was finding rhythms in all types of organisms. What eluded these investigators, however, was the specific location of the mammalian biological clock.

In 1967, Curt Richter published a study suggesting that ablation of the hypothalamus led to circadian behavioral arrhythmicity[29]. Exactly who should receive credit for the discovery of the central pacemaker is still hotly debated, but in 1972, two groups independently identified the suprachiasmatic nuclei of the hypothalamus (SCN) as the biological clock in mammals. Data from Robert Moore and Nicholas Lenn identified the retinohypothalamic tract projecting from the retina—long thought to be the primary sensor of circadian light in mammals—to the SCN[30]. Simultaneously, Friedrich Stephan and Irving Zucker concluded that the SCN were the pacemaker by electrolytic lesion of specific nuclei in the hypothalamus[31]. Only lesioning of the SCN produced behavioral arrhythmicity. Progress in the field quickened as the SCN were found to exhibit rhythmicity of neuronal firing rates *in vivo*[32, 33] and *in vitro*[34]. The SCN were firmly

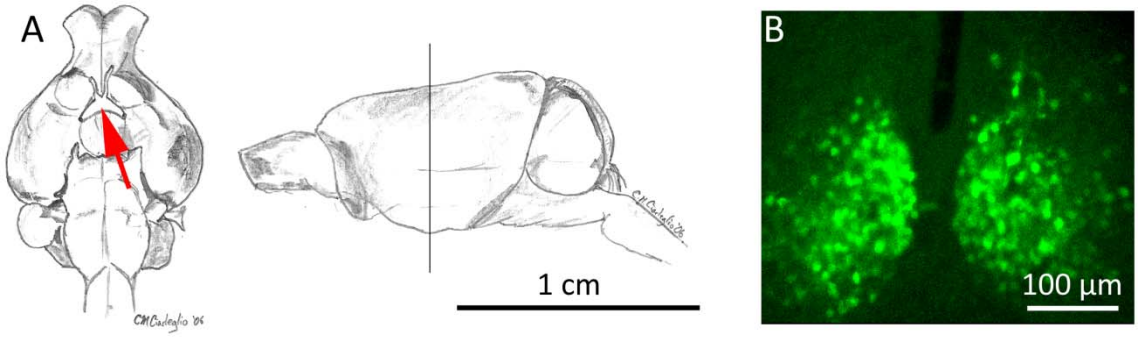

Figure I-3. | **Murine suprachiasmatic nuclei of the hypothalamus. a** | *Left*, in this ventral sketch of the mouse brain, the SCN are located in the hypothalamus, just dorsal to the caudal extreme of the optic chiasm (**red** arrow). *Right*, in this sagittal view of the mouse brain, coronal SCN slice cultures are typically made on the vertical black line. Thick horizontal scale bar represents 1 cm. **b** | *Per1*::GFP reporter expression in neurons of a coronal hypothalamic slice culture during the circadian day. See Section 1.7: Model Mice. Thick horizontal scale bar represents 100 µm.

established as the master circadian pacemaker in mammals by transplant studies that rescued behavioral rhythmicity in SCN-lesioned animals, and conveyed upon the transplant recipient the donor's circadian period[35].

The SCN are medially located in the anterior hypothalamus, dorsal to the optic chiasm and inferio-lateral to the third ventricle in mice (Fig. I-3a), the model organism of choice for this dissertation. Each nucleus is about 200µm wide at its widest point on the coronal plane, 200-250µm dorso-ventrally, and about 500-600µm from the rostral to caudal extremes. Each nucleus of the SCN is densely packed with about 10,000 small (~10µm-wide) neurons, most of which are GABA-ergic[36, 37]. These neurons fluoresce green in transgenic reporter mice (Fig. I-2b), and due to their density, the SCN are readily identifiable in a coronal brain section as translucent bulbs above a darker optic chiasm in back-lighting (Fig. I-4). These neurons increase their spike-rate frequency during the circadian day[32, 38-40], and upregulate night-time firing-rate in response to phase-shifting light-pulses[41, 42].

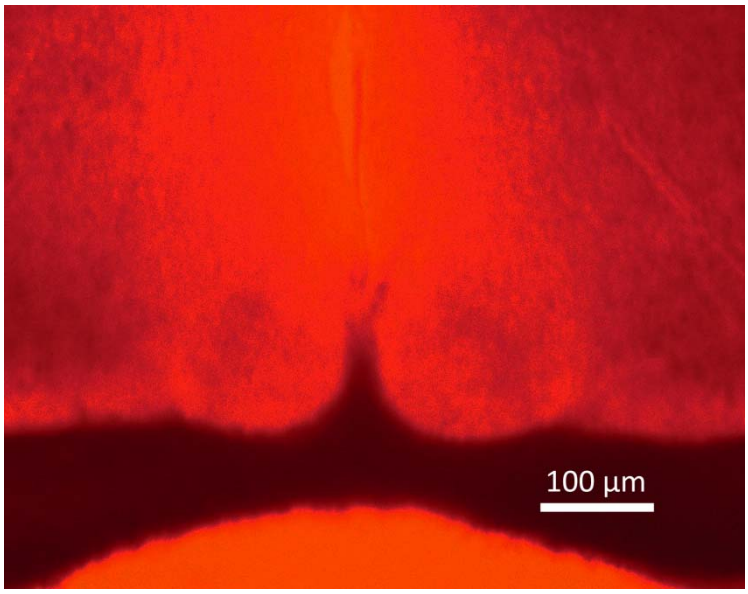

Figure I-4. | **Coronal hypothalamic slice in dim red backlighting.** Scale bar represents 100 µm.

Section 1.4: Circadian Genes and Neurochemisty

The Transcription/Translation Feedback Loop.

Several "clock genes" take part in an interlocking transcriptional and translational feedback loop to activate and repress each other in a manner that results in a ~24-hour period (for review see [43]; Fig. I-5). The key circadian genes in mammals include *Bmal1* and *Clock* (or also *Npas2*), which activate the E-box promoter for the *Period* genes *Per1* and *Per2*, and the *Cryptochrome* genes *Cry1* and *Cry2*. While *Clock* is constitutively expressed, *Bmal1*[e] peaks in expression during the subjective circadian night, or "lights-off"[44]. The transcriptional factor Rora serves to activate *Bmal1* transcription, and further, competes with Rev-Erbα for binding to *Bmal1*'s promoter[45]. CLOCK and BMAL1 dimerize in the cytoplasm after translation, are phosphorylated by an as-yet-unknown kinase, and then translocate back into the nucleus to bind to E-boxes that upregulate *Per*, *Cry* and *Rev-Erbα* expression—forming the "positive arm" of the negative feedback loop.

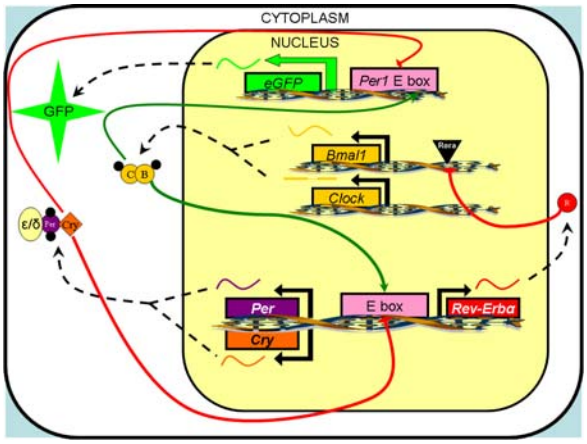

Figure I-5. | **Genetic mechanisms of the circadian neuron.** Mammalian neuronal circadian rhythms are governed by an intricate gene-protein feedback loop known as the Transcription/Translation Feedback Loop (TTFL). Black dashed arrows represent movement of transcripts out of the nucleus for translation; **green** arrows represent the positive loop where the resultant proteins activate transcription of *Per*, *Cry* and *Rev-Erbα*; **red** lines represent the negative loop where the resultant proteins inhibit their own transcription in the case of Per and Cry, or inactivate *Bmal1* transcription by competing with Rora as in the case with *Rev-Erbα*. The production of a short half-life GFP reporter is linked to transcriptional activation of *Per1* (See Section 1.7: Model Mice).

After translation, either PER1 and CRY1 or PER2 and CRY2 dimerize, and then are phosphorylated by Casein kinase I ε/δ. This serves to either degrade the proteins, or to repress their own transcription in the "negative arm" of the feedback loop by translocating back into the

[e] Also *Bmal2*, though its role is unclear.

nucleus and inhibiting their own promoter's activation by BMAL1/CLOCK. Concurrently, Rev-Erbα inhibits *Bmal1* transcription by competing with Rora for promoter binding in a second "negative feedback loop." Because the *Per* genes are highly transcribed during the circadian day[44], they are a useful measure of circadian period *ex vivo* (see Figs. I-3 and I-5; Section 1.7: Model Mice).

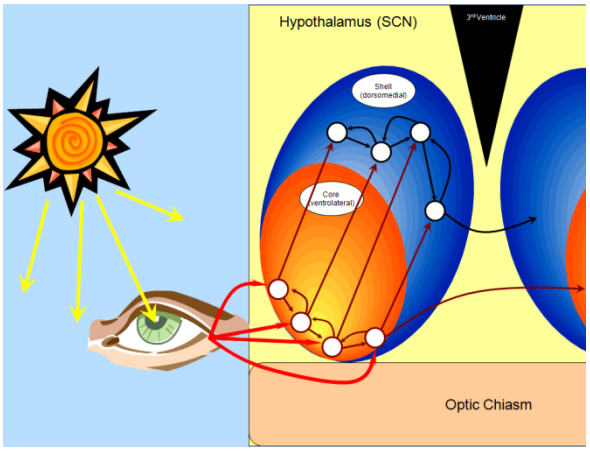

Figure I-6. | **Gross organization of the SCN and its projections.** The retinohypothalamic tract projects from melanopsin ganglion cells of the retina along the optic nerve to innervate the SCN, which has classically been divided into a ventrolateral "core" region (**orange**) which projects bilaterally and to a dorsomedial "shell" region (**blue**). Many core VIP-ergic neurons in the SCN (**maroon**) receive glutamatergic innervation (**red** arrows) from the retina via the retinohypothalamic tract that signals "lights-on." These neurons send VIP-ergic projections (**maroon** arrows) to other VIP-ergic neurons, into the shell, and into the core of the other SCN. Shell neurons (**black**) receive VIP-ergic innervation, and project (**black** arrows) to other shell neurons, and to the other SCN shell.

The SCN is innervated by the retina and is characterized by anatomically localized neuropeptides.

The mammalian circadian clock is entrained to the external environment primarily by light[19]. Light presented during the early night phase-delays[f] the onset of locomotor activity, while light presented in the late night phase-advances[g] the onset of activity. This phase-shifting process occurs when conventional photoreceptors and specialized melanopsin ganglion cells (MGCs)[46] within the retina signal photic information to the SCN via glutamatergic innervation by the retinohypothalamic tract (RHT)[47-50]. Early work suggested that this innervation occurs on a group of neuropeptide-producing neurons located in the ventrolateral "core" of the SCN[30, 51],

[f] A phase-delaying stimulus resets the phase of the circadian rhythm such that an animal's activity, for example, would begin later the next circadian day than would be predicted had the stimulus not reset the phase.

[g] A phase-advance is similar to a phase-delay, though activity would begin earlier the subsequent day rather than later.

however recent studies suggest that projections from melanopsin ganglion cells actually innervate the entire nucleus more extensively than previously thought[52]. There are slight species-specific differences in the pattern of innervation, but most rodent models follow a general layout. Studies on light-induced expression of the immediate-early gene c-*Fos* suggest that many retinorecipient cells express vasoactive intestinal polypeptide (VIP) and gastrin-releasing peptide (GRP)[53-56]. Extensive work by Robert Moore and colleagues have identified a conserved anatomical pattern of neuropeptide expression in SCN from multiple rodent models[47, 57-59]. In addition to the retinorecipient core, the SCN is also characterized by a dorsomedial shell that produces arginine vasopressin (AVP), met-enkephalin and angiotensin II[47]. Core neurons innervate not only each other, but the shell of the same nucleus as well[60]. There are internuclear connections between the two cores and the two shells (Fig. I-6).

VIP plays a role in circadian entrainment and behavior.

VIP is a secreted peptide in the glucagon family that is expressed rhythmically in these core cells, with a peak during the night in 12:12 light-dark (LD) conditions, but not in constant lighting conditions (DD and LL)[61-65]. Exposure to constant light has been shown to significantly depress VIP concentrations in the rat SCN[66] in a light-dose-dependent manner[67]. This result is supported by *in vitro* data suggesting that NMDA phase-delays neuronal firing activity in rats, and causes a drop in the VIP content of core cells[68]. These same cells respond to pulses of light during the dark period by upregulating *Per1* and *Per2* expression[41, 69-71] and producing a phase-shift[17]. Previous studies have shown that VIP is sufficient to phase-advance when applied alone at CT 20-24 *in vivo*, and moderately sufficient to phase-delay when applied alone at CT 12-14 in hamsters[72]. Altogether, these results strongly suggest a key role for VIP in photic entrainment.

VIP signals via a G protein-coupled receptor in SCN.

Prepro-vasoactive intestinal polypeptide is the precursor from which VIP and peptide

histidine isoleucine (PHI) are derived, and both are structurally similar to pituitary adenylate cyclase-activating polypeptide (PACAP). All three share binding affinity for three receptor types in the brain—$VPAC_1$, $VPAC_2$ and PAC_1, but VIP has a higher specificity for the VPAC receptor subtypes. $VPAC_2$ (gene name *Vipr2*) is a G protein-coupled receptor that is highly expressed in the mammalian SCN, and its mRNA shows a biphasic pattern of expression in LD and DD[73]. Signaling through this receptor activates adenylyl cyclase to increase the concentration of cyclic AMP (cAMP), and it has been shown that rhythms in firing activity in the SCN are responsive to the phase-dependent phase-shifting effects of VIP and $VPAC_2$ agonists via PKA and MAPK *in*

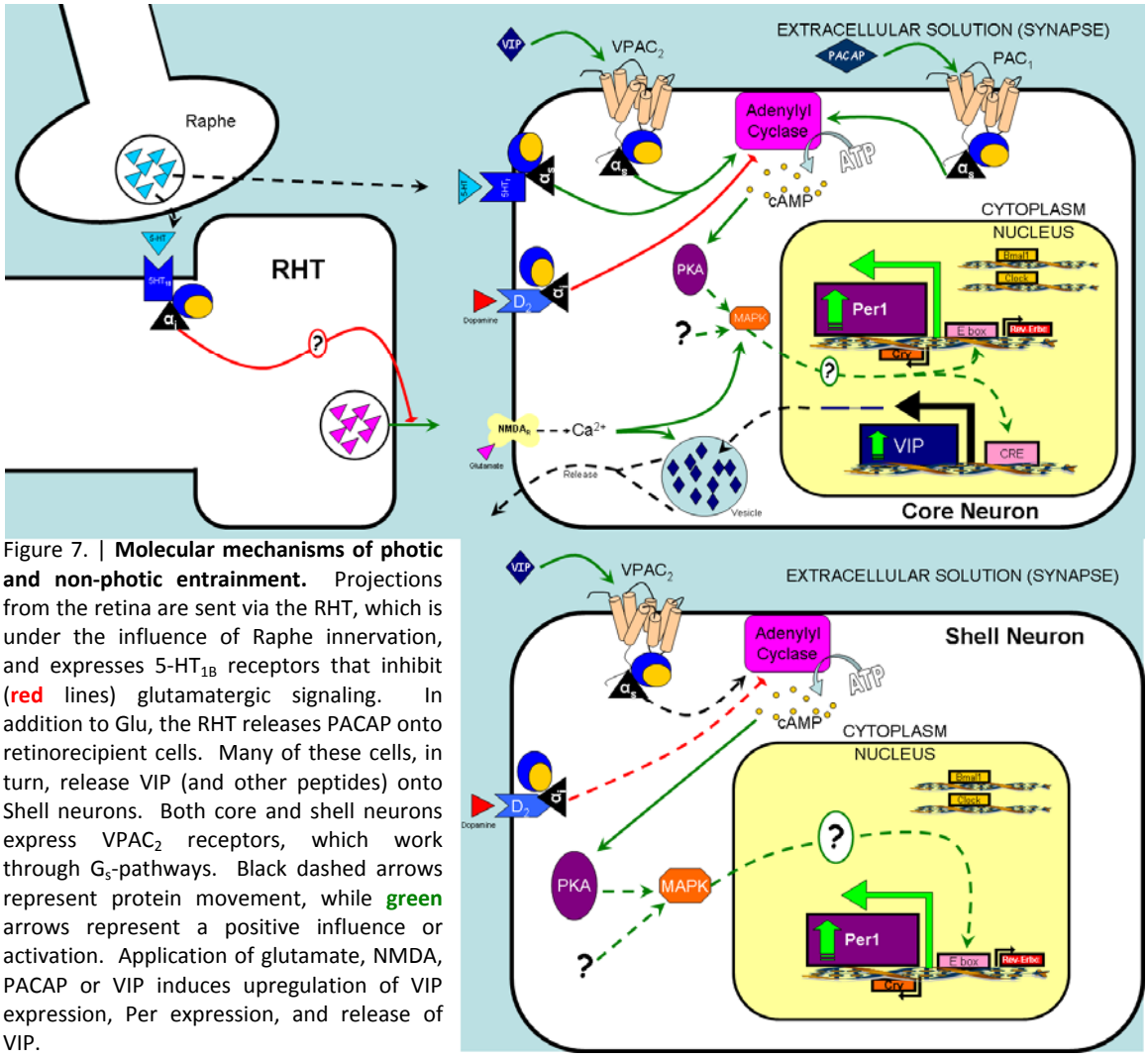

Figure 7. | **Molecular mechanisms of photic and non-photic entrainment.** Projections from the retina are sent via the RHT, which is under the influence of Raphe innervation, and expresses $5\text{-}HT_{1B}$ receptors that inhibit (**red** lines) glutamatergic signaling. In addition to Glu, the RHT releases PACAP onto retinorecipient cells. Many of these cells, in turn, release VIP (and other peptides) onto Shell neurons. Both core and shell neurons express $VPAC_2$ receptors, which work through G_s-pathways. Black dashed arrows represent protein movement, while **green** arrows represent a positive influence or activation. Application of glutamate, NMDA, PACAP or VIP induces upregulation of VIP expression, Per expression, and release of VIP.

vitro[74, 75] which induces *Per1* and *Per2* gene expression[76] similar to light (Fig. I-7). Specifically, application of VIP or $VPAC_2$ agonists suppress spontaneous firing *in vitro*[77]. These data strongly support a role for $VPAC_2$ as the essential VIP receptor in the mammalian circadian clock.

The mammalian circadian clock can be set by non-photic stimuli.

The primary zeitgeber for entrainment of the circadian clock is light, but non-photic stimuli such as novelty and arousal can also phase shift the clock[78]. Non-photic input is thought to arise in part from the median Raphe nucleus using serotonin as a neurotransmitter[79], and from the intergeniculate leaflet (IGL) of the thalamus using Neuropeptide Y (NPY) as a neurotransmitter[80]. Early studies showed that VIP-ergic neurons were under the influence of serotonergic innervation[81], and that treatment with the serotonin-depleting reagents parachlorophenylalanine (pCPA)[82] or 5,6-dihydroxytryptamine[83] causes a marked decrease in VIP immunoreactivity—an effect that can be reversed with 5-HT_{1B} receptor agonist[83]. This depletion initiates the rhythmic property of VIP mRNA expression in DD[84], and suggests that serotonin works antagonistically to light[85, 86]. The increase of available serotonin by treatment with monoamine oxidase inhibitors (MAOI) or by knocking out the MAO_A gene increases VIP expression in rats[87] and mice[88] respectively. 5-HT_{1B} receptors are localized to the RHT[89], suggesting an indirect effect on VIP expression by modulation of glutamate release. Similarly, 5-HT_{1A} or 5-HT_7 receptors are located on the core neurons of the SCN, and allow serotonin to directly modulate VIP release and neuronal activity[89]. Because serotonin plays a role in non-photic entrainment and modulates the SCN directly[90], mice with VIP signaling-deficiency—and thus lacking robust responses to photic stimuli—may have enhanced responses to non-photic stimuli.

Section 1.5: Human Circadian Genetics

Humans exhibit most of the same circadian characteristics as mice. Humans exhibit strong circadian rhythms in temperature, melatonin, cortisol, attention, and activity. Like mice, the central circadian pacemaker is located in the hypothalamus, which is entrained by photic and non-photic input. Unlike mice, humans are diurnal: active in the daytime.

Despite this major behavioral difference, the genes that govern circadian rhythms in mice are also expressed in humans in the same temporal pattern. As with all genes, circadian genes are prone to heritable mutations over time. These conserved variants have been identified in many of the circadian genes, with significant phenotypic consequences that have driven the field of circadian geneticists to create mouse models of the genetic change and further our understanding of circadian protein roles, function and dysfunction.

Perhaps the most obvious human circadian rhythm is the sleep/wake cycle. Much effort has been made to identify genetic causes for circadian sleep disorders, which have been defined by the International Classification of Sleep Disorders (ICSD)[91] as "a persistent or recurrent pattern of sleep disturbance due primarily to alterations in the circadian timekeeping system or a misalignment between the endogenous circadian rhythm and exogenous factors that affect the timing or duration of sleep." Six disorders have been recognized as true circadian rhythm sleep disorders (CRSD) by the ICSD and include: Advanced Sleep Phase Syndrome (ASPS or FASPS), Delayed Sleep Phase Syndrome (DSPS), non-24 hour sleep-wake disorder (N-24; also known as free-running disorder or FRD), irregular sleep-wake rhythm/phase (ISWR), jet lag and shift work. For a detailed discussion from the American Academy of Sleep Disorders Task Force, please see [92, 93].

FASPS has, to date, been the only circadian disorder found to display true Mendelian inheritance, and is characterized by the afflicted people exhibiting a ~4-hour advanced phase

angle of sleep onset every day. These people wake up in the very early morning (1-4 am) and fall asleep very early as well (6-7 pm), even in the presence of social pressure to stay awake[94, 95]. While this disorder is likely to have many genetic sources, two such sources have been identified as either of two complementary mutations: a S662G mutation in the *hPer2* phosphorylation site[96] or a T44A mutation in the phosphate transfer domain of the Casein Kinase 1 δ (CK1δ)[97].

DSPS etiology has not been as straightforward. DSPS it is the most common of the CRSDs, and is characterized by extremely late bedtimes (2-6 am) and midday wake times (10 am – 2 pm). While there is one reported case of inherited DSPS where the genetic defect is unknown[98], a length polymorphism located in exon 18 of the *Per3* gene has shown the most promising association with the phenotype[99, 100]. A simple nucleotide polymorphism (SNP) in the *Clock* gene (3111T>C) has also been a promising genetic lead, with people carrying the C/C genotype exhibiting strong evening preference, though not DSPS *per se*. Like FASPS, however, there are likely many genetic causes for the phenotype that have yet to be identified.

N-24 is common in blind people and is a result of a lack of perception of photic entraining stimuli which then leads to the person free-running through the geophysical days. N-24, therefore, does not necessarily have a primary genetic component. ISWR is characterized by the absence of circadian sleep-wake and its cause is unknown. Jetlag is the unpleasant physiological and psychological after-effects of traveling across multiple time zones, and its severity is proportional to the number of time zones crossed, direction of travel (west to east is considered more severe for humans), sleep deprivation, presence of zeitgebers at the destination and individual tolerance[93]. While the cause of jetlag is known to be the misalignment of circadian phase with the geophysical phase at the destination (or disruption/misalignment of multiple internal endogenous oscillators), much work has been done to alleviate the symptoms and

elucidate their root causes. To date, no major genetic studies have been undertaken in humans regarding N-24, ISWR or jetlag.

The final recognized CRSD, shift work disorder, is caused by circumstances similar to jetlag, in that misalignment of circadian phase with the zeitgebers (light, social pressure, stimulants) during the work shift cause unpleasant after-effects or sleepiness, especially in people on a rotating schedule[92, 93]. Individuals involved in shift work (estimated at 1 in 5 American workers[101]), have been, due to their unique circumstances, a useful pool of human subjects for circadian rhythms research, and several studies have taken advantage of this pool to study how genetic polymorphisms in circadian genes associate with shift work tolerance, sleep strategy and other CRSDs. Chapter V of this dissertation discusses a population of predominantly European American shift work nurses at Vanderbilt University, and compares SNP frequencies within this population to other geographical groups[2]. A future study using this genetic dataset, in combination with survey results from the Vanderbilt shift work nurses will outline how genetic polymorphisms associate with lifestyle and sleep strategy within this group.

Characteristics of human mental health display an intriguing association with circadian rhythms. The symptoms of jetlag and shift work briefly described above offer evidence that disruption of circadian phase angle can lead not only to side-effects, but suggest the possibility of more serious conditions. A strong circadian rhythm of mood, for example, has been noted in patients with severe depression, and is codified in the DSM-IV as a criterion for the melancholic subtype of major depression. It has been noted that the patients with mood disorders often exhibit altered circadian phase in body temperature, cortisol and even melatonin (for review, see [102, 103]). There are also many seasonal-related ailments that will be discussed more thoroughly in the next section (Section 1.6: Seasonality). It has been suggested that the connection between mood disorder and circadian rhythms may involve the literal connection

between the serotonergic Raphe nuclei of the brainstem and the SCN, both directly and through the intergeniculate leaflet (IGL) of the thalamus. There are several 5-HT receptors expressed in the SCN (as discussed in the previous chapter, Figure I-7), and the interplay between the circadian system and the serotonergic system is thought to be extensive, at both the molecular and tissue levels. In combination with the extant data on the role of clock genes in normal and abnormal human circadian rhythmicity, these data suggest not only that circadian genes could play a potentially huge role in mental health, but also that human circadian neural organization is an appropriate starting point for research into treatments for mental disorders.

We cannot, of course, easily and non-invasively study human SCN network organization directly. Instead, we must use model systems such as the mouse in which transgenic manipulations can be performed and from which live tissue can be collected acutely. Expression of circadian genes is thought to be conserved across the species, despite the difference in behavioral timing preference. Like mice, human *Period* is expressed during the daytime, and *Bmal1* is expressed at night. Conventional wisdom suggests that SCN neural activity is inhibitory in nocturnal animals, but excitatory or disinhibitory in diurnal animals. How the SCN accomplish this behavioral switch while maintaining conserved mammalian machinery is unknown. As further data regarding the neural organization of the SCN is gathered using mouse transgenic models, our understanding of human circadian function and dysfunction will continue to grow as well.

Section 1.6: Seasonality

After the moon-forming impact, the new Earth was left spinning on an axis slightly off perpendicular to the planet's orbit around the sun. While this is not thought to be unusual, the planet is thought to continue normally either with a floating axis or right its axis to

perpendicular (with respect to its orbit around a star) with time[104]. The gravitational influence of the nascent moon served to stabilize this off-kilter axis, creating the seasons. The amount of seasonal daily light, or photoperiod, varies from the most light on the first day of summer, to the least on the first day of winter. The range of light per day depends on latitude, with the most extreme latitudes receiving the most extreme photoperiods. As life flourished on the planet, strategies for thriving with seasonal changes in photoperiod developed, and are maintained today. The ability to predict oncoming hardship in the winter, or abundance in the summer is thought to increase fitness in plants and animals alike. For plants like trees, the shorter day indicates a decrease of higher energy short-wavelength light and the coming colder temperatures. The trees lose their foliage at this time of year and go relatively dormant. As day-length increases, photoperiod signals the oncoming warmth and a transition to photosynthesis and an increase in foliage and gamete production occur.

In animals, change in photoperiod indicates a necessity for behavioral change. For nocturnal animals, summer photoperiod means that all activity has to be squeezed into a shorter night, and with the abundance of growing plant-life, it is the prime-time of year to breed, and thus some male animals experience explosive gonadal growth while females become receptive to mating. As winter approaches, photoperiod indicates a time for hibernation and/or pelage change—lighter color and thicker coat to prepare for winter cold.

Not all animals experience these physiological changes, but those that do are said to be photoperiodic. Mice (*Mus musculus*) are thought not to be photoperiodic, but they do experience a behavioral reorganization to changes in photoperiod. In their seminal paper on entrainment, Pittendrigh and Daan[15] demonstrated that rodents[h] compress their main activity bout (α) in long photoperiods. Additionally, this compression of α results is an after-effect, or

[h] Including non-photoperiodic mice.

transient reorganization of the circadian rhythm that is evident in constant conditions. Specifically, the compression of α evident in long photoperiods correlates with a decreased free-running period in mice.

The reorganization of the clock and how this accounts for behavioral changes had remained a mystery until recently, with the development of *in vivo* electrophysiological and *ex vivo* circadian gene reporter techniques. *In situ* hybridization (ISH) from Bill Schwartz and colleagues found that expression of circadian genes was different in animals taken from short (8L:16D) and long (16L:8D) photoperiods[105, 106]. Work from the lab of Johanna Meijer as recently as 2006 showed that *in vivo* electrical activity of mouse SCN from more extreme photoperiods[i] was dramatically different, and they postulated that season was encoded by change in neuronal phase distribution[107-109]. At least three laboratories[j] then took advantage of *Period* gene reporters to address whether this change was evident *ex vivo*. The Honma group won the race using a *Per1*::Luc reporter mouse developed in their lab using a construct donated by the Tei Lab[k]. Using 100μm coronal slices of hypothalamus, they found that anterior slices demonstrated a weak double-oscillation, and they suggested that this was the elusive morning and evening oscillators[110]. The Ebihara group then published a more in-depth study of season encoding using horizontal slices from the same reporter mouse[111]. Our group, in the lab of Doug McMahon, found similar results, but also focused on the developmental impact of photoperiod on SCN organization and plasticity (see Chapter IV).

It has become fairly clear that the phase distribution of neuronal circadian rhythms is highly correlated with behavioral reorganization between winter and summer photoperiods. How or if this then leads to behavioral after-effects, however, is unknown. After-effects have been

[i] 6L:18D for short photoperiod; 18L:6D for long photoperiod.
[j] Ken-Ichi Honma of Hokkaido University; Shizufumi Ebihara of Nagoya University; Douglas McMahon of Vanderbilt University.
[k] Hajime Tei, Mitsubishi Kagaku Institute of Life Sciences.

primarily studied in T-cycles[l]. Aton and Herzog showed that *in vitro* rhythms in electrical activity are not reflective of the behavioral change in free-running period (FRP). This paradoxical effect is supported by work from the Harrington lab[112, 113].

An understanding of the seasonal effects of light is critical in explaining aberrations in human health. Changes in seasonal photoperiod have been associated with mood disorders and mental disease in humans. Seasonal Affective Disorder (SAD), for example, is a mood disorder that affects between 0.4% and 2.7% of the United States population every year and is treated with bright light therapy or selective serotonin reuptake inhibitors (SSRI)[114-116]. A 5-8% winter-spring excess of births have been reported for both schizophrenia and mania/bipolar disorder[117-119]. There is a spring and summer excess of births for autism[120-122], and a winter-spring excess of births for neurosis[123, 124]. Winter-born humans have been reported to show both stronger morning-preference than the other seasons on a Morningness-Eveningness Questionnaire[125, 126], and significantly lower (sadder) Global Seasonality scores than individuals born in the summer[127]. These studies suggest that birth season—or perhaps the seasonality of late gestation—imprint the organization of the brain systems that control cognition, emotion and/or circadian rhythmicity.

Section 1.7: Model Mice

With their large SCN[m] and our ability to perform transgenic manipulations, the house mouse (*Mus musculus*) has proven an invaluable model system in which to study mammalian circadian neurobiology. Mice are nocturnal[n] (Fig. I-1), and some strains of inbred mice[o] represent an excellent circadian model organism, exhibiting robust, consolidated behavioral activity rhythms

[l] Day-length ≠ 24-hours.
[m] Relative to their overall brain size.
[n] Active at night.
[o] C57Bl/6J, C3H, and a hybrid of the two strains called B6C3.

with a period slightly shorter than 24-hours. Because gestation is only 21 days and they can reproduce as young as 6 weeks of age, mice offer high fecundity at a low cost when compared to primates and other rodents. Additionally, transgenic approaches are far more advanced in mice than in any other mammal.

As previously noted, the high amplitude rhythm of *Period* gene expression provides a convenient means by which molecular rhythms can be measured (Figs. I-3 and I-5). Several laboratories have taken advantage of this mechanism by creating transgenic reporter mice. Around the year 2000, Sandra Kuhlman designed a *Per1*-promoter driven short half-life green fluorescent protein (GFP) reporter mouse strain (abbreviated *Per1*::GFP) in the lab of Douglas McMahon (Fig. I-3b, see [128]). This mouse strain, while originally designed as a guided missile to identify *Per1*-expressing neurons for electrophysiological recording[41, 129, 130], has been the workhorse of my studies, and reliably reports the cellular expression of *Per1* promoter activity in the SCN by fluorescent protein production (Fig. I-8).

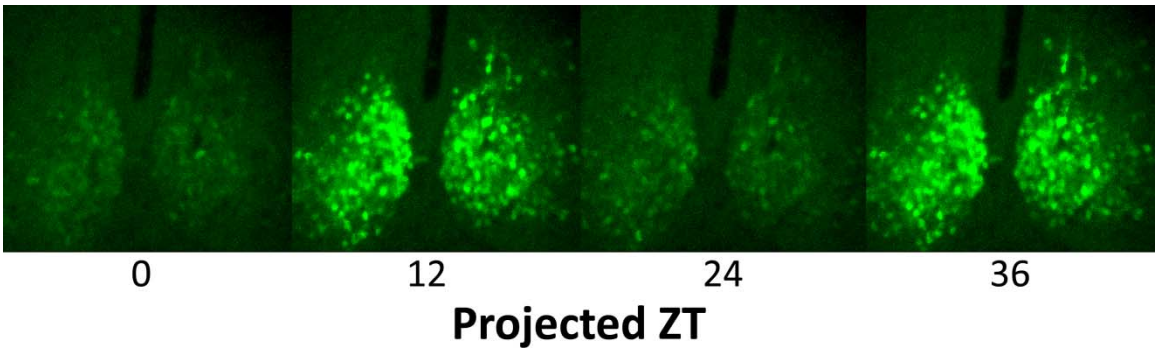

Figure 8. | **Representative example of the circadian expression of *Per1*::GFP in SCN neurons over 36 hours *ex vivo* in projected Zeitgeber Time.** Brain slices from mice carrying the *mPer1*::GFP were cultured and the gene expression dynamics of their SCN were assayed via confocal microscopy.

The other reporter mouse line used in these studies was created by Seung-Hee Yoo and Shin Yamazaki in the laboratory of Joe Takahashi, in which the gene for firefly luciferase was attached to the mouse *Per2* gene, and inserted as a knockin (called PER2::LUC). Each strain has

advantages and weaknesses. The *Per1*::GFP mouse line is on a hybrid B6C3 background and is only reliably fluorescent for the first 4-5 days *ex vivo* of adults, but the line offers fast integration images of *Per1* promoter-driven expression at the single cell level. The PER2::LUC knockin is on the preferable C57Bl strain, their SCN circadian reporter expression can last for years in culture, and one can monitor up to 36 samples with a LumiCycle (Actimetrics) photo-multiplier tube, but due to the slow integration time needed for single-cell resolution, imaging technology cost and time resources are prohibitive, making the line more appropriate for tissue-level work. Other reporter mouse lines not used in this dissertation include $Per1_{Tokyo}$::LUC and $Per1_{Tokyo}$::GFP strains sharing the same *Per1* promoter from the laboratory of Hajime Tei, and a recently designed *Per2*::LUC_{SV} mouse strain from the Takahashi lab with more robust luminescence than the previous PER2::LUC knockin strain. For the purposes of this dissertation, only the *Per1*::GFP (and PER2::LUC[p]) line were used in these studies and bred to other mutant mice as indicated.

In 2002, Harmer *et al*.[131] succeeded in knocking out the $VPAC_2$ receptor gene *Vipr2* with dramatic results: though the knockout mice (*Vipr2*$^{-/-}$) are able to roughly entrain to a light-dark cycle with behavioral activity onset at around lights-off, they are completely arrhythmic in DD, and show ~8 hour phase advance the first day in DD. These animals also show a depressed rhythmicity in clock gene expression[131]. Later evidence suggests that these mice do not entrain to the light-dark cycle as well as first reported[132, 133]. Electrophysiological analyses of these mice indicate a loss of the typical midday peak in firing activity, a result that was mimicked by chronic application of a $VPAC_2$ antagonist in control mice[132]. Immunohistochemical analyses revealed a lack of light-induced expression of immediate-early gene *pERK* in the core of the SCN, suggesting that they lack the ability to gate photic stimuli and that they possess a disconnect between the clock and its normal path of entrainment[134]. Evidence using crosses with both the PER2::LUC

[p] Kindly donated by Shin Yamazaki and Joe Takahashi; though not reported in this work.

and *Per1*::GFP reporter mouse lines suggest that the SCN neurons in neonatal *Vipr2*$^{-/-}$ mice are less capable of maintaining *in vitro* synchrony than controls[135].

In 2003, Colwell *et al*.[136] showed that a *VIP* knockout mouse (*VIP*$^{-/-}$; also deficient for PHI since they are the same gene) shows behavioral characteristics similar to the *Vipr2*$^{-/-}$ mouse, with an unusual phase angle of entrainment in LD and arrhythmicity in DD. They also exhibit the ~8 hour phase advance the first day in DD, and completely ignore phase-delaying light-pulses, suggesting a similar disconnect between the photic pathway and the clock as seen in [134]. Unlike in the *Vipr2*$^{-/-}$ mouse, application of VIP rescues the spontaneous firing activity of SCN neurons *in vitro*[136]. A study on both knockout mice showed that a significantly smaller proportion of rhythmically firing neurons exist in their SCN than in controls[133]. Taken together, these data implicate VIP and its receptor in mediating photic stimuli to, and synchrony within, the SCN. The inherent cellular desynchrony[135] and the disconnect between the clock and photic pathway[134] make these mouse models powerful tools to study uninhibited pathways of non-photic entrainment, and to identify how cellular pacemakers are organized in the central mammalian clock.

Section 1.8: Objectives, Relevance and Impact

In the 30+ years since the discovery of the SCN as the central mammalian clock, various groups of circadian researchers have used genetic, anatomical and molecular studies to elucidate the mechanisms by which the these nuclei control circadian physiology and behavior. The overall objective of this dissertation was to determine the genetic and molecular organization of the SCN network, and elucidate how the SCN interacts with the environment to produce measurable behavioral and physiological circadian rhythms. I have taken advantage of transgenic mouse lines to report on and model function and dysfunction in the mammalian SCN

as representative of the organization in higher mammals such as humans, and I have taken the study of circadian biology one step further in analyzing the evolutionary pressures of circadian genes within human populations.

The studies reported in this dissertation address several key questions in neuroscience and chronobiology. 1) How do neurons within the SCN organize as a network, and how does this network control behavior? Chapter II examines the role of SCN organization in behavioral output, and finds that, very much like the coding found in the voluntary motor system, the SCN neural network encodes behavioral phase vector as a population, with the temporal direction determining the phase of behavioral onset, and the strength of that vector determining the behavioral coherence. 2) I next asked what role VIP plays in network synchrony within the SCN, and in light-signaling to the SCN. Chapters II and III use a *VIP*$^{-/-}$ mouse line, which leads to an absence of neuronal synchrony within the SCN, to suggest that the role of VIP communication in the SCN is to modulate the timing and coherence of population vector encoding by SCN neurons in response to light and behavioral feedback. 3) In the absence of proper light signaling found in *VIP*$^{-/-}$ mice, I asked how locomotor behavior feeds-back on the circadian pacemaker and affects the clock and its entrainment. While Chapter II uses wheel measurements of activity exclusively, Chapter III reports activity measurement by infrared motion detection that suggest that locomotor activity on a wheel leads to modulation of masking and greater integration of weakly rhythmic behavioral components in mice.

Using the findings of Chapters II and III as an interpretive guide, 4) I next ask how seasonal photoperiod changes are encoded by the SCN. 5) Furthermore, does light, or more specifically seasonal photoperiod during development, hard-wire the rhythmic character of neurons within the SCN? The data in Chapter IV suggest that the answer to the former (4) very much depends on the answer to the latter question (5). Seasonal photoperiod was found to be encoded at

both the neuronal and SCN network levels, and its plasticity was dependent on the photoperiod in which the mice developed.

The final topic addressed in this dissertation makes the translational leap from a mouse model that represents human circadian organization to actual humans themselves. 6) I asked how geography has affected the distribution of circadian gene variants in the human species, and how might this distribution be explained by the environment in which each population is found. Chapter V suggests that while the frequencies of many of the most common human circadian genetic variants are significantly different across populations, these differences are the result of genetic drift rather than natural selection.

Each of these questions carries translational and clinical significance. In defining the properties of the mouse circadian neural network, we have identified the SCN as a quintessential model for basic neuroscientists to study how neural networks govern behavior. Furthermore, the mechanisms by which the SCN organize in response to seasonal photoperiod are applicable to humans and human mental health. Finally, the study of polymorphic human circadian genes lays a foundation for future research on the behavioral and physiological consequences of these gene variants, and possibly provides a means by which circadian ailments can be treated.

Using genetic knockouts, molecular reporters and behavioral analyses, this dissertation will explore the relationship between circadian genes, the SCN neural network in which these genes are expressed, and finally the behavioral output that results from this network. I will investigate how light not only entrains the adult clock, but also serves to imprint clock organization during development, and also how circadian behavior can feedback on itself and reorganize. The mammalian circadian system is complicated, with multiple layers of feedback at each level of organization (Figure I-9), but while this dissertation may leave some questions unanswered, it is

my hope that the data are presented in a logical and meaningful way, and that it spawns even further questions for future research.

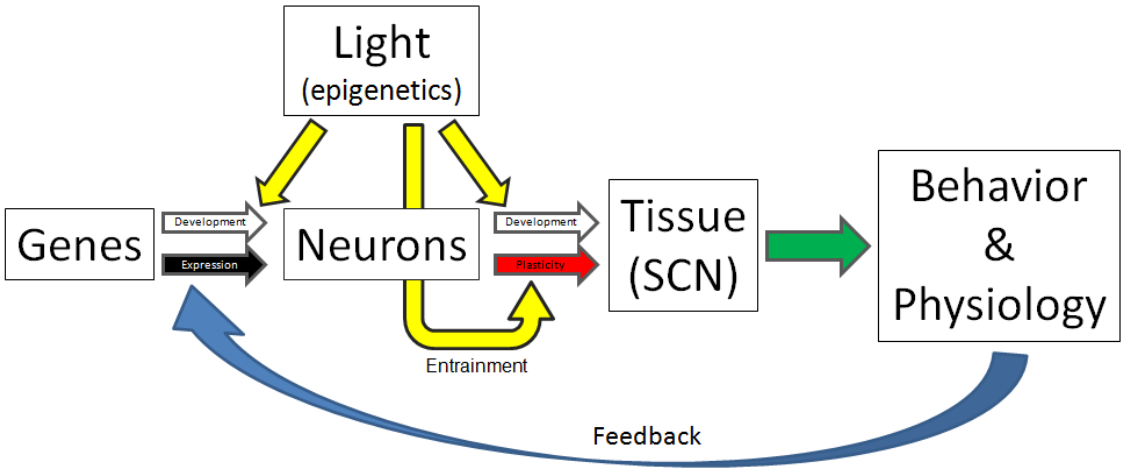

Figure I-9. | **Levels of mammalian circadian organization examined in this dissertation, and the layers of feedback between levels.**

CHAPTER II

POPULATION ENCODING BY CIRCADIAN CLOCK NEURONS ORGANIZES CIRCADIAN BEHAVIOR[q]

Christopher M Ciarleglio[1,2], Karen L Gamble[2], John C Axley[2], Benjamin R Strauss[2], Jeremiah Y Cohen[1], Christopher S Colwell[3], and Douglas G McMahon[1,2]

[1] Neuroscience Graduate Program, Vanderbilt University, Nashville, TN
[2] Department of Biological Sciences, Vanderbilt University, Nashville, TN
[3] Department of Psychiatry and Biobehavioral Sciences, UCLA, Los Angeles, CA

Section 2.1: Summary Abstract

Mammalian circadian rhythms are orchestrated by the suprachiasmatic nuclei (SCN) of the hypothalamus. The SCN are composed of circadian clock neurons but the mechanisms by which these populations of neuronal oscillators encode rhythmic behavior are incompletely understood. We have used *ex vivo* real-time gene expression imaging of the neural correlates of circadian behavior, combined with genetic disruption of vasoactive intestinal polypeptide (VIP), a key SCN signaling molecule, to examine the neural basis of circadian organization in the SCN. We show that the coherence and timing of clock neuron rhythms are correlated with the coherence and timing of behavioral rhythms within individual mice, and that the degree of disruption of SCN neuronal organization correlates with the degree of behavioral disruption within individuals. Our results suggest that the SCN encode circadian phase as a temporal population vector of its constituent neurons such that as the neuronal population becomes desynchronized, phase information becomes ambiguous.

[q] Ciarleglio *et al*. (2009). Population Encoding by Circadian Clock Neurons Organizes Circadian Behavior. *J. Neurosci*.

Section 2.2: Introduction

The master circadian clock in mammals is a gene-driven neural network that temporally regulates behavior and physiology. It is composed of ca. 20,000 neurons, and is located in the suprachiasmatic nuclei of the hypothalamus (SCN)[137]. At a gross level, the SCN's control of circadian behavior is clearly established as SCN lesions result in behavioral circadian arrhythmicity[31, 138, 139] that can be restored by SCN transplants[140]. At a more refined level, it is unclear how neurons within the SCN neural network act to control or regulate circadian behavior.

Vasoactive intestinal polypeptide (VIP) is a key signaling molecule expressed in neurons of the retino-recipient region of the SCN, where it is rhythmically released in a light cycle and can reset the phase of the clock in response to nighttime light pulses[61-65, 72]. Mice lacking VIP-ergic signaling show marked circadian abnormalities such as an inability to phase shift in response to light pulses and blunted endogenous behavioral circadian rhythms[131, 136]. In addition, neonatal SCN from *VIP*$^{-/-}$ mice exhibit reduced synchrony of neuronal spike frequency rhythms[133] and of neuronal clock gene expression of rhythms[135]. Manipulation of this SCN signaling molecule offers the opportunity to perturb SCN organization and to test the relationship between clock network organization and the control of behavior.

Using *ex vivo* real-time clock gene expression imaging of SCN networks and neurons in which SCN are acutely explanted and characterized from behaviorally characterized VIP-deficient mice, we sought to ascertain the aspects of SCN network organization that define behavioral circadian organization. Our findings indicate that within individual mice the degree of behavioral circadian disruption resulting from loss of VIP is correlated with the degree of desynchrony in the SCN neural network and that the onset of behavioral activity coincides with a specific phase of SCN rhythms. These results suggest that in the circadian clock, the overall pattern and

organization of rhythmic neuronal activity that drives the temporal organization of locomotor behavior is encoded by the mean temporal population vector of SCN neuron rhythms.

Section 2.3: Materials & Methods

Animals and housing. Mice with a targeted *VIP* gene disruption[136] were backcrossed four generations to mice (B6C3 hybrid from Jackson Labs) carrying the *mPer1*::d2EGFP transgene[128] yielding *Per1*::GFP$^{+/+}$, *VIP*$^{+/-}$ mice which were bred in a 12L:12D light cycle (LD) to yield experimental mice. Male offspring 3-5 weeks of age were placed in litter-filled wheel cages (Coulbourn Instruments, Whitehall, PA) with food and water *ad libitum*. All mice were entrained to 12L:12D light cycles for 9-22 days, and then either euthanized and their SCN explanted to assay SCN molecular rhythms *ex vivo* as part of the LD experimental group, or maintained in constant darkness (DD) for an additional 20-60 days and then euthanized and their SCN explanted to assay SCN rhythms *ex vivo* as part of the DD group. Animals were euthanized by cervical dislocation between Zeitgeber Time (ZT) 9-12 in LD (where ZT 12 is lights-off), or Circadian Time (CT) 9-13 in DD (where CT 12 is the onset of activity). Behavioral onset of mice behaviorally arrhythmic in DD could not be assigned. They were euthanized along with their rhythmic counterparts and their SCN rhythm phases are reported as time *ex vivo*. All animal care was conducted in accordance with Vanderbilt University IACUC guidelines.

Behavioral analyses. Wheel-running activity was monitored and recorded in 5-minute bins using ClockLab software (Actimetrics, Evanston, IL). Behavior was analyzed using ClockLab Analysis software, and activity was quantified as the number of wheel revolutions occurring during 5-min bins. In LD, the proportions of activity during lights-on and lights-off, as well as the total amount of activity per day were determined for the last 9 days in LD using the "activity profile" function. In DD, activity was measured for the first 20 days in darkness. Chi-squared periodogram analysis

yielded rhythmic power as a measure of the amplitude and coherence of behavioral rhythms[136]. Linear regression[16] was also used to project behavioral onset (CT12) in rhythmic animals to establish a consistent time of euthanization (CT 9-13).

Ex vivo culture. After behavioral characterization, mouse brains were extracted and blocked in cold sampling media as previously described[141]. One or two 200-µm coronal hypothalamic sections per animal were made on a Vibroslicer (Campden Instruments, Lafayette, IN). SCN were isolated by trimming the surrounding hypothalamic tissue and placed on a Millicell (Millipore) culture membrane insert in 37°C recording media[141], conditioned with GIBCO N-2 supplement (Invitrogen, Carlsbad, CA) and contained in 35-mm culture dishes (Falcon, BD, Franklin Lakes, NJ). Dishes were then sealed with sterile high-vacuum grease and placed in a custom 6-well aluminum chamber heated to 35.5°C by a voltage-regulator.

Confocal imaging. The 6-well chamber containing cultured slices was placed on an automated stage on a laser-scanning confocal microscope (LSM5 PASCAL, Zeiss, Germany) with GFP excitation at 488 nm, and bandpass emission recorded between 505-555 nm. Three Z-stack images totaling 40-µm in depth were taken of each slice every hour for 90 hours. Focus was adjusted manually to account for slice swelling and flattening as needed.

Ex vivo analyses. Raw LSM files of SCN time-lapse imaging were compiled in MetaMorph (Molecular Devices, Downingtown, PA). The Z-stack for each time-point was compressed into a single maximum projection image from which a background subtraction was made (Close-Open morphological filter with a 75 pixel-round sequential average). Whole SCN or single cells were selected as regions of interest (ROI) from the resultant time-series stack, and time-lapse intensity measurements were made and exported to an in-house program created in R (http://www.r-project.org/) that allowed selection of minima and maxima for each SCN or cell, and calculation of phase. The first 12 hours *ex vivo* were omitted from the analyses. Peaks in

fluorescence were visually scored as having a clear rising and falling phase above baseline fluorescence, and the number of circadian peaks per SCN or per cell was determined by 3-person independent visual scoring. For the purposes of this study, SCN or cells with two or more peaks were considered rhythmic. Overall slice fluorescence was determined by the total integrated fluorescence over hours 12-36 *ex vivo* divided by the area.

Statistical analysis. Circular statistics and Rayleigh vector plots were performed in Oriana 2.0 (Rockware, Golden, CA). Statistics were calculated for each animal for further comparison. Means were statistically compared in SPSS 14.0 (SPSS, Chicago, IL) with independent samples *t*-tests (two-tailed) and one-way analyses of variance (ANOVA) followed by post-hoc Fisher's Least Significant Difference tests, except for when the variances were not homogeneous, as indicated by a significant Levene's test. In these cases, nonparametric Kruskal-Wallis or Median tests were used. For correlational analysis, Pearson's product moment correlations were used. Significance was ascribed at $p < 0.05$.

Section 2.4: Results

VIP$^{-/-}$ *Per1::GFP mice exhibit weakened, phase advanced circadian behaviors*.

VIP knockout mice have been previously shown to exhibit specific circadian behavioral deficits, including altered light entrainment in LD and disrupted free-running circadian rhythms in DD[136]. To confirm that these traits persisted following breeding onto the *Per1*::GFP circadian reporter background, we examined the circadian behavior of VIP knockout (VIP$^{-/-}$), heterozygous (VIP$^{+/-}$) and wildtype (VIP$^{+/+}$) *Per1*::GFP mice in LD and DD (Fig. II-1). In light/dark cycles all genotypes exhibited primarily nocturnal locomotor patterns, but VIP$^{-/-}$ mice had less robust partitioning of activity into the night (dark) portion of the cycle, performing a greater percentage of wheel-running during the light-phase than the other genotypes (Median test,

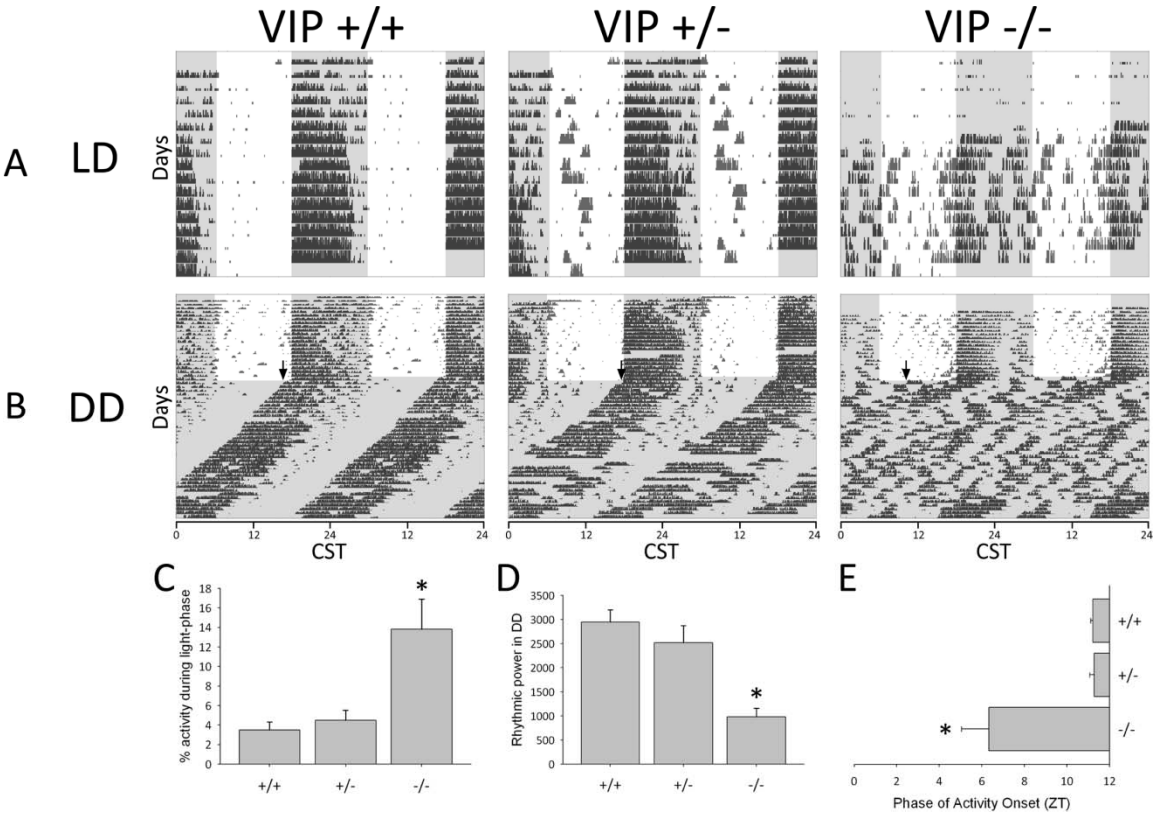

Figure II-1. | ***VIP* knockout *Per1*::GFP mice exhibit altered circadian behavior.** Left to right: example *VIP* wildtype (+/+), heterozygous (+/-) and knockout mice (-/-) on the *Per1*::GFP reporter background. **a** | Double-plotted actograms illustrate circadian behavior in a 12L:12D light cycle (LD). CST indicates Central Standard Time. **b** | Double-plotted actograms illustrate circadian behavior in constant darkness (DD). Black arrow represents the phase of activity onset on the first day in DD. (**a**, **b**) Black ticks represent activity in 5-minute bins; white background denotes lights-on; gray background denotes lights-off. **c** | Percentage of total wheel-running activity during the light-phase in LD for $VIP^{+/+}$ (N = 14), $VIP^{+/-}$ (N = 16) and $VIP^{-/-}$ (N = 16) mice. **d** | Rhythmic power in constant darkness as measured by χ^2 periodogram amplitude for $VIP^{+/+}$ (N = 8), $VIP^{+/-}$ (N = 9) and $VIP^{-/-}$ (N = 8) mice. **e** | Time of activity onset on the first day in constant darkness for $VIP^{+/+}$ (N = 7), $VIP^{+/-}$ (N = 9) and $VIP^{-/-}$ (N = 8) mice. Error bars represent SEM; asterisks (*) represent significance at $p < 0.05$.

$\chi^2(2) = 3.76$, $p < 0.05$, Fig. 1a, c). In constant darkness $VIP^{-/-}$ mice exhibited severely disrupted free running circadian behavior compared to wildtype and heterozygous mice. They lacked clear, coherent circadian rhythms (Fig. II-1b), and exhibited a significant reduction in rhythmic power in periodogram analysis ($F(2, 22) = 13.4$, $p < 0.01$, Fig. II-1d). At the transition from LD into DD, many $VIP^{-/-}$ mice did exhibit an initial behavioral onset during the first day in DD that was phase advanced by 5-6 hours compared to the onsets of $VIP^{+/-}$ and $VIP^{+/+}$ mice (Kruskal-Wallis, $\chi2(2) = 8.8$, $p < 0.05$, Fig. II-1e). These results demonstrate that the signature circadian deficits

associated with the lack of VIP signaling in the SCN—weakened light entrainment, disrupted endogenous rhythms and advanced phase angle of activity onset[136]—are preserved in *VIP*$^{-/-}$ *Per1*::GFP mice.

VIP$^{-/-}$ *Per1::GFP mice exhibit desynchronized, phase advanced SCN neuronal rhythms*.

We next characterized the SCN organization of the mice behaviorally characterized in Fig. II-1 by measuring circadian rhythms in the expression of *Per1* promoter-driven short half-life GFP in acute, *ex vivo* hypothalamic slice culture[128, 129, 141, 142]. After behavioral characterization in LD or DD, coronal SCN slices from each mouse were acutely explanted into organotypic slice culture. Cultures were imaged hourly for 90 hours on a confocal microscope, providing an assay of SCN network organization that could then be correlated with the animal's previous behavior, genotype and lighting condition.

Fig. II-2a-c show the SCN tissue and the SCN neuron *Per1*::GFP rhythms from the individual mice that were behaviorally characterized in Fig. II-1. Each column shows imaging data from an individual mouse matching the corresponding genotype and condition in Fig. II-1 (i.e., the data in the LD, *VIP*$^{+/+}$ column in Fig. II-2a-c are imaging data from the SCN explant of the mouse for which the behavioral record is Fig. II-1a LD, *VIP*$^{+/+}$, *etc.*). Overall SCN rhythmicity, as measured by the integrated *Per1*::GFP fluorescence of the SCN, was robustly rhythmic in explants from *VIP*$^{+/+}$ and *VIP*$^{+/-}$ mice in LD and DD, but was significantly disrupted in *VIP*$^{-/-}$ explants in both LD and DD (Fig. II-2a). Like locomotor behavior of *VIP*$^{-/-}$ mice at the LD to DD transition, *Per1*::GFP gene expression in explants from LD *VIP*$^{-/-}$ mice often exhibited a detectable initial onset cycle, followed by damped or disrupted rhythmicity during subsequent cycles *ex vivo* (Fig. II-2a), suggesting that de-afferentation of the explant may mimic the LD to DD transition. SCN explants from *VIP*$^{-/-}$ mice maintained in DD exhibited disrupted tissue-level circadian rhythms (Fig. II-2a) similar to their disrupted circadian behavior (Fig. II-1a).

At the cellular level, individual SCN neurons exhibited robust circadian rhythms in reporter gene expression in explants from all genotypes maintained in both LD and DD, even in *VIP*$^{-/-}$ mice with disrupted behavioral and SCN rhythms. Fig. II-2b shows all the cellular rhythms from the corresponding SCN slices in Fig. II-2a, whereas Fig. II-3 shows a limited number of typical cellular

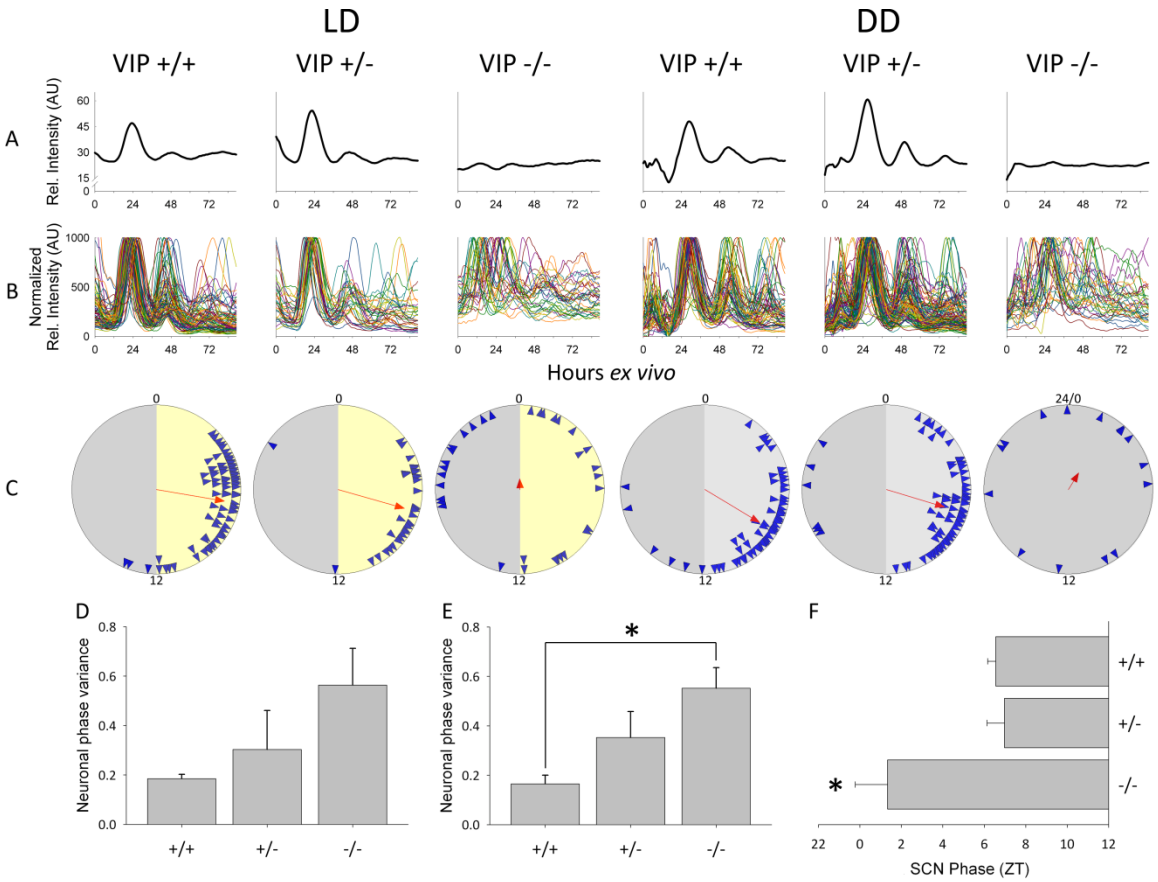

Figure II-2. | ***Ex vivo* circadian gene expression rhythms from SCN and clock neurons.** Left to right: example *ex vivo* SCN *Per1*::GFP imaging data from *VIP* wildtype (+/+), heterozygous (+/-) and knockout mice (-/-). **a** | Representative relative fluorescence intensity plots of *ex vivo* SCN for each of the *VIP* genotypes from LD (*left*) and DD (*right*) over 90 hours. **b** | Representative normalized relative fluorescence intensity plots of individual neurons over 90 hours *ex vivo*. **c** | Rayleigh plots from LD (*left*) and DD (*right*). Blue arrowheads represent the 50% peak rising phases of individual rhythmic neurons from a representative mouse of a particular genotype. Red arrow indicates the mean phase vector of rhythmic neurons, where length is inversely proportional to the neuronal phase variance, and the direction indicates timing relative to the previous light cycle in LD or previous behavioral cycles in DD. For LD (*left*), numbers indicate projected ZT, where projected ZT 0-12 is represented with a yellow background and projected ZT 12-24(0) is represented with a gray background; for DD (*right*), numbers indicate CT, where CT 0-12 is represented with a light gray background and CT 12-24(0) is represented with a darker gray background. For the *VIP*$^{-/-}$ mouse in DD, in which CT could not be reliably assigned, the phases of neurons are plotted as time *ex vivo*. **d** | Neuronal phase variance in SCN from *VIP*$^{+/+}$ (N = 4), *VIP*$^{+/-}$ (N = 5) and *VIP*$^{-/-}$ (N = 4) mice maintained in LD. **e** | Neuronal phase variance in SCN from *VIP*$^{+/+}$ (N = 7), *VIP*$^{+/-}$ (N = 8) and *VIP*$^{-/-}$ (N = 7) mice maintained in DD. **f** | SCN phase from *VIP*$^{+/+}$ (N = 9), *VIP*$^{+/-}$ (N = 9) and *VIP*$^{-/-}$ (N = 6) mice previously maintained in LD. Error bars represent SEM; asterisks (*) represent significance at $p < 0.05$.

rhythms from the same slices to better illustrate the properties of individual cellular rhythms. Rayleigh vector plots of the distribution of neuronal *Per1*::GFP rhythm phases revealed that the degree of synchrony in neuronal rhythms—as shown by vector arrow length—was reduced in *VIP*$^{-/-}$ mouse explants, particularly in DD (Fig. II-2c). Further quantitative analysis of the imaging data showed that in explants from mice maintained in LD, there was a trend toward increased neuronal phase variance within each mouse as the number of functional *VIP* alleles decreased, with *VIP*$^{-/-}$ explants exhibiting the highest degree of neuronal phase variance ($F(2, 10) = 2.0$, $p = 0.19$, Fig. II-2d). Similarly, in explants from mice in DD, the variance of the individual cell phases within each animal was significantly greater in *VIP*$^{-/-}$ explants than in *VIP*$^{+/+}$ explants (Kruskal-Wallis, $\chi2(2) = 9.171$, $p = 0.01$, Fig. II-2E). Finally, the onset phase (10% rise) of the first *Per1*::GFP cycle *ex vivo* occurred 5-6 hours earlier in *VIP*$^{-/-}$ SCN compared to *VIP*$^{+/-}$ and *VIP*$^{+/+}$ SCN ($F(2,21) = 4.1$, $p<0.05$, Fig. II-2f), similar to the onset of behavioral rhythms at the LD to DD transition. The lack of detectable synchrony in SCN neuronal phases across slices from *VIP*$^{-/-}$ mice in DD (Fig. II-4), in which the time axis is hours *ex vivo*, indicated that dissection and transition to *ex vivo* conditions did not set neuronal phase.

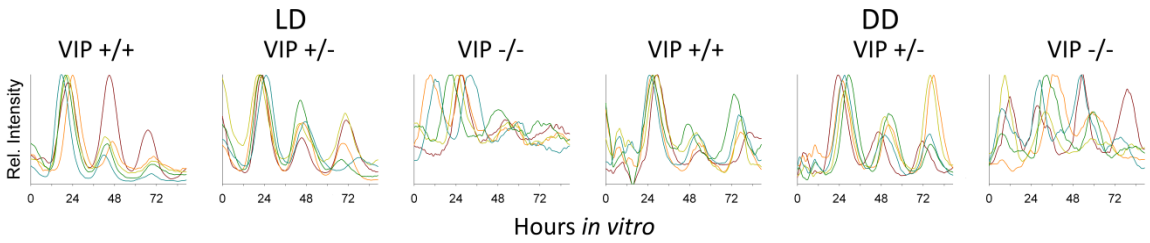

Figure II-3. | **Representative examples of 5 neurons in SCN slices** from mice of all *VIP* genotypes (see Fig. II-2b) maintained in LD (*left*) and in DD (*right*).

SCN neuronal phase distribution sets behavioral coherence and timing.

Given the striking correspondence of changes in the neuronal phase distribution with alterations in circadian behavior that we observed across mouse populations with altered VIP

communication, we next tested if SCN neuronal phase organization was correlated with circadian behavioral characteristics within individual mice across *VIP* genotype and lighting condition. Indeed, the proportion of wheel-running activity that occurred during the light-phase

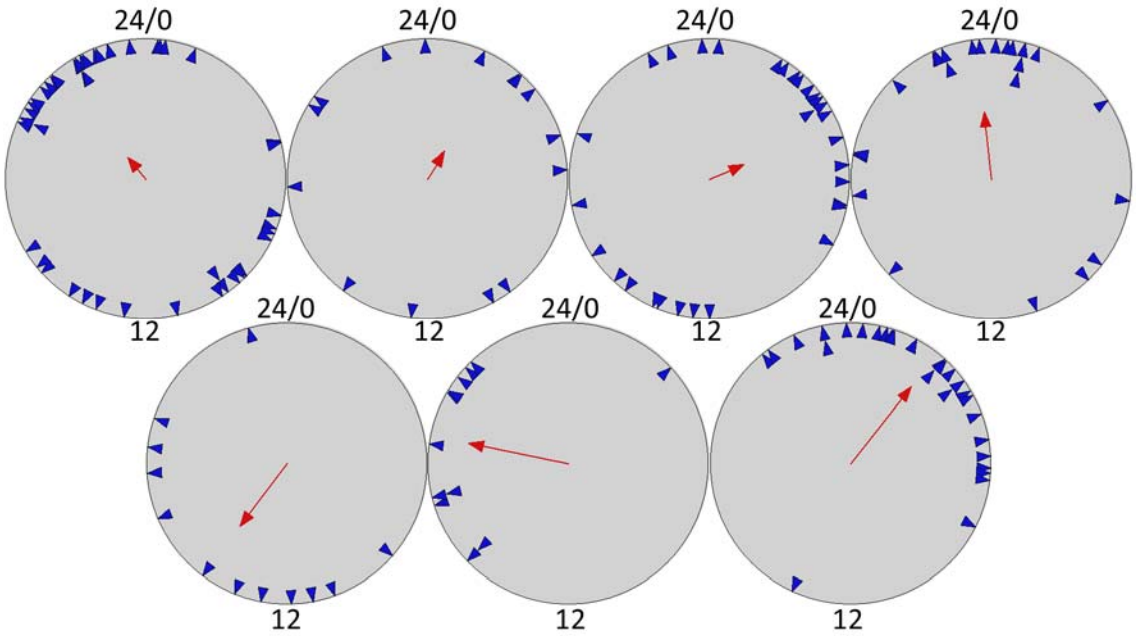

Figure II-4. | **Rayleigh plots of rhythmic neuron phases from *VIP*$^{-/-}$ mice in DD (N = 7).** Blue arrowheads represent the 50% peak rising phases of individual rhythmic neurons. Red arrow indicates the mean phase vector of rhythmic neurons within each animal, where arrow length is inversely proportional to the neuronal phase variance, and arrow direction indicates timing relative to the time of dissection. Numbers indicate the phases of neurons plotted as time *ex vivo* in hours.

of LD cycles was significantly and positively correlated with increased neuronal phase variance within individual animals across all genotypes (i.e., increased daytime activity was associated with decreased neuronal synchrony in all mice; $r(15) = 0.568$, $p < 0.05$, Fig. II-5a). Similarly, behavioral rhythmic power was significantly and negatively correlated with neuronal phase variance within individual animals across *VIP* gene dosage (i.e., decreased behavioral rhythmic power was associated with increased neuronal desynchrony in all mice; $r(18) = -0.641$, $p < 0.01$, Fig. II-5b). In addition to the correlations of neuronal phase variance with the coherence of behavioral rhythms, the timing of molecular rhythms in the SCN neural network also correlated

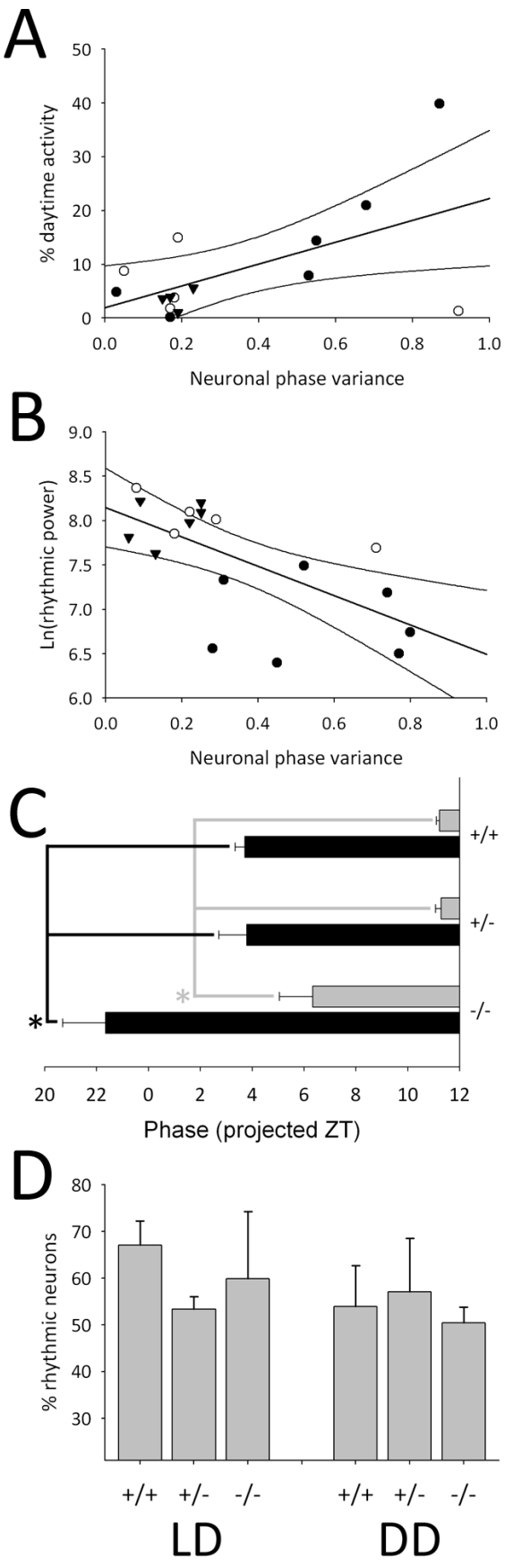

Figure II-5. | **Correlation of SCN neuronal rhythms with behavioral characteristics. a** | Plot of % daytime wheel-running activity vs. neuronal phase variance for individual mice (N = 15) by *VIP* genotype maintained in LD. **b** | Plot of rhythmic power vs. neuronal phase variance for individual mice (N = 18) by *VIP* genotype maintained in DD. (**a**, **b**) Closed circles represent $VIP^{-/-}$ mice, open circles represent $VIP^{+/-}$ mice and triangles represent $VIP^{+/+}$ mice. Thick black line represents single order regression, and the thin black lines represent the 95% confidence interval. **c** | Phase of SCN *Per1*::GFP onset (10% rising phase) on the first day *ex vivo* from mice maintained in LD (black bars) and onset of behavioral activity on the first day in DD (gray bars). For number of animals, see Fig. II-1E and Fig. II-2F. **d** | Plot of the percent of rhythmic neurons (2+ peaks) per SCN slice for mice maintained in LD (*left*) or in DD (*right*). LD: $VIP^{+/+}$ (N = 5), $VIP^{+/-}$ (N = 5) and $VIP^{-/-}$ (N = 4); DD: $VIP^{+/+}$ (N = 6), $VIP^{+/-}$ (N = 8) and $VIP^{-/-}$ (N = 7). Error bars represent SEM; asterisks (*) represent significance at $p < 0.05$.

with the timing of behavioral activity. In SCN from mice maintained in LD, both the onset of the *Per1*::GFP rhythm (10% above baseline on the rising phase) during the first cycle *ex vivo* and the onset of behavioral activity during the first cycle in DD were phase advanced by 5-6 hours in $VIP^{-/-}$ mice compared to other genotypes (Fig. II-5c).

Whereas the characteristics of circadian behavior mirrored SCN neuronal phase distribution and onset time, there was no significant correlation between other aspects of SCN rhythms and circadian behavior. Overall levels of *Per1*::GFP expression, measured as fluorescence intensity, were similar across *VIP* genotypes ($F(2, 70) = 1.359$, $p = 0.26$) and there was no correlation between the number or percent of rhythmic neurons in an individual animal's SCN explant and the behavioral rhythmic power of that mouse in DD (Pearson's product moment correlation for: number, $r(20) = 0.255$, $p = 0.28$ and percent, $r(20) = 0.238$, $p = 0.31$). Furthermore, the percentage of rhythmic neurons in individual SCN explants was similar across *VIP* genotypes and across lighting conditions (LD: $F(2, 11) = 2.7$, $p = 0.11$; DD: $F(2, 18) = 1.3$, $p = 0.29$, Fig. II-5d and Fig. II-6).

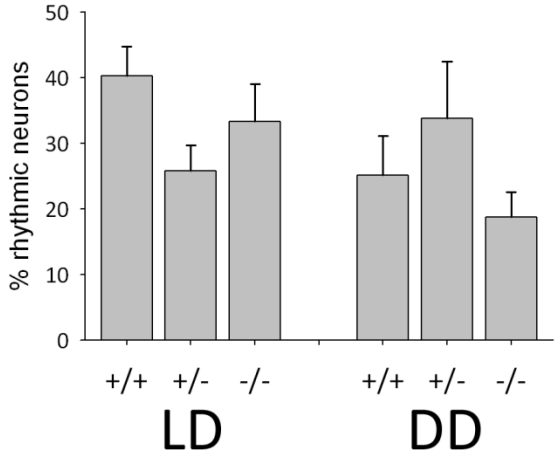

Figure II-6. | **Plot of the percent of rhythmic neurons (3+ peaks) per SCN slice for mice of all *VIP* genotypes maintained in LD (*left*) and in DD (*right*).** LD: $VIP^{+/+}$ (N = 5), $VIP^{+/-}$ (N = 5) and $VIP^{-/-}$ (N = 4); DD: $VIP^{+/+}$ (N = 6), $VIP^{+/-}$ (N = 8) and $VIP^{-/-}$ (N = 7). Error bars represent SEM.

Section 2.5: Discussion

In this study, we have disrupted SCN network organization by targeted deletion of a key communicating molecule, VIP, and then assayed the circadian behavior and the neural correlates of circadian behavior by *ex vivo* real-time gene expression imaging of circadian clock neurons in the SCN of individual mice. Our principal findings are that the timing (phase) and coherence (power) of circadian behavior is encoded by the timing and degree of synchrony of SCN neuronal rhythms. The timing and strength of circadian locomotor rhythms is encoded by the timing and strength of the SCN average neuronal temporal population vector.

Targeted knockout of the *VIP* gene disrupts the circadian neural network by leading to neuronal de-synchronization and results in stereotypical behavioral deficits such as increased daytime wheel running and arrhythmicity in constant darkness. In this study, we found that the weakened behavioral rhythms and phase-advanced DD behavioral onset in adult $VIP^{-/-}$ *Per1*::GFP mice reflect the less synchronized and phase advanced patterns of neural rhythms recorded *ex vivo* in the SCN of the same individual animals. Specifically, the degree of degradation of behavioral rhythmic coherence was correlated with the degree of degradation of rhythmic coherence in the population of SCN neurons within an individual (Fig. II-5a-b). We also found that the first peak of SCN network *Per1*::GFP expression maintains a constant phase relationship to activity onset across *VIP* genotypes, with the initial rise in gene activity anticipating behavioral activity onset by 7-8 hours and matching the 5-6 hour phase advance of activity in the $VIP^{-/-}$ mice. Unexpectedly, we also found that while SCN neuronal synchrony was disrupted in $VIP^{-/-}$ mice, SCN neurons from $VIP^{-/-}$ mice exhibited robust rhythmicity in similar number and proportion to SCN neuronal molecular rhythms from $VIP^{+/-}$ and $VIP^{+/+}$ mice.

There are both similarities and differences between our results and the results from previous circadian studies using VIP communication-deficient mice. Our study used acutely

explanted, *ex vivo* SCN from adult *VIP*$^{-/-}$ mice to assay circadian behavior and establish circadian neural correlates within individual mice. In contrast, previous studies used reconstituted dispersed neonatal SCN networks or reorganized neonatal SCN explants that had been maintained chronically *in vitro* for 2 or more weeks before recording, and then inferred a relationship of *in vitro* findings to adult circadian behavior based on genotype[133, 135]. Our finding that compromised VIP signaling leads to de-synchronization of SCN clock neurons is in accordance with studies of neonatal SCN networks, and strengthens the conclusion that VIP acts as a synchronizing substance in the SCN[133, 135, 143]. In addition, we have now demonstrated directly the previous speculation that the de-synchronization of SCN neurons is accompanied by loss of behavioral rhythmic coherence within individuals. Our results demonstrating preservation of the number and proportion of individual neuronal rhythms in explanted adult *VIP*$^{-/-}$ SCN stand in contrast to the neonatal VIP studies in which there was significant loss in the proportion of rhythmic neurons following loss of VIP communication in SCN networks[133, 135]. A study of VIP receptor knockout adult animals also revealed a surprisingly high proportion of rhythmic but desynchronized SCN neurons[144]. The reasons for these differences are unknown, but could be explained by a number of factors including a difference in the role of VIP in mature vs. neonatal SCN networks, differences in culture time (4 days vs. 2-3 weeks), access to a running wheel or compensation in the adult by upregulation of other signaling molecules in the SCN network such as GRP that could sustain cellular rhythms[135]. Whatever the precise cause, it is clear that one inference drawn from the neonatal SCN studies, that cellular de-synchronization in the SCN necessarily leads to reduced cellular rhythmicity, does not hold in the case of VIP communication, or in the case of disruption of SCN neuronal synchrony by constant light, where cellular rhythm robustness is also preserved in the face of cellular desynchrony[141, 142].

Our findings have significant implications for understanding how the SCN neural network encodes and drives circadian behavior. The present study of *VIP* gene-dosage effects, in combination with work on mice exposed to constant light[141, 142], demonstrates a strong correlation between the timing and coherence of circadian locomotor behavior, and the timing and coherence of neuronal phases within the SCN, represented as the temporal direction and magnitude of the population vector of SCN neuronal rhythms. Work on neonatal SCN and SCN neurons from *Tau*-mutant hamsters and *Clock*$^{\Delta 19}$-mutant mice, has suggested that behavioral circadian period is approximated by the population average period of the individual neurons that comprise the SCN[38, 39]. Similarly, chimeric SCN composed of wildtype and *Clock*$^{\Delta 19}$-mutant SCN neurons drive circadian behavior with the intrinsic period of the majority of neurons[145]. The present data suggest that, similar to period, the timing (phase) of behavioral onset is encoded by the average phase of the neural population represented as a temporal population vector with the temporal direction of the vector determining the time of activity onset and the magnitude of the vector determining the coherence of the behavioral rhythms. In this way, the manner in which the circadian network encodes behavioral phase is not unlike the population coding observed in the voluntary motor system, in which the spatial direction of targeted limb movements is coded by the average population vector of directional motor neurons in the cortex[146].

This concept of population encoding can be extended to the paired SCN and to multiple neuronal populations within each SCN to account for exceptional circumstances in which SCN neuronal sub-populations can encode bimodal circadian behavioral output. For example, "splitting" of behavioral circadian rhythms in response to constant light correlates with antiphase oscillation of the gene expression rhythms in the SCN neurons of the paired SCN[142, 147]. Similarly, seasonal light cycles induce changes in the distribution of neuronal phases within the

SCN[108, 110, 111] that likely encode for photoperiodic changes in circadian behaviors. Population coding in the SCN has these potential advantages: 1) the summation of neuronal phases may lead to greater accuracy and precision of circadian behavioral activity onset similar to the increase in precision of period gained by population encoding[38, 39]; 2) a network composed of neurons with variable phase relationship and a population encoded output to behavior can flexibly encode the amplitude and phase of changing environmental stimuli (such as seasonal light cycles) and through the phase organization of the neuronal population, drive circadian behavior appropriately. VIP is a signal for light stimuli within the SCN network as well as a synchronizing agent. Thus, the overall role of VIP communication in the SCN appears to be to modulate the timing and coherence of population vector encoding by SCN neurons to adjust circadian behavior to environmental light input.

Section 2.6: Chapter Acknowledgements

This work was supported by NIH grants RO1 MH63341 to D.G.M., F31 MH080547 to C.M.C., NS043169 to C.S.C., P30 EY008126 to J.D. Schall and T32 MH64913 to E. Sanders-Bush. The authors would like to thank Terry Page for his helpful comments and Tongrong Zhou for technical assistance.

Section 2.7: Author Contributions

CMC & DGM conceived experimental design; CMC, JCA and BRS performed experiments and compiled results; CMC & KLG performed statistical analyses; CMC & DGM wrote the paper; and CSC provided critical comment and the *VIP*$^{-/-}$ mouse line.

CHAPTER III

CONSOLIDATION OF CIRCADIAN BEHAVIOR BY LOCOMOTOR FEEDBACK IN VIP DEFICIENT MICE

Christopher M Ciarleglio[1,2], Karen L Gamble[2], John C Axley[2], Christopher S Colwell[3] and Douglas G McMahon[1,2]

[1] Neuroscience Graduate Program, Vanderbilt University, Nashville, TN
[2] Department of Biological Sciences, Vanderbilt University, Nashville, TN
[3] Department of Psychiatry and Biobehavioral Sciences, UCLA, Los Angeles, CA

Section 3.1: Summary Abstract

Mammalian circadian rhythms are generated in the suprachiasmatic nuclei of the hypothalamus (SCN), the central mammalian circadian pacemaker, and are entrained by both photic and non-photic stimuli via input from the retina and other brain regions. One of the key modalities of non-photic entrainment involves feedback of locomotor activity on the circadian clock. Here, we have used mice with a genetic knockout of vasoactive intestinal polypeptide (*VIP*), a key intercellular signaling neuropeptide within the SCN, to disrupt their circadian rhythms and investigate the extent to which wheel-running influences the circadian system and interacts with VIP-signaling. *VIP* wildtype, heterozygous and knockout mice were raised in a 12L:12D light cycle and then put through a series of lighting and wheel-access conditions while their behavioral circadian rhythms were monitored using infrared motion detection. Our findings indicate that wheel-running induces greater integration of rhythmic behavioral components and that VIP signaling is necessary for integration of weak or ultradian rhythms into coherent circadian behavioral output.

Section 3.2: Introduction

The master circadian pacemaker is a self-sustained oscillator in mammals that is located in the suprachiasmatic nuclei of the hypothalamus (SCN), a bilateral structure at the base of the brain that receives input from the retina and other brain regions in order to synchronize its phase with, or entrain to, the external environment. Vasoactive intestinal polypeptide (VIP) is a signaling neuropeptide expressed by neurons in the ventral region of the SCN[47, 50, 54] that is rhythmically released in light-dark cycles[61-65]. VIP signaling has been shown to be an essential component of photic entrainment and SCN organization as VIP can reset the phase of behavioral rhythms[72, 148] and VIP promotes both cellular and behavioral rhythmic coherence[133, 149]. VIP knockout mice have been characterized as exhibiting circadian behavior that is shortened in period, weakened in power and advanced in phase compared to wildtype mice[136].

Also contributing to the organization of the SCN are other, non-photic entrainment modalities that include feedback of locomotor activity on the circadian clock. Hamsters forced to run during the subjective day, for example, have been shown to phase advance their circadian behavioral activity independent of light[12]. Furthermore, wheel-running increases the rate at which re-entrainment occurs in mice after light-induced phase shifts[150]. While this mode of non-photic entrainment is thought to be mediated by serotonergic innervation of the SCN[151], the extent to which wheel-running influences the circadian system—both physiologically and behaviorally—is not completely understood.

Here we have examined the effects of locomotor feedback from wheel-running and its interaction with disruption of the circadian system by loss of VIP. Our findings indicate that wheel-running induces greater integration of rhythmic behavioral components and that VIP signaling is necessary for integration of weak or ultradian rhythms into coherent circadian behavioral output.

Section 3.3: Materials and Methods

Animals and housing. Mice with a targeted *VIP* gene disruption[136] were backcrossed at least four generations to mice (B6C3 hybrid from Jackson Labs) carrying the *mPer1*::d2EGFP transgene[128] yielding *Per1*::GFP$^{+/+}$, *VIP*$^{+/-}$ mice (for use in [149]), which were bred in a 12L:12D light cycle (LD) to yield experimental mice. Male offspring 4-5 weeks of age were placed in litter-filled wheel cages (Coulbourn Instruments, Whitehall, PA) equipped with infrared (IR) motion detector (Spy2 from Visonic, Tel Aviv, Israel) and food and water *ad libitum*. Mice were split into two groups that were subjected to an identical light paradigm, but with differing wheel-access to control for order-effects. All mice were entrained to a 12L:12D light cycle for 4 weeks, whereupon the light cycle was advanced 6 hours for 2 weeks, and then delayed 6 hours to the original light cycle for an additional 2 weeks. The lights were then turned off to allow the animals to run in constant conditions for about 3 weeks. Each animal was subjected to 7 distinct phases in which the mouse had free access to a wheel or in which the wheel was locked. The first group (A), had the following order of wheel-access: open for 10 days (phase 1), locked for 10 days (phase 2), then open for about 7 weeks (phase 3: same light cycle as phase 1-2; phase 4: advanced 6 hours; phase 5: delayed 6 hours; phase 6: constant darkness), then finally locked in constant darkness for a week (phase 7). The second group had exactly the opposite order, with access to the wheel in phases 2 and 7 to control for the possibility of order-effects (Fig. III-1a). Wheel-running and IR activity was monitored and recorded in 5-min bins using ClockLab Software (Actimetrics, Evanston, IL). All animal care was conducted in accordance with Vanderbilt University IACUC guidelines.

Behavioral analyses. IR behavior was analyzed using ClockLab Analysis software (Actimetrics), and activity was quantified as the number of IR activations occurring during 5-min bins. The free-running period, rhythmic power, *alpha*, amount of activity during lights-on and lights-off, as

well as the total amount of activity per day were determined for each phase using the chi-squared periodogram and activity profile options in the "Batch Analysis" function. Phase of activity onset was determined by eye in ClockLab's actogram function. As a component measurement of consolidation, bout analyses were exported using the Actogram "bout" function in ClockLab, with a bout defined as a period of activity whereupon the activity level never falls below 1 count/min for longer than 40 minutes. Consolidation was addressed descriptively as combination of factors: *alpha*, amount of activity, number of bouts, average bout-length and the average length of the maximum bout per day. The velocity of phase shifts was calculated by eye as the number of days needed for an animal to resume its previous onset phase angle and duration after a phase shift.

Statistical analysis. Means were statistically compared in SPSS 14.0 (SPSS, Chicago, IL) by univariate analyses including repeated measures. For data with non-homogeneous distributions, the Sheirer-Ray-Hare extension of the nonparametric Kruskal-Wallis Test was performed[152]. Post-hoc Fisher's Least Significant Difference tests were performed on parametric data and post-hoc Dunnett's T3 test were performed on non-parametric data. Significance was ascribed at $p < 0.05$.

Section 3.4: Results

Using simultaneous wheel and infrared motion detectors (IR), we monitored activity in mice and assessed the contributions of VIP gene-dosage and wheel-activity to circadian behavioral organization. Mice were raised in a 12L:12D light cycle and then put through a series of lighting and wheel-access conditions while their behavioral circadian rhythms were monitored (Fig. III-1a). Because the activity signal readout by IR persisted during both locking and unlocking of the wheel, we used the uninterrupted IR data to analyze circadian behavior.

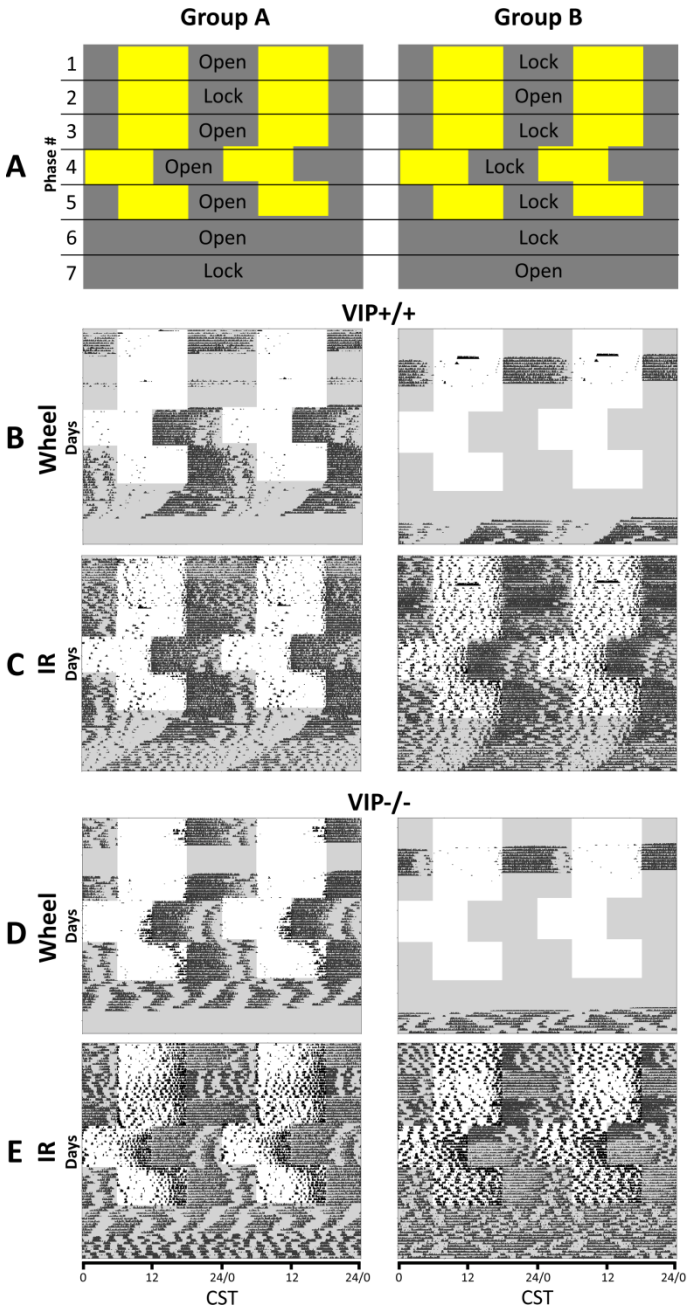

Figure III-1 | **Wheel-locking and light cycle paradigm with representative actograms.** Group A (*left*) and Group B (*right*) show an opposite order of wheel-access over an identical light and dark paradigm (**a**). Lights-on is indicated as a yellow or white background; darkness is indicated by gray background; "Open" indicates the mice in that particular group had access to an unlocked wheel during that phase of time; "Lock" indicates the mice in that particular group had their wheel locked during that phase of time. Phases are indicated by numerals at left. **b**-**e** | Double-plotted actograms illustrate circadian behavior in the light paradigms illustrated in (**a**) as recorded by wheel-running (**b** and **d**) or infrared motion detection (**c** and **e**). Black ticks represent activity in 5-minute bins. Note: the mouse in Group A (Fig. 1b) did run on the wheel during Phase 3, but the recording switch became dislodged and did not report the activity. **b**-**c** | Representative actograms from *VIP* wildtype ($VIP^{+/+}$) mice. **d**-**e** | Representative actograms from *VIP* knockout mice ($VIP^{-/-}$).

Wheel-running does not affect circadian period or power.

VIP$^{-/-}$ mice exhibited specific circadian deficits in behavioral period and rhythmic power (Fig. III-1d-e vs. *VIP*$^{+/+}$ mice in Fig. III-1b-c). We used χ^2 periodogram analyses to measure the circadian periodic components of behavior, and found that many of the *VIP*$^{-/-}$ mice did exhibit a significant circadian component in constant darkness (mean±SEM: 22.5±0.15h, N = 7 out of 9 mice). Statistical analyses of these measurements further suggested that the period of *VIP*$^{-/-}$ mice was significantly shorter than *VIP*$^{+/-}$ and *VIP*$^{+/+}$ mice (mean±SEM: *VIP*$^{+/-}$, 23.6±0.094h, N = 17; *VIP*$^{+/+}$, 23.6±0.15h, N = 7; RM ANOVA, $F(2) = 21.3$, $p < 0.001$; LSD, $p < 0.001$, Fig. III-2a), as previously reported[133, 136]. Free-running period across genotypes was not, however, affected by wheel-running (RM ANOVA, $F(1, 28) = 0.6$, $p = 0.436$, Fig. III-2a).

Further analyses of periodogram measurements indicated a relationship between genotype and lighting condition affecting rhythmic power. Overall, *VIP*$^{+/+}$ and *VIP*$^{+/-}$ mice had significantly greater rhythmic power (mean±SEM: *VIP*$^{+/-}$, 1090.8±50.7, N = 18; *VIP*$^{+/+}$, 1054.2±68.0, N = 10) than *VIP* knockout mice (mean±SEM: 721.6±62.0, N = 12; RM ANOVA, $F(2, 37) = 11.6$, $p < 0.001$; LSD, $p < 0.001$, Fig. III-2b). Specifically, *VIP*$^{-/-}$ mice exhibited significantly less robust rhythmicity than mice carrying a functional *VIP* allele in both LD (RM ANOVA, $F(2, 34) = 4.4$, $p < 0.05$; LSD, $p < 0.01$, Fig. III-2c) and in DD (RM ANOVA, $F(2, 27) = 16.7$, $p < 0.001$; LSD, $p < 0.001$, Fig. III-2d). As one would anticipate, mice had overall greater periodic amplitude in LD (mean±SEM: 1170.0±52.3, N = 40) than they did in DD (mean±SEM: 741.1±26.0, N = 40; RM ANOVA, $F(1, 37) = 95.6$, $p < 0.001$, Fig. III-2b). Wheel-running, again, had no significant main effect on rhythmic power (LD: $F(1, 34) = 1.5$, $p = 0.231$; DD: $F(1, 27) = 1.8$, $p = 0.188$).

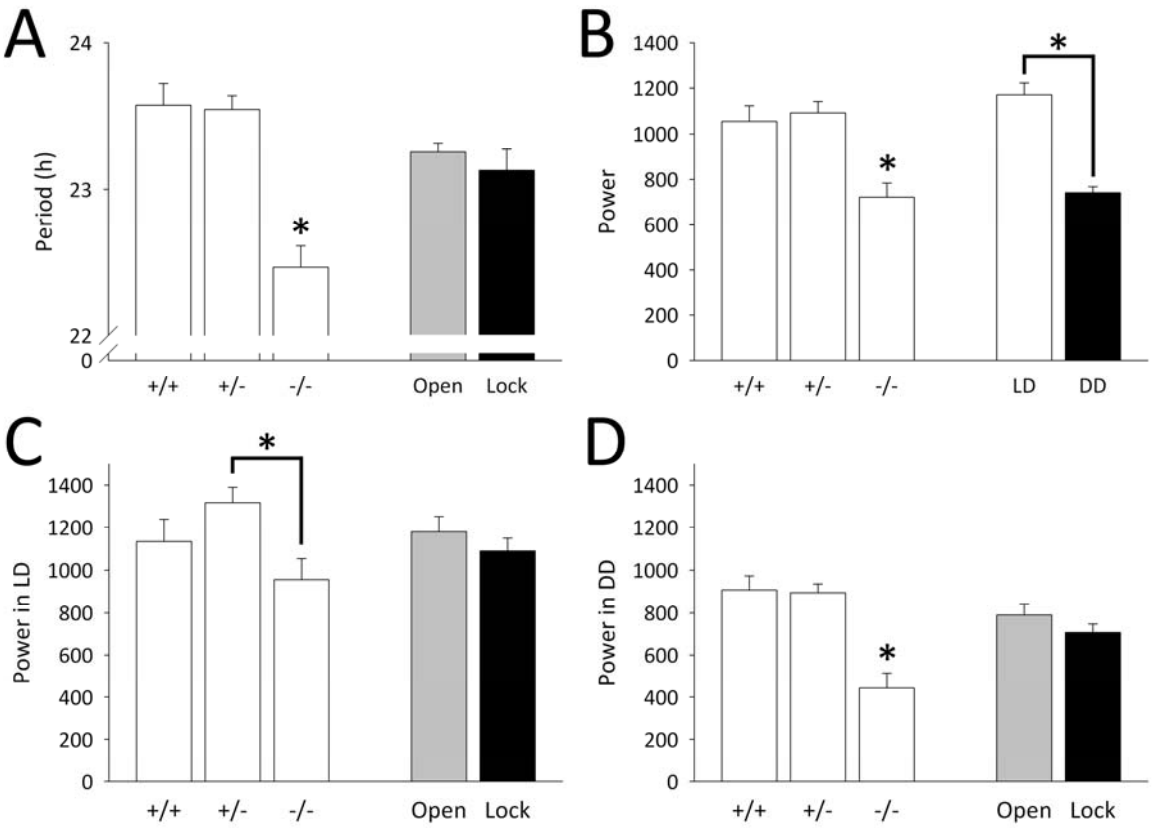

Figure III-2 | ***VIP*$^{-/-}$ mice exhibit significantly altered circadian behavior.** *VIP* wildtype ($^{+/+}$), heterozygous ($^{+/-}$) and knockout mice ($^{-/-}$); "Lock" indicates mice had their wheel locked, "Open" indicates mice had access to a functional wheel. **a** | Two-way ANOVA main effects for χ^2 periodogram analyses of genotype-specific and wheel-running effects on free-running period. **b** | Two-way ANOVA main effects for χ^2 periodogram analyses of genotype-specific and light-dependent effects on overall rhythmic amplitude (power) in LD and DD. **c**-**d** | Two-way ANOVA main effects for χ^2 periodogram analyses of genotype-specific and wheel-running effects on rhythmic amplitude (power) in LD (**c**) and DD (**d**). Error bars represent SEM; asterisks (*) represent significance at $p < 0.05$.

Wheel-running enhances masking and the rate of advancing phase shifts in VIP$^{-/-}$ *mice.*

We found that overall, *VIP*$^{-/-}$ mice exhibited a significantly earlier onset of activity in LD (mean±SEM: ZT 9.5±0.46 hours, N = 10) than did *VIP*$^{+/-}$ and *VIP*$^{+/+}$ mice (mean±SEM: *VIP*$^{+/-}$, ZT 11.8±0.34 hours, N = 18; *VIP*$^{+/+}$, ZT 11.6±0.48 hours, N = 9; RM ANOVA, $F(2, 34) = 5.3$, $p = 0.01$, Fig. III-3a §). Interestingly, this genotype effect was exaggerated in *VIP*$^{-/-}$ mice with a locked wheel, in that *VIP*$^{-/-}$ mice began their activity ~2 hours earlier than when they had an open wheel, and 2.5-3 hours earlier than the overall onset in *VIP*$^{+/-}$ and *VIP*$^{+/+}$ mice (RM ANOVA, $F(2, 34) = 4.8$, $p < 0.05$, Fig. III-3a *).

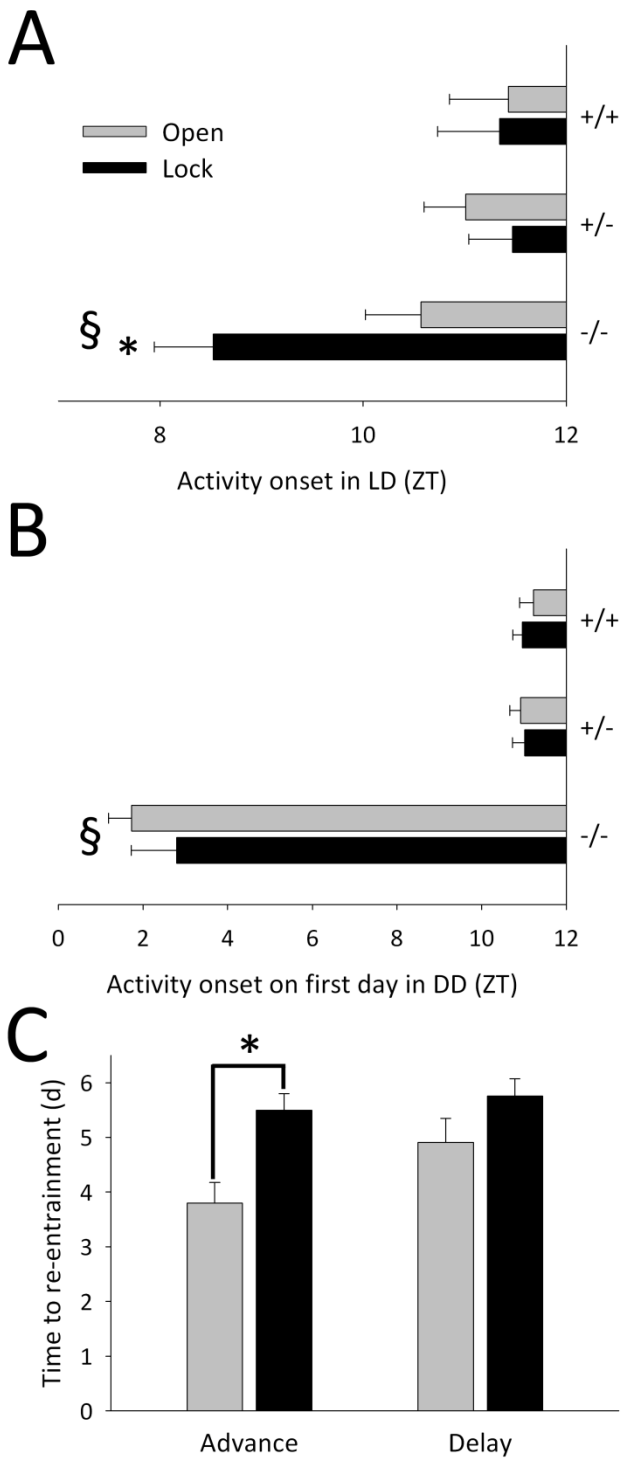

Figure III-3 | **Wheel-running affects entrainment in mice.** *VIP* wildtype ($^{+/+}$), heterozygous ($^{+/-}$) and knockout mice ($^{-/-}$); "Lock" indicates mice had their wheel locked and is represented by black bars, "Open" indicates mice had access to a functional wheel and is represented by gray bars (see inset legend, Fig. III-3a). § indicates that $VIP^{-/-}$ mice have an overall earlier onset of activity on the first day in DD when compared to $VIP^{+/-}$ and $VIP^{+/+}$ mice. **a** | Time of activity onset in LD. **b** | Activity onset on the first day in DD in projected ZT. **c** | Two-way ANOVA main effects for wheel-running effects on time to re-entrainment after a 6-hour advance or a 6-hour delay. Error bars represent SEM; asterisks (*) represent significance at $p < 0.05$.

Previous studies on *VIP*$^{-/-}$ mice identified a significantly advanced onset of activity on the first day in constant darkness[133, 136, 149]. We found that *VIP* knockout mice in this study also had a significantly earlier onset of activity on the first day in DD (mean±SEM: *VIP*$^{-/-}$, ZT 2.3±0.35 hours, N = 10; *VIP*$^{+/-}$, ZT 11.0±0.26 hours, N = 17; *VIP*$^{+/+}$, ZT 11.1±0.37 hours, N = 10; Kruskal-Wallis, $H(2, 31) = 20.7$, $p < 0.001$; Dunnett T3, $p < 0.001$, Fig. III-3b §). Despite a clearly more advanced phase angle in LD (Fig. III-3a), *VIP*$^{-/-}$ mice with a locked wheel started their activity on the first day in DD at about the same phase as *VIP*$^{-/-}$ mice with an open wheel, suggesting that the actual entrained phase angle of *VIP*$^{-/-}$ mice was similar with locked and open wheels, but that wheel-running enhanced negative masking in LD.

We next sought to quantify any genotype or wheel-dependent differences in the ability of mice to phase shift their behavior. We found that *VIP* gene-dosage had no effect on the rate of re-entrainment (see Methods) of mice to phase advance or phase delay of the light cycle by 6 hours (+6 h: Two-way ANOVA, $F(2, 33) = 0.5$, $p = 0.634$; -6 h: $F(2, 32) = 1.1$, $p = 0.343$). While there was no effect of wheel-access on phase delays (Two-way ANOVA, $F(1, 32) = 2.4$, $p = 0.13$, Fig. III-3c), wheel-running decreased the number of days necessary for the mice to resume their previous phase angle after a phase advance (Two-way ANOVA, $F(1, 33) = 12.3$, $p < 0.01$, Fig. III-3c).

Wheel-running consolidates circadian and ultradian activity bouts.

In order to assess the effect of wheel-running on circadian behavior, we measured several factors: (1) *alpha*, the duration of the main circadian activity bout, (2) partitioning of activity into night and day, (3) number of ultradian bouts of activity per day, (4) length of ultradian bouts and (5) maximum ultradian bout-length. (1) In LD, we found that wheel-running significantly lengthened *alpha* for all genotypes (RM ANOVA, $F(1, 34) = 7.9$, $p < 0.01$, Fig. III-4a). In contrast, wheel-running in DD had no effect on *alpha* duration (RM ANOVA, $F(1, 29) = 0.059$, $p = 0.81$, Fig.

III-4B). In both LD and DD, *VIP*$^{-/-}$ mice exhibited a significantly shorter *alpha* than heterozygote and wildtype mice, regardless of wheel access (RM ANOVA, LD: $F(2, 34) = 12.6$, $p < 0.001$; LSD, $p < 0.01$, Fig. III-4a; DD: $F(2, 29) = 15.0$, $p < 0.001$; LSD, $p < 0.01$, Fig. III-4b).

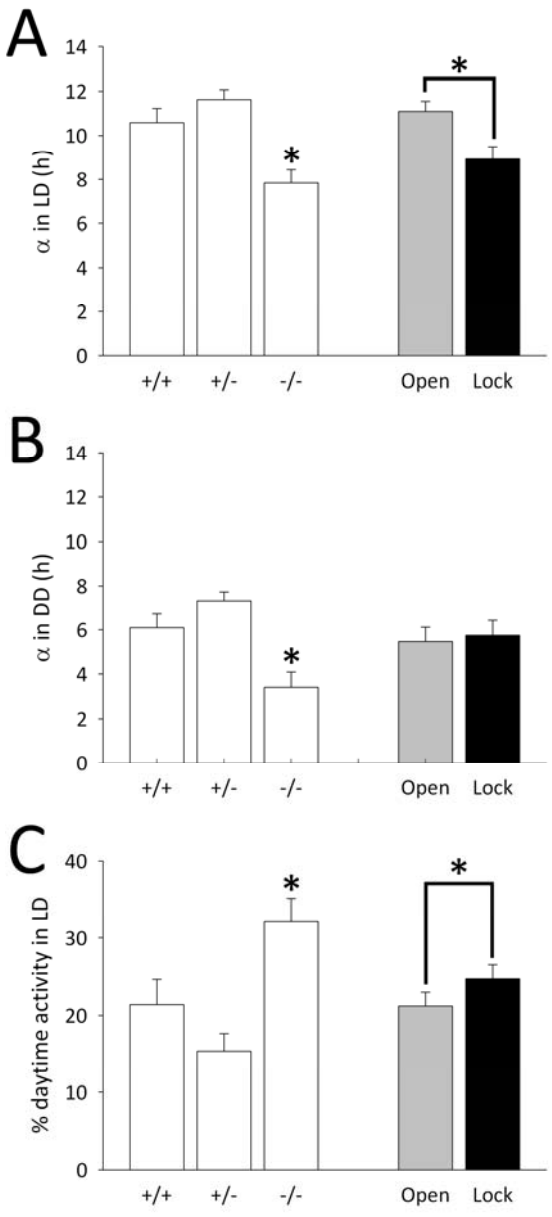

Figure III-4 | **Wheel-running increases *alpha* in LD, and decreases the percentage of daytime activity.** *VIP* wildtype ($^{+/+}$), heterozygous ($^{+/-}$) and knockout mice ($^{-/-}$); "Lock" indicates mice had their wheel locked, "Open" indicates mice had access to a functional wheel. **a**-**b** | Two-way ANOVA main effects for genotype-specific and wheel-running effects on length of *alpha* in LD (**a**) and DD (**b**). (C) Two-way ANOVA main effects for percentage of total activity during the light-phase in LD as a function of genotype or wheel-running. Error bars represent SEM; asterisks (*) represent significance at $p < 0.05$.

(2) We next asked whether there was a genotype-specific or wheel-dependent change in the partitioning of activity into night and day in LD or DD. We found a significantly larger percentage of total activity occurred during the light-phase in *VIP*$^{-/-}$ mouse activity (mean±SEM: 32.1±3.0%, N = 10) than in heterozygous and wildtype mouse activity (mean±SEM: *VIP*$^{+/-}$, 15.4±2.3%, N = 18; *VIP*$^{+/+}$, 21.4±3.2%, N = 9; RM ANOVA, $F(2, 34) = 9.7$, $p < 0.001$; LSD, $p < 0.05$, Fig. III-4c). Across all genotypes, mice with a locked wheel had a larger percentage of daytime activity than mice allowed to run (RM ANOVA, $F(1, 34) = 7.2$, $p < 0.05$, Fig. III-4c).

(3) Upon visual inspection, some mice exhibited a clear difference in ultradian behavioral bout organization with a locked and unlocked wheel in DD (Fig. 1d-e and Fig. III-5a). We tested whether there were genotype-specific or wheel-dependent differences in the average number of daily activity bouts per animal per day. We found that the number of bouts in LD was indeed dependent on the presence of an unlocked wheel, and that access to an open wheel significantly decreased the number of bouts across all genotypes (RM ANOVA, $F(1, 41) = 27.7$, $p < 0.001$, Fig. III-5b). There were overall genotype differences as well, with *VIP*$^{-/-}$ mice exhibiting a greater number of bouts in LD (mean±SEM: 7.3±0.30 bouts, N = 14) than heterozygous and wildtype mice (mean±SEM: *VIP*$^{+/-}$, 5.8±0.25 bouts, N = 19; *VIP*$^{+/+}$, 6.3±0.33 bouts, N = 11; RM ANOVA, $F(2, 41) = 7.6$, $p < 0.01$; LSD, $p < 0.05$, Fig. III-5b).

(4) As one would expect from these results, as the number of bouts per day decreased with access to an open wheel, their length increased (RM ANOVA, $F(1, 34) = 25.1$, $p < 0.001$, Fig. III-5c). *VIP*$^{-/-}$ mice exhibited the smallest bout-length (mean±SEM: 100.8±9.4 minutes/bout, N = 10); significantly smaller than *VIP*$^{+/-}$ mice (mean±SEM: 135.1±7.0 minutes/bout, N = 18, LSD -/- v. +/-, $p < 0.01$) and trending smaller than *VIP*$^{+/+}$ mice (mean±SEM: 123.0±9.9 minutes/bout, N = 9; RM ANOVA, $F(2, 34) = 4.3$, $p < 0.05$; LSD -/- v. +/+, $p = 0.11$). We further found an interaction suggesting that the change in bout-length due to wheel-activity was exaggerated in mice

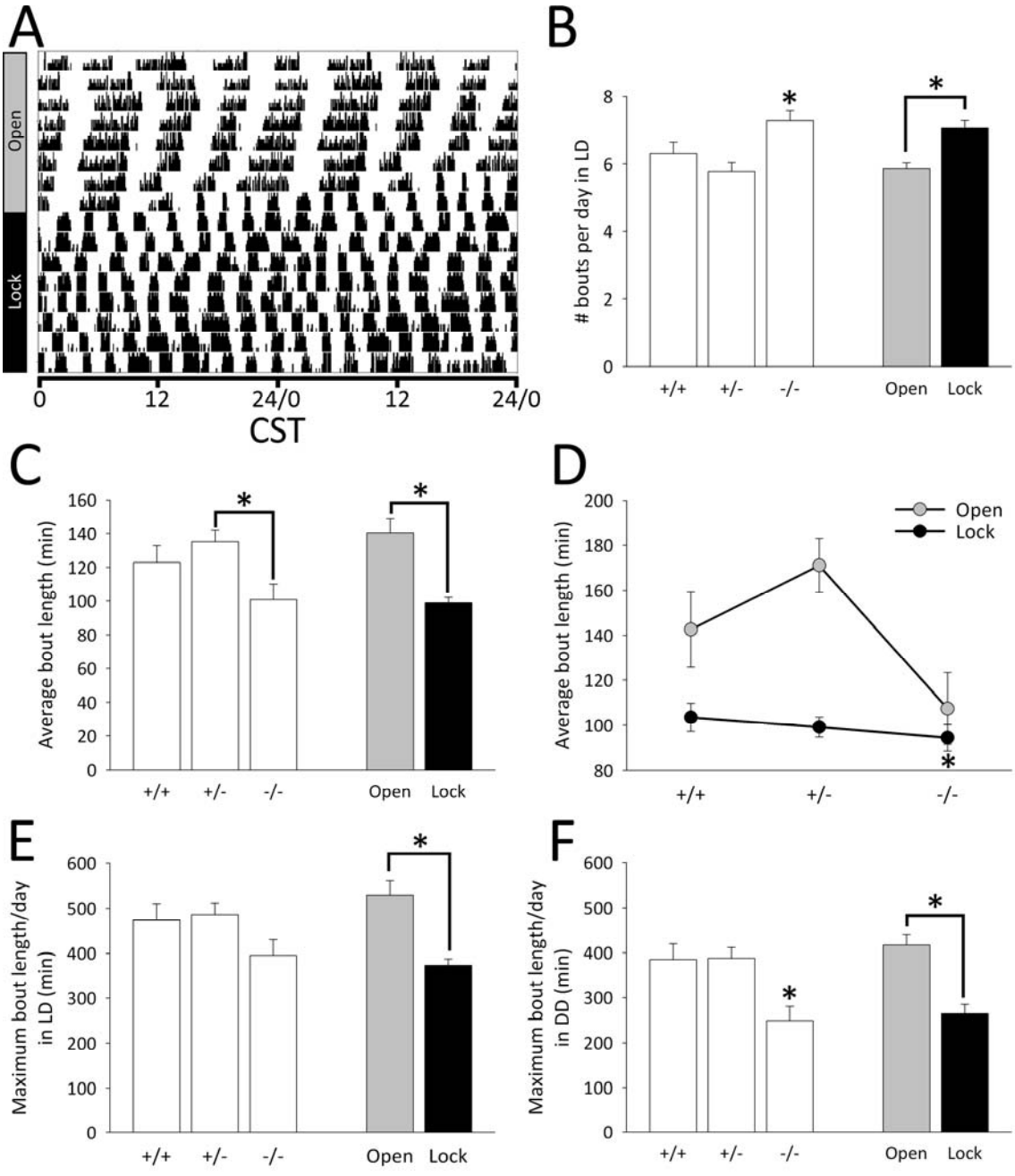

Figure III-5 | **Wheel-running increases behavioral consolidation in mice.** *VIP* wildtype ($^{+/+}$), heterozygous ($^{+/-}$) and knockout mice ($^{-/-}$); "Lock" indicates mice had their wheel locked, "Open" indicates mice had access to a functional wheel. **a** | Representative DD portion of an actogram (Fig. III-1c, *left*) from a *VIP*$^{-/-}$ mouse with an unlocked wheel ("Open" on gray sidebar) and a locked wheel ("Lock" on black sidebar). **b** | Two-way ANOVA main effects for number of bouts per day in LD as a function of genotype and wheel-running. **c** | Two-way ANOVA main effects for average bout-length per day in LD as a function of genotype and wheel-running. **d** | Two-way ANOVA interaction plot between genotype and wheel-running for average bout-length per day. Locked wheels are indicated by closed circles; wheel-running is indicated by open circles. **e** | Two-way ANOVA main effects for average length of the longest (maximum) bout per 24-hour day in LD as a function of genotype and wheel-running. **f** | Two-way ANOVA main effects for average length of the longest (maximum) bout per 24-hour day in DD as a function of genotype and wheel-running. Error bars represent SEM; asterisks (*) represent significance at $p < 0.05$.

possessing at least one functional *VIP* allele (RM ANOVA, Genotype x Wheel access, $F(2, 34) = 5.0$, $p < 0.05$, Fig. III-5d), suggesting that VIP is necessary for wheel-running to affect bout-length in LD.

(5) As a final component of behavioral consolidation, we measured the average duration of the longest ultradian bout per animal per 24-hour period. This bout contributes greatest to the characteristics of *alpha*, and for our purposes can be measured independently of circadian period. We found that the average length of this bout increased with wheel-access across all genotypes in both LD (RM ANOVA, $F(1, 34) = 27.2$, $p < 0.001$, Fig. III-5e) and DD (RM ANOVA, $F(1, 32) = 34.1$, $p < 0.001$, Fig. III-5f). While we did not find a genotype-specific change of maximum bout-length in LD (RM ANOVA, $F(2, 34) = 2.3$, $p = 0.115$, Fig. III-5d), we did find that this bout-length was significantly decreased in $VIP^{-/-}$ mice in DD (RM ANOVA, $F(2, 32) = 6.9$, $p < 0.01$; LSD, $p < 0.01$, Fig. III-5e).

Section 3.5: Discussion

This study offers a detailed examination of how the locomotor feedback from wheel-running interacts with VIP gene-dosage to affect circadian behavioral organization. Our principal findings are that wheel-running contributes to the integration of multiple circadian and/or ultradian oscillators, and that a role for VIP is implicated in organizing mouse behavior in response to wheel-running.

$VIP^{-/-}$ *mice exhibit circadian behavior deficits independent of wheel activity.*

Chi-squared periodogram analysis showed that there was a significant circadian periodic component in the behavior of $VIP^{-/-}$ mice, and that their period was significantly shorter than mice with functional *VIP* alleles (Fig. III-2a) as reported previously[133, 136]. Because locomotor activity, especially linked to wheel-running, has been shown to shorten behavioral period in

rats[153, 154], and mice [155], one would expect all rhythmic animals with wheel-access to have a shorter free-running period than when the wheel is locked; however, we found that access to a wheel did not affect the period of the rhythm in this study, possibly due to mouse background/strain differences between the studies. Periodogram analysis did suggest, however, that rhythmic amplitude, or power, was reduced in *VIP*$^{-/-}$ mice as previously shown[136, 149] (Fig. III-2b-d).

Locomotor activity affects masking of VIP$^{-/-}$ *mice.*

The maintenance of the mouse phase angle in LD was found to be dependent not only on genotype, but also access to an unlocked wheel. While *VIP*$^{-/-}$ mice exhibited an overall earlier onset of activity in LD than did *VIP*$^{+/-}$ and *VIP*$^{+/+}$ mice, we also found that *VIP*$^{-/-}$ mice with a locked wheel exhibited a significantly earlier onset of activity in LD than did *VIP*$^{-/-}$ mice with an unlocked wheel (Fig. III-3a). This interaction was interesting given how it might affect one of the classical behavioral phenotypes associated with VIP-signaling deficient mice: specifically that these mice exhibit an unusually large phase advance on the first day in constant darkness[131-133, 136, 149, 156]. The results of this study are consistent, but with an interesting twist: despite the clear difference in LD between the onset of activity in *VIP*$^{-/-}$ mice with an open wheel and those with a locked wheel, both groups start their activity at about the same circadian time on the first day in DD (Fig. III-3b). This suggests that both groups (locked wheel and open wheel *VIP*$^{-/-}$ mice) maintain a consistent phase angle of entrainment regardless of wheel-running status, but that those animals with access to an open wheel exhibit enhanced masking in LD that is not apparent in *VIP*$^{-/-}$ mice with a locked wheel. This phenotype is absent in *VIP*$^{+/-}$ and *VIP*$^{+/+}$ mice, suggesting that the robust nature of the circadian clock in these mice may overcome any subtle changes evident in the knockout mice.

We found that *VIP* genotype did not have an effect on the rate of re-entrainment to 6-hour shifts in the light cycle, but that wheel-running did decrease the number of days necessary to advance 6-hours (Fig. III-3c). This result makes sense in light of the phase dependence of non-photic entrainment. With a 6-hour advance of the light cycle, darkness falls in the middle-to-late part of the circadian "day," where non-photic stimuli (such as wheel-running) and dark-pulses have the greatest phase-advancing effect[157]. In contrast, a 6-hour delay of the light cycle pushes the circadian "day" into the animals' circadian "night" and results in masking of wheel-running activity, thus resulting in a similar time to re-entrainment with a locked or an unlocked wheel (Fig. III-3c).

Consolidation

After completing an initial characterization of genotype and wheel-effects on the circadian characteristics of period, rhythmic power and phase, we sought to describe the effect of those variables on behavioral consolidation. At a gross level, we hypothesized that the weakly rhythmic tendency of $VIP^{-/-}$ mice would manifest as a decrease in overall consolidated behavior, and further that locomotor activity would modulate this phenotype by promoting consolidation. A problem arises, however, in defining "behavioral consolidation." Our results indicate that $VIP^{-/-}$ mice had significantly shorter *alpha* lengths than heterozygote and wildtype mice did in both LD and DD (Fig. III-4a-b), and that wheel-access lengthened *alpha*, but only in LD. This finding suggests that in the absence of light, wheel-running is less effective in consolidating rhythmic behavior—at least that measured by *alpha*—possibly due to the lack of rhythmically-released VIP typically found in SCN under LD[61-65]. In order to confirm that this lengthening of *alpha* was actually a consolidation of activity rather than a wheel-running mediated increase of overall activity in the mice, we next asked how genotype and wheel-access affected the second component of consolidation: the partitioning of activity into day and night. In finding no

statistical differences in the amount of daily activity among genotypes and between wheel-access groups, our results suggest that the lengthening of *alpha* is indeed due to the redistribution of activity into a more consolidated circadian bout rather than due to wheel-induced hyperactivity. $VIP^{-/-}$ mice did, however, exhibit a higher percentage of daytime (lights-on) activity than $VIP^{+/-}$ and $VIP^{+/+}$ mice did (Fig. III-4c). In addition to this main effect of genotype, we found that wheel-running decreased the percent of daytime activity, suggesting that the non-photic stimulus may reinforce nocturnal partitioning of behavior, or may enhance masking to light as discussed above.

The third and fourth components of consolidation that we measured in a light-dark cycle were the average number of daily bouts and the average length of those bouts. We reasoned that more consolidated behavior would consist of relatively fewer bouts with greater average length than unconsolidated behavior. Given the *alpha* results discussed above, we hypothesized that knocking-out a key synchronizing chemical in the SCN[133, 135, 144, 149] would lead to less consolidation by these measures, and that wheel-running would modulate this effect such that it would lead to greater consolidation than in the locked wheel condition. We chose to measure bout number and length in LD alone because they could, in theory, be measured as daily averages independent of circadian period—a complication precluding the analyses of these measurements in DD. Our results in LD indicated that the average number of daily bouts was significantly increased in $VIP^{-/-}$ mice (Fig. III-5b), as would be expected given the decreased length of *alpha*, with increased daytime activity and similar total activity when compared to heterozygotes and wildtype mice. It would also follow that since total daily activity is similar across genotypes, a greater number of bouts could only be possible if the length of those bouts decreased, as demonstrated by $VIP^{-/-}$ mice in Fig. III-5c. Perhaps even more interesting is the finding that wheel-running not only increases average bout-length, but exhibits an interaction

with genotype in that the lengthening effect of wheel-running is dependent upon the presence of a functional *VIP* allele in mice (Fig. III-5d). This result suggests that VIP is necessary for the consolidating effects of wheel-running in LD, and therefore plays a critical role mediating the locomotor activity contribution to rhythmic component integration by the SCN.

The final component of consolidation we measured was the "daily maximum bout," or the average length of the longest daily bout per mouse. This measurement is similar to *alpha* in that it can be identified as the primary time of activity in a day. The daily maximum bout is distinguished from *alpha* in that it only consists of a single bout, whereas *alpha* may consist of many. We chose to measure this factor because, while we are looking for the average over several 24-hour days, it is not dependent on the circadian period of the mouse. Furthermore, it allows us to see more subtle genotype or wheel-running induced changes than *alpha* does. We reasoned that consolidated activity would be represented by a relatively longer average maximum bout than unconsolidated behavior. We therefore hypothesized that the results for average maximum bout measurements would reflect the results for *alpha*. We found that, like *alpha*, wheel-running increased the length of the average maximum bout in LD (Fig. III-5e). Unlike *alpha* measurements, the relatively greater sensitivity of this measurement revealed a wheel-running dependent increase in average maximum bout-length in DD as well (Fig. III-5f), suggesting that wheel-running may at least subtly affect consolidation in the absence of light. Furthermore, the length of the daily maximum bout in $VIP^{-/-}$ mice had a tendency to be shorter in LD (Fig. III-5e) and was significantly shorter in DD (Fig. III-5f).

Ultradian components are unmasked in VIP signaling-deficient mice.

While the absence of VIP results in apparent circadian arrhythmicity, the behavior of $VIP^{-/-}$ mice is not truly arrhythmic *per se*; rather these mice exhibit ultradian rhythms similar to those noted in early SCN lesion studies[31, 138] and studies of animals kept in continuous illumination[158-

[161] (Fig. III-1). This continuity of phenotypes is not unexpected since constant light has been shown to depress VIP immunoreactivity substantially in rodents[66, 67]. Removing a key intra-SCN signaling molecule allowed us to study the organizational effect of locomotor activity with less interference from light, the main entraining factor[134]. Figure III-6 is a visual illustration of the effect of wheel-running on *VIP*$^{-/-}$ mice. These representative actograms show that, regardless of the order of wheel-access, wheel-running leads to more consolidated activity than when the wheel is locked. The nature of these underlying rhythmic components is not understood. Knocking out the master integrator may unmask innate, perhaps ultradian, rhythmic components from other non-circadian pacemakers or may simply fail to synthesize many uncoupled individual extra-SCN circadian pacemakers into a single coherent phase[149, 162]. Our results suggest the existence of one or more high frequency ultradian oscillators yet to be identified. Furthermore, these results in *VIP*$^{-/-}$ mice support the hypothesis that the SCN serve not only as the master circadian clock, but also as the master integrator of other rhythmic components produced in the mammalian body[137].

Conclusions

Our findings have significant implications for understanding the relationship between *VIP* gene-dosage and/or locomotor activity in organizing circadian behavior. This study, in combination with other studies[131, 133-136, 149, 156], demonstrate the unique behavioral deficits of VIP-signaling deficient mice. Our results are unique in that all measurements were made with a passive infrared motion detector and further address the role wheel-running has on circadian behavioral output. We found that wheel-running leads to modulation of masking and greater integration of weakly rhythmic behavioral components in all mice. Furthermore, our results demonstrate several intriguing interactions between wheel-running and light or *VIP* gene-

dosage which suggest that proper light-signaling is necessary for appropriate behavioral responses to wheel-induced consolidation of activity and maintenance of phase.

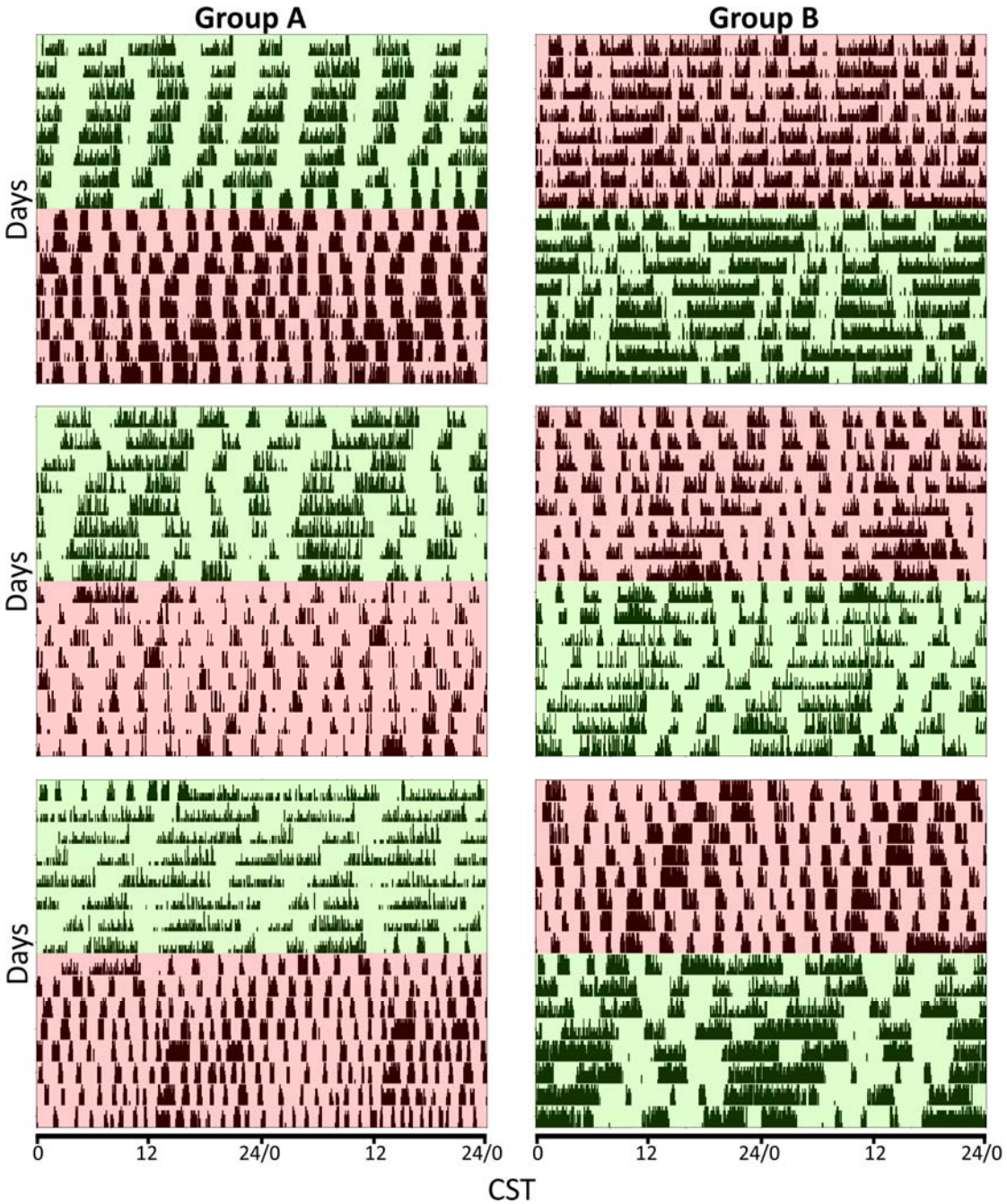

Figure III-6 | **Wheel-running consolidates weak or ultradian rhythmicity in *VIP*$^{-/-}$ mice.** Six representative IR actograms of *VIP* knockout behavior in DD. *Top left* actogram is also found in Fig. 1d-e (*left*) and Fig. III-5a, and is repeated here for reference. Black ticks represent activity in 5-minute bins; Group A (*left*) has access to a functional wheel first (**green**) followed by a locked wheel (**red**), and Group B (*right*) has an opposite order of wheel-access.

Section 3.6: Chapter Acknowledgements

This work was supported by NIH grants RO1 MH63341 to D.G.M., F31 MH080547 to C.M.C., RO1 NS043169 to CSC and T32 MH64913 to E. Sanders-Bush.

Section 3.7: Author Contributions

CMC & DGM conceived experimental design; CMC and JCA performed experiments and compiled results; CMC & KLG performed statistical analyses; CMC & DGM wrote the paper; and CSC provided critical comment and the *VIP*$^{-/-}$ mouse line.

CHAPTER IV

PHOTOPERIODIC INPUT DURING PERINATAL DEVELOPMENT INFLUENCES ORGANIZATION OF THE CIRCADIAN CLOCK

Christopher M Ciarleglio[1,2], John C Axley[2], Benjamin R Strauss[2], Jeremiah Y Cohen[1], Karen L Gamble[2] and Douglas G McMahon[1,2]

[1] Neuroscience Graduate Program, Vanderbilt University, Nashville, TN
[2] Department of Biological Sciences, Vanderbilt University, Nashville, TN

Section 4.1: Summary Abstract

The circadian clock's ability to entrain seasonally to varying day-length, or photoperiod, is crucial for determining seasonal aspects of behavior and physiology in many species. Light input has been shown to powerfully influence neural and behavioral development; however, whether seasonal photoperiod can affect the developmental organization of the circadian clock is unknown. We now report that circadian pacemaker properties of the suprachiasmatic nuclei (SCN—the central neural pacemaker in mammals), as read out by circadian reporter gene rhythms, can be developmentally imprinted by photoperiod, and that seasonal changes in photoperiod reorganize not only the phase relationships of the neurons that comprise the SCN, but also the circadian gene-expression rhythms of those clock neurons. Our results suggest that seasonal light exposure, and furthermore maturation during a particular season, dramatically and persistently alter the properties of the mammalian circadian neural network. An understanding of the nature of the SCN response to seasonal photoperiod is crucial to elucidating the role of light in influencing brain development and in assessing the etiology of seasonal affective disorders in humans.

Section 4.2: Introduction

A near-ubiquitous property of living organisms is the possession of an innate circadian clock that synchronizes to external timing factors, such as the presence or absence of light at certain times of day. Non-equatorial species are subjected not only to daily rhythms of light and dark, but also to seasonal changes in the amount of light received per day throughout the year. Adaptation of the innate circadian system to changes in seasonal light is called seasonality, and the physiological effects of seasonality are known as photoperiodism. Photoperiodism can consist of seasonal pelage, weight and/or reproductive changes, as well as behavioral and migratory changes. Seasonal encoding is thought to occur in the suprachiasmatic nuclei of the hypothalamus (SCN), the central circadian pacemaker in the mammalian brain. Recent reports have suggested that the circadian phase relationship of neurons within the SCN change in response to seasonal light cycles such that they become more desynchronized in long photoperiod (summer) and more tightly synchronized in short photoperiod (winter), leading to an overall broadening or narrowing of circadian electrical activity and gene expression waveforms, respectively [108, 110, 111].

A recent report on the development of frog tadpoles suggested that light could effectively imprint the neural circuitry of the adult frog SCN, leading to changes in camouflage behavior [163]. Development in constant light has been shown to readily and persistently alter the neural organization of the SCN in developing mice, and lead to disrupted behavior that can be correlated with the amount of neuronal phase desynchrony in the SCN [141]. Light can also imprint the developing visual system such that deprivation during the critical period of visual cortical development leads to persistent reduction in visual acuity [164]. Taken together, these results indicate that light has a powerful epigenetic effect on development, but it is unknown whether physiologically relevant exposure to light, such as the amounts seen in differing

seasons, can affect the developmental organization of the non-image forming visual system like the mammalian SCN.

In this study, we investigate the role of seasonal photoperiod in the developmental organization of the mouse SCN, and attempt to ascertain the mechanisms by which the SCN reorganize to encode seasonal change in adulthood. Our results suggest that seasonal light exposure, and furthermore maturation during a particular season, dramatically and persistently alter the properties of the mammalian circadian neural network.

Section 4.3: Materials and Methods

Animals. Breeding mice (B6C3 hybrid; AANAT function unknown) homozygous for the mPer1::d2EGFP transgene [128] were placed in light-tight boxes under short (8:16), equinox (12:12) or long (16:8) photoperiod. Pups were born and reared in the parental/developmental light cycle until weaning (~p21). Male mice were then placed in wheel-cages with litter, food and water *ad libitum* in one of the three photoperiods for ~28 days. At the end of behavioral characterization, animals were killed by cervical dislocation between ZT 9-12 to assay SCN rhythms. All animal care was conducted in accordance with Vanderbilt University IACUC rules and regulations.

Ex vivo culture. After behavioral characterization, mouse brains were extracted and blocked in cold sampling media as previously described [141]. One or two 200-µm coronal hypothalamic sections per animal were made on a Vibroslicer (Campden Instruments, Lafayette, IN). SCN were isolated by trimming the surrounding hypothalamic tissue and placed on a Millicell (Millipore) culture membrane insert in 37°C recording media [141], conditioned with GIBCO N-2 supplement (Invitrogen, Carlsbad, CA) and contained in 35-mm culture dishes (Falcon, BD,

Franklin Lakes, NJ). Dishes were then sealed with sterile high-vacuum grease and placed in a custom 6-well aluminum chamber heated to 35.5°C by a voltage-regulator.

Confocal imaging. The 6-well chamber containing cultured slices was placed on an automated stage on a laser-scanning confocal microscope (LSM5 PASCAL, Zeiss, Germany) with GFP excitation at 488 nm, and bandpass emission recorded between 505-555 nm. Three Z-stack images totaling 40-μm in depth were taken of each slice every hour for 90 hours. Focus was adjusted manually to account for slice swelling and flattening as needed.

Ex vivo analyses. Raw LSM files of SCN time-lapse imaging were compiled in MetaMorph (Molecular Devices, Downingtown, PA). The Z-stack for each time-point was compressed into a single maximum projection image from which a background subtraction was made (Close-Open morphological filter with a 75 pixel-round sequential average). Whole SCN or single cells were selected as regions of interest (ROI) from the resultant time-series stack, and time-lapse intensity measurements were made and exported to an in-house program created in R (http://www.r-project.org/) that allowed selection of minima and maxima for each SCN or cell, and calculation of phase [1]. This totaled some 5, 538 neurons, and 48 mice. The first 12 hours *ex vivo* were omitted from the analyses. Peaks in fluorescence were visually scored as having a clear rising and falling phase above baseline fluorescence, and the number of circadian peaks per SCN or per cell was determined by study-blind visual scoring. For the purposes of this study, SCN or cells with two or more peaks were considered rhythmic.

Operational definitions. Zeitgeber Time (ZT) is defined as the time of day relative to the light cycle such that ZT 0 is lights-on (dawn) and ZT 12 is lights-off (dusk). *Phase* is defined as the timepoint halfway between the 50% rising timepoint and the 50% falling timepoint on the first peak of the GFP-expression waveform. *Risetime* is defined as the time from 10-90% on the rising side of the first peak in the waveform. *Duration* is the total time between the 50% rising

timepoint and the 50% falling timepoint on the first peak of the waveform. *Neuronal variance* is the variation in neuronal phase determined by circular statistics in Oriana 2.0 (Rockware, Golden, CA). *Period* was defined as the time from the first to second cycle of *Per1*::GFP expression in each neuron. *Ex vivo* slice culture, being an acute extraction of brain tissue from an adult mouse, can be traumatic to the tissue, but we believe that the earliest cycles of the culture are most indicative of *in vivo* conditions [129, 141, 142]. Therefore, these first two cycles served as the best indicator of neuronal period.

Statistical analysis. Circular statistics were performed in Oriana software. Statistics were calculated for each animal for further comparison. Means were reported per mouse and statistically compared in SPSS 14.0 (SPSS, Chicago, IL) with two-way analyses of variance (ANOVA) followed by post-hoc Least Significant Difference (LSD), except for when the variances were not homogeneous, as indicated by a significant Levene's test. In these cases, the Sheirer-Ray-Hare extension of the nonparametric Kruskal-Wallis Test was performed [152], followed by a non-parametric post-hoc Dunnett T3 test. Significance was ascribed at $p < 0.05$.

Section 4.4: Results

Using transgenic *Per1* promoter-driven green fluorescent protein reporter mice, we investigated the effects of development in different seasonal photoperiods on the organization of the SCN circadian clock. Our findings indicate that the SCN of mice exhibit imprinting and/or plasticity in response to seasonal light changes in a manner dependent on the photoperiod experienced during the first three weeks of postnatal life (developmental photoperiod). These results are novel in that they show photoperiod-dependent changes in both tissue-level organization and in neuronal properties of the circadian clock, and these results also show a

possible biological mechanism which may account for mental health phenotypes associated with birth season in humans.

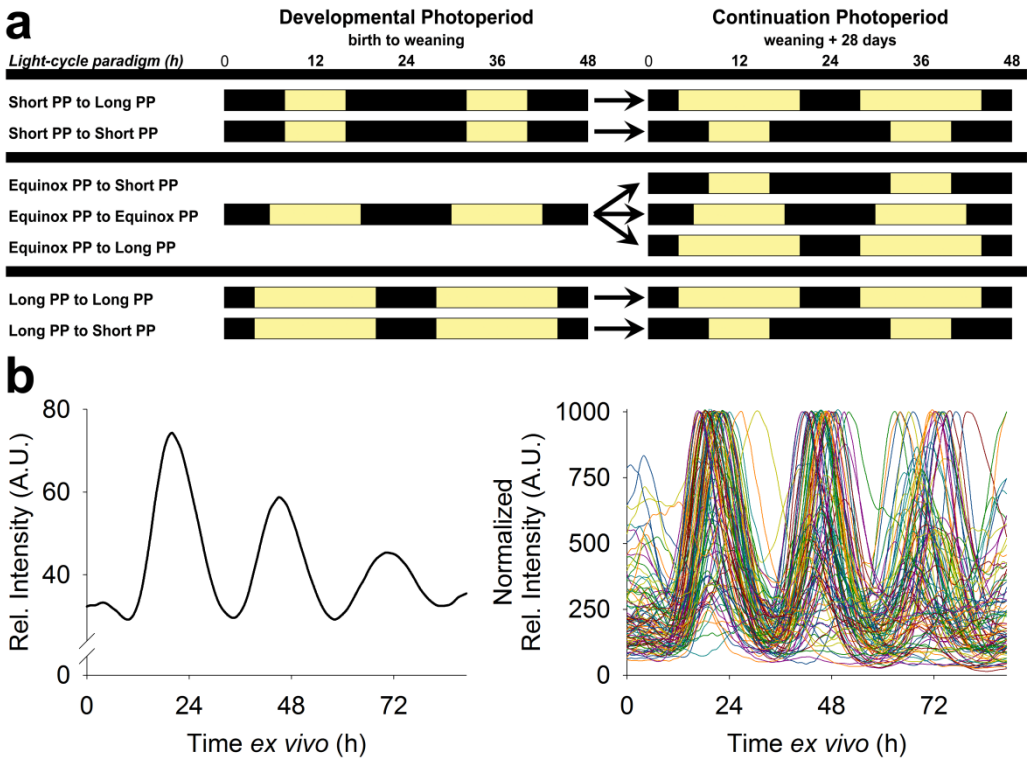

Figure IV-1 | **Experimental design and representative SCN tissue and neuronal time-lapse recordings. a** | Mice were born and matured in a particular developmental photoperiod (PP) of short (8:16), equinox (12:12) or long (16:8) until weaning (*left*). At ~p21, mice were placed individually into wheel-cages under a continuation photoperiod for ~28 days (*right*). Yellow bars represent "lights-on," and black bars represent "lights-off." **b** | Representative time-series examples of SCN (*left*) and neuronal (*right*) *Per1*::GFP expression recordings taken from a single coronal hypothalamic slice on a confocal fluorescent microscope over ~90 hours.

Table IV-1 | **Results of two-way ANOVA.** Analyses included two main-effects: 1) the effects of maturing from birth to weaning in a particular developmental photoperiod (PP), and 2) the effects of transition to a particular continuation PP for ~28 days. Finally, the analyses considered the interaction between developmental and continuation PPs, and how these two factors contributed to *Per1*:GFP circadian gene expression properties in the SCN and SCN neurons *ex vivo*. Significance (bold) was ascribed at $p < 0.05$.

	Developmental PP main-effects			*Continuation PP* main-effects			*Development x Continuation* interaction		
Characteristic	d.f.	*F* or *H*	*p*	d.f.	*F* or *H*	*p*	d.f.	*F* or *H*	*p*
SCN									
Phase	2, 39	0.897	0.416	1, 39	25.901	**< 0.001**	2, 39	5.7	**< 0.01**
Period	2, 25	2.79	0.081	1, 25	2.822	0.105	2, 25	0.919	0.412
Risetime	2, 39	0.994	0.379	1, 39	45.66	**< 0.001**	2, 39	0.699	0.503
Duration	2, 39	5.888	**< 0.01**	1, 39	29.54	**< 0.001**	2, 39	8.152	**< 0.001**
Neuronal									
Variance	2, 36	1.019	0.601	1, 36	17.206	**< 0.001**	2, 36	1.57	0.456
Period	2, 32	4.593	**< 0.05**	1, 32	7.219	**< 0.05**	2, 32	1.566	0.224
Risetime	2, 36	0.197	0.822	1, 36	9.193	**< 0.01**	2, 36	0.95	0.396
Duration	2, 36	4.533	**< 0.05**	1, 36	10.218	**< 0.01**	2, 36	2.807	0.074

We developed mice from birth to weaning (~P21) in one of three light cycles—a short-day, winter-like photoperiod of LD 8:16; an equinox photoperiod of LD 12:12; or a long-day, summer-like photoperiod of LD 16:8 (developmental photoperiod; Fig. IV-1a, *left*). Mice were then subjected to one of the three photoperiods for an additional four weeks (continuation photoperiod; Fig. IV-1a, *right*). At the end of this interval, SCN were removed and *ex vivo* imaging of SCN tissue and neuronal *Per1*::GFP rhythms were performed to assess the impact of these seasonal light cycle manipulations on clock ensemble (Fig. IV-1b, *left*) and clock neuronal properties (Fig. IV-1b, *right*).

SCN clock properties depend on developmental photoperiod.

Measuring the circadian waveform properties of *Per1*::GFP expression in the SCN of mice subjected to various developmental and continuation photoperiods (Fig. IV-1), we discovered that some tissue-level SCN characteristics displayed plasticity (*i.e.* they were set by the continuation photoperiod) while other characteristics were imprinted (*i.e.* they were set by the developmental photoperiod or an interaction between the developmental and continuation photoperiods). Previous work suggests that encoding of seasonal photoperiod occurs at the tissue-level in SCN as a broadening (long-day) or narrowing (short-day) of overall electrical activity waveform *in vivo* [108] or circadian gene expression waveform *ex vivo* [110, 111]. These studies used the same developmental paradigm for all mice (LD 12:12), and then subjected the mice to different photoperiods in adulthood, what we herein refer to as "continuation photoperiod."

We first asked whether this SCN-level waveform broadening or narrowing in response to continuation photoperiod occurs in our mouse strain as well, and we also asked if this change in relative circadian gene expression waveform depended at all on exposure to differing developmental photoperiod. We analyzed two measurements: 10-90% risetime and mid-rise to the mid-fall peak duration. We found that indeed, risetime, which is an indirect measure of the

increase in *Per1* transcriptional activation (via the *Per1*::GFP reporter) on the rising phase of the circadian gene expression rhythm, was plastic across all developmental photoperiods. Figure IV-2a represents the main-effects of developmental photoperiod (*left*) and continuation photoperiod (*right*) from results of a two-way ANOVA and demonstrates that SCN from mice subjected to a long-day continuation photoperiod had greater risetimes than SCN from mice

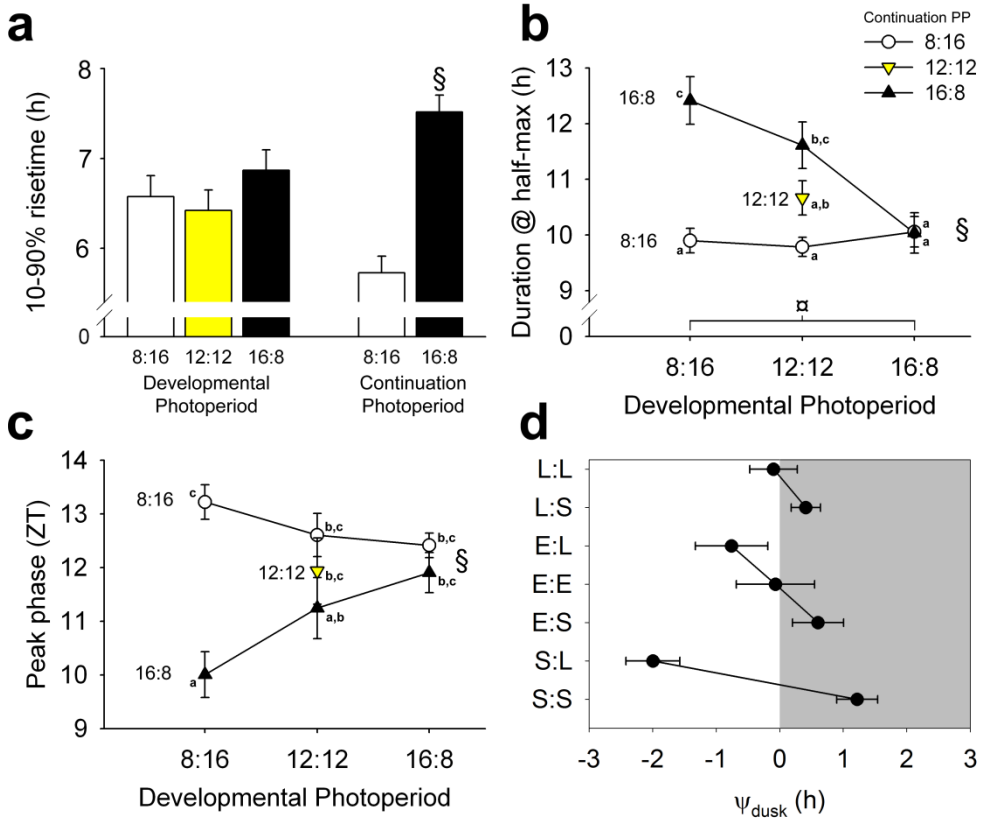

Figure IV-2 | **Developmental photoperiod affects SCN circadian rhythm properties. a-b** | SCN tissue-level *Per1*::GFP expression waveform properties. **a** | Two-way ANOVA main-effects for 10-90% risetime of the first peak *ex vivo*. **b** | Two-way ANOVA interaction plot for duration from 50% rise to 50% fall of the first peak *ex vivo*. Developmental photoperiod on X-axis; continuation photoperiod: short (LD 8:16) represented by open circles, equinox (LD 12:12) represented by yellow inverted triangles and long (LD 16:8) represented by black triangles (see inset legend). **c** | Two-way ANOVA interaction plot for peak phase of *Per1*::GFP expression in SCN. **d** | Dusk asymmetry index demonstrating the phase relationship (ψ) between peak of tissue-level *Per1*::GFP expression (Fig. IV-2c) and dusk. White background represents "lights-on," while grey background represents "lights-off." Photoperiodic paradigm represented as "Developmental:Continuation" with "L" representing long photoperiod, "E" representing equinox photoperiod and "S" representing short photoperiod. Error bars represent SEM. ¤ represents the presence of a significant main effect for developmental photoperiod; § represents the presence of a significant main effect for continuation photoperiod; interactions are indicated by letters such that means sharing a letter are not significantly different. Significance ascribed at $p < 0.05$.

subjected to a short-day continuation photoperiod regardless of the developmental photoperiod they had experienced (mean±SEM: 7.5±0.19h, N = 22 *vs.* 5.7±0.19h, N = 23, Table IV-1 and Fig. IV-2a *right*). These results corroborate the findings of previous studies [108, 110, 111].

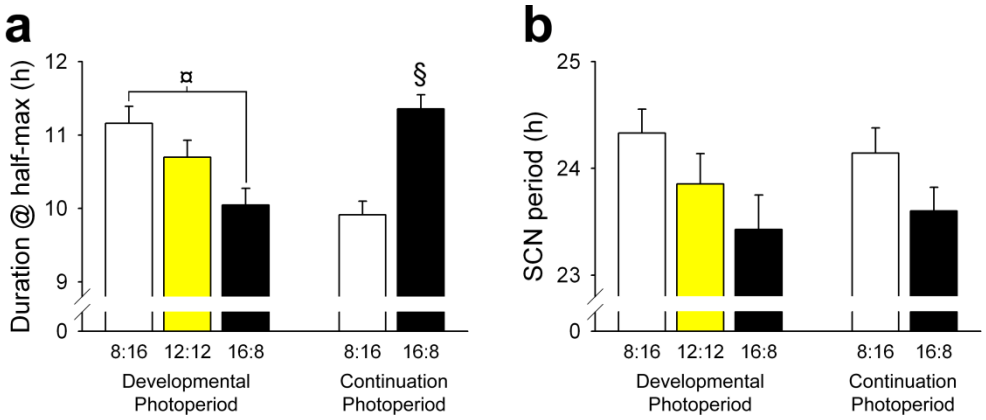

Figure IV-3 | **Duration of Per1::GFP expression in the SCN changes in response to both developmental and/or continuation photoperiods. a** | Two-way ANOVA main-effects for Per1::GFP expression duration from 50% rise to 50% fall of the first peak *ex vivo*. **b** | Two-way ANOVA main-effects for SCN period (1st to 2nd cycles) *ex vivo*. Error bars represent SEM. ¤ represents the presence of a significant main effect for developmental photoperiod; § represents the presence of a significant main effect for continuation photoperiod. Significance ascribed at $p < 0.05$.

Table IV-2 | **Mean ± SEM for all groups.**

	SCN Properties				Neuronal Properties			
Dev PP:Cont PP	Phase (ZT)	Period (h)	Risetime (h)	Duration (h)	Variance	Period (h)	Risetime (h)	Duration (h)
Long:Long	11.9 ± 0.37 [b,c]	22.8 ± 0.39	7.8 ± 0.23	10.0 ± 0.36 [a]	0.25 ± 0.034	23.1 ± 0.25	6.1 ± 0.18	9.2 ± 0.17
Long:Short	12.4 ± 0.23 [b,c]	24.0 ± 0.18	6.0 ± 0.49	10.1 ± 0.27 [a]	0.17 ± 0.017	24.5 ± 0.34	5.6 ± 0.08	9.1 ± 0.19
Equinox:Long	11.2 ± 0.57 [a,b]	23.8 ± 0.34	7.5 ± 0.28	11.6 ± 0.42 [b,c]	0.28 ± 0.030	23.9 ± 0.25	5.8 ± 0.09	9.7 ± 0.17
Equinox:Equinox	11.9 ± 0.62 [b,c]	23.8 ± 0.64	6.3 ± 0.45	10.7 ± 0.31 [a,b]	0.20 ± 0.020	24.5 ± 0.43	5.8 ± 0.18	9.7 ± 0.36
Equinox:Short	12.6 ± 0.40 [b,c]	24.0 ± 0.63	5.3 ± 0.09	9.8 ± 0.17 [a]	0.19 ± 0.033	24.4 ± 0.50	5.7 ± 0.11	9.3 ± 0.11
Short:Long	10.0 ± 0.42 [a]	24.2 ± 0.47	7.3 ± 0.56	12.4 ± 0.43 [a]	0.25 ± 0.013	24.6 ± 0.22	6.0 ± 0.16	9.9 ± 0.20
Short:Short	13.2 ± 0.32 [c]	24.4 ± 0.17	5.9 ± 0.20	9.9 ± 0.22 [c]	0.25 ± 0.020	24.9 ± 0.23	5.5 ± 0.18	9.1 ± 0.08

Unlike risetime, peak duration, which is an indicator of both the increase and decrease of *Per1* transcriptional activation on the rising and falling phases of the *Per1*::GFP reporter waveform, was found to be dependent on both developmental and continuation light cycles due to a complex interaction between these two experimental variables. Figure IV-2b represents the interaction between developmental photoperiod (*X-axis*) and continuation photoperiod (*symbols on graph as indicated*) as found by a two-way ANOVA, and demonstrates that long photoperiod developed mice exhibited a conserved duration of peak *Per1*::GFP expression in

response to seasonal changes in light, while short photoperiod developed mice exhibited different durations in short-day and long-day continuation photoperiods (Table IV-1; see Table IV-2 for mean±SEM and Fig. IV-3a for main-effects of Two-way ANOVA). As the duration of the light phase in developmental photoperiod was increased, the duration of *Per1*::GFP expression at half-maximum became less plastic and more imprinted (Fig. IV-2b). These results indicate that while the rate of increase of *Per1* transcriptional activation (risetime) may respond to changes in seasonal light input with plasticity, the overall tissue-level waveform (duration) responds to seasonal light cycle changes in a developmentally imprinted manner.

We next asked if, given the stark changes in circadian gene expression waveform, there was an effect of developmental or continuation photoperiod on the phase angle of this waveform to the light cycle before the animal was killed. We found that, as with waveform duration, there was a significant interaction between developmental and continuation photoperiods in that long-day photoperiod developed mice exhibited a conserved SCN phase in response to seasonal changes in light, whereas short-day photoperiod developed mice exhibited different SCN phases in short-day and long-day continuation photoperiods (Table IV-1, Fig. IV-2c; see Table IV-2 for mean±SEM). In other words, as the light portion of the developmental photoperiod was increased, SCN phase became less plastic and more imprinted (Fig. IV-2c). Figure 2d shows that as developmental photoperiod was increased, the phase angle to dusk, or relationship between SCN phase and lights-off, was increasingly conserved.

Finally, we asked if *ex vivo* SCN period was affected by developmental and/or continuation photoperiods, and found only a suggestive trend (Table IV-1; see Table IV-2 for mean±SEM and Fig. IV-3b for main-effects of Two-way ANOVA).

Clock neuron properties depend on developmental photoperiod.

Previous studies using mice developed in an equinox (LD 12:12) photoperiod and then subjected to different seasonal continuation photoperiods have indicated that seasonality is encoded by alterations in the phase relationships of neurons in the SCN [108, 110, 111]. Seasonal encoding at the tissue-level, therefore, has until now been thought of as a purely plastic process involving individual neural oscillators falling out of phase with each other in long photoperiod and becoming more synchronized in short photoperiod [109]. These previous studies emphasized network encoding of seasonal signals and provided no evidence that seasonal light influenced neuronal properties to contribute to seasonal encoding. We now show that in addition to network encoding, the circadian characteristics of SCN neurons not only respond to changes in seasonal light cycle, but do so in a manner that depends on developmental light history.

We first sought to characterize the relationship between seasonality and distribution of neuronal clock phases within the SCN. We found that this property, as measured by the neuronal phase variance, was plastic across all developmental photoperiods. Figure IV-4a represents the main-effects of developmental photoperiod (*left*) and continuation photoperiod (*right*) from results of a two-way ANOVA and demonstrates that SCN from mice subjected to a long-day continuation photoperiod had greater neuronal phase variance than SCN from mice subjected to a short-day continuation photoperiod, regardless of the developmental photoperiod they had experienced (mean±SEM: 0.29±0.015, N = 20 *vs.* 0.17±0.015, N = 22, Table IV-1, Fig. IV-4a). These results corroborate previous studies demonstrating that SCN from mice matured in a LD 12:12 exhibited photoperiod-dependent changes in neuronal phase relationships within the SCN that likely underpin the photoperiod-dependent broadening or narrowing of the tissue-level *Per1*::GFP expression waveform (Fig. IV-2a-b) [108-111].

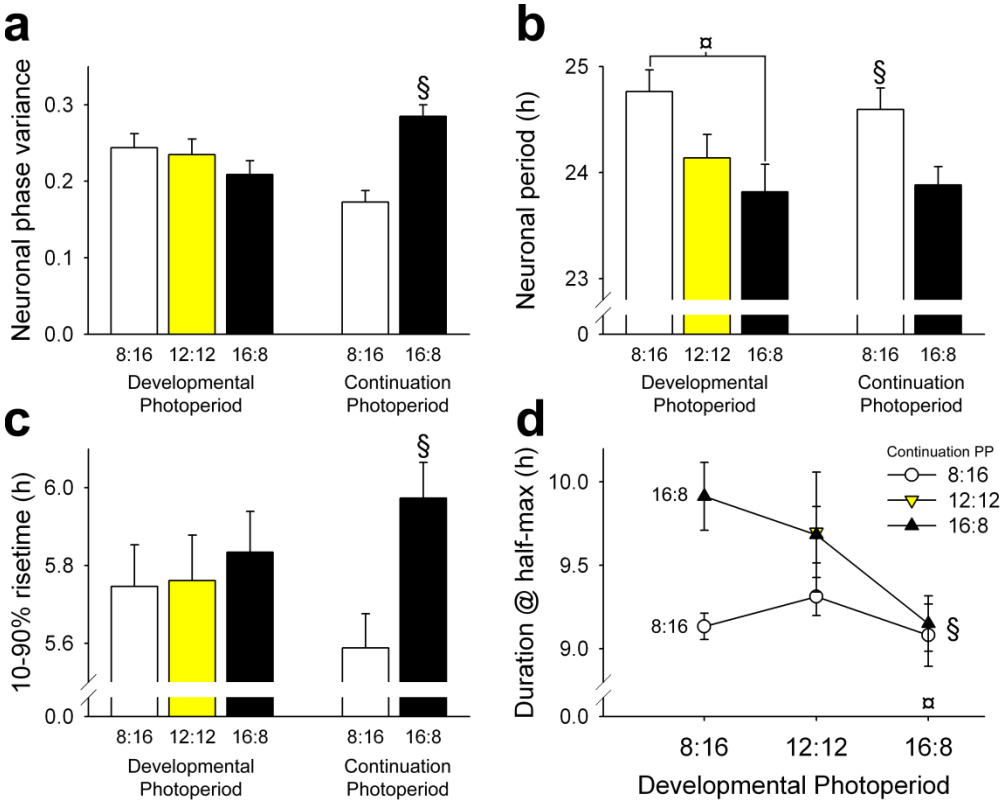

Figure IV-4 | **SCN neurons exhibit changes in circadian rhythm properties in a developmental photoperiod-dependent manner. a** | Two-way ANOVA main-effects for neuronal phase variance of *Per1*::GFP expression in SCN as measured by circular statistics (0 = no phase variance; 1 = complete phase variance). **b-d** | SCN neuronal-level *Per1*::GFP expression properties. **b** | Two-way ANOVA main-effects for period from the first to second cycles of *Per1*::GFP expression in SCN neurons. **c** | Two-way ANOVA main-effects for 10-90% risetime of the first peak *ex vivo*. **d** | Two-way ANOVA interaction plot for duration from 50% rise to 50% fall of the first peak *ex vivo*. Developmental photoperiod on X-axis; continuation photoperiod: short (LD 8:16) represented by open circles, equinox (LD 12:12) represented by yellow inverted triangles and long (LD 16:8) represented by black triangles (see inset legend). Error bars represent SEM. ¤ represents the presence of a significant main effect for developmental photoperiod; § represents the presence of a significant main effect for continuation photoperiod. Significance ascribed at $p < 0.05$.

We next asked if in SCN neurons, as in the SCN as a whole, there were seasonal light-induced changes in circadian properties that might contribute to seasonal encoding, and we found that there were effects on neuronal period and neuronal waveform. There were two main-effects on neuronal period that may explain the strong trend seen at the tissue-level. First, SCN neurons from mice developed in a short photoperiod had a significantly longer neuronal period (mean±SEM: 24.8±0.2h, N = 15) than SCN neurons from mice developed in long photoperiod (mean±SEM: 23.818±0.3, N = 11; LSD post-hoc, $p < 0.05$; Table IV-1 and Fig. IV-4b

"¤" *left*). SCN neurons from mice developed in an equinox photoperiod displayed an intermediate period (mean±SEM: *12:12*, 24.1±0.2h, N = 12; Table IV-1 and Fig. IV-4b *left*). Second, SCN neurons from mice subjected to a short continuation photoperiod also had a significantly longer neuronal period than SCN neurons from mice subjected to a long continuation photoperiod (mean±SEM: 24.6±0.2h, N = 15 *vs.* 23.9±0.2h, N = 12; Table IV-1 and Fig. IV-4b "§" *right*). It is worth noting that while we did not find a significant interaction for neuronal period between the developmental and continuation photoperiods, SCN neurons from mice developed in a long-day photoperiod did exhibit the most extreme response to seasonal light change: SCN neurons from long-day:long-day mice exhibited the shortest period of the study (mean±SEM: 23.1±0.25h, N = 8) while SCN neurons from long-day:short-day mice exhibited a much longer period (mean±SEM: 24.5±0.34h, N = 6, Fig. IV-4b).

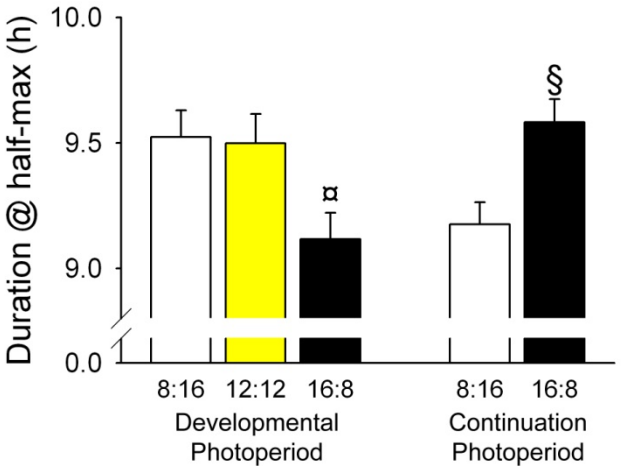

Figure IV-5 | **Duration of Per1::GFP expression in SCN neurons changes in response to developmental and/or continuation photoperiod.** Two-way ANOVA main-effects for duration from 50% rise to 50% fall of the first peak *ex vivo*. Error bars represent SEM. ¤ represents the presence of a significant main effect for developmental photoperiod; § represents the presence of a significant main effect for continuation photoperiod. Significance ascribed at $p < 0.05$.

We also found that the circadian waveform of individual SCN neurons was altered by photoperiod. Just as in the SCN as a whole, risetime was found to be a plastic property of neurons. SCN neurons from mice subjected to a long-day continuation photoperiod exhibited

greater overall risetimes than SCN neurons from mice subjected to a short-day continuation photoperiod, regardless of the developmental photoperiod they had experienced (mean±SEM: 6.0±0.09h, N = 20 *vs.* 5.6±0.09h, N = 22, Table IV-1 and Fig. IV-4c). We also found that, like the SCN as a whole, the effects of photoperiod on the duration of peak width in SCN neurons are more complicated. Duration of neuronal *Per1*::GFP waveform was dependent on both developmental and continuation light cycles: SCN neurons from mice subjected to a long-day continuation photoperiod exhibited significantly longer durations than SCN neurons from mice subjected to a short-day continuation photoperiod (mean±SEM: 9.6±0.09h, N = 20 *vs.* 9.2±0.09h, N = 22; Table IV-1, Fig. IV-4d "§" and Fig. IV-5 *right*). We also found that SCN neurons from mice developed in a long photoperiod exhibited an overall *shorter* duration (mean±SEM: 9.1±0.11h, N = 15) than SCN neurons from mice developed in an equinox or a short photoperiod (mean±SEM: *12:12*, 9.5±0.12h, N = 12; *8:16*, 9.5±0.11h, N = 15; LSD post-hoc, $p < 0.05$; Table IV-1, Fig. IV-4d "¤" and Fig. IV-5 *left*). While not reaching statistical significance, there was a strong trend towards an interaction between these two experimental variables that might explain the main-effects of the two-way ANOVA (Table IV-1, $p = 0.074$). Thus, the waveform of individual neurons changed in response to seasonal light cycles in a developmentally-imprinted manner such that as the deviation of the light phase increased, the duration of neuronal *Per1*::GFP expression on each cycle became less plastic and more imprinted, just as in the SCN as a whole. Taken together, these results indicate that seasonality is not exclusively encoded by altered phase relationships between neurons within the SCN as previously proposed [108, 109], but rather that changes occur at the molecular level within individual neurons that may also contribute to seasonal encoding.

Section 4.5: Discussion

Previous studies of seasonal encoding in mice have been performed by subjecting LD 12:12 developed mice to seasonal continuation light cycles, and have reported that encoding occurs at the tissue level due to the plasticity of neuronal circadian phase relationships [108, 110, 111]. Our approach in this study was more complex, involving two independent variables (developmental photoperiod and continuation photoperiod) and two-way ANOVA to tease apart the contributions of each of these variables to seasonal encoding. While this approach does not allow for exactly the same comparisons within a single developmental photoperiod, it affords a powerful (and statistically sound) analysis of the overall main-effects of 1) maturing in a developmental photoperiod, or 2) transitioning into a continuation photoperiod during adulthood. Additionally, a two-way ANOVA can 3) account for any interaction between the two variables (Table IV-1).

We initially began this study by attempting to reproduce the results of the previous work on equinox photoperiod developed mice. Our results (from within the omnibus two-way ANOVA discussed below) corroborate those studies in that SCN from mice developed in equinox photoperiod exhibited plasticity in risetime and duration (Fig. IV-2b). Specifically, SCN from mice subjected to a long continuation photoperiod exhibited greater *Per1*::GFP expression risetimes than did SCN from mice subjected to a short continuation photoperiod (Fig. IV-2a, *right*; see Table IV-2 for mean±SEM within equinox developed mice). Similarly, SCN from mice developed in an equinox photoperiod and then subjected to a long continuation photoperiod exhibited greater overall duration of *Per1*::GFP expression on each cycle—waveform broadening—than did SCN from mice subjected to a short continuation photoperiod (Fig. IV-2b; see Table IV-2 for mean±SEM). These results confirm the previous findings that SCN electrical activity and circadian gene expression waveforms change shape within equinox developed mice

when they are subjected to different seasonal photoperiods [108, 110, 111]. Furthermore, our results also confirm that these changes at the tissue-level are, at least in part, due to changes in neuronal circadian phase relationship at the cellular-level. Specifically, we find that the SCN from mice subjected to a long continuation photoperiod exhibited greater neuronal phase variance of *Per1*::GFP expression than did SCN from mice subjected to a short continuation photoperiod (Fig. IV-4a *right*; see Table IV-2 for mean±SEM within equinox developed mice). Taken together, these results suggest that seasonal encoding occurs at the tissue-level by alteration of neuronal synchrony—at least in animals matured in an equinox photoperiod. None of the previous studies reported a continuation photoperiod dependent change in neuronal properties other than phase, and our study also failed to reveal any significant neuronal waveform changes within this developmental group.

A previous study using *Per1*::GFP reporter mice indicated that animals developed and matured in constant light (LL) exhibited disrupted SCN tissue-level circadian rhythms, but intact neuronal clock function [141]. In particular, this study found that while mice developed in a 12:12 light-dark cycle exhibited robust SCN tissue-level circadian rhythms, their counterparts developed in LL exhibited damped SCN rhythms due to neuronal asynchrony. As an extension of these results, we asked if seasonal light cycles could similarly influence the neural organization of the developing mammalian clock. Using a developmental paradigm similar to that used previously in hamsters [165], we sought to characterize what differences, if any, existed between mice developed on a short or long photoperiod and then either maintained in that developmental photoperiod or switched into the opposite continuation photoperiod after weaning (Fig. IV-1a).

Simply put, we found that seasonal encoding is not as straightforward as the results from LD 12:12 developed mice would suggest. At the tissue-level, SCN *Per1*::GFP risetime was

completely plastic, increasing in long continuation photoperiods and decreasing in short continuation photoperiods regardless of developmental photoperiod (Fig. IV-2a). This result is not at odds with the results from equinox developed mice. However, in measuring SCN *Per1*::GFP waveform duration, we found that the equinox-developed mice discussed above exhibited an intermediate phenotype between the plasticity of short photoperiod developed mice and the imprinting of long photoperiod developed mice (Fig. IV-2b; see Table IV-2 for mean±SEM). This result suggests that seasonal encoding of waveform duration at the tissue level is dependent on developmental photoperiod, yielding a plastic response to continuation photoperiod in short-day developed mice and an imprinted response to continuation photoperiod in long-day developed mice.

This unexpected result led us to wonder if, with the variable shape of the circadian gene expression waveform, there might also be an effect of the two factors (developmental photoperiod and continuation photoperiod) on the *Per1*::GFP waveform's peak phase. The phase relationship, or phase angle, between the environmental entraining factor (light) and the circadian clock is perhaps the most important characteristic in circadian biology. What we found was that, like duration, the peak phase of *Per1*::GFP expression was dependent on the interaction between developmental photoperiod and continuation photoperiod such that the SCN from long-day developed mice exhibited a conserved phase angle to dusk that was absent in short-day developed mice. As with duration, the SCN from equinox photoperiod developed mice exhibited an intermediate phenotype (Fig. IV-2c-d).

We next sought to explain these tissue-level results by characterizing the neuronal circadian phenotype. As discussed above, we found that neuronal phase variance is completely plastic, responding to long continuation photoperiod with increased phase variance and to short continuation photoperiod with relatively decreased phase variance, regardless of

developmental conditions (Fig. IV-4a). How then can we explain the developmental effect of photoperiod on SCN circadian gene expression waveform duration? The only explanation can be derived from seasonal changes in neuronal properties, which had not been previously reported. For the first time, we report that photoperiod does indeed change the waveform characteristics of neuronal circadian rhythms, but only when taking into account the developmental photoperiod. We found that, as in the SCN, risetime is plastic across all developmental photoperiods, such that neuronal *Per1*::GFP risetime increased in long continuation photoperiods and decreased in short continuation photoperiods (Fig. IV-2c). This result, however novel, does not explain the tissue-level imprinting completely. The reason may instead lie in the characteristics of neuronal duration. Similar to what we reported at the tissue level, there is a strong trend towards an interaction between developmental photoperiod and continuation photoperiod ($p = 0.07$) such that SCN neurons from mice developed in a long photoperiod exhibit conserved, short durations while SCN neurons from mice developed in a short photoperiod exhibit plasticity in duration, ranging from the longest in short:long mice to the shortest in short:short mice (Fig. IV-4d).

We also found that, while there was only a trend towards significance at the tissue-level, seasonal photoperiod does affect neuronal period. Specifically, SCN neurons from mice developed in a long photoperiod exhibit significantly shorter periods than SCN neurons from mice developed in a short photoperiod (Fig. IV-4b, *left*), and SCN neurons from mice subjected to a long continuation photoperiod generally exhibited significantly shorter periods than SCN neurons from mice developed in a short photoperiod (Fig. IV-4b, *right*). It is worth noting that, while not significant, the means of each group of mice (at both the tissue and cellular levels) hint at an interaction such that period is imprinted in short photoperiod developed mice and plastic in long photoperiod developed mice—exactly the opposite of the interaction seen in SCN phase

and SCN/neuronal duration (Fig. IV-3b and IV-4b; see Table IV-2 for mean±SEM). All together, these results establish that photoperiod can influence the developing biological clock at both the network and cellular levels.

While our results clearly demonstrate how seasonal encoding occurs in the SCN, the mechanisms by which light causes these results are not yet clear. It is well established that photic signals are transmitted to the SCN clock via a specialized subset of retinal ganglion cells that express the photopigment melanopsin [166, 167]. These intrinsically photoreceptive ganglion cells (ipRGCs) detect light and functionally project to the SCN as early as the day of birth in rodents [168-170], and thus provide a likely pathway by which developmental photoperiod influenced SCN organization in our study. Maternal-neonatal behavioral interactions could also have played some role in the influence of photoperiod on the developing biological clock, however, previous results with mice raised in LL suggest that light input is the predominant signal [141]. IpRGCs also contribute to the pupillary light response, melatonin suppression and acute regulation of sleep/wake states and are thus the basis for a subcortical non-image forming visual system [171-176]. The seminal studies of Hubel and Wiesel originally identified imprinting of functional characteristics of visual cortical cells and circuits in response to visual deprivation in the early postnatal period [164, 177-182]. The present study extends developmental imprinting to the circadian non-image forming visual system and suggests that light history may have extensive effects on brain maturation.

These results are intriguing in light of a recent report on the epigenetic effects of illumination during the development of dopamine neurons in the frog SCN [163]. That study found that as the amount of light to which frog tadpoles were exposed during development increases, the number of inhibitory dopamine neurons also increases, thus imprinting the retinohypothalamic-SCN circuitry and allowing finer control of skin pigmentation. Our results in

the mouse provide analogous evidence for photoperiod-dependent imprinting of the mammalian SCN.

Furthermore, our results provide an *ex vivo* correlate of studies reporting the effect of developmental photoperiod history on neurophysiology in rodents. Hamsters (*Phodopus sungorus*) subjected to a developmental and post-weaning paradigm similar to that used in this study exhibited imprinting of anxiety behaviors for some measures, and continuation photoperiod modulation of depressive and anxiety behaviors for other measures [165, 183]. Studies like this reveal an important truth that is often overlooked in research on photoperiodism: while behavioral activity and physiology may exhibit photoperiodic differences between groups, there are other concurrent measureable neurological changes that take place. Our results on the seasonally and developmentally dependent maintenance of phase angle may provide the mechanism by which the brain encodes torpor and lipid composition [184], imprints immune response [185, 186], and organizes aggressive behavioral output [187], to name a few examples. Because these animal models are thought to represent physiological correlates of humans, the results of these studies and this current study have broad implications for human health.

Our results indicate that developmental seasonal imprinting of the mouse biological clock leads to differential responses to subsequent seasonal change. Humans are not considered to be strongly seasonal organisms, yet there is substantial evidence that seasonal change and birth season influence mood disorders [188]. Seasonal Affective Disorder (SAD), for example, is a mood disorder that affects between 0.4% and 2.7% of the United States population every year and can be treated with circadian light therapy [114-116]. Winter-born individuals show significantly lower (sadder) Global Seasonality scores than individuals born in the summer [127], and there is a significant excess of winter-spring births for schizophrenia, mania/bipolar disorder and neurosis [117-119, 123, 124]. In addition, there is a spring and summer excess of births for autism [120, 122]. Taken

together, the elucidation of the mechanisms by which the mammalian SCN encodes season and is seasonally imprinted during development may provide insight into the causes of behavioral predispositions to seasonal change.

We have demonstrated that the mouse SCN biological clock network and its constituent neurons exhibit imprinting and/or plasticity of functional characteristics in a manner that is dependent on the photoperiod experienced during perinatal development. The SCN from mice developed in a long photoperiod are imprinted so that they respond to subsequent changes in seasonal photoperiod by conserving phase angle to dusk and with conserved *Per1* circadian waveforms at the tissue and cellular levels, while the rate of rise of *Per1* expression can still be modulated. SCN from mice developed in a short-day photoperiod respond to subsequent changes in seasonal day-length differently, however, with maintained plasticity in SCN rhythm phase and all aspects of tissue-level and neuronal waveform properties—only neuronal period is imprinted in short-day photoperiod developed mice.

Section 4.6: Chapter Acknowledgements

The authors would like to thank Jeremiah Y. Cohen for kindly providing custom software programming and Terry Page for his thoughtful comments. This work was supported by NIH grants P50 MH078028 to R. D. Blakely, T32 MH64913 to E. Sanders-Bush and F31 MH080547 to C.M.C.

Section 4.7: Author Contributions

CMC & DGM conceived experimental design; CMC, JCA and BRS performed experiments and compiled results; CMC & KLG performed statistical analyses; and CMC & DGM wrote the paper.

CHAPTER V

GENETIC DIFFERENCES IN HUMAN CIRCADIAN CLOCK GENES AMONG WORLDWIDE POPULATIONS[r]

Christopher M. Ciarleglio*[1], Kelli Ryckman[2], Stein V. Servick[1], Akiko Hida[1], Sam Robbins[4], Nancy Wells[4], Jennifer Hicks[4], Sydney A. Larson[1], Joshua P. Wiedermann[1], Krista Carver[4], Nalo Hamilton[4], Kenneth K. Kidd[5], Judith R. Kidd[5], Jeffrey R. Smith[2], Jonathan Friedlaender[6], Douglas G. McMahon[1], Scott Williams[2], Marshall L. Summar[3], and Carl Hirschie Johnson[1]

*Neuroscience Graduate Program
[1]Dept. of Biological Sciences
[2]Dept. of Medicine and Center for Human Genetics Research
[3]Dept. of Pediatrics and Genetics
[4]Vanderbilt University School of Nursing
Vanderbilt University, Nashville, TN 37235

[5]Department of Genetics, Yale University School of Medicine, New Haven, CT 06510

[6]Department of Biological Anthropology (*emeritus*), Temple University, Philadelphia, PA 19106

Section 5.1: Summary Abstract

The daily biological clock regulates the timing of sleep and physiological processes that are of fundamental importance to human health, performance, and well-being. Environmental parameters of relevance to biological clocks include (i) daily fluctuations in light intensity and temperature, and (ii) seasonal changes in photoperiod (day-length) and temperature; these parameters vary dramatically as a function of latitude and locale. In wide-ranging species other than humans, natural selection has genetically optimized adaptiveness along latitudinal clines. Is there evidence for selection of clock gene alleles along latitudinal/photoperiod clines in humans? A number of polymorphisms in the human clock genes *Per2*, *Per3*, *Clock*, and *AANAT* have been reported as alleles that could be subject to selection. In addition, this investigation

[r] Ciarleglio *et al*. (2008). Genetic Differences in Human Circadian Clock Genes Among Worldwide Populations. *J Biol Rhythms.* **23**(4): 330.

discovered several novel polymorphisms in the human *Arntl* and *Arntl2* genes that may have functional impact upon the expression of these clock transcriptional factors. The frequency distribution of these clock gene polymorphisms is reported for diverse populations of African Americans, European Americans, Ghanaians, Han Chinese and Papua New Guineans (including five sub-populations within Papua New Guinea). There are significant differences in the frequency distribution of clock gene alleles among these populations. Population genetic analyses indicate that these differences are likely to arise from genetic drift rather than from natural selection.

Section 5.2: Introduction

Eukaryotic and prokaryotic organisms manifest daily (circadian) rhythms controlled by endogenous biochemical oscillators[14]. In mammals, this biological clock regulates the timing of sleep and physiological processes–including feeding behavior, lipid and carbohydrate metabolism, sleep, and blood pressure control–that are of fundamental importance to human health, performance, and well-being[14]. These daily oscillations are controlled by a circadian clock composed of autoregulatory transcription/translation feedback loops of the expression of central clock genes, especially *Clock*, *Bmal1/Arntl*, *Bmal2/Arntl2, Per1*, *Per2*, *Per3*, *Cry1*, and *Cry2*[14, 189]. The clock-controlled hormone melatonin also plays an important role in circadian and sleep systems[190]. Perturbation of the central clock genes by mutation or knockout in mice elicits phenotypes ranging from arrhythmicity[191-193] to metabolic syndrome/obesity[194], altered insulin/glucose responsiveness[195], and increased susceptibility to cancer[196].

In humans, disorders of the biological clock have been strongly implicated in sleep disorders, shiftwork, alertness/performance, cardiovascular disease, and mental health[14, 197]. For example, in depression, there is often a daily variation in mood (depression worse in morning) with

altered phasing of the cortisol secretion rhythm (and other rhythms)[14, 102]. Recent studies have shown that clock gene polymorphisms are associated with several syndromes, including sleep and mood disorders, for example: (i) variants in *Per2* and *CKIδ* with "Familial Advanced Sleep Phase Syndrome" (FASPS[96, 97]), (ii) variants of *Per3* with delayed sleep phase syndrome[100] and extreme diurnal preference[99], (iii) a variable number of tandem repeats in exon 18 of *Per3* (VNTR) with sleep structure and dysfunction[198], (iv) a single nucleotide polymorphism (SNP) in the promoter of the human arylalkylamine N-acetyl-transferase gene (*AANAT*) with short sleep duration[199], and (v) a polymorphism in the 3' UTR of *Clock* with diurnal preference[200], and sleep disorders[201].

A previous paper reported that a biallelic tandem repeat polymorphism (VNTR) in the human *Per3* gene exhibited significantly different allelic frequencies between Papua New Guineans (0.19) *versus* East Asians (0.80-0.89), whereas European/American/African populations had intermediate frequencies (0.6~0.7)[202]. We therefore tested whether these geographical/ethnic differences in allelic frequency were common in other biological clock genes or whether this phenomenon was specific to the VNTR polymorphism of *Per3*. This study reports the frequency distribution of previously reported polymorphisms of potential functional significance in *PER2*, *PER3*, *CLOCK*, and *AANAT* in African Americans, European Americans, Han Chinese, Papua New Guineans, and Africans from Ghana. Because Papua New Guinean samples may be genetically diverse, we also perform analyses on subpopulations within Papua New Guinea. In addition, we performed systematic screening and characterization of common exonic and promoter polymorphisms in the *ARNTL* (aka *hBmal1* or *hMop3*[203]) and *ARNTL2* (aka *hBmal2* or *hMop9*[204]) genes by single-stranded conformation polymorphism (SSCP) analyses and sequencing, and report the discovery of several novel polymorphisms. We use population genetic analyses on these clock gene polymorphisms (i) to understand population stratification,

(ii) to assess selection/drift, and (iii) as a basis for future association analyses of clock gene polymorphisms with phenotypes of behavioral and/or medical significance.

Section 5.3: Materials and Methods

Study subjects. DNA samples were collected from unrelated human subjects from various global populations, including: African-American (n = 48 from the Coriell Cell Repository), European-American (n = 422 collected at Vanderbilt), Han Chinese (n = 48 from the Coriell Cell Repository), New Guinean (n = 66), and Ghanaian (n = 48, randomly selected from a cohort of unrelated individuals of the Ga ethnic group that were collected as part of an ongoing study of the genetic basis of hypertension and cardiovascular disease[205]). The PNG samples are further subdivided into separate sub-populations as follows: Sepik (n = 18), Madang (n = 4), Gimi (n = 10), Goroka (n = 11), and Nasioi/Bougainville (n = 23). The study was approved by all relevant institutional review boards and participating individuals.

DNA isolation and primer design. For the European-American (EA) samples collected at Vanderbilt, 5 cc whole blood was collected from each subject and DNA was isolated from lymphocytes by the Vanderbilt DNA core facility. For the Nasioi, Gimi, and Goroka PNG samples, DNA was isolated from lymphoblast cell lines grown at Yale University. Previously reported primers were used for the *Per2*, *Per3* and *Clock* variants (Table V-1). For *Arntl* and *Arntl2*, forward and reverse primers yielding ~200 bp amplicons were generated to cover the promoter regions, exons, and intronic regions immediately flanking exons in a series of overlapping fragments (Table V-1). These primers were designed with an annealing temperature of ~55°C.

SSCP screening and genotyping. Each amplicon was PCR amplified from the genomic DNA using one of two protocols: Platinum PCR Supermix (Invitrogen, Carlsbad, CA, USA) was used for *Per2*, *Per3* and *Clock*. For *Arntl* and *Arntl2*, AmpliTaq Gold (Applied Biosystems, Foster City, CA, USA)

was used with the provided PCR Buffer II and $MgCl_2$. Loading dye (4X = 40 mM EDTA, 0.1% bromophenol blue, 0.1% xylene cyanol prepared in deionized formamide) was added to all PCR products. These products were then denatured at 94°C for 3 min, rapidly cooled to 4°C, and separated in MDE electrophoresis gels (Lonza, Basel, Switzerland) at 15 W in 0.6x TBE running buffer at 4°C for 8–14 h. Gels were developed by silver staining to visualize bands[206]. In the case of the *Arntl* and *Arntl2* genes, we used SSCP to screen for common polymorphisms in the EA population (defined as those polymorphisms present in 5% or more of the population). As an initial screening cohort, we chose 20 random EA subjects (~ 5% of the total population) to look for novel variants and to verify the existence of known polymorphisms within each of the amplicons analyzed (80 amplicons for *Arntl* and 62 amplicons for *Arntl2*). The screening set was estimated to provide 98% power to detect a polymorphism with a minor variant frequency of 0.10, and 87% power with a frequency of 0.05. Each amplicon was amplified by PCR and then run on an acrylamide gel for SSCP analysis. Samples that represented the most common SSCP banding pattern and also any samples that exhibited an uncommon band shift pattern were sequenced as described below to confirm the common sequence and to identify polymorphisms (for the less common patterns).

In the cases of the *Per2*, *Per3*, *Clock*, and *AANAT* genes, we used previously reported primers or redesigned primers to produce ~200 bp amplicons that are roughly centered upon the site of SNPs that have already been described (Table V-1). For the *Per2* and *Clock* genes, we discovered novel SNPs that were located within the amplicons in addition to the targeted SNP. Finally, SNP allele frequencies in all genes were determined on all the samples in the indicated five populations using the SSCP patterns as confirmed by sequencing. Results from the genotyping analyses using SSCP were concordant with the existing data in dbSNP for allele frequencies in the different populations, indicating the fidelity of this method.

Sequence analysis. Amplicons with band-shifts were PCR amplified as stated above, cleaned with the QIAQuick PCR Purification Kit (QIAGEN, Valencia, CA), and sequenced with an ABI 3730xl DNA Analyzer (Applied Biosystems). Control and shifted sequences were aligned using Clustal W, and variants were compared to dbSNP build 126 for *Homo sapiens* (NCBI, Bethesda, MD, USA).

Statistical analyses. Allelic and genotypic distributions were compared between ethnic groups using Fisher's exact tests. Hardy-Weinberg Equilibria (HWE) were calculated for each marker using Fisher's exact tests. Haplotype frequencies were estimated using an expectation maximization (EM) algorithm that reconstructs haplotypes and determines frequencies that maximize the likelihood of the genotypic data[207, 208]. Differences in haplotype distributions between populations were determined using a regression approach [209]. Wright's F_{ST} estimates were calculated between each population and within the Papua New Guinea sub-populations using a method developed by Weir and Cockerham[210]. Wright's F_{ST} is a measure of population differentiation that ranges from 0 to 1 with 0 indicating no differentiation and 1 indicating highly differentiated populations. The above analyses were performed with either Stata version 9, Powermarker[211], or Tools for Population Genetic Analysis (TFPGA, version 1.3 available at http://www.marksgeneticsoftware.net/); all gave virtually the same results.

Section 5.4: Results

SSCP screening of polymorphisms in Arntl and Arntl2.

Based on the previous study of the geographical frequency distributions of the *Per3* VNTR, we assessed the allele frequency of the clock gene SNPs in five populations: European Americans (EA), African Americans (AA), Ghanaians (GA), Han Chinese (HC), and Papua New Guineans (PNG)[202]. Because PNG populations are known to be genetically heterogeneous[212], we

assayed several subpopulations within PNG to determine if the study of Nadkarni and coworkers[202] provided data that reflected PNG as a whole or only certain subpopulations within PNG.

In addition to genotyping previously reported SNPs within the clock genes *Clock*, *Per2*, *Per3*, and *AANAT*, we identified several novel SNPs in the promoter and exonic regions of the key clock genes *Arntl* and *Arntl2* using SSCP gel analyses[206]. Our criterion for a "common" polymorphism was frequency greater than five percent in the initial screening cohort. This screening strategy identified 11 SNPs in *Arntl* and *Arntl2* that were chosen for further characterization (Table V-1). Of these 11 SNPs, three were novel variants in *Arntl* and three others were unreported variants in *Arntl2* (Table V-1). Not only did our SSCP method reveal these six novel polymorphisms in the *Arntl* and *Arntl2* genes, it also revealed one new SNP in *Clock* and three new SNPs in *Per2* in the amplicons designed to uncover the previously reported SNPs (Table V-1). Two previously reported SNPs in *Per2* and *Per3* for which rs# have not been assigned are referred herein as c.1984A>G[96] and c.2460A>G[100] (see Table V-1 for the location of all SNPs discussed in this paper along with the primer pairs we used).

Among the *Arntl* SNPs, ss95215855 was the only variant found exclusively in the EA population (Table V-2 and Fig. V-1). The other two SNPs in *Arntl* were both intronic (Table V-1) and occurred in non-EA populations at low frequency (Table V-2, Fig. V-1). We screened eight polymorphisms in the *Arntl2* gene in the EA population (Tables V-1 and V-2, Fig. V-1), of which five were polymorphic in all populations (Table V-2). The first (rs5797225) was a TTG repeat in the 5' region that is likely to act as promoter of *Arntl2*. This polymorphism consisted of either 7, 8, 9, or 10 TTG repeats, with the 8 or 9 repeat structure being most common in all populations (Table V-2, Fig. V-1). The next two polymorphisms (rs7137588 and rs11048972) were within 19-bp of

Table V-1. | **Variants discussed in this study with details as indicated.**

Gene	*Location*	*Genomic size (bp)*	*Chromosomal position*	*SNPs (nomenclature)*	*SNPs (SNPdb b.130)*	*Placement*	*Base Change*	*Protein Change*	*genomic seq*	*coding seq*	*flanking seq*	*Primers (forward and reverse, 5'-3')*	*Ref.*
Arntl	11p15.2	109 487	13286395	g.30475T>G	ss95215854	intronic	T>G	n/a	ENSG00000133794		catg**t**ttaa	GTGGTGAGAAATGGTCAC	
-602550												CATGCTAACAATGCTCAG	
			13288144	c.-173A>C	ss95215855	5'UTR	A>C	n/a	ENSG00000133794	ENST00000256172	CCCA**A**GCTT	GTCCAATGGATTTAAAGGAC	
												CTGGTAACCTCCACAGA	
			13335041	c.180-137G>A	ss95215856	intronic	G>A	n/a	ENSG00000133794	ENST00000256172	cact**g**tgtc	CAGACAAAGATGACCCTC	
												CCTTGGTGTTCTGTATATTC	
Arntl2	12p11.23	87 478	27374970	rs5797225	rs5797225	promoter	-/TTG	n/a			gttg**ttg**ttgt	CCTGGCTTCTGTGTTATTTA	
												GTCCTTTTAGCATTCTGCT	
			27375106	rs7137588	rs7137588	promoter	G>C	n/a			cgtg**g**ttcc	ATCTAAGTGGCTTTAGGG	
			27375125	rs11048972	rs11048972	promoter	A>G	n/a			atgg**a**caaa	TCATTGCTAAGTACTCAGG	
			27375128	c.-2145A>G	ss95215857	promoter	A>G	n/a	ENSG00000029153		acaa**a**ggag		
			27375878	rs10548381	rs10548381	promoter	-/CTA	n/a			ttct**cta**ctaa	CATCTCTGAACTTCTGTTTC	
												CTTGGCTTTCCAGACAAG	
			27420486	rs4964059	rs4964059	intronic	A>C	n/a			ctct**a**tcaa	GGAGAATGGTTCATGTAGAC	
			27420525	c.201-21T>C	ss95215858	intronic	T>C	n/a	ENSG00000029153	ENST00000261178	gata**ttt**ta	ACTCACCATGTACCATCTC	
			27464992	g.87738A>G	ss95215859	3' flanking	A>G	n/a	ENSG00000029153	ENST00000261178	aaata**t**ttc	CTTCCTGTCACAGGGATG	
								n/a				GCCAAAACAATATGTAAG	
Clock	4q12	114 337	55996126	rs1801260	rs1801260	3'UTR	T>C	n/a			GGCA**T**AGCC	TCCAGCAGTTTCATGAGATGC	Katzenberg et al. (1998)
-601851			55996140	*227A>G	ss95215860	3'UTR	A>G	n/a	ENSG00000134852	ENST00000381325	TGAC**A**GTGT	GAGGTCATTTCATAGCTGAGC	
Per2	2q37.3	44 406	238830546	c.1902-80G>T	ss95215861	intronic	G>T	n/a	ENSG00000132326	ENST00000254657	tatg**g**gcac	GGCACTTGGGTGTCGGTTTCTC	Shiino et al. (2003)
-603426			238830402	rs2304669	rs2304669	exonic	A>G	syn			TGGC**A**CTGC	CCCCTATCGGGCTATGGTGGA	
			238830383	c.1984A>G	c.1984A>G	exonic	A>G	S>G	ENSG00000132326	ENST00000254657	AGAG**A**GTGT		
			238830376	c.1991C>T	ss95215862	exonic	C>T	A>V	ENSG00000132326	ENST00000254657	GTGG**C**GTCG		
			238830375	rs2304670	rs2304670	exonic	G>A	syn			TGGC**G**TCGC		
			238830372	rs2304671	rs2304671	exonic	G>A	syn			CGTC**G**CTCA		
			238830273	c.2186+29C>T	ss95215863	intronic	C>T	n/a	ENSG00000132326	ENST00000254657	gaga**g**cagt		
Per3	1p36.23	60 853	7792555	rs35426314	rs35426314	exonic	G>A	V>M			GAGC**G**TGTC	ATGATTCTAGATGAGCTCTGCGGTGG	Ebisawa et al. (2001)
-603427			7792635	rs228669	rs228669	exonic	T>C	syn			CCAG**T**GGGC	GAACCGAGGTAGTACAGAAAACACGATG	
			7809991	rs35733104	rs35733104	exonic	C>T	syn			CTTA**C**CTCG	ACCTCGAGCCCGACCTTCCCACCTG	
			7810060	c.2460A>G	c.2460A>G	exonic	A>G	syn	AB047532	ENST00000361923	CTGC**A**CCGG	CAAAAACGATGGCGACAACAGAGGACA	
			7810080	rs228696	rs228696	exonic	T>C	L>P			GGGC**T**GCCC		
			7810086	rs35899625	rs35899625	exonic	T>G	L>W			CCC**TT**GTCC		
			7810166	rs228697	rs228697	exonic	C>G	P>A			CCCC**C**CTGT		
			7810192	rs17031614	rs17031614	exonic	G>A	syn			CATC**G**TTTT		
			del(3031-3084nt)	AB047536	AB047536	exonic	VNTR	-18aa				GAAGATTAAAGTGTCTTTTCATGTGCCCTTAC	Ebisawa et al. (2001)
												AATGTCTGGCATTGGAGTTTGAAACATTAG	
			7819720	rs10462021	rs10462021	exonic	A>G	H>R			TCTC**A**TGGG	CGGGAAAAGAACCCTGTGTCTTATTCAG	Ebisawa et al. (2001)
												CTACCTGGCCAAAATACATGAGTATATGAC	
AANAT	17q25.1	2 549	71974704	rs3760138	rs3760138	intronic	G>T	n/a			GTGT**G**AGCT	CTCTGCAGGGGGTCAAAAG	
-600950			71974983	rs4238989	rs4238989	intronic	C>G	n/a			TGGG**C**TTGT	CATCTCTAATCCCTGCTCTGTCAC	

NOTE: SNPs are identified by either rs or ss number with the exception of two SNPs, one in Per2 (c.1984A>G) and the other in Per3 (c.2460A>G), which were labeled by the convention described in[213]. Previously unreported single nucleotide polymorphisms (SNPs) are referred to by "ss" numbers; these have been submitted to dbSNP and will be publicly available as rs numbers in Build 130. OMIM references for each gene are shown below the gene names. Chromosomal locations are based on the NCBI Build 36.1 for the human genome (release date March 2006).

each other in the *Arntl2* promoter region and were variable in all populations (Table V-2, Fig. V-1). One other common SNP occurs within the putative promoter of *Arntl2* (rs10548381) and another SNP (rs4964059) occurs in the intron between exons 2 and 3 (ss95215857, ss95215858, and ss95215859 do not appear in Table V-2 because they are very rare). One of the SNPs in *Arntl2* departed from HWE at the $p < 0.05$ level (rs4964059) and two SNPs departed from HWE at the $p < 0.01$ level (rs10548381 and ss95215857, Table V-2). Each of these departures was limited to a single population, and for two of these three the populations may represent either recent admixture among distinct populations (rs10548381 in African Americans) or stratification (rs4964059 in PNG).

Table V-2. | **Allele frequencies of polymorphisms in all populations with deviations from Hardy-Weinberg Equilibrium (HWE).**

Gene	*Allele*	*African American*	*European American*	*Ghanaian African*	*Han Chinese*	*Papua New Guinea*
Arntl						
ss95215854	T	1	0.99	0.93	1	1
ss95215855	A	1	0.97	1	1	1
ss95215856	G	0.98	0.99	0.98	0.99	0.96
Arntl2						
rs5797225	GTT (7)	0.01	-	-	-	-
	GTT (8)	0.49	0.71	0.51	0.48	0.71
	GTT (9)	0.5	0.29	0.46	0.51	0.28
	GTT (10)	-	-	0.03	0.01	0.01
rs7137588	G	0.86	0.73	0.87	0.93	0.75
rs11048972	A	0.98	0.94	0.87	0.98	1
ss95215857	A	1	0.96**	1	1	1
rs10548381	+/CTA	0.93*	0.9	0.98	0.98	0.99
rs4964059	A	0.91	0.67	0.88	0.43	0.43*
ss95215858	T	0.99	1	1	1	1
ss95215859	A	1	1	1	1	1
Clock						
rs1801260	T	0.86	0.74*	0.83	0.92	0.83
ss95215860	A	1	1	1	1	0.96
Per2						
rs2304669	A	0.97	0.87	0.99	0.94	0.94
c.1984A>G	A	1	1	1	1	1
ss95215862	C	N/A	1	N/A	N/A	N/A
rs2304670	G	0.9	0.93	0.87	0.94	1
rs2304671	G	0.96	0.93	0.96	0.89	1
Per3						
rs35426314	G	1	1	1	1	1
rs228669	C	0.96**	0.97	0.99	0.99	1
rs35733104	C	1	1	1	1	1
c.2460A>G	A	1	1	1	1	1
rs228696	C	0.95*	0.97	0.98	1	1
rs228697	C	0.98	0.99	1	0.95	0.83
rs17031614	G	1	1	1	1	1
AB047536	4-repeat	0.59	0.66	0.64	0.81**	0.41
rs10462021	A	0.93	0.83	0.96	1	0.98
AANAT						
rs4238989	G	0.74	0.53	0.87	0.53	0.51

*Deviation from HWE at $p < 0.05$

**Deviation from HWE at $p < 0.01$

N/A indicates that the marker was not genotyped for that population.

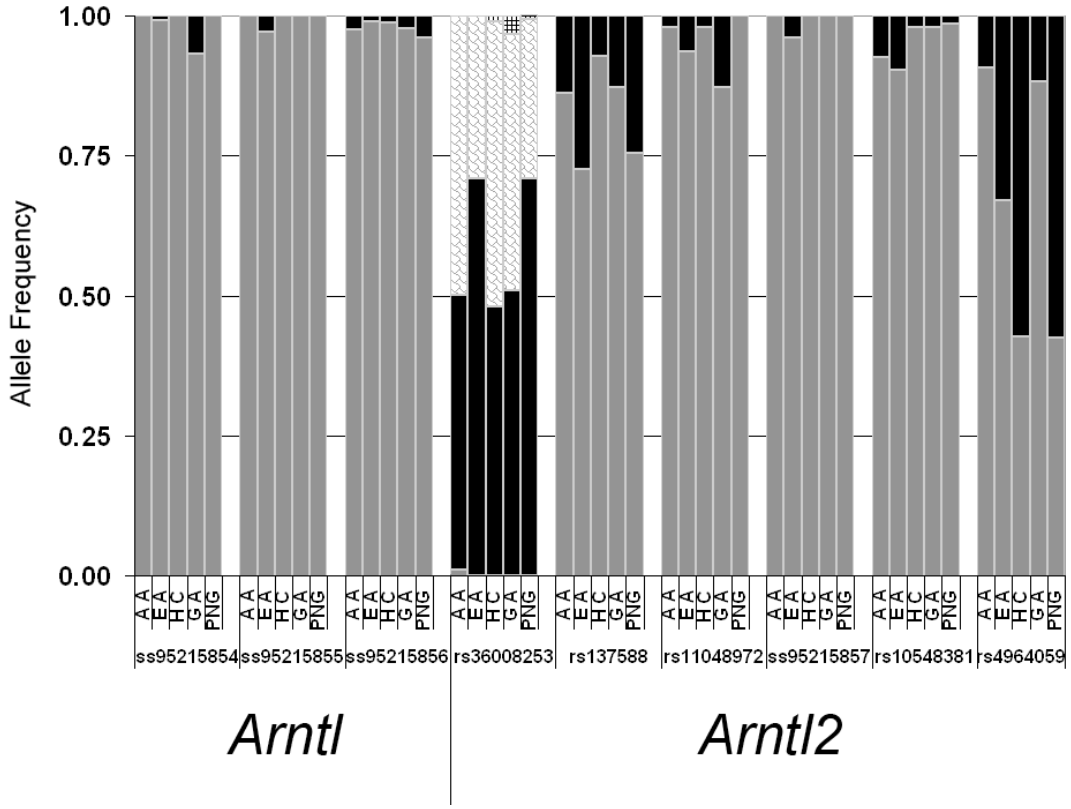

Figure V-1. | **Histogram plots of *Arntl* and *Arntl2* SNPs across five populations** (AA = African American, EA = European Americans, HC = Han Chinese, GA = Ghana Africans, and PNG = Papua New Guineans). Gray is the common allele, black is the less common.

Population analyses of Arntl*,* Arntl2*,* Clock*,* Per2*,* Per3*, and* AANAT *genes*.

We also analyzed previously reported SNPs in the central clock genes *Clock*, *Per2*, and *Per3*, and in the *AANAT* gene that encodes the rate-limiting enzyme of melatonin biosynthesis (Table V-1). Our rationale for including these SNPs in the study was three-fold. The first was to compare our systematic analyses with that of the only previous population genetic study of a clock gene SNP, namely of the VNTR SNP in *Per3*[202]. The second reason for studying these previously reported SNPs is that many of them have been reported to have functional significance. Finally, our third rationale was that many of them are sufficiently common in human populations that they might have some value in explaining common syndromes that might be associated with clock gene polymorphisms (in contrast, while the SNPs in *Per2* and *CKI*δ have potent effects upon the timing of sleep and activity[96, 97], they are so uncommon that

they are unlikely to have any real explanatory power for disorders in the general population). We again used the SSCP method to assess the frequency of these SNPs by designing primers to amplify ~200 bp amplicons around the reported SNPs. We then sequenced representatives of every different SSCP pattern we observed for every amplicon. This method was successful in identifying the reported SNPs and in addition, we discovered novel SNPs in *Clock* and *Per2* within these amplicons (Table V-1).

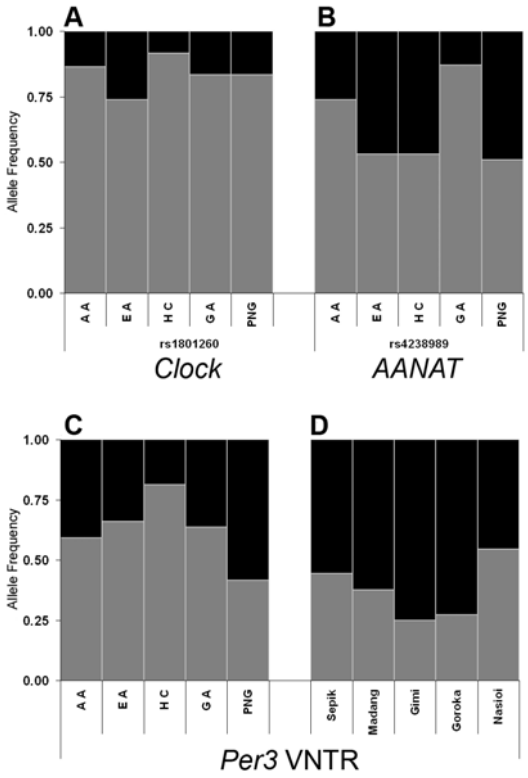

Figure V-2. | **Proportion plots of allele frequency** in **a** | *hClock* (rs1801260), **b** | *hAANAT* (rs4238989), **c** | and *hPer3* (AB047536) across five populations (AA = African American, EA = European Americans, HC = Han Chinese, GA = Ghana Africans and PNG = Papua New Guineans). Gray is the common allele, black is the less common. **d** | Proportion of the VNTR SNP of *Per3* in five Papua New Guinea subpopulations. Gray is the 4-repeat and black is the 5-repeat. VNTR = variable number of tandem repeats; SNP = single nucleotide polymorphism.

SNPs rs1801260 (in *Clock*) and rs4238989 (in *AANAT*) were polymorphic in all populations we studied (Table V-2 and Fig. V-2a-b). SNP ss95215860 in *Clock,* a previously unreported SNP we identified in the PNG population was unique to PNG (Table V-2). The c.1984A>G SNP in *Per2*

that is associated with FASPS[96] was not detected in any of our populations (Table V-2). In the process of SSCP screening for c.1984A>G, however, we identified other *Per2* SNPs, including three novel SNPs, ss95215861, ss95215862, and ss95215863 with extremely low frequencies (<0.01), and three SNPs that have been previously identified (rs2304669, rs2304670, and rs2304671) (Table V-2). For most of the SNPs in *Per3*, there was a low but detectable frequency of polymorphisms in our populations (Table V-2). The most polymorphic of the *Per3* variants was the VNTR repeat (AB047536) that has been associated with delayed sleep phase syndrome and sleep structure dysfunction[100, 198] and that has been reported to exhibit significantly different allelic frequencies among populations[202]. This polymorphism is a four or five tandem repeat of a 54 bp sequence in exon 18 of *Per3*. We confirm that the 4-repeat allele is the most common in all populations except for the PNG population, where the 5-repeat is most common (Table V-2, Fig. V-2c). The 5-repeat is least common in the Han Chinese population (19%), and is approximately the same (34-41%) in the EA, African-American, and Ghanaian populations.

Deviation from Hardy/Weinberg Equilibrium (HWE) for all the SNPs of sufficient frequency are indicated in Table V-2 (four SNPs were present in such low frequency that they were not studied further: ss95215861, ss95215863, rs35899625, and rs3760138). Including the *Arntl2* SNPs that were out of HWE as noted above, there were two loci that deviated from HWE in the EA population, one of which had a nominal *p*-value < 0.01 (Table V-2). In the Han Chinese and Papua New Guinea populations there was one SNP in each that deviated from HWE; however, only the SNP in the Han population deviated with a nominal $p < 0.01$. In African-Americans there were three SNPs that deviated from HWE, two of which had a nominal *p*-value ($p < 0.01$). None of these appears significant in the context of multiple tests. There were significant allele and genotype differences between many of the populations we compared (Tables V-3 and V-4). The populations that differed the most in both allelic and genotypic distributions were European

Table V-3. | **Allele Frequency Differences (*p*-values listed).**

Gene	*AA vs EA*	*AA vs GA*	*AA vs HC*	*AA vs PNG*	*EA vs GA*	*EA vs HC*	*EA vs PNG*	*GA vs HC*	*GA vs PNG*	*HC vs PNG*
Arntl										
ss95215854	1	0.012	N/A	N/A	0.001	1	0.579	0.038	<0.001	N/A
ss95215855	0.098	N/A	N/A	N/A	0.094	0.092	0.014	N/A	N/A	N/A
ss95215856	0.271	0.618	0.241	0.708	0.068	0.606	0.004	0.246	0.458	0.242
Arntl2										
rs5797225	<0.001	0.263	0.97	0.001	<0.001	<0.001	0.168	0.442	0.003	0.001
rs7137588	0.004	0.682	0.107	0.045	0.001	<0.001	0.526	0.238	0.018	0.001
rs11048972	0.117	0.01	0.623	0.172	0.033	0.062	<0.001	0.001	<0.001	0.163
ss95215857	0.041	N/A	N/A	N/A	0.04	0.041	0.003	N/A	N/A	N/A
rs10548381	0.588	0.085	0.095	0.036	0.007	0.007	0.001	0.617	0.648	0.638
rs4964059	<0.001	0.486	<0.001	<0.001	<0.001	<0.001	<0.001	<0.001	<0.001	0.884
ss95215858	0.103	1	1	0.418	N/A	N/A	N/A	N/A	N/A	N/A
ss95215859	1	N/A	N/A	N/A	1	1	0.131	N/A	N/A	N/A
Clock										
rs1801260	0.006	0.687	0.164	0.566	0.034	<0.001	0.012	0.128	0.86	0.078
ss95215860	1	N/A	N/A	0.074	1	1	<0.001	N/A	0.072	0.073
Per2										
rs2304669	0.001	0.351	0.175	0.217	<0.001	0.064	0.02	0.12	0.033	0.781
c.1984A>G	1	N/A	N/A	N/A	1	1	0.138	N/A	N/A	N/A
rs2304670	0.221	0.508	0.423	<0.001	0.062	0.688	<0.001	0.126	<0.001	0.005
rs2304671	0.307	0.721	0.105	0.031	0.385	0.125	<0.001	0.111	0.027	<0.001
Per3										
rs228669	0.534	0.061	0.203	0.035	0.36	0.33	0.037	1	0.431	0.428
c.2460A>G	0.19	N/A	N/A	N/A	0.195	0.202	1	N/A	N/A	N/A
rs228696	0.196	0.27	0.03	0.014	1	0.159	0.057	0.234	0.177	N/A
rs228697	0.079	0.498	0.462	<0.001	0.579	0.007	<0.001	0.06	<0.001	0.01
rs17031614	1	N/A	N/A	N/A	1	1	0.129	N/A	N/A	N/A
AB047536	0.291	0.517	0.001	0.016	0.743	0.002	<0.001	0.004	0.001	<0.001
rs10462021	0.008	0.534	0.01	0.172	<0.001	<0.001	<0.001	0.118	0.243	0.268
AANAT										
rs4238989	0.001	0.02	0.003	0.002	<0.001	0.902	0.664	<0.001	<0.001	0.674

AA = African American, EA = European American, GA = Ghanaian African, HC = Han Chinese, PNG = Papua New Guinea
N/A indicates test was not performed because marker was fixed for the same allele in all populations.

Table V-4. | **Genotype Frequency Differences (*p*-values listed).**

Gene	*AA vs EA*	*AA vs GA*	*AA vs HC*	*AA vs PNG*	*EA vs GA*	*EA vs HC*	*EA vs PNG*	*GA vs HC*	*GA vs PNG*	*HC vs PNG*
Arntl										
ss95215854	1	0.017	N/A	N/A	<0.001	0.426	0.241	0.026	<0.001	N/A
ss95215855	0.058	N/A	N/A	N/A	0.154	0.166	0.012	N/A	N/A	N/A
ss95215856	0.259	1	0.602	0.455	0.245	0.605	0.019	0.58	0.451	0.232
Arntl2										
rs5797225	<0.001	0.665	0.903	0.001	<0.001	<0.001	0.083	0.864	0.004	0.001
rs7137588	0.009	0.893	0.251	0.182	0.004	<0.001	0.362	0.391	0.146	0.003
rs11048972	0.1	0.014	1	0.165	0.017	0.062	<0.001	0.009	<0.001	0.169
ss95215857	0.134	N/A	N/A	N/A	0.153	0.148	0.063	N/A	N/A	N/A
rs10548381	0.031	0.55	0.364	0.198	0.04	0.027	0.003	1	0.641	1
rs4964059	<0.001	0.596	<0.001	<0.001	<0.001	<0.001	<0.001	<0.001	<0.001	0.607
ss95215858	0.102	1	1	N/A	N/A	N/A	N/A	N/A	N/A	N/A
ss95215859	1	N/A	N/A	N/A	1	1	0.127	N/A	N/A	N/A
Clock										
rs1801260	0.035	0.334	0.45	0.169	0.046	<0.001	0.011	0.015	0.839	0.011
ss95215860	0.197	N/A	N/A	0.418	0.199	0.194	<0.001	N/A	0.071	0.071
Per2										
rs2304669	0.01	0.614	0.469	0.354	0.001	0.199	0.073	0.116	0.03	1
c.1984A>G	1	N/A	N/A	N/A	1	1	0.132	N/A	N/A	N/A
rs2304670	0.238	0.786	0.603	<0.001	0.077	0.864	<0.001	0.206	<0.001	0.005
rs2304671	0.488	1	0.087	0.028	0.499	0.182	<0.001	0.098	0.026	<0.001
Per3										
rs228669	0.121	0.622	1	0.074	0.344	0.326	0.012	1	0.463	0.412
c.2460A>G	0.193	N/A	N/A	N/A	0.188	0.205	0.245	N/A	N/A	N/A
rs228696	0.113	1	0.115	0.032	0.717	0.065	0.093	0.245	0.18	N/A
rs228697	0.073	0.526	0.419	0.002	1	0.001	<0.001	0.054	<0.001	0.042
rs17031614	1	N/A	N/A	N/A	1	1	0.127	N/A	N/A	N/A
AB047536	0.38	0.386	<0.001	0.044	0.521	<0.001	<0.001	0.015	0.003	<0.001
rs10462021	0.013	0.841	0.019	0.309	0.002	<0.001	<0.001	0.122	0.449	0.258
AANAT										
rs4238989	0.006	0.125	0.02	0.009	<0.001	0.926	0.835	<0.001	<0.001	0.734

AA = African American, EA = European American, GA = Ghanaian African, HC = Han Chinese, PNG = Papua New Guinea
N/A indicates test was not performed because marker was fixed for the same allele in all populations.

Americans as compared with Ghanaians. In comparisons of these two populations, the common variant was more frequent in EA (except for the rs10462021 SNP in *Per3*). As expected, there were few allelic or genotypic differences between Ghanaians and African-Americans (Tables V-3 and V-4).

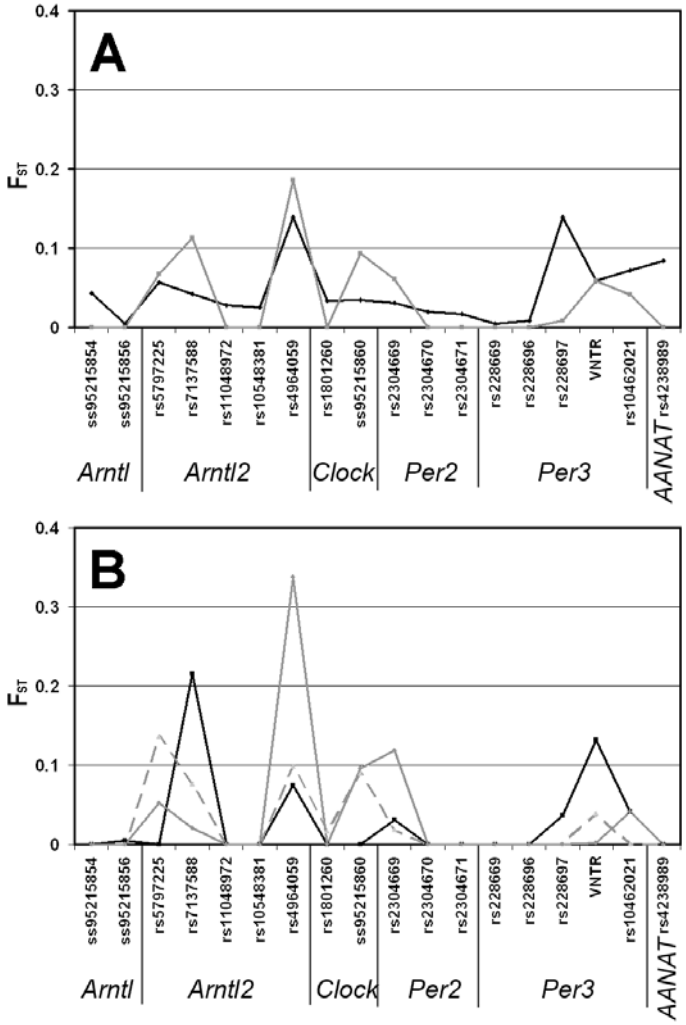

Figure V-3. | **F_{ST} values for SNPs (theta P).** Two comparisons are shown—the 5 populations together (panel **a**) and the PNG subpopulations (panel **b**). In panel **a**, the black line is an average FST across all populations with all PNG subpopulations combined into 1; the gray line is the F_{ST} across all PNG subpopulations compared simultaneously. Panel B is the pairwise comparison of PNG subpopulations. Black solid traces are EH vs. NA, dashed traces are EH vs. Coastal, gray solid traces are NA vs. Coastal. EH = Eastern Highlands population (Gimi and Goroka pooled); NA = Nasioi (Bougainville); and Coastal = Sepik and Madang pooled. SNP = single nucleotide polymorphism; PNG = Papua New Guinean.

Loci were excluded from haplotype and F_{ST} analyses if four or more populations had only one of the two alleles. Haplotypes for *Arntl2*, *Per2*, and *Per3* differ in frequency among the populations (Tables V-5 and V-6). In particular, for *Arntl2* the comparisons revealed significant differences ($p < 0.001$) for all of the population comparisons except when comparing Ghanaians to African-Americans. There were also significant differences in haplotype comparisons when comparing PNG to the other populations (Tables V-5 and V-6). F_{ST} averaged across all five populations was below 0.1 for all polymorphisms (Table V-7 & Fig. V-3a, black trace), with the exception of *Arntl2* (rs4964059) and *Per3* (rs228697) ($F_{ST} = 0.139$ for both SNPs). Comparing the PNG subpopulations among each other shows two SNPs (rs7137588 and rs4964059 in *Arntl2*) for which F_{ST} exceeds 0.1 and one that nearly exceeds 0.1 (ss95215860 in *Clock*), indicating greater genetic differentiation among PNG populations than across the global samples (Fig. V-3a, gray trace).

Table V-5. | **Haplotype frequencies across five populations.**

Haplotype	*African American*	*European American*	*Ghanaian African*	*Han Chinese*	*Papua New Guinea*
Arntl					
T-G	0.98	0.98	0.92	0.99	0.96
G-G	N/A	0.01	0.06	N/A	N/A
Arntl2					
8-G-A-+-A	0.47	0.56	0.49	0.38	0.39
8-G-A-+-C	N/A	<0.01	N/A	0.03	0.07
8-C-A-+-C	0.02	0.11	N/A	0.04	0.22
9-G-A-+-A	0.34	0.07	0.36	0.02	0.02
9-G-A-+-C	0.02	0.05	0.02	0.48	0.26
9-C-A-+-C	0.04	0.06	N/A	0.01	0.01
9-C-G---C	0.01	0.05	N/A	<0.01	N/A
Per2					
A-A-G	0.1	0.07	0.11	0.05	N/A
A-G-A	0.04	0.07	0.03	0.1	N/A
A-G-G	0.82	0.73	0.83	0.78	0.94
G-G-G	0.03	0.13	0.01	0.06	0.06
Per3					
C-C-C-4-A	0.52	0.48	0.59	0.76	0.29
C-C-C-4-G	0.07	0.16	0.04	N/A	0.02
C-C-G-4-A	0.02	0.01	N/A	0.05	0.1
C-C-C-5-A	0.33	0.3	0.34	0.18	0.52
C-C-G-5-A	N/A	N/A	N/A	<0.01	0.06

Order of SNPs for each haplotype is as follows:
Arntl: (ss95215854/ss95215856)
Arntl2: (rs5797225/rs7137588/rs11048972/rs10548381/rs4964059)
Per2: (rs2304669/rs2304670/rs2304671)
Per3: (rs228669/rs228696/rs228697/AB047536/rs10462021)
N/A indicates that the haplotype was not present in that population.

Table V-6. | **Haplotype trend regression (*p*-values listed).**

Haplotype	*AA vs EA*	*AA vs GA*	*AA vs HC*	*AA vs PNG*	*EA vs GA*	*EA vs HC*	*EA vs PNG*	*GA vs HC*	*GA vs PNG*	*HC vs PNG*
Arntl (2 SNPs)	0.84	0.044	0.309	0.474	0.001	0.714	0.099	0.062	0.171	0.123
Arntl2 (5 SNPs)	<0.001	0.795	<0.001	<0.001	<0.001	<0.001	<0.001	<0.001	<0.001	<0.001
Per2 (3 SNPs)	0.04	0.876	0.099	0.006	0.006	0.105	<0.001	0.024	0.011	<0.001
Per3 (5 SNPs)	0.07	0.27	0.006	<0.001	0.005	<0.001	<0.001	0.061	<0.001	<0.001

AA = African American, EA = European American, GA = Ghanaian African, HC = Han Chinese, PNG = Papua New Guinea
Order of SNPs for each haplotype is as follows:
Arntl: ss95215854/ss95215856
Arntl2: rs5797225/rs7137588/rs11048972/rs10548381/rs4964059
Per2: rs2304669/rs2304670/rs2304671
Per3: rs228669/rs228696/rs228697/AB047536/rs10462021

Table V-7. | **F_{ST} values (theta P) for the five populations together and for the PNG subpopulations.**

Gene	*FST*	*FST (PNG only)*
Arntl		
ss95215854	0.043	N/A
ss95215855	0.013	N/A
ss95215856	0.005	0
Arntl2		
rs5797225	0.057	0.067
rs7137588	0.042	0.113
rs11048972	0.028	N/A
ss95215857	0.02	N/A
rs10548381	0.025	0
rs4964059	0.139	0.186
ss95215858	0.012	N/A
ss95215859	0	N/A
Clock		
rs1801260	0.034	0
ss95215860	0.035	0.093
Per2		
rs2304669	0.031	0.061
c.1984A>G	0	N/A
rs2304670	0.02	N/A
rs2304671	0.017	N/A
Per3		
rs228669	0.005	N/A
c.2460A>G	0	N/A
rs228696	0.008	N/A
rs228697	0.139	0.008
rs17031614	0	N/A
AB047536	0.059	0.059
rs10462021	0.072	0.041
AANAT		
rs4238989	0.084	0

N/A indicates test was not performed because marker was fixed for the same allele in all populations.

Stratification within the PNG sub-populations.

Nadkarni and coworkers[202] reported that the VNTR polymorphism of *Per3* (AB047536) exhibited significantly different allelic frequencies in PNG (0.19), as compared to East Asians (0.80-0.89) and European/American/African populations (intermediate frequencies of 0.6~0.7). However, PNG populations can be very diverse genetically[212], and the previous study did not give the origin(s) of its PNG study population. We therefore performed our analyses using 3 populations within Papua New Guinea (Sepik/Madang, Gimi, and Goroka) and one population from the nearby island of Bougainville (Nasioi). We found that there is very significant variation of clock gene polymorphisms among the PNG sub-populations. For example, the 4-repeat variant of VNTR ranged in allele frequency from 25% (Gimi) to 54% (Nasioi) (Fig. V-2d). This result implies that Nadkarni and coworkers[202] might have studied a distinct sub-population within PNG and that their results might not be reflective of PNG populations in general. The VNTR was not the only polymorphism that showed significant variation among PNG subpopulations, as implied by the allele frequencies and F_{ST} values for PNG (Fig. V-3a and Tables V-7-8) and as is more explicity shown by the F_{ST} comparisons among the PNG sub-populations (Fig. V-3b and Table V-9, including pairwise comparisons between the PNG population and the other populations, Table V-10). There are numerous F_{ST} values greater than 0.10 when the PNG sub-populations are compared, e.g., in the rs5797225, rs7137588, rs4964059, rs2304669, and VNTR polymorphisms. In fact, the F_{ST} values for most of those SNPs exceed that of the VNTR polymorphism when compared among the PNG sub-populations (F_{ST} is only greater than 0.1 for the VNTR polymorphism when the Eastern Highlands sub-population is compared with the Nasioi sub-population, Table V-9). These data support the idea that genetic differentiation among the PNG populations is greater than that across much of the rest of the world.

Table V-8. | **Allele frequencies for all polymorphisms in the Papua New Guinea (PNG) sub-populations with deviations from Hardy/Weinberg Equilibrium (HWE).**

Gene	*Allele*	*Eastern Highlands*	*Nasioi*	*Coastal*
Arntl				
ss95215854	T	1	1	1
ss95215855	A	1	1	1
ss95215856	G	0.93	0.98	0.98
Arntl2				
rs5797225	GTT (7) GTT (8)	-0.83	-0.74	-0.57**
	GTT (9)	0.17	0.24	0.43
	GTT (10)	-	0.02	-
rs7137588	G	0.57	0.89	0.78
rs11048972	A	1	1	1
ss95215857	A	1	1	1
rs10548381	+	1	0.98	0.98
rs4964059	C	0.57	0.35	0.8
ss95215858	T	1	1	1
ss95215859	A	1	1	1
Clock				
rs1801260	T	0.88	0.85	0.77
ss95215860	A	1	1	0.89
Per2				
rs2304669	A	0.95	1	0.86
c.1984A>G	A	1	1	1
rs2304670	G	1	1	1
rs2304671	G	1	1	1
Per3				
rs35426314	G	1	1	1
rs228669	C	1	1	1
rs35733104	C	1	1	1
c.2460A>G	A	1	1	1
rs228696	C	1	1	1
rs228697	C	0.76	0.89	0.84**
rs17031614	G	1	1	1
AB047536	5-repeat	0.74	0.46	0.57
rs10462021	A	1	0.93	1

*indicates deviation from HWE at $p < 0.05$; **indicates deviation from HWE at $p < 0.01$

Eastern Highlands = Gimi and Goroka
Nasioi = Bouganville
Coastal = Sepik and Madang

Table V-9. |. **F_{ST} values for clock gene SNPs among the PNG populations.**

Gene	*EH vs NA*	*EH vs Coastal*	*NA vs Coastal*
Arntl			
ss95215856	0.005	0	0
Arntl2			
rs5797225	0	0.136	0.052
rs7137588	0.216	0.077	0.021
rs10548381	0	0	0
rs4964059	0.075	0.099	0.337
Clock			
rs1801260	0	0.017	0
ss95215860	N/A	0.09	0.096
Per2			
rs2304669	0.031	0.019	0.119
Per3			
rs228697	0.036	0	0
AB047536	0.132	0.039	0.002
rs10462021	0.041	N/A	0.041
AANAT			
rs4238989	0	0	0

N/A indicates test was not performed because marker was fixed for the same allele in all populations.

Eastern Highlands = Gimi and Goroka

Nasioi = Bouganville

Coastal = Sepik and Madang

Table V-10. | **F_{ST} values (theta P) for all pair-wise combinations of populations.**

Gene	*AA vs EA*	*AA vs GA*	*AA vs HC*	*AA vs PNG*	*EA vs GA*	*EA vs HC*	*EA vs PNG*	*GA vs HC*	*GA vs PNG*	*HC vs PNG*
Arntl										
ss95215854	0	0.06	N/A	N/A	0.11	0	0	0.049	0.074	N/A
ss95215855	0.012	N/A	N/A	N/A	0.011	0.011	0.013	N/A	N/A	N/A
ss95215856	0	0	0	0	0.001	0	0.027	0	0	0.007
Arntl2										
rs5797225	0.092	0	0	0.086	0.068	0.101	0	0	0.062	0.095
rs7137588	0.041	0	0.012	0.027	0.048	0.094	0	0.006	0.035	0.091
rs11048972	0.01	0.069	0	0.017	0.025	0.011	0.034	0.07	0.143	0.016
ss95215857	0.017	N/A	N/A	N/A	0.017	0.017	0.02	N/A	N/A	N/A
rs10548381	0	0.02	0.021	0.037	0.029	0.029	0.037	0	0	0
rs4964059	0.115	0	0.404	0.389	0.094	0.11	0.112	0.366	0.354	0
ss95215858	0.043	0	0	0.004	N/A	N/A	N/A	N/A	N/A	N/A
ss95215859	0	N/A	N/A	N/A	0	0	0	N/A	N/A	N/A
Clock										
rs1801260	0.036	0	0.003	0	0.018	0.076	0.02	0.021	0	0.021
ss95215860	0	N/A	N/A	0.024	0	0	0.078	N/A	0.024	0.024
Per2										
rs2304669	0.039	0	0	0.001	0.058	0.015	0.017	0.025	0.023	0
c.1984A>G	0	N/A	N/A	N/A	0	0	0	N/A	N/A	N/A
ss95215862	1	N/A	N/A	N/A	1	1	1	N/A	N/A	N/A
rs2304670	0.001	0	0.001	0.112	0.018	0	0.04	0.018	0.15	0.064
rs2304671	0.001	0	0.026	0.04	0	0.007	0.039	0.022	0.045	0.124
Per3										
rs228669	0	0.009	0.008	0.04	0.001	0.001	0.013	0	0.003	0.003
c.2460A>G	0	N/A	N/A	N/A	0	0	0	N/A	N/A	N/A
rs228696	0.006	0.002	0.042	0.051	0	0.009	0.011	0.012	0.016	N/A
rs228697	0	0.01	0.003	0.1	0	0.056	0.313	0.041	0.139	0.053
rs17031614	0	N/A	N/A	N/A	0	0	0	N/A	N/A	N/A
AB047536	0.002	0	0.102	0.05	0	0.048	0.108	0.066	0.083	0.27
rs10462021	0.032	0	0.063	0.017	0.057	0.101	0.078	0.032	0	0.011
AANAT										
rs4238989	0.075	0.044	0.076	0.094	0.206	0	0	0.23	0.246	0

AA = African American, EA = European American, GA = Ghanaian African, HC = Han Chinese, PNG = Papua New Guinea
N/A indicates test was not performed because marker was fixed for the same allele in all populations.

Section 5.5: Discussion

The function of biological clocks is to provide temporal information to the organism so that physiological and/or behavioral responses can be coordinated during the daily cycle to maximize adaptiveness. Environmental parameters of relevance to biological clocks include daily fluctuations in light intensity and temperature and seasonal changes in day-length and temperature[14]. These parameters vary dramatically as a function of latitude and locale. Therefore, biological clocks within wide-ranging species may be genetically "tuned" by natural selection to optimize adaptiveness along latitudinal clines or other location-dependent factors. Indeed, *Drosophila melanogaster* exhibits such genetic polymorphisms in circadian clock genes along latitudinal clines[214, 215]. *Homo sapiens* is a species that is distributed to practically every terrestrial niche on earth. Therefore it is of interest to study levels and patterns of variation in human circadian clock genes to assess the evolutionary mechanism that may have shaped these patterns.

Our study is the first systematic report of the frequency distribution of polymorphisms in multiple clock genes. We chose two groups of polymorphisms to study: (i) previously reported polymorphisms of potential functional significance in *Per2*, *Per3*, *Clock*, and *AANAT*, and (ii) polymorphisms in *Arntl* and *Arntl2* identified by a systematic SSCP screen of promoter and exonic regions. This screen revealed several novel polymorphisms in *Arntl* and *Arntl2*. We studied five diverse populations (including subpopulations within Papua New Guinea) from very different latitudes and environments. Significant differences between the populations were found for allelic and genotypic frequencies. For the reported clock gene polymorphisms that also appear in HapMap, our allele frequencies are nearly identical to the HapMap data for most of the assays (Table V-2), confirming the accuracy of the SSCP method. There were 7 out of 145 SNP/population combinations that were out of Hardy Weinberg Equilibrium (HWE)–well within

the range expected for a Type 1 error at the $p < 0.05$ level (7/145 = 4.8%). Moreover, none of the SNPs show more than one population deviating from HWE (Table V-2). Of note, one of these is in the combined PNG population that is probably not a single panmictic population[212], as shown by the large F_{ST} values among the discrete populations.

On the basis of the SNPs for which allelic and genotypic frequency differences could be calculated for all five populations, EA and Ghanaians differed the most. In contrast, there were very few allelic or genotypic differences between the Ghanaian and African-American samples. As expected, haplotype comparisons revealed similar patterns (Tables V-5-6). It is interesting that the most common haplotype for all populations was the same for *Per2* and *Arntl*, but that this was not the case for *Arntl2* and *Per3*. For *Arntl2,* the most common haplotype in the Han population was exceedingly rare in all other populations except PNG, where it was the second most common haplotype. In *Per3,* the most common haplotype in PNG was second most common in all of the other populations (Table V-5).

The PNG population was less different from the EA, African-American, and Ghanaian populations than the EA-Ghanaian difference when the PNG samples were pooled, in contrast to expectations based on the previous report[202]. As might be expected in terms of geographic distance, the PNG population as a whole was most similar to the Han Chinese in terms of individual SNP allele frequencies (Table V-3), but this difference was not as clear from the haplotype analyses. This might indicate a very different history of the PNG founding chromosomes. Upon examining sub-populations within PNG, it became clear that even the VNTR SNP–studied by Nadkarni & coworkers[202] and used to argue that PNG is a genetic outlier–has very different allele frequencies among sub-populations. For example, in the Nasioi sub-population, the VNTR allele frequency is close to that in the non-PNG populations (EA/GA/AA). Therefore, the very low VNTR frequency (19% for the 4-repeat allele) reported by Nadkarni &

coworkers[202] does not reflect PNG as a whole. Moreover, the F_{ST} analyses that compare the three PNG sub-groups indicate much larger F_{ST} values among the PNG sub-groups (Fig. V-3b and Table V-9) than among any of the five global populations (Fig. V-3a and Table V-7). Because it is difficult to imagine that the environment within the PNG region is more heterogeneous than the environments inhabited by EA vs. Han Chinese vs. African-Americans vs. Ghana Africans vs. Papua New Guineans, it is unlikely that the differences in allele frequency we observe are due to natural selection acting in response to environmental pressures. Genetic similarities based on large numbers of autosomal markers place the Nasioi sub-population sample close to the East Asian populations and far from the European and African populations[216]. Some, but not all, of the markers we examined follow this pattern.

Therefore, it seems likely that the differences in the clock gene allele distributions that we have observed are due to genetic drift (e.g., possibly a founders' effect). Most of the genetic heterogeneity among Papua New Guineans has likewise been attributed to genetic drift[212]. In particular, our data do not support selection of clock gene alleles on the basis of latitude/photoperiod, which might be predicted to affect the evolution of circadian clock genes (as in *Drosophila*[214, 215]). Our Ghana and PNG samples are the best defined in terms of latitude and both are close to the equator where the annual photoperiod will be nearly constant at 12 h light/12 h dark (LD 12:12). Nevertheless, the allele frequencies are very different between the Ghana and PNG populations. Our other populations (EA, AA, and HC) are less well defined geographically and have been subject to admixture. Nevertheless, these populations come from latitudes ranging between 22-70°N. At 22°N, the annual photoperiod ranges between LD 13.2:10.8 (summer) and LD 10.4:13.6 (winter), whereas around 60°N photoperiods range between LD 18.4:5.6 (summer) and LD 5.4:18.6 (winter). (At 70°N there is no night in mid-summer and no day in mid-winter.) Therefore, EA and HC populations will experience a broad

range of annual photoperiodic changes and there is no evidence from an EA/HC comparison to GA/PNG to suggest a selective pressure for annual photoperiod. Our analysis is of central clock genes (and of a melatonin synthesis gene); perhaps the central clock mechanism has been mechanistically constrained in humans and has therefore not been subject to natural selection along latitudinal clines (in contrast to the situation in *Drosophila*[214, 215]). However, because the most important input signal for the entrainment of circadian pacemakers is light, it is very possible that the light input pathway has been optimized by natural selection for specific latitudes/photoperiods. Therefore, while we have not found evidence for natural selection acting on central clock genes, our data do not exclude the possibility that genes encoding input pathway components (e.g., melanopsin) will show genetic evidence for natural selection.

Finally, we discovered several new SNPs, including some relatively common polymorphisms in *Arntl* and *Arntl2*. These polymorphisms may affect the expression of these two critical clock genes. For example, because 5'UTR regions are often involved in translational control, the novel ss95215855 SNP of *Arntl* could affect the translational efficiency of *Arntl* mRNA. In addition, common SNPs in the *Arntl2* gene affect regulatory regions such as the promoter (rs5797225, rs7137588, rs11048972, ss95215857, and rs10548381) and intronic regions (rs4964059 and ss95215858). For example, the rs7137588 SNP is in the recognition motif for the EBP-80 transcriptional factor, and therefore this SNP could affect transcriptional regulation of *Arntl2*. In addition to being key components of the central circadian clockwork, the ARNTL/BMAL1 and ARNTL2/BMAL2 transcriptional factors also mediate a large number of output pathways controlled by the clock via E-box containing promoters. Therefore, polymorphisms in the regulatory regions of the *Arntl* and *Arntl2* genes have the potential to affect many clock-regulated output processes.

Our study unveiled significant differentiation among populations for clock gene allele, genotype and haplotype frequencies that can serve as a basis for future association analyses of clock gene polymorphisms with phenotypes of behavioral and/or medical significance. Although it is impossible based on the present data to determine the motivating factors in the patterns of differentiation, it appears unlikely that these differences are due to consistent patterns of natural selection but rather are more likely to be caused by random processes. This conclusion is based on the large scale differences among the Ghana and PNG populations that should have similar photoperiod and temperature regimes as compared to the other populations studied.

Section 5.6: Chapter Acknowledgements:

We thank Matthew Pullen and Kontip C. Mahautmr for technical assistance, the Vanderbilt University DNA Core for DNA storage and sequencing, and Vanderbilt's General Clinical Research Center (supported in part by grant M01 RR-00095 from the National Center for Research Resources, NIH) for DNA isolation and storage. This research was supported by a Discovery Grant from Vanderbilt University, the Vanderbilt Joint Center for Nursing Research, U01 HL065962 (to Dr. Dan Roden), and grants from the National Institute of Mental Health (R01 MH043836 to CHJ and R01 MH063341 to DGM). CMC was supported by T32 and P50 awards from the National Institute of Mental Health (T32 MH064913; P50 MH078028).

CHAPTER VI

SUMMARY

The research in this dissertation was envisioned as a multidisciplinary assessment of circadian clock organization in mammals, emphasizing the molecular and genetic characteristics of rhythms in mice and men. The end result is a far cry from what was expected when the research was originally proposed, and occurred at a pace far faster than anticipated given advances in microscopy techniques and computerized analyses. Despite the unexpected nature of the outcomes (and perhaps because of them), the results suggest how circadian genes and light act together to organize the SCN neural network, and thus affect behavioral and neurological phenotype.

Section 6.1: Master Pacemakers or Population Encoding?

In 2005, Ohta *et al*. showed quite convincingly that constant light (LL) could not only decouple the left and right SCN, but also lead to neuronal asynchrony in a handful of mice[142]. These neural characteristics readily explained the behavioral phenotypes seen in these mice, but constant light as a tool for studying neural circuitry was cumbersome. Most mice took months in LL to split or become arrhythmic—time that could be considered a confound since aging inherently changes circadian properties. Rather than continue waiting long durations of time for light to desynchronize the clock, we sought a genetic alternative.

It has been suggested that all ~20,000 neurons of the SCN are endogenous and self-sustained[40], but this hypothesis had come under scrutiny as evidence mounted in favor of a model in which only a small subset of these neurons were true endogenous pacemaker cells. In

electrophysiological studies, for example, a much reduced proportion of SCN neurons from *VIP*$^{-/-}$ or *Vipr2*$^{-/-}$ mice displayed rhythmic firing patterns when compared to wildtype mice[132, 133]. Experiments using PER2::Luciferase and *Per1*::GFP SCN explants from *Vipr2*$^{-/-}$ neonates showed reporter damping and a lack of neuronal synchrony in the absence of VIP signaling[135]. The first study reported in this dissertation sought to characterize the relationship between the neurons in the SCN and their resultant behavioral output.

When originally proposed, we had two hypotheses regarding why *in vitro* reporter expression was damped in the SCN of VIP signaling-deficient mice, and subsequently what the proper role of each neuron was in the SCN. Hypothesis 1 suggested that all SCN neurons contributed equally to the timekeeping properties of the wildtype tissue[40], and also to behavior. According to this hypothesis, VIP-deficiency knocked-down the amplitude of the clock gene expression[131], resulting in damping (Fig. VI-1a). Conversely, hypothesis 2 proposed that only a subset of neurons were truly endogenous pacemakers among other slave oscillators. In the absence of the central synchronizing neuropeptide, the background noise from these desynchronized/arrhythmic slave neurons would therefore account for the observed tissue damping in VIP-deficient mice (Fig. 1b). As reported in Chapter II, it would seem that neither of these models is completely correct. Instead, both hypothesized mechanisms appear to seem to contribute to the organization of the SCN. As proposed in hypothesis 1, we found no difference in the number of rhythmic neurons between wildtype, heterozygote and VIP knockout mice. The tissue-level reporter damping, however, was almost certainly due to desynchrony of neurons with robust rhythmic amplitude. These results support a hybrid model in which equal numbers of neurons express rhythmic *Per1*::GFP expression across VIP genotypes, and the observed damping of VIP signaling-deficient SCN is due to neuronal desynchrony. Furthermore,

and more significantly, the synchrony of neurons within the SCN directly correlates with the robustness of rhythmic circadian behavior.

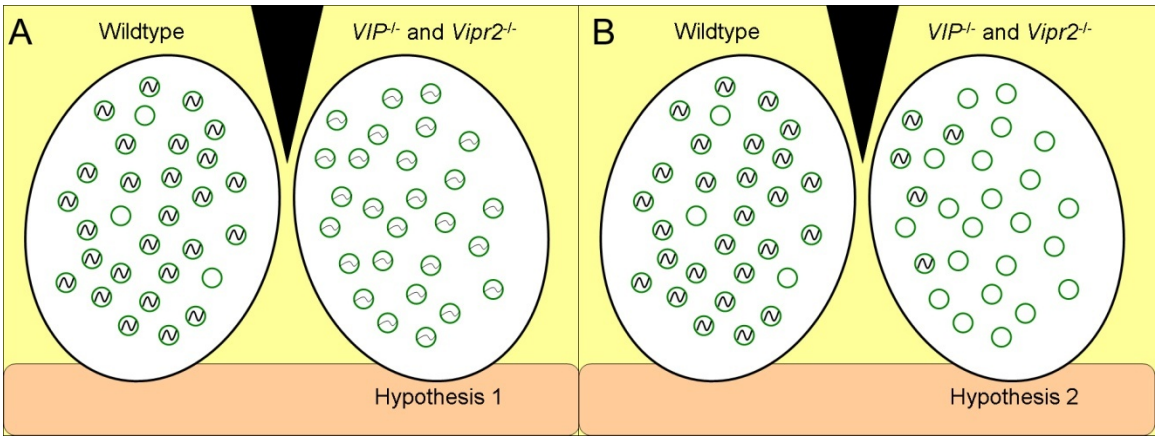

Figure VI-1. | **Hypotheses regarding which cells constitute the endogenous pacemakers of the SCN.** While most neurons in a wildtype SCN produce high-amplitude rhythms, **a** | all SCN neurons in *VIP*$^{-/-}$ or *Vipr2*$^{-/-}$ mice produce low amplitude rhythms in synchrony or asynchrony, resulting in damping; or **b** | only a subset of truly endogenous master pacemaker neurons in the SCN from *VIP*$^{-/-}$ or *Vipr2*$^{-/-}$ mice produce high amplitude rhythms while other neurons have none. Tissue damping results from the small number of oscillating neurons being drowned out by the majority of arrhythmic neurons.

We originally believed that if there were a small subset of rhythmic neurons within the SCN, as proposed in hypothesis 2 (Fig. VI-1), we would be able to discern a correlation between individual cells and individual bouts of activity. In retrospect, this expectation was unreasonable given the limits of the time-series imaging technique and data suggesting that SCN lesioned mice could have behavioral rhythms restored by inserting a packet of SCN neurons that prevents synaptogenesis[217]. In other words, control of rhythmic circadian behavior by the SCN is paracrine, rather than synaptic, thus making control of behavior by individual neurons on a one-bout to one-neuron basis highly unlikely.

Instead, our results suggest a far more reasonable solution: behavioral activity onset receives contributions from all of these rhythmic SCN neurons—a type of mean population vector. Our findings have significant implications for understanding how the SCN neural network encodes and drives circadian behavior. The timing of behavioral onset is encoded by

the vector average phase of the neural population with the temporal direction of the vector determining the time of activity onset and the magnitude of the vector determining the coherence of the behavioral rhythms. Our results further support the assertions that VIP is a signal for light stimuli within the SCN network as well as a synchronizing agent. Thus, the overall role of VIP communication in the SCN appears to be to modulate the timing and coherence of population vector encoding by SCN neurons to adjust circadian behavior to environmental light input.

Section 6.2: Locomotor Activity, VIP and *Ultradian* Rhythms

In 2005, during the construction of the light-tight circadian boxes in which mice would be behaviorally characterized, Hide Ohta and I became concerned about the limitations of our activity-monitoring system. Wheel-running is and has always been the primary method by which circadian behavioral activity is monitored in rodents. The problem with the *status quo*, however, is that wheel-running itself has been shown to actually change the characteristics of the circadian clock. Specifically, it was thought that nocturnal behavior may be reinforced via the serotonergic system through daily wheel-running mediated feedback[85, 86]. To address this inherent bias in our setup, I devised a means by which an infrared motion detector could be mounted in our existing wheel-cages and report the on- and off-wheel locomotor activity of mice through our existing ClockLab system.

Late in that year and in early 2006, upon the departure of Dr. Ohta, I inherited a line of $VIP^{-/-}$ mice that had been characterized as having several unusual behavioral phenotypes. Fortuitously, I chose to test the lab's new IR system on this line of mice and report my findings, however preliminary, at a conference for the Society for Research on Biological Rhythms (May, 2006). Colwell *et al* (2003) had demonstrated that these mice failed to phase shift in response

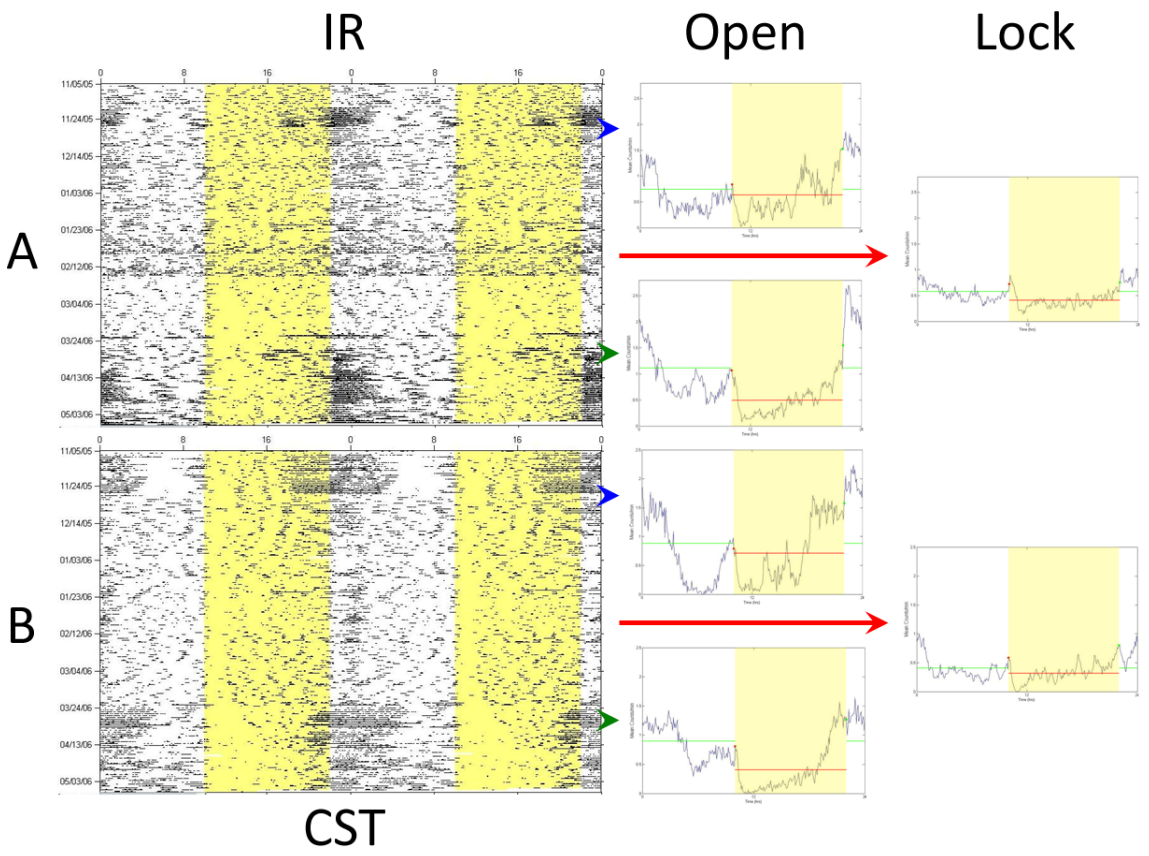

Figure VI-2. | **Wheel-running consolidates locomotor rhythms in VIP$^{-/-}$ mice.** VIP knockout mice were left in LD 12:12 and monitored for an initial 25 days in dual wheel-IR cages (blue arrowhead). Wheels were then locked (red arrow) for 110 days and monitored with IR alone, before being unlocked (green arrowhead) for 57 days. *Left*, representative double-plotted IR actograms from two wheel-locked VIP$^{-/-}$ mice (**a-b**). *Right*, mean activity profiles over the given days. The green line represents the mean counts/minute during lights-off; the red line represents the mean counts/minute during lights-on. "Lights-on" indicated by yellow background.

to light pulses[136]. In combination with results from the knockout of VIP's principle receptor in the SCN ($VPAC_2$) indicating a similar behavioral phenotype[131, 218] and an apparent immunity to light at the molecular level[134], the VIP-/- mice appeared to be ideal candidates to study non-photic entrainment. Of course, in part due to the study in Chapter II[1], we now know that photic gating in the SCN is not absent in VIP signaling-deficient mice as suggested (see [134]) *per se*, but rather severely altered such that light affects desynchronized SCN neurons at random phases of their circadian rhythms, resulting in a weak/absent phase shifting vector. But at the time, these mice, which were on a hybrid sv129 background, seemed a promising alternative to constant

light as a tool for studying neural circuitry and behavior in an animal with disrupted photic input. Figure VI-2 is a slight variation of an actual figure that appeared on the poster for that conference in 2006, and suggests—at least upon visual inspection—that wheel-running can, even in a light-dark cycle, consolidate rhythmic behavior. These preliminary data were the foundation of Chapter III of this dissertation.

The principal findings reported in Chapter III are that wheel-running does indeed consolidate activity by possibly contributing to the integration of multiple circadian and/or ultradian oscillators. The persistence of a strong ultradian phenotype (Fig. III-6) suggests that knocking out the master integrator may unmask other innate rhythmic components from other non-circadian pacemakers or may simply fail to synthesize many uncoupled individual extra-SCN circadian pacemakers into a single coherent phase [1, 162]. Importantly, these results in *VIP*$^{-/-}$ mice support the hypothesis that the SCN serve not only as the master circadian clock, but also as the master integrator of other rhythmic components produced in the mammalian body [137].

There is an interesting relationship between light, VIP and serotonin that begs for speculation on the role of each in these processes. VIP is rhythmically released in light-dark cycles, but not in constant dark [61-65]. Exposure to constant light has been shown to significantly depress VIP concentrations in the rat SCN [66] in a light-dose dependent manner [67]. The behavioral phenotype of arrhythmic mice kept in continuous illumination [141, 142, 158-161] is visually similar to the behavioral phenotype of *VIP*$^{-/-}$ and *Vipr2*$^{-/-}$ mice [1, 131, 133, 136]. These mice also exhibit ultradian rhythms similar to those noted in early SCN lesion studies [31, 138]. For the purposes of this dissertation, *VIP*$^{-/-}$ mice were thought of as a genetic model of wildtype mice kept in constant light or with lesioned SCN. This approach allowed us to study the underlying periodic components without performing surgical lesions in adult mice or aging them in LL, and removing a key intra-SCN signaling molecule allowed us to study the organizational effect of locomotor

activity with less interference from light[134]. The results of Chapter III suggest a further interaction between VIP-ergic and serotonergic systems: wheel-running activity correlates positively with 5-HT release in the SCN [153], and depletion of this non-photic circadian modulator leads to greater daytime activity [79, 219, 220]; also, antagonism between light and 5-HT exists such that in the night-time absence of light, serotonin may reinforce nocturnal behavior through daily wheel-running mediated feedback [85, 86]. Since light signaling is impaired in VIP-signaling deficient mice [134, 136], the effects of wheel-access are exaggerated in *VIP*$^{-/-}$ mice as evidenced by better partitioning of activity with a nighttime bias, and greater consolidation with access to a wheel, such that there is less daytime activity even in the *VIP*$^{-/-}$ mice with access to a wheel. Perhaps the greater release of serotonin onto the SCN after locomotor activity accounts for these results.

This study brings to light a fundamental complication found in most circadian behavioral studies: wheel-running, the primary method of activity monitoring in the circadian field, is not the most desirable means by which to minimize exposure to the Heisenberg Uncertainty Principle[221]. In our efforts not to affect the circadian phenomena we are observing, it is best not to make the animals work to demonstrate their behavioral properties when that work—in this case wheel-running—may alter the results. Passive monitoring by such methods as beam-break and infrared motion detection is preferable when the wheel may feedback on the circadian system and drive resulting behavior rather than simply report it. Certainly, new methods of quantification using these systems need to be developed and perfected.

Section 6.3: Developmental Imprinting of Seasonal Encoding

In 2006, perinatal development in continuous illumination was shown to disrupt the organization of the mouse SCN in adulthood, even when the mothers were rhythmic[141]. For Dr.

Ohta, whose primary occupation was as a pediatrician, this finding was significant given that most hospital neonatal intensive care units (NICU) expose their premature babies to constant light for convenience and ease of patient care. This result, therefore, suggests that NICUs may actually be doing undue harm to their infants and increasing the likelihood that they will face circadian related disorders (see Section 1.5: Human Circadian Genetics). As my direct supervisor in Dr. McMahon's lab, Dr. Ohta's interest in developmental neurobiology meshed well with my own, and his study served an important role in the development of the experiments reported in Chapter IV.

In early 2007, an interesting paper was published addressing how, electrophysiologically, the brain encodes seasonal changes in photoperiod[108]. The multiunit array approach, while able to demonstrate the overall photoperiod-dependent changes that occur in the SCN's electrical waveform, was unable to clearly demonstrate how single neurons and the neural network organized to encode season. Convinced that the *Per1*::GFP mouse line in our lab provided the perfect model to allow us to characterize neuronal *and* tissue properties in *ex vivo* SCN, I went to work entraining equinox developed mice to short (LD 8:16), equinox (LD 12:12) or long (LD 16:8) photoperiods. As these data were being analyzed, another paper using a similar approach (*Per1*::Luc) was published that provided clearer evidence that the degree of neuronal phase variance within the SCN changed in response to photoperiod, accounting for the tissue-level electrical and circadian gene expression waveform changes between short-day and long-day mice[110]. A question persisted in our minds, however, about whether light at physiological levels—such as seen in differing seasonal photoperiods—had the ability to alter SCN organization during development in a manner similar to that seen in continuous illumination[141].

The findings reported in Chapter IV suggest that light does indeed have an epigenetic effect on the development of mouse SCN, even at physiologically relevant photoperiodic durations.

Constant light was an extreme example, rarely confronted in nature (the polar latitudes), while photoperiods are confronted at almost every other non-equatorial latitude. Chapter IV reported several important advances in our understanding of seasonality and seasonal encoding: 1) seasonal encoding occurs at both the tissue- and cellular-levels; 2) the organization of the adult SCN and its ability to reorganize in response to seasonal photoperiod input are imprinted during development, possibly by classical epigenetic means; 3) perhaps the most salient individual finding was that SCN from mice developed in a short-day light cycle exhibited an inability to properly conserve phase angle of *Per1* expression to dusk while the SCN from long photoperiod developed mice exhibit conservation of phase angle to dusk (Fig. IV-2c-d). In combination with results from other studies on affect in other rodent models[165, 183, 187, 222], these results provide significant fuel for speculation on the implications for human health. Could a seasonal misalignment in the phase relationship between the environmental light cycle and the circadian gene expression in the human SCN account for the seasonal affective disorders, and might development—either *in utero* or postnatal—imprint susceptibility to mental disease state in adults? These questions would be difficult to answer in humans, where electroencephalography on hypothalamus is nearly impossible. We can, however, reliably track the output of other circadian rhythms as a marker. For example, our results are reminiscent of a study on humans that suggested SAD might be related to (or at least present with) an increase in the duration of melatonin production during the winter light cycle in SAD patients that is not seen in normal people or summertime SAD patients [223]—much like the tissue-level change in *Per1*::GFP waveform reported in Chapter IV.

From a purely genomic standpoint, our results are intriguing given their epigenetic implications. A recent report on the epigenetic effects of illumination during the development of dopamine neurons in the frog SCN suggested that as the amount of light to which frog

tadpoles were exposed during development increases, the number of inhibitory dopamine neurons also increases, thus imprinting the retinohypothalamic-SCN circuitry and allowing finer control of skin pigmentation[163]. Our results in the mouse provide analogous evidence for photoperiod-dependent imprinting of the mammalian SCN that raise two important questions: 1) might this imprinting be the result of changes in monoaminergic neural circuitry in the mouse SCN as in the frog SCN? and 2) might these results have important implications for behavior in mammals? While the answer to the first question will have to wait for future studies to simply count the number of monoaminergic neurons present in the SCN after developing in the photoperiodic paradigm provided in Figure IV-1, evidence to answer the second question may already be extant. Besides the evidence offered in this dissertation, the most intriguing of these studies may be developmental photoperiod's imprinting of affect in hamsters [165], but further studies in mice regarding the effect of photoperiod on mood must be undertaken.

As is so often the case in biology, while Dr. Ohta's study of constant light disruption on the developing mouse SCN was a catalyst for the questions addressed in Chapter IV, it was not alone. Early studies of behavioral circadian rhythms noted an interesting phenomenon in rodents exposed to different photoperiods: as *alpha*[s] gets compressed by a long photoperiod, free-running period decreases [19]. Until this study, the *in vitro* correlates of this after-effect have never been identified. Our results show a clear effect of photoperiod—both developmentally and in seasonal adaptation—on neuronal period *ex vivo*. While likely not interesting to the general public, an *ex vivo* demonstration of photoperiod-dependent period change was a fascinating discovery for me. The result is downplayed in dissertation Chapter IV (and the subsequent publication) due to an inability to link it with a behavioral phenotype[t], but this one

[s] The main bout of locomotor activity that occurs at night in nocturnal rodents.
[t] Because the mice were killed straight out of a light-dark cycle, no behavioral free-running period could be measured.

early result (Fig. VI-3) was a singular driving force leading me to ask what switching the light cycle from a short developmental photoperiod to a long continuation photoperiod (or vice-a-versa) might do. Without this finding, I likely would have cut my losses, as it were, and stopped experimenting on developmental photoperiods all together. Instead, switching mice from their developmental photoperiod to a different continuation photoperiod allowed us to use a powerful statistical approach to measure the interaction between development and plasticity, which in turn identified the complex relationship between light and the developing clock. Before we can fully understand the implications of the *ex vivo* period findings, further work using *in vivo* electrophysiology or imaging (via bioluminescence or fluorescence) must be done to establish the correlation between what we found in the culture dish and actual mouse behavior.

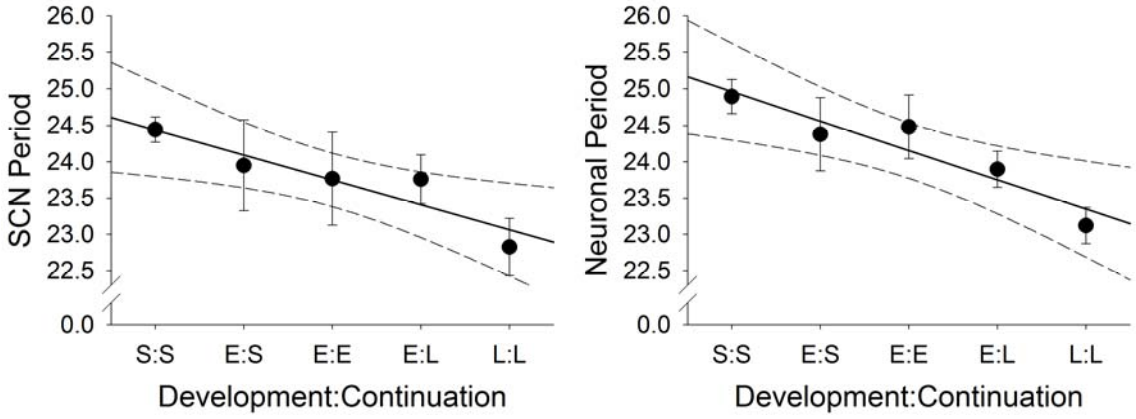

Figure VI-3. | **Exposure to long photoperiod decreases SCN *Per1*::GFP period *ex vivo*. a** | SCN period. **b** | SCN neuronal period. Black line represents the fitted regression; dashed line represents the 95% confidence interval. Photoperiodic paradigm represented as "Developmental:Continuation" with "L" representing long photoperiod, "E" representing equinox photoperiod and "S" representing short photoperiod. Error bars represent SEM.

Section 6.4: Circadian Genes, Geography and Evolution

As was discussed in the introduction of this dissertation, the fact that circadian rhythms have become a ubiquitous characteristic of life on earth is fascinating given the tumultuous history of the planet. One of the chief pieces of evidence for the evolutionary importance of

circadian rhythms comes from the work of Carl Johnson, with whom I did my first full rotation in graduate school. As a part of that rotation, I began testing and redesigning primers with which several cohorts of human subjects could be screened for circadian gene variants that would ultimately be associated with phenotype. I continued this project, which was done in collaboration with Marshall Summar and Doug McMahon, through the rest of my rotations and into the first couple years of graduate school. The cohorts tested consisted of a geographically diverse sampling, coming from China, Ghana, Papua New Guinea, and the United States (African and European American cohorts). While a relatively small sampling, both in number per cohort and in actual geographical setting, it was our hope that screening for genetic variants in the human circadian genes would give us some insight to their evolutionary conservation. Chapter V was only the first of what I hope are many studies to come out of this work.

In Chapter V, we discovered several new and intriguing SNPs, and reported the population frequencies for these and previously identified variants. The overall finding of this study was that differences seen in variant frequencies between populations were likely due to genetic drift rather than natural selection. This study serves as a jumping-off point for more interesting association analyses between the variants reported and actual, quantifiable phenotypes. The main cohort of subjects investigated in this project were Vanderbilt University Medical Center Nurses—mostly Caucasian. In addition to providing a sample of blood for DNA extraction at nursing orientation, these men and women also took an extensive survey on their sleep and circadian habits which were then painstakingly analyzed by Dr. Karen Gamble. Those results have provided interesting information on how shift-work nurses adjust their sleep schedules to compensate throughout their normal rotation. Additionally, a few atypical subject groups (Nighteaters, unipolar depressed, autism) were studied for association between symptoms of their disorder and circadian gene variants. Preliminary data are quite compelling, but yet to be

validated. It is our hope that all of these data will be associated with the variants reported in Chapter V, and offer insight into the role of circadian genes in mental and behavioral function and dysfunction.

Section 6.5: Conclusions

This dissertation has run the gamut from genes to behavior, from mice to men. It has been difficult at times to integrate the chapters of this dissertation into a single coherent narrative because they were not always specifically in the same vein. However, the general thematic arc of how genes may control behavior in rodents and humans, and of how the expression of these genes is altered by light during and after development has broad appeal.

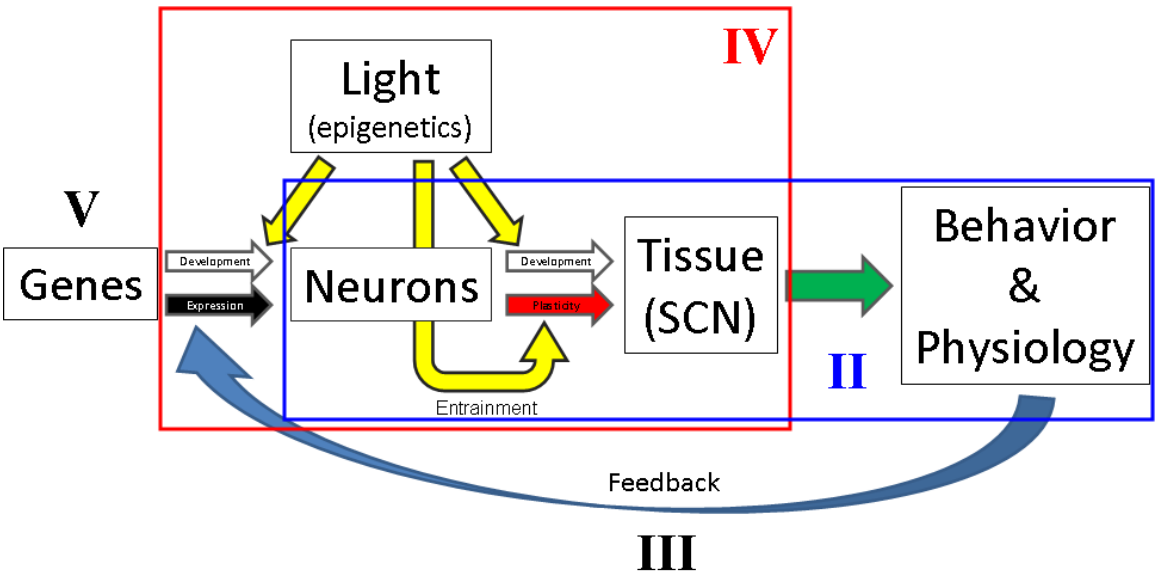

Figure VI-4. | **Integrative schematic of levels of mammalian circadian organization examined in this dissertation, and the layers of feedback between levels.** Chapters denoted by Roman numerals.

Chapter V of this dissertation reported the population frequencies of circadian gene variants in humans as the first part of a multi-pronged effort to assess their geographical divergence and to associate them with behavioral or neurological phenotypes. In addition to donating a DNA

sample, most of the subjects in this and upcoming studies had also filled out extensive questionnaires on mood, mental, sleep and other behavioral characteristics in order to elucidate the role of those genes in typical and atypical biology (Fig. VI-4). Chapters II and III started at the other end of the spectrum—behavior—and worked backwards, assessing how measured behavioral activity correlates to characteristics of circadian gene expression at the tissue and cellular levels (Fig. VI-4 *blue box* and *Feedback arrow*). The results suggested that the degree of rhythmic synchrony between SCN neurons *ex vivo*—as measured by a *Per1* reporter—strongly correlate with the strength of rhythmic behavior *in vivo*. Additionally, the function of a circadian-related neuropeptide, VIP, is crucial in the proper organization of the SCN and its subsequent behavioral output. Locomotor behavior also consolidates clock function in the SCN and therefore behavior as well. This relationship between genes (like those studied in humans in Chapter V) and behavior (as measured in mice in Chapter II, III, and in humans as an eventual addendum to Chapter V) is crucial to our understanding of function and dysfunction at all levels of the circadian system.

Chapter IV is undoubtedly my favorite part of this dissertation (Fig VI-4 *red box*). It combines the methods of Chapter II with questions raised by the geographical distribution of Chapter V to confront a real-world problem: how does photoperiod affect development at the tissue and cellular level? Our results provide a possible mechanism by which the neurological or behavioral characteristics seen in adulthood can be explained by neural reorganization of and development in different photoperiods. Many of the human circadian gene-related disorders explored in the course of Chapter V may be, according to the data provided in Chapter IV, imprinted by photoperiod during development. It is indeed a stretch to assume a one-to-one correlation between the neurophysiological organization of a mouse developed in a certain season and the neurophysiological organization of a human developed in the same season, but

as members of the mammalian class, it is plausible. The apparent epigenetic effect of light should not come as a surprise: light is the primary zeitgeber by which circadian phase is set. Entrainment must involve transcriptional and/or translational modification in the SCN by light (or, more accurately, from structures sensing light and relaying the information to the SCN). Thus light's ability to imprint the clock—a subcortical visual processing center—is as understandable as light's ability to imprint processing in the visual cortical centers of the brain.

While almost all of the results reported here were completely unexpected, much has been learned—both in the field and personally. Overall my results suggest that circadian genes and light act together to organize the mammalian SCN neural network, and thus affect behavioral and neurological phenotypes. It is my hope that these studies have served to stimulate further research into their implications for human health.

Section 6.6: Future Directions

The volume of data collected in pursuit of my doctorate is far greater than what was (or could be) presented in this dissertation. While the experimental phase of my research has been complete for some time, analyses have been cumbersome and slow due not only to the volume, but also the complexity of the data. It is my hope that a collaboration with a biostatistician will allow us to revisit much of these leftover data, which I believe is a rich source of information on anatomical location, sustained rhythmicity and waveform dynamics. Until then, however, the simpler analyses performed for this dissertation will have to suffice.

As I complete my graduate work, I find myself looking forward with great enthusiasm. In the immediate future, I will continue characterizing a mouse possessing a severe knockdown of serotonin expression. These Pet-1 "knockout"[u] mice[224, 225] will serve as a powerful tool to

[u] They do express an extremely low level of serotonin, but not an absence.

address many of the questions raised in this dissertation: 1) is 5-HT necessary for proper retinohypothalamic tract innervation of the SCN? 2) Do these knockouts possess any circadian behavioral deficits? 3) Do these knockouts possess altered light or non-photic responsiveness? 4) Can any behavioral or neurological characteristics be explained by the molecular phenotype of the SCN and its constituent neurons? 5) How do these molecular rhythms react to pharmacological treatment? 6) What role does 5-HT play in seasonal imprinting and/or adaptation? Preliminary data suggests that these mice *do* possess several unusual behavioral characteristics, such as a delayed phase angle of activity offset in LD and a long free-running period that may be explained by a complementarily long SCN *Per1*::GFP period. It will be fascinating to see what the PRC of these animals looks like, and together with answers to the questions posed above, should answer many of the serotonin-related questions raised in this dissertation.

As progress in the field continues to quicken, it is my hope that our understanding of mammalian circadian biology will soon span the gap, uninterrupted, from molecules to mind.

APPENDICES

Section A.1: Regional Analysis from Ciarleglio *et al* (2009)[1]

Background

As a part of the original set of analyses done for [1], I attempted to find any regional-specific pattern of *Per1*::GFP expression in the coronal SCN slices. My hope was that such an analysis might identify the truly endogenous pacemaker neurons. The nucleus was divided evenly into four quadrants: dorsomedial, ventromedial, ventrolateral and dorsolateral. The phases at half-max of the first peak of rhythmic neurons were plotted on a template, and color-coded to denote four distinct phase ranges. Those neurons whose phase occurred CT 0-4 were coded red, CT >4-8 coded orange, CT >8-12 coded yellow, and CT 12-0 coded green (Fig. A.1-1).

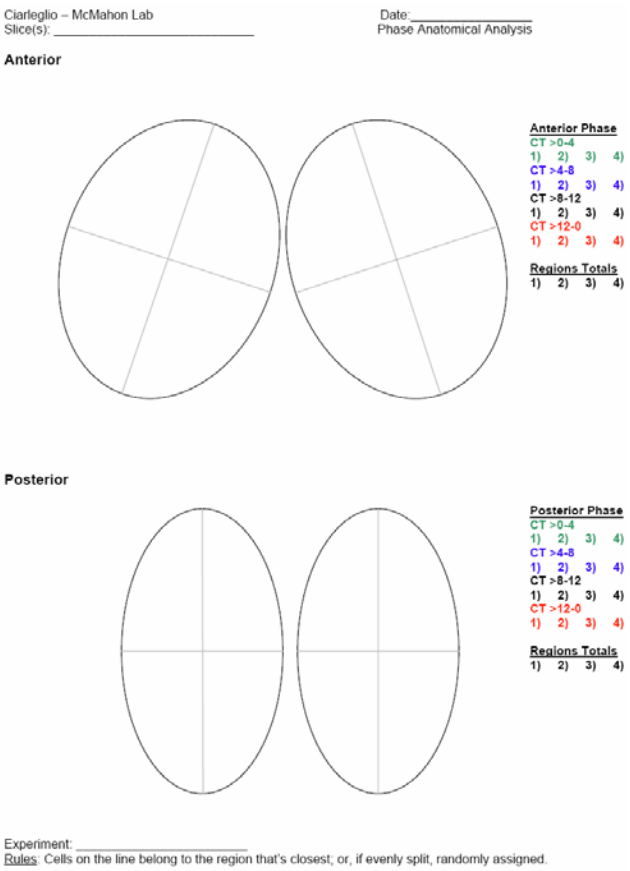

Figure A.1-1. | **Regional analysis template for phase.** Note: these were hand-drawn, so I used green, blue, black and red pens rather than the colors in the final output figures (A.2-3 and A.2-4).

Results & Discussion

There were no overall phase differences across genotypes in either LD or DD (LD: $\chi^2(6) = 9.43$, $p = 0.1506$; DD: $\chi^2(6) = 8.49$, $p = 0.2042$), nor was there a difference in phase across regions in acutely extracted SCN from rhythmic mice in DD ($\chi^2(9) = 9.19$, $p = 0.4197$; Note: no *VIP*$^{-/-}$ mice included in this analysis). In LD, however, there was a significant phase x region effect wherein the resulting phase of neurons expressing *Per1*::GFP depended on the region in which the neuron was located, independent of genotype ($\chi^2(9) = 26.0$, $p = 0.0020$; Fig. A.1-2). For example, over half of the total neurons whose 50% phase occurs between projected ZT 8-12 are located in the ventromedial region, while the dorsomedial region possesses nearly half of the ZT 0-4 as well as half of the ZT 12-0 phased neurons (Fig. A.1-2).

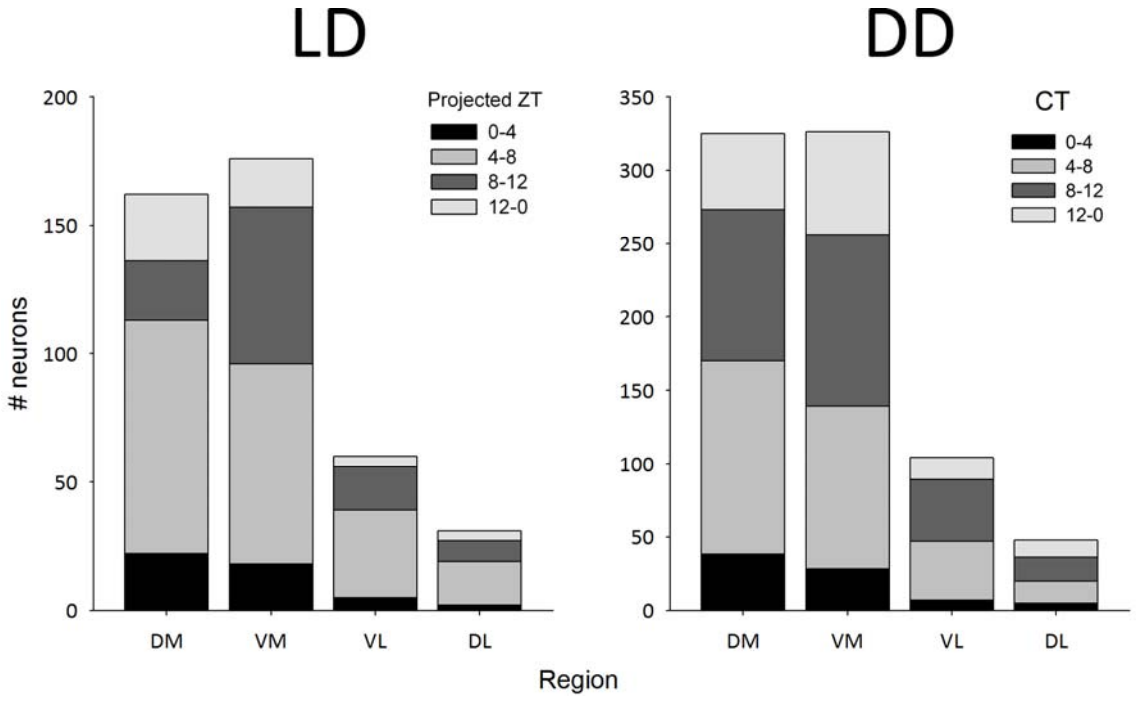

Figure A.1-2. | **Stacked bar graph illustrating overall regional differences in phase of *Per1*::GFP expressing neurons in mice from LD (*left*) or DD (*right*).**

We found a relationship between genotype and phase within each region such that there is a difference among genotypes in the distribution of neuronal phases within the medial two regions of the SCN (DM: $F(6) = 63.695$, $p < 0.0001$; VM: $F(6) = 53.675$, $p < 0.0001$) (Fig. A.1-3 and A.1-4).

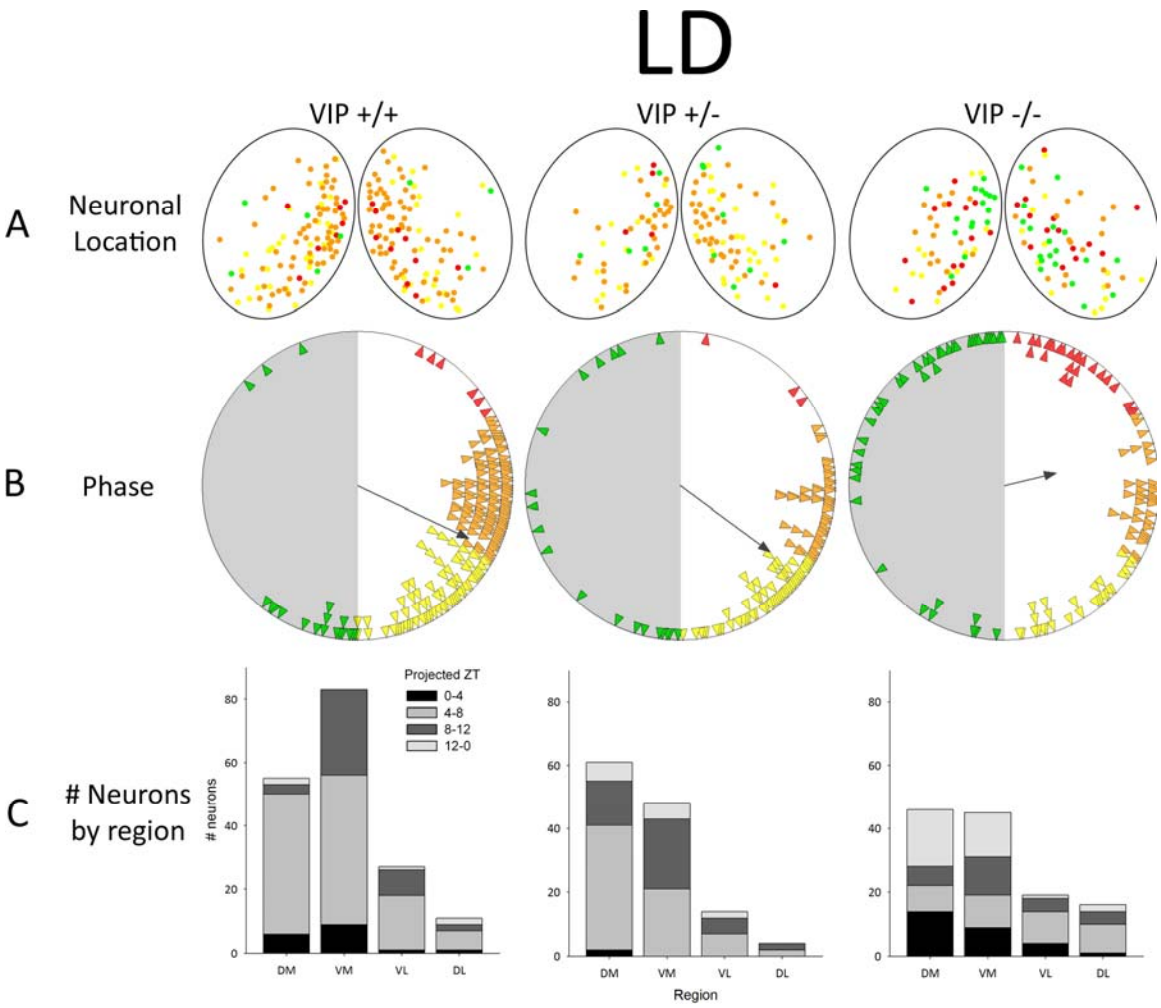

Figure A.1-3. | **Genotype-specific assignment of neuronal *Per1*::GFP phase is dependent on region in LD.** $VIP^{+/+}$ (*left*), $VIP^{+/-}$ (*center*) and $VIP^{-/-}$ (*right*). **a-b** | Phase of rhythmic neurons by color: CT 0-4 were coded red, CT >4-8 coded orange, CT >8-12 coded yellow and CT 12-0 coded green. **a** | Composite image of anatomical position and phase (by color) of neurons in SCN from all mice. **b** | Rayleigh plots. Arrowheads represent the 50% peak rising phases of all rhythmic neurons from a particular genotype. Black arrow indicates the mean phase vector of rhythmic neurons, where length is inversely proportional to the neuronal phase variance, and the direction indicates timing relative to the previous light cycle in LD. Projected ZT 0-12 is represented with a white background and projected ZT 12-24(0) is represented with a gray background. **c** | Stacked bar graphs illustrating the composite number of neurons of each phase in each region across all genotypes. DM = dorsomedial; VM = ventromedial; VL = ventrolateral; DL = dorsolateral.

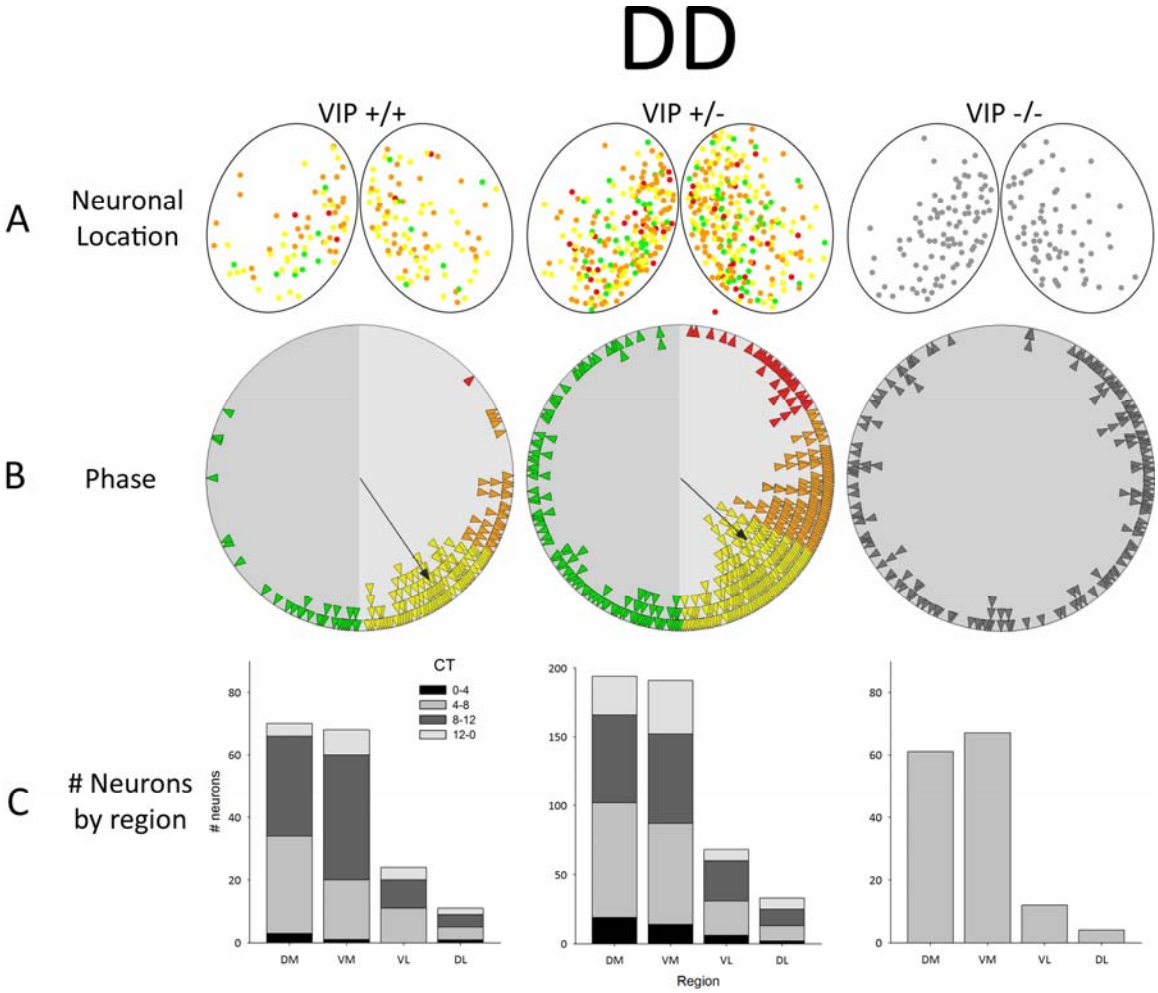

Figure A.1-4. | **Genotype-specific assignment of neuronal *Per1*::GFP phase is dependent on region in DD.** *VIP*$^{+/+}$ (*left*), *VIP*$^{+/-}$ (*center*) and *VIP*$^{-/-}$ (*right*). **a-b** | Phase of rhythmic neurons by color: CT 0-4 were coded red, CT >4-8 coded orange, CT >8-12 coded yellow and CT 12-0 coded green. **a** | Composite image of anatomical position and phase (by color) of neurons in SCN from all mice. **b** | Rayleigh plots. Arrowheads represent the 50% peak rising phases of all rhythmic neurons from a particular genotype. Black arrow indicates the mean phase vector of rhythmic neurons, where length is inversely proportional to the neuronal phase variance, and the direction indicates timing relative to the previous light cycle in LD. CT 0-12 is represented as a light gray background and CT 12-24(0) is represented as a darker gray background. **c** | Stacked bar graphs illustrating the composite number of neurons of each phase in each region across all genotypes. DM = dorsomedial; VM = ventromedial; VL = ventrolateral; DL = dorsolateral. For *VIP*$^{-/-}$ mice (*right column*), an assignment of phase was not possible, so arrowheads in **b** represent time *ex vivo*.

These results suggest that while the medial portion of the SCN was most densely populated, the rhythmic expression of *Per1* occurred proportionally in a clockwise fashion in the left nucleus, and a counter-clockwise fashion in the other nucleus. If one were to choose the dorsomedial region of the SCN as an arbitrary starting point for the wave of expression, one would see the ventromedial expression follow, then the ventrolateral, and finally the

dorsolateral regions. This is not to say that expression in one region is exclusive of the others, but rather that the percent of rhythmic neurons within a phase group increases region by region throughout the day.

This analysis was not powerful enough to identify master pacemaker cells (if they even exist), but my hope is that these data will provide some insight into *Per1* transcriptional activation—at least in these mice.

Section A.2: Mouse Colony Maintenance

Records are kept of all mice genotyped or bred in the facility, as in Figure A.1-1.

		Genotype									
#	Sex	*P1* ::GFP	*P1* ::Luc	*P2* ::LUC	*Pet1* ::YFP	*Pet1* KO	Color	Born?	Father	Coffin/Cage	Notes
1	M	+				+/-	Black	1/20/2009	Buddy	515048	
2	M	+				-/-	Brown	1/20/2009	Buddy	515048	
3	F		+			+/-	Agouti	1/1/2009	Caesar	515179	
4	F		+			-/-	White	1/1/2009	Caesar	515179	
5	M			+/-	+		Black	1/5/2009	Hide	515978	The Axe
6	M F						L R O A W				
7	M F						L R O A W				

Figure A.2-1. | **Mouse genotyping records**.

Tailing

Mice are numbered using the ear-punch method from the University of Virginia (Fig. A.2-2a) or via ear-tags from National Band & Tag Co. (Newport, KY) (Fig. A.2-2b).

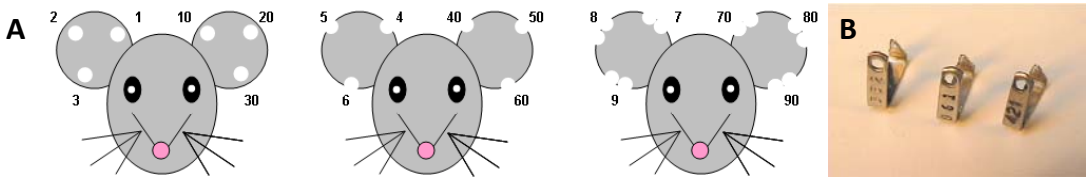

Figure A.2-2. | **Mouse identification numbering**. **a** | Ear-notch pattern from the University of Virginia. **b** | Ear-tags from National Band & Tag Co.[v]

1 cm is removed from tip of mouse tail using a #10 scalpel blade after animal numbering. For animals >P25, cold ethanol (70%) should be used as a pre-operative anesthetic (Fig. A.2-3). Tailing takes place in a hood.

[v] http://www.nationalband.com/1005b.htm

Figure A.2-3. | **Mouse tailing items**. Ice bucket with a petri dish containing 70% ethanol, #10 scalpel, ear-punch (FST), 1.5 mL tubes and pliers for ear-tags.

Tail DNA Isolation

i. Tail Lysis Buffer (1L)
   a. 50mL 2M Tris-Cl (pH=8.0)→$[100mM]_{final}$
   b. 20mL 500mM EDTA (pH=8.0) →$[10mM]_{final}$
   c. 25mL 20% SDS→$[0.5\%]_{final}$
   d. 40mL 5M NaCl→$[200mM]_{final}$
   e. 865mL autoclaved Milli-Q H_2O

ii. Protein Precipitation Solution (100mL)
   a. 57.81g Ammonium Acetate→$[7.5M]_{final}$
   b. Up to 100mL H_2O

iii. DNA Hydration Solution (**TE** 500mL)
   a. 5mL 1M Tris-Cl (pH=8.0)→$[10mM]_{final}$
   b. 1mL 500mM ETA (pH=8.0)→$[1mM]_{final}$
   c. Fill up to 500mL with autoclaved Milli-Q H_2O

1. Clip <1 cm of mouse tail OR ear punch skin. Place in sterile tube on ice or dry ice.
2. To tube add 600µl Tail Lysis Solution and 20µl Proteinase K (20 mg/mL #25530-049 from Invitrogen).
3. Place tubes in water-bath @ 55˚C for 1-3 hours to overnight or until no visible pieces of skin or bone present.
4. Remove tubes and cool on ice.
5. Add 100µl Protein Precipitation Solution (7.5M Ammonium Acetate) and vortex to completely break up any solid piece of tissue remaining. Mixture will become cloudy.
6. Spin @ 10000-13000 rpm for 3-5 minutes. Place tubes back on ice.
7. Move supernatant to fresh tube and discard pellet. If a pellet did not form:

a. Vortex for 20 seconds
b. Incubate on ice for 5 minutes
c. Centrifuge @ 10000-13000 rpm for 3 minutes

8. Add 300µl 100% Isopropanol (2-propanol) to each tube.
9. Mix gently by inverting at least 50 times (this isolates the DNA)
10. Centrifuge @ 10000-13000 rpm for 5 minutes. Place tubes in the same position in centrifuge so the DNA pellet forms at the same location in each tube (easier to locate then-i.e. hinge on the outside ring of the centrifuge).
11. Carefully pour off supernatant into a waste container, making sure your pellet remains in tube.
12. Add 500µl 70% ethanol and mix tube to wash the pellet.
13. Centrifuge @ 10000-13000 for 2-3 minutes.
14. Carefully pour off ethanol to waste container and blot tube on paper towel.
15. Allow the ethanol to dry off, but not drying out the pellet. Usually about 30 minutes.
16. Add 30µl DNA Hydration solution (TE) to each tube. Rehydrate it by incubating the samples at 65˚ C for 1 hour or at room temperature overnight.
17. Store at 4˚ C for short term or at -20˚ C for long term.

Genotyping

Per1::GFP Genotyping

1 reaction (20 µl per Rxn):
2µl 10x PCR Buffer II
2µl 10x $MgCl_2$ [25mM]
0.5µl 10 mM dNTP
0.2µl FpRpGFP @ [20µM]
0.1µl AmpliTaq Gold (@5U/µl)
1µl Tail DNA
14.2µl H2O

Primers (-20°C)
FpGFP: 5’ CCT GGT CGA GCT GGA CGG CGA CGT AAA 3’
RpGFP: 5’ CCG GCG GGA AGC CAT GGC TAA GCT T 3’

Per1::GFP Thermocycler Conditions:
95°C for 7:30
95°C for 1:00 for 32 cycles
60°C for 1:00
72°C for 1:30
72°C for 5:00
4°C hold

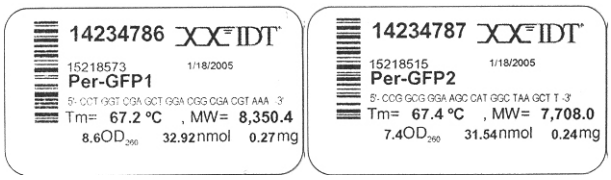

Figure A.2-4. | ***Per1*::GFP primers from IDT.**

PER2::LUC Genotyping

1 reaction (20 µl per Rxn):
2µl 10x PCR Buffer II
2µl 25mM $MgCl_2$
0.5µl 10 mM dNTP
0.4µl Primers: P1 @ [10µM], P2 @ [10µM], P3 @ [10µM]
0.1µl AmpliTaq Gold (@5U/µl)
1µl Tail DNA
14µl H_2O

Primers (-20°C)
P1 (mPer2e23F): (3771) 5' CTG TGT TTA CTG CGC GAG T 3' (3789)
P2 (mPer2e23R—deleted in target): (4000) 5' GGG TCC ATG TGA TTA GAA AC 3' (3981)
P3 (LUC): (cds 529) 5' TAA AAC CGG GAG GTA GAT GAG A 3' (508)

PER2::LUC Thermocycler Conditions:
94°C for 7:30
94°C for 1:00 for 35 cycles
55°C for 1:00
72°C for 1:00
72°C for 15:00
4°C hold

229bp WT
680bp Luc+

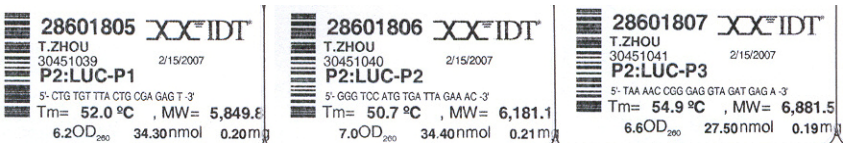

Figure A.2-5. | **PER2::LUC primers from IDT.**

Pet-1 KO Genotyping
Adapted from Roxanne Murphy, Case Western University
Adapted from Melinda Peters, Vanderbilt University (Weeber Lab)

1 reaction (30 µl per Rxn):
3µl 10x PCR Buffer II
3µl 10x $MgCl_2$
1µl 10 mM dNTP
1µl Primers: 5'PET @ [20µM], 5' LOX @ [20µM], 3' PET @ [20µM]
0.5 µl AmpliTaq Gold (@5U/µl)
1 µl Tail DNA
20.5µl H2O

Primers (-20°C)
3’ PET: 5’ GCC TGA TGT TCA AGG AAG ACC TCG G 3’
5’ PET: 5’ CGC ACT TGG GGG GTC ATT ATC AC 3’
5’ LOX: 5’ CGG TGG ATG TGG AAT GTG TGC G 3’

Pet-1 KO Thermocycler Conditions:
94°C for 7:30
94°C for 50 sec for 38 cycles
62°C for 30 sec
72°C for 40 sec
72°C for 15:00
4°C hold

209 bp WT
361 bp KO

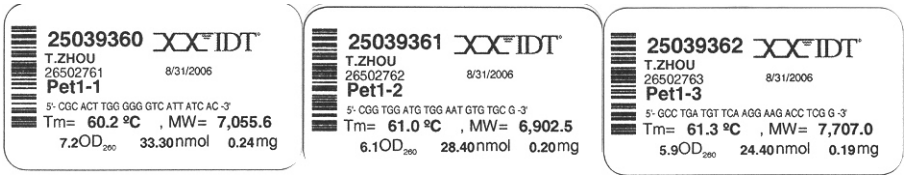

Figure A.2-6. | ***Pet-1* primers from IDT.**

VIP KO Genotyping

i. 5x PCR Buffer (100mL)
   a. 3.63g Tris base (pH=9.15)→$[300mM]_{final}$
   b. 1.1889g $(NH_4)_2SO_4$ →$[90mM]_{final}$
   c. 0.148g $MgSO_4$→$[6mM]_{final}$
   d. Fill to 100mL with autoclaved Milli-Q H_2O
ii. $MgSO_4$ (100mL)
   a. 0.616g $MgSO_4$
   b. Fill to 100mL with autoclaved Milli-Q H_2O
iii. 10x PCR Buffer II (100mL w/ optional Mg^{2+})
   a. 1.576g Tris-Cl→$[100mM]_{final}$
   b. 0.745g KCl→$[500mM]_{final}$
   c. *optional* 0.952g $MgCl_2$→$[25mM]_{final}$
   d. Fill to 100mL with autoclaved Milli-Q H_2O

1 reaction (20 µl per Rxn):
4µl 5x PCR Buffer
2.4µl $MgSO_4$
0.7µl 10 mM dNTP
1.2µl VIP primer mix
0.4µl DMSO
0.2µl TitaniumTaq (BD/Clontech #639208)

1µl Tail DNA
10.1µl H_2O

Primers (-20°C)
(V1) VIPF5-: 5' TTA CCT GAT TCG TTT GCC AAT GAG TGA C 3'
(V2) VIPF4+: 5' TTT CAA GGT GTG GGG CTA GAG ACA TAC A 3'
(N) ONEO 10-: 5' GGC CCG GAG ATG AGG AAG AGG AGA ACA G 3'

VIP Thermocycler Conditions:
95°C for 5:00
95°C for 30 sec for 11 cycles
70°C→ 60°C for 35 sec
72°C for 2:00

96°C for 30 sec for 22 cycles
60°C for 35 sec
72°C for 2:00

72°C for 7:00
4°C for 20:00
25°C hold

318bp WT
708bp VIPKO

Agarose Gel

1. 1g agarose (=1%)
2. up to 100mL 1x TBE or TAE
3. microwave High until dissolved
4. add 4µl/100mL EtBr to gel
5. allow gel to cool and solidify
6. add 4x loading dye to each sample
7. load ½ sample into each well
8. flank with 5µl 1kb Ladder
9. run @ 100-150mV

Section A.3: Suprachiasmatic Nuclei (SCN) Slice Culture for Rodents

A. Slice Culture

i. Sampling Media (can be made at half volume in 1 bottle of HBSS)

a. In 900mL Hank's Buffered Saline Solution (HBSS from Gibco 14175-103), add:
b. 10mL Penicillin (25U/mL) & Streptomycin (25ug/mL from Sigma - P4333 100mL)
c. 5mL NaHCO3 (7.5% from Sigma – S8761)
d. 10mL Hepes (1M, pH 7.2 from Sigma – H0887)
e. Bring volume to 1000mL total in volumetric flask
f. Filter sterilize
g. Store at 4°C in light-proof container up to 3 weeks

ii. Recording Media

a. Into sterile beaker with 800mL sterile (Sigma W3500 500mL water), add:
b. Entire bottle (10g) of Dulbecco's Modified Eagle's Medium (DMEM) (Sigma D-2902 already includes L-glutamine 0.584g/L)
c. 2.5mL Penicillin (25U/mL Final) & Streptomycin (25ug/mL Final) (Sigma p4333)
d. 4.7mL NaHCO3 (7.5%)
e. 10mL Hepes (1M, pH 7.2)
f. 3.5g Glucose (Sigma 7021) or 7.8mL 45% Glucose solution (Sigma G8769)
g. Bring volume to 1000mL total
h. Filter sterilize
i. Store at 4°C in light-proof container up to 3 weeks

iii. Materials (all sterile *in order of appearance*)

P1000 pipettor
precut P1000 tips
P200 tips
1 sterile bulbed pipette
#10 and #11 blades
Large scissors
Small curved scissors (FST 14091-11)
Whatman #2 filter paper
15mL conical tube
Submersion box
Chuck
Superglue
Autoclaved Aluminum foil packet
flint lighter
KimWipes (regular & E-XL)
Campden Instruments Integraslice 7550MM
Styrofoam ice bucket
aliquoted N2 supplement (Invitrogen)
P200 pipettor
P100 tips
2 sterile Falcon ten-twenty-nine Petri dishes
2 scalpels
Fine forceps
Medium scissors (FST 14070-12)
35mm culture dish(es), cut
Tube rack
Millicell 0.4um culture insert (PICMORG50)
Heated Lids (Bioptechs special order)
WPI Blade SS for Integraslice #501632
UV sterilized Pyrex dishes (1 ½)
Bunsen burner
Electric trigger pipettor
aluminum foil
round ice bucket
dissection microscope

Preliminary preparation

Figure A.3-1. | **Proper hood organization.**

1. >10 minutes prior to culture, place the following instruments and objects into hood for UV sterilization as indicated in Fig. A.3-1:
    a. P1000 pipettor (set at 1000uL) and P200 pipettor (set at 200uL)
    b. Autoclaved precut P1000 tips, regular P1000 tips and P200 tips
    c. 2 sterile Falcon ten-twenty-nine Petri dishes
    d. 1 sterile bulbed pipette, cut
    e. Autoclaved vacuum grease-filled 10mL syringe
    f. 2 scalpels with 1 #10 blade and 1 #11 blade
    g. Hanging on rack:
        i. fine forceps
        ii. Large scissors for decapitation
        iii. Medium scissors for skull
        iv. Small curved scissors for extraction and nerves
    h. Several sterile 35mm culture dishes with lids
    i. All heated lids cleaned thoroughly with EtOH
    j. Whatman #2 filter paper
    k. Tube rack with sterile 15mL tube
    l. Sterile culture insert(s)
    m. Integraslice materials
        i. Submersion box
        ii. Chuck
        iii. WPI blade
        iv. Superglue
    n. Autoclaved Pyrex dishes (1 ½ sets)
    o. Autoclaved Aluminum foil packet
    p. Bunsen burner (connected to gas) and a flint lighter
    q. Electric trigger pipettor
2. Be sure to have enough KimWipes and KimWipe E-XL

3. Place some aluminum foil on countertop between Integraslice and dissection microscope
4. Fill both ice buckets to top with fresh ice. The round one goes on foil (*left*), the Styrofoam one goes on the right of the dissection microscope.
5. Turn on dissection microscope with bottom red illumination.

Under sterile-field conditions in hood…

1. Cut a 35mm culture dish just below the line (total height = 6 mm) using a flame-heated #10 scalpel. Be sure to shape the dish so that it properly fits into the heated lid. Cover with native lid and put aside to sterilize under UV.
2. Using a sterile 10mL serological pipette, transfer 9.9mL sterile recording media to 15mL sterile tube with the electric trigger pipettor, close and place in incubator at 37°C.

Figure A.3-2. | **Culture room bench organization**. Integraslice**,** dissection microscope and ice buckets.

3. Place Sampling media bottle in Styrofoam ice bucket at 4°C.
4. Carefully open the foil surrounding the Pyrex dishes and
    a. Place one ½ dish upside-down in round ice bucket.
    b. Tear off a piece of foil to cover top of Styrofoam ice bucket, sterile side up.
5. Pour 40mL Sampling media into the full Pyrex dish.
    a. Place the full Pyrex dish on the foil in the Styrofoam bucket.
6. Dip a Whatman filter paper into dish (or submersion box), and place on upside-down ½ dish in the round ice bucket. Place a dry piece of filter paper next to it.
7. Assemble Integraslice with blade and submersion box. Be careful that hands are EtOH-sterilized.

a. Turn on Integraslice and set cutting frequency to 70, and adjust height and speed accordingly.

8. Pour sampling media into submersion box.

Sacrifice and Isolation

1. Sacrifice mouse or other rodent by cervical dislocation.
2. With course scissors, decapitate animal and remove eyes.
3. With medium and fine-curved scissors, extract brain being careful not to damage the optic chiasm.
4. Drop the freshly extracted brain ventral-side-up onto the filter paper.
5. If performing a coronal slice, go to step 6. If performing horizontal slice, skip to step 9.
6. With #11 scalpel, remove cerebellum and caudal cortex, being careful to keep slice perfectly perpendicular to the midline (longitudinal fissure).
7. With the same blade, remove all forebrain immediately anterior (rostral) to the optic chiasm.
8. Pat-dry the caudal side of the brain with dry filter paper to remove excess liquid—this makes the superglue stick more reliably.
9. Put 1 drop of superglue on the chuck, and place the brain rostral-side-up (ventral-side-up for horizontal slicing) on the chuck with fine forceps.
    a. Dry any excess glue with a KimWipe
10. Submerge chuck and brain into sampling media.
11. Lower vibrating blade into sampling media and slice through chiasm at a thickness of 200um and no faster than 0.17mm/sec through SCN.
12. Turn off lights.
13. With the cut, bulbed pipette and a pair of fine forceps, remove selected slices to the Pyrex dish on ice with sampling media in it.
14. Using sharp forceps, place a hole in the right side of the basal ganglia in order to see the proper orientation of the slices as they come out.
15. As slices are being made, one may use the dissection microscope to study the previous slices under dim red light, and may take pictures of the slices with the digital camera.
    a. If one wishes to keep an “anterior” and a “posterior” slice, orient the slices for cutting (step 17) such that the anterior slice has the basal ganglia hole on the right (when ventral side down) and the posterior slice has the basal ganglia hole on the left.
16. Dr. Hide Ohta recommends that a “good” slice is a posterior section in which one can see the suprachiasmatic nuclei (SCN) and a shadow of the chiasm directly behind them, as in Figure A.3-3. But follow this guideline if only 1 slice is to be kept.

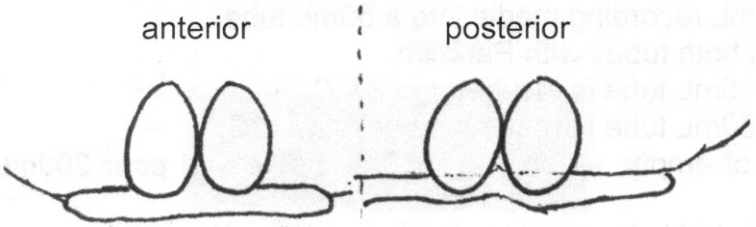

Figure A.3-3. | **Proper slice selection.** Coronal slices through suprachiasmatic nuclei of the hypothalamus showing the slight difference between a more anterior cut and the preferred posterior slice.

17. When a good slice is found, steady it in the dish with the #11 scalpel and use the #10 scalpel to evenly cut out the SCN in a "D" shape as in Figure A.3-4.

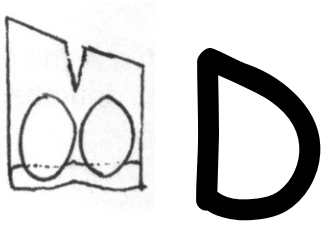

Figure A.3-4. | **Cutting the proper coronal slice.** Coronal slice through the preferred posterior SCN showing the "D"-shaped cut to distinguish the correct side for microscopy.

Culture (in hood under sterile-field conditions)

1. Fetch the recording media from the incubator.
2. Using the P1000, transfer 1000uL into the 35mm culture dish.
    a. Keep covered at all times, blocking light with foil if possible.
3. Using fine forceps, angle a culture membrane slowly into the dish, like a coverslip on a slide so that no bubbles form.
4. Using a cut P1000 tip on the P1000 pipette, transfer the slice (over the culture dish top) onto the membrane so that it maintains a "D" orientation.
5. Use a P200 to remove excess media from the top, making sure to keep the slice in the dead-center of the membrane (unless placing 2 or more on the same membrane, in which case evenly space).
6. "Frost the cake" by squeezing vacuum grease around heated-lid rim, and press onto dish to seal. Be sure the lid is on flat and steady.
7. Move the dish to the confocal microscope.

Proceed to "Live Culture" Confocal microscopy…

B. Live Culture Confocal microscopy (Multi-Unit)

Note: it is best to allow the Confocal laser to equilibrate over some period of time (usually 5 hours) before using it. This can be problematic, however, because this requires the Mercury fluorescent bulb to be on aimlessly as well (if you use it). Use discretion.

Startup

1. Make sure laser box is in "Standby" mode.
2. Make sure black knob is at 9 o'clock.
3. Turn on "Power Enable" (O→I).
4. Turn on "Emission Key" clockwise.
5. Run in "Standby Mode" for 10 minutes.
6. Toggle switch from "Standby" to "Laser Run".
7. Turn on Voltmeter.
    a. Red probe in top right hole, black probe in bottom right hole.

8. Crank up the black knob until the Voltmeter reads ~650 mV (0.650 V).
9. Turn on the temperature regulator and put the "Set Temp." at 35.5°C.
10. Turn on smaller voltage regulator and adjust it to stay at ~2.5 V as new lids are added.
11. Activate powerstick under computer.
12. Make sure stage controller (top of rack) is on and the Z-axis keypad is not frozen.
13. Turn on the computer, and sign in as "Confocal" (password: "silvioconte").

For "Live Culture" Confocal Microscopy

14. Turn on the "Air" to float the table.
15. Place the 6-well aluminum chamber securely on the stage, and insert the temperature sensor into the hole on the side with putty. Also, attach wires for current from the temperature regulator.
16. Allow the chamber to reach set temperature.
17. Screw in the Achroplan 20x long-working-distance objective (LD Achroplan 20x/0.4 Korr Ph2) and set the inherent focus to 0.5 (the thickness of the heated glass).

Setting up Multiple Slices

1. Quickly transfer the culture dish(es) to the 6-well chamber and attach the voltage regulator to the heated lid(s) to avoid condensation.
2. Putty the dish(es) into the well to stabilize it (them).
3. Using dim red light (keep on setting #1 on the filter wheel), drop the objective down and center the slice.
4. Focus down properly.
5. *See next section for computer setup.* On the "Stage" control of the computer, click zero and "Mark position." This is your first position.
6. Go to the next slice in the sequence, and follow steps 9-11 until all slices are accounted for.
7. Pull out the silver slider tube on the right side of the microscope to allow the photo-multiplier-tube (PMT) to get a look.

Confocal Computer Settings for MultiTime Series

1. Start up PASCAL with the laser on (Fig. A.3-5)

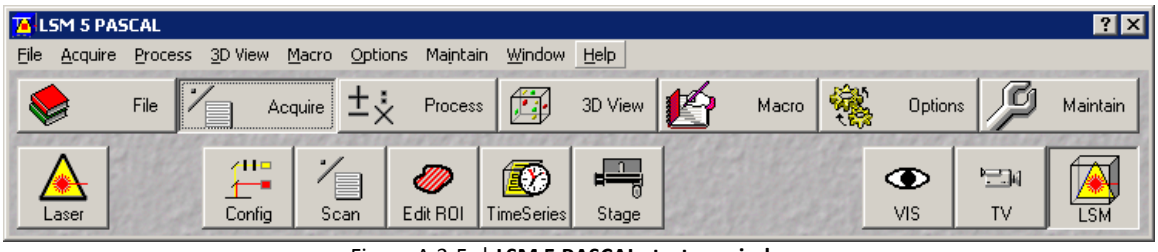

Figure A.3-5. | **LSM 5 PASCAL startup window.**

2. Create a new image database ("File" menu)
3. "Config" → "Config" → "GFP Bandpass" → Apply → Close "Config" (Fig. A.3-6)

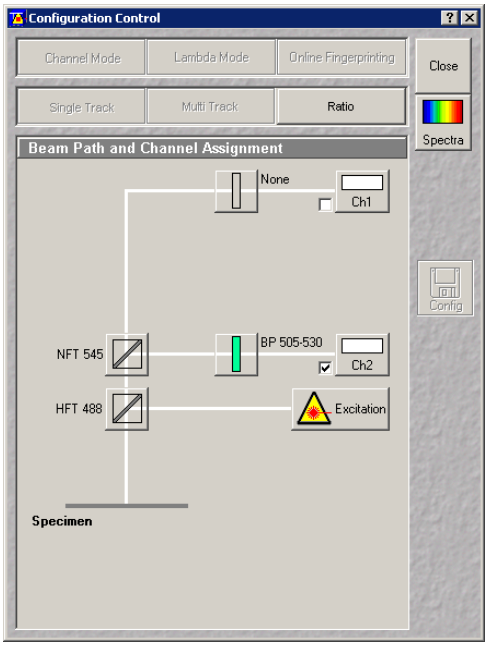

Figure A.3-6. | **LSM 5 PASCAL Configuration Control window.** "GFP Bandpass" loaded.

4. "Scan"
    a. "Mode" (Fig. A.3-7a)
        i. Objective: LD Achroplan 20x/0.4 Korr Ph2
        ii. Speed: 7 @ mean of 16 lines
        iii. Data Depth: 12 bit, unidirectional
        iv. Zoom, Rotation and Offset: *to taste*

A

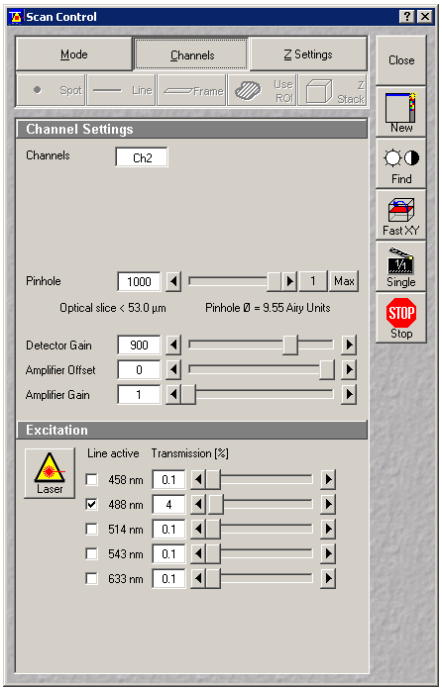

B

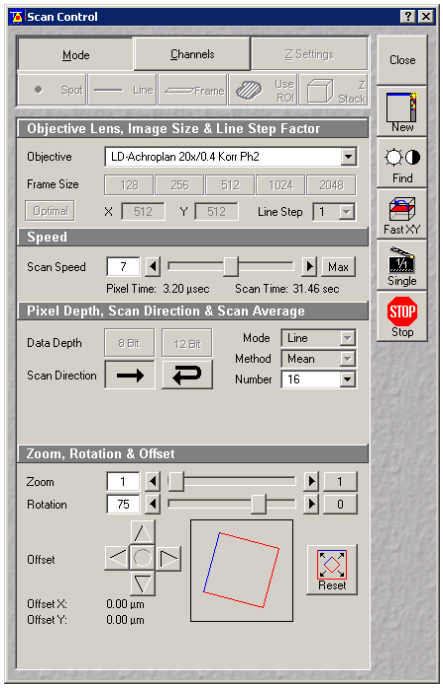

Figure A.3-7. | **LSM 5 PASCAL Scan Control window.** a | "Mode" tab. b | "Channels" tab.

b. “Channels” (Fig. A.3-7b)
    i. Pinhole: Max
    ii. Detector gain: Max to orient SCN in frame, then ~900
    iii. Amplifier offset: *to taste with “Palette” option*
    iv. Amplifier gain: 1
    v. Excitation: 488 nm checked *and laser excitation increased as necessary (usually 4% when the laser is healthy, though each new laser has its own settings)*
c. Z settings
    i. Z sectioning: depressed
    ii. Number of slices: 3
    iii. Interval (um): 20
    iv. Current slice: 2

5. “Stage” (Fig. A.3-8)

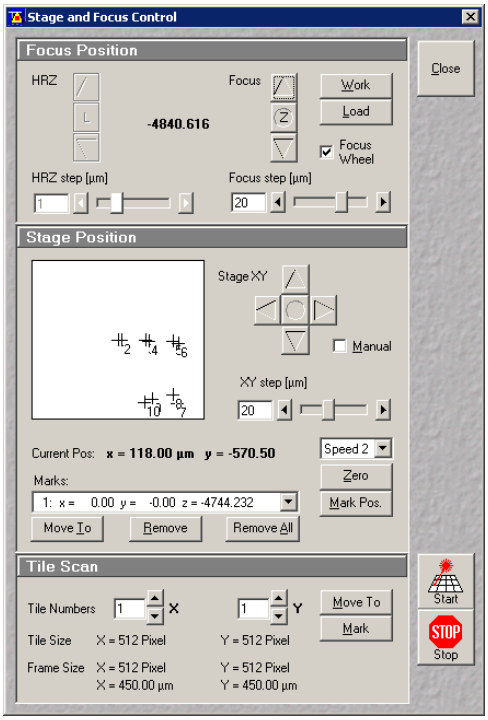

Figure A.3-8. | **LSM 5 PASCAL Stage and Focus Control window.**

6. MultiTime Macro (Fig. A.3-9)
    a. Depress “Multiple Locations” tab.
        i. Depress “GR-G-L” tab.
        ii. “Experiment Repitions”: 150
        iii. “Views”: 1
        iv. “Group Repititions”: 5
    b. Block 1 Parameters; Location 1
        i. “Wait Interval (min)”: 60 min

ii. Depress “Define Configuration”

c. Configuration, Time Interval and Number of Scans

i. Set configuration settings in the Scan Control window to taste, and then name a configuration for each slice and “Save Conf.”

ii. Check “ZStackXY”

iii. “Base File Name” should be the part number (i.e. “Part01”)

iv. “Select Image Database” to the one you created.

v. “Options”: Choose whether to make the objective go to the “loading position” before moves. Also clear previous TEMP files.

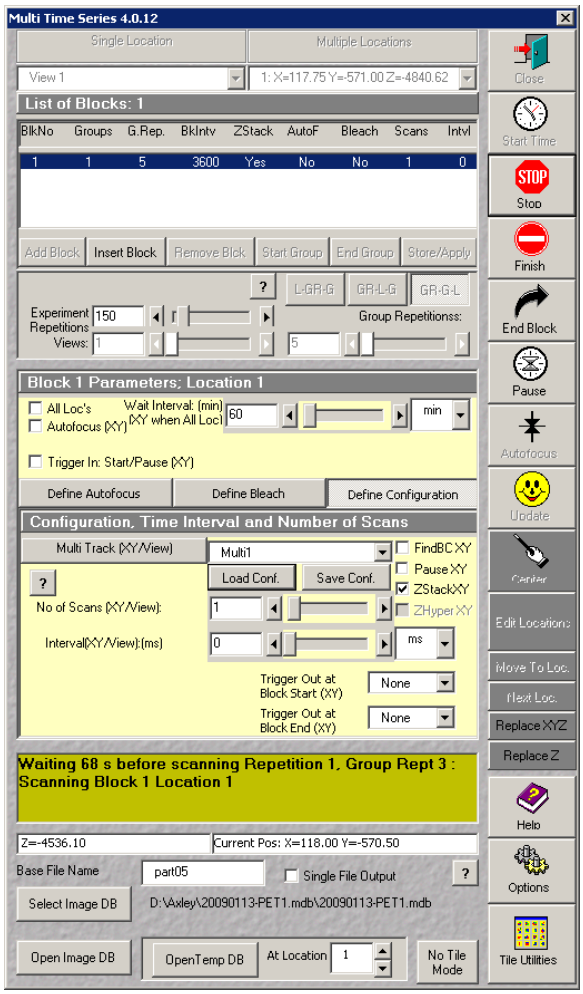

Figure A.3-9. | **LSM 5 PASCAL MultiTime 4 Macro window.**

These are the basic settings, but of course, one must play around with the focus to get the slice at optimal level. This is accomplished using “FastXY” in the “Scan” menu. At this point, one can rotate, move, focus or normalize the palette. Click Stop.

General Procedures for Time Series Imaging

1. Once all slices are properly centered and their configurations saved, imaging may commence.
2. Press "Start Time".
3. Slices are generally made between CT9-12, or late subjective day, and the first Z-stack is taken at CT12. Images should be taken ON THE HOUR to avoid later confusion.
4. The Laser scans the deepest layer first (the more negative number on the Z-axis), then the middle layer, and then finally the most superficial layer.
5. The Z focus will have to be adjusted as the slice settles over the first 36 hours.
    a. Every 3-4 hours, click "Finish" on the "MultiTime" menu. Images are concatenated and saved automatically, but in the event of a crash, they are backed up individually in the TEMP folder.
    b. Using the "FastXY" and incremental focus on the "Stage" control, center and adjust the middle layer to the best depth at all positions, being sure to hit "Replace XYZ" after every adjustment and restart the Time Series by pressing "Start Time" at the appropriate hour-mark.
        i. It is best not to further normalize the image using the palette midstream because it will be a jumpy contrast/brightness change in the movie.
6. Try to capture at least 90 consecutive hours of good fluorescence.

C. Live Culture Confocal microscopy (Single-Unit)

Note: it is best to allow the Confocal laser to equilibrate over some period of time (usually 5 hours) before using it. This can be problematic, however, because this requires the Mercury fluorescent bulb to be on aimlessly as well (if you use it). Use discretion.

Startup

18. If using epifluorescence, start FluoArc. Otherwise, skip to step 2.
19. Make sure laser box is in "Standby" mode.
20. Make sure black knob is at 9 o'clock.
21. Turn on "Power Enable" (O→I).
22. Turn on "Emission Key" clockwise.
23. Run in "Standby Mode" for 10 minutes.
24. Toggle switch from "Standby" to "Laser Run".
25. Turn on Voltmeter.
    a. Red probe in top right hole, black probe in bottom right hole.
26. Crank up the black knob until the Voltmeter reads ~650 mV (0.650 V).
27. Turn on the temperature regulator and put the "Set Temp." at 35.5°C.
28. Turn on smaller voltage regulator and adjust it to stay at ~2.5 V as new lids are added.
29. Activate powerstick under computer.
30. Make sure stage controller (top of rack) is on and the Z-axis keypad is not frozen.
31. Turn on the computer, and sign in as "Chris" (password: "silvioconte").

For "Live Culture" Confocal Microscopy

32. Turn on the "Air" to float the table.

33. Place the 6-well aluminum chamber securely on the stage, and insert the temperature sensor into the hole on the side with putty. Also, attach wires for current from the temperature regulator.
34. Allow the chamber to reach set temperature.
35. Screw in the Achroplan 20x long-working-distance objective (LD Achroplan 20x/0.4 Korr Ph2) and set the inherent focus to 0.5 (the thickness of the heated glass).

Setting up the Single Slice

8. Quickly transfer the culture dish to the 6-well chamber and attach the voltage regulator to the heated lid so as to avoid condensation.
9. Putty the dish into the well to stabilize it.
10. Using dim red light (keep on setting #1 on the filter wheel), drop the objective down and center the slice.
11. Focus down properly.
12. *For epifluorescence:* turn off the red light and switch the filter wheel to FITC (position #3), and pull out the black slider.
    a. A good slice will usually fluoresce under FITC excitation, but this may not always be the case.
13. Replace the slider position, and turn the wheel to #1 for the laser. Also, pull out the silver slider tube on the right side of the microscope to allow the photo-multiplier-tube (PMT) to get a look.

Confocal Computer Settings for Time Series

7. Start up PASCAL with the laser on.
8. "Config" → "Config" → "GFP Bandpass" or "GFP Longpass" → Apply → Close "Config"
9. "Scan"
    a. "Mode"
        i. Objective: LD Achroplan 20x/0.5W Korr
        ii. Speed: 3 (or 7 @ mean of 16 lines)
        iii. Data Depth: 12 bit
        iv. Zoom, Rotation and Offset: *to taste*
    b. "Channels"
        i. Pinhole: Max
        ii. Detector gain: Max to orient SCN in frame, then ~900
        iii. Amplifier offset: *to taste with "Palette" option*
        iv. Amplifier gain: 1
        v. Excitation: 488 nm checked *and laser excitation increased as necessary (usually 4% when the laser is healthy, though each new laser has its own settings)*
    c. Z settings
        i. Z sectioning: depressed
        ii. Number of slices: 3
        iii. Interval (um): 20
        iv. Current slice: 2
10. Time Series
    a. Number: ∞ (or 150)
    b. Time Interval
        i. "SliceLiveImage" and Apply

ii. StartT

These are the basic settings, but of course, one must play around with the focus to get the slice at optimal level. This is accomplished using "FastXY" in the "Scan" menu. At this point, one can rotate, move, focus or normalize the palette. Click Stop.

General Procedures for Time Series Imaging

7. Once a slice is properly aligned and normalized on the screen, one may begin the time series by clicking "StartT" in the "Time Series" menu.
8. Slices are generally made between CT9-12, or late subjective day, and the first Z-stack is taken at CT12.
9. The Laser scans the deepest layer first (the more negative number on the Z-axis), then the middle layer, and then finally the most superficial layer.
10. The Z focus will have to be adjusted as the slice settles over the first 36 hours.
    a. Every 3-4 hours, click "Stop" on the "Time Series" menu and save the images as an MDB database, being careful to record how many timepoints were taken, and what part in the sequence the file is (i.e. is this the first or second time you've had to stop the time series to adjust?)
    b. Using the FastXY and manual SLOW focus (or incremental focus on the "Stage" control in the software), adjust the middle layer to the best depth and restart the Time Series by pressing "StartT" at the appropriate hour-mark.
        i. It is best not to further normalize the image using the palette midstream because it will be a jumpy contrast/brightness change in the movie.
11. Try to capture at least 90 consecutive hours of good fluorescence. It may be beneficial to allow the slice to settle before starting recording. This can range in time from several hours to several weeks (in neonatal tissue), all in an incubator (in sealed, sterile pouch).

D. MetaMorph Analyses

1. On the Confocal Room computer, transfer the LSM files to the "Analysis" computer with Molecular Devices MetaMorph 7.5 software and purple dongle.
2. Start MetaMorph Offline (MDS Software).
3. Be sure "McMahon" Taskbar is running.
4. Open all LSM parts of a single location (i.e. part01_L1_Sum.LSM, part02_L1_Sum.LSM, *etc.*) by dragging the icons to the MetaMorph window.
5. Create a stack.
    a. Click "Add Plane" on the McMahon taskbar (Fig. A.3-10 and A.3-11a).
        i. Source: select the second highest stack (for example, if there are 10 parts, this would be Part09) and "All Planes".
        ii. Resultant stack: the highest stack (for example, if there are 10 parts, this would be Part10) and "Top".
        iii. Check "Close image after adding".

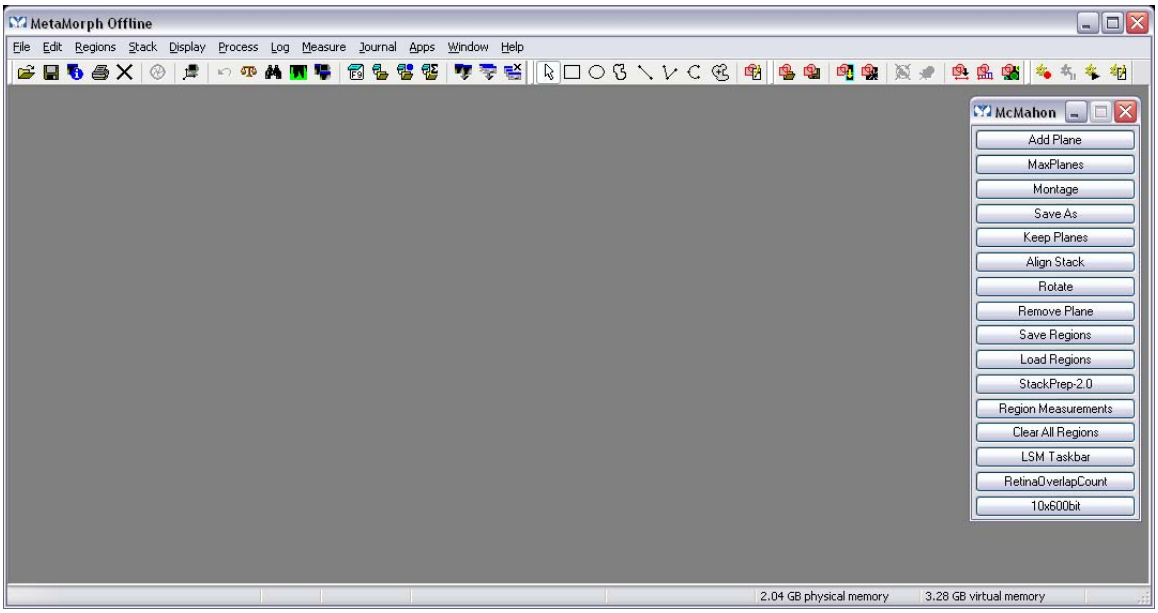

Figure A.3-10. | **MetaMorph Offline 7.5 Software window.** McMahon taskbar with prerecorded "journals" on right.

b. Click "MaxPlanes" on the McMahon taskbar. The code for this journal is © 2007 by C.M.Ciarleglio for open use by the McMahon Lab and its collaborators.
    i. this macro will take a Maximum image for each timepoint and trim the stack to exactly 90 planes (hours 0-89).

A B C

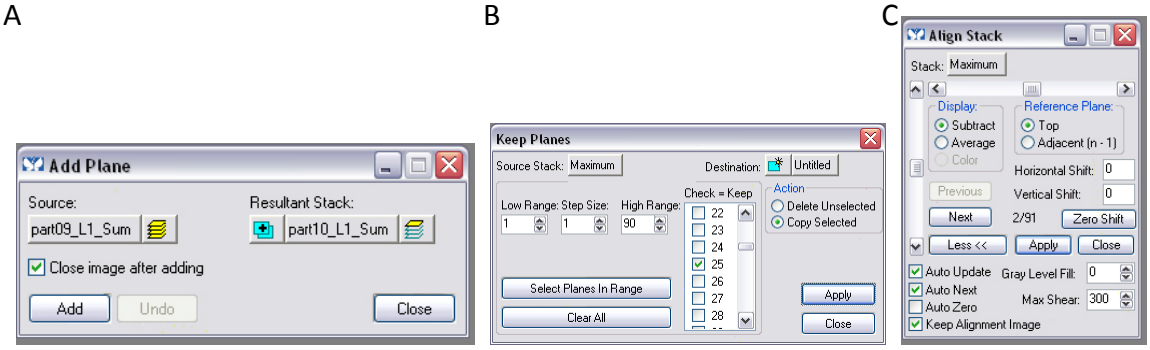

Figure A.3-11. | **Creating a stack. a** | Add Plane window. **b** | Keep Planes window. **c** | Align Stack window.

6. Align the stack.
    a. Find the best image in the stack (usually around plane 25), and click "Keep Planes" on the McMahon taskbar (Fig. A.3-11b).
        i. select only that plane, make sure that "Copy Selected" is checked, and hit apply.
        ii. click "Add Plane" on the McMahon taskbar and add the copied plane to the top of the Maximum stack (Fig. A.3-11a). This will serve as a reference.
    b. Click "Align Stack" on the McMahon taskbar (Fig. A.3-11c). Align images to both the "Top" image and the "Adjacent (n-1)" image.

c. Rotate as needed (not often) by clicking “Rotate” on the McMahon taskbar.
d. Close the “Align Stack” window, then the “Alignment window”. SAVE the stack accordingly.

7. Background subtraction.
   a. Click “StackPrep-2.0” on the McMahon taskbar. The code for this journal is © 2007 by C.M.Ciarleglio for open use by the McMahon Lab and its collaborators.
      i. This journal does a Morphological background subtraction with the settings shown in Figure A.3-12.

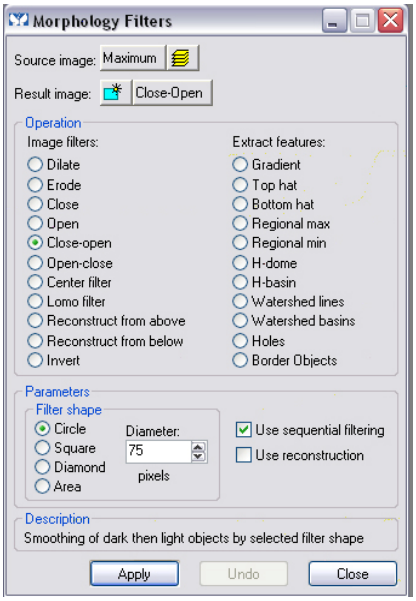

Figure A.3-12. | **Morphology Filters window as set up in the “StackPrep 2.0” macro.**

8. Click “Remove Plane” on the McMahon taskbar and check the first plane. This will bring the number of planes back to 90.
9. SAVE stack as a “MetaSeries Single/Multi-plane TIFF(*.tif).” Repeat steps 4-9 for next locations.
10. Using the background-subtracted stack, click “Region Measurements” on the McMahon taskbar and make sure the “Graph” tab is active. Using a Region of Interest (ROI) tool, select cells (or larger regions) and see their circadian profile on the graph (Fig. A.3-13).
11. When all ROIs are selected, click “Open Log” on the “Region Measurements” window.
    a. “Open Data Log” window
       i. select “Dynamic Data Exchange”
       ii. click OK
    b. “Export Log Data” window
       i. select “Microsoft Excel”
       ii. Sheet name: Sheet1
       iii. Starting Row: 1
       iv. Starting Column: 1
       v. Hit OK.
       vi. MS Excel will open.
    c. click “F9: Log Data”

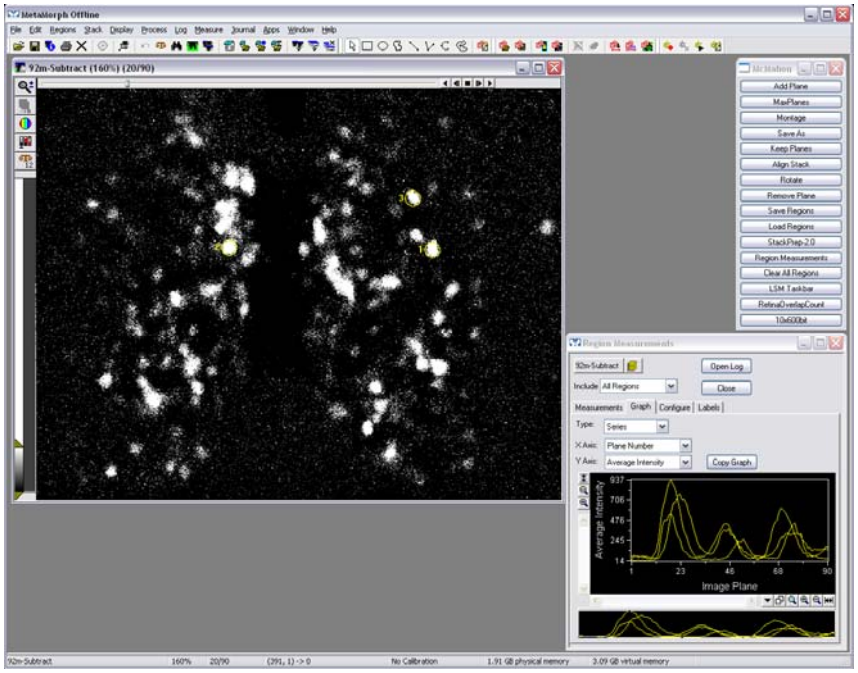

Figure A.3-13. | **Cell selection.**

E. TheCohenProject®[w]

1. Save the exported Excel spreadsheet as a comma-delimited text file (*.CSV) (Fig. A.3-14).
2. The folder system for TheCohenProject® should be set up on a Windows OS computer as in Fig. A.3-15.

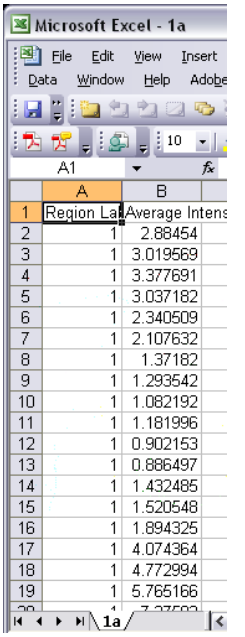

Figure A.3-14. | ***.CSV file layout.**

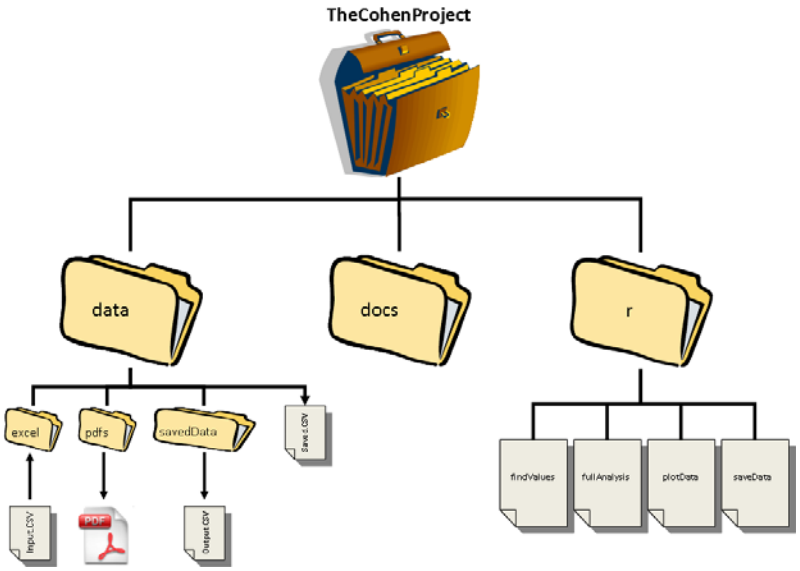

Figure A.3-15. | **TheCohenProject® folder layout for Windows OS.**

[w] © 2007 by J.Y.Cohen for use by McMahon Lab.

3. *.R files located in the folder: \TheCohenProject\r\
    a. “findvalues.r” code

```
#########################################################
### Find values of interest for GFP intensity plots ###
###                                                  ###
### Written by Jeremiah Cohen for Chris Ciarleglio  ###
### December, 2007                                   ###
#########################################################

# cells is the matrix of GFP intensities
# cellNo is which cell number to analyze in cells
# resolution is the resolution (in hrs) of the smoothing spline

findValues <- function(cells, cellNo = 1, session = '48a', resolution = 0.1,
 sampleTime)
{
 options(locatorBell = FALSE)
 cell <- cells[((cellNo - 1) * sampleTime + 1) : (cellNo * sampleTime), 2]
 if (sampleTime != 117){
  predictCell <- predict(smooth.spline(x = 0 : (sampleTime - 1), y = cell),
   seq(0, (sampleTime - 1), resolution))
 }
 if (sampleTime == 117){
  predictCell <- predict(smooth.spline(x = c(0 : 13, seq(14.5, 65.5,
   by = .5)), y = cell), seq(0, 65.5, resolution))
 }
 winDialog('ok', message = 'Choose two points surrounding each extremum.')

 x11(height = 8, width = 10)
 plot(predictCell$x, predictCell$y, type = 'l', xlab = 'Time (h)',
  ylab = 'Intensity', bty = 'l', main = paste('Session ', session, ' cell ',
  cellNo, sep = ''))
 if (sampleTime == 90) points(0 : 89, cell, cex = .75)
 if (sampleTime == 117) points(c(0 : 13, seq(14.5, 65.5, by = .5)), cell, cex = .75)
 abline(v = 12, lty = 2, col = 'gray')
 locatePeaks <- locator()

 plot(predictCell$x, predictCell$y, type = 'l', xlab = 'Time (h)',
  ylab = 'Intensity', bty = 'l', main = paste('Session ', session, ' cell ',
  cellNo, sep = ''))
 if (sampleTime == 90) points(0 : 89, cell, cex = .75)
 if (sampleTime == 117) points(c(0 : 13, seq(14.5, 65.5, by = .5)), cell, cex = .75)
 abline(v = 12, lty = 2, col = 'gray')
 abline(v = locatePeaks$x, col = 'gray')

 if (length(locatePeaks$x)%%6 != 0){
  qa <- winDialog('ok', message =
   'You did not choose the correct number of points. Please redo this cell.')
  graphics.off()
  return(NA)
 }
 qa <- winDialog(type = 'yesno', message = 'Are you ok with your picks?')
 if (qa == 'NO'){
  graphics.off()
  return(NA)
 }

 # Find the local extrema
 xTroughs1 <- vector(); xPeaks <- vector(); xTroughs2 <- vector()
 yTroughs1 <- vector(); yPeaks <- vector(); yTroughs2 <- vector()
 for (i in seq(1, length(locatePeaks$x), by = 6)){
  temp1 <- which.min(abs(predictCell$x - locatePeaks$x[i]))
  temp2 <- which.min(abs(predictCell$x - locatePeaks$x[i + 1]))
  xTroughs1 <- c(xTroughs1, temp1 + which.min(predictCell$y[temp1 : temp2]) -
```

```
  1)
 yTroughs1 <- c(yTroughs1, min(predictCell$y[temp1 : temp2]))
 temp3 <- which.min(abs(predictCell$x - locatePeaks$x[i + 2]))
 temp4 <- which.min(abs(predictCell$x - locatePeaks$x[i + 3]))
 xPeaks <- c(xPeaks, temp3 + which.max(predictCell$y[temp3 : temp4]) - 1)
 yPeaks <- c(yPeaks, max(predictCell$y[temp3 : temp4]))
 temp5 <- which.min(abs(predictCell$x - locatePeaks$x[i + 4]))
 temp6 <- which.min(abs(predictCell$x - locatePeaks$x[i + 5]))
 xTroughs2 <- c(xTroughs2, temp5 + which.min(predictCell$y[temp5 : temp6]) -
  1)
 yTroughs2 <- c(yTroughs2, min(predictCell$y[temp5 : temp6]))
}

# Phase and time at half-peak, 10% of peak, and 90% of peak of rise
yTenRise <- predictCell$y[xTroughs1] + (predictCell$y[xPeaks] - predictCell$
 y[xTroughs1])/10
yFiftyRise <- predictCell$y[xTroughs1] + (predictCell$y[xPeaks] - predictCell$
 y[xTroughs1])/2
yNinetyRise <- predictCell$y[xTroughs1] + 9 * (predictCell$y[xPeaks] -
 predictCell$y[xTroughs1])/10
xTenRise <- vector(); xFiftyRise <- vector(); xNinetyRise <- vector()
for (i in 1 : length(xTroughs1)){
 xTenRise[i] <- xTroughs1[i] + which.min(abs(predictCell$y[xTroughs1[i] :
  xPeaks[i]] - yTenRise[i]))
 xFiftyRise[i] <- xTroughs1[i] + which.min(abs(predictCell$y[xTroughs1[i] :
  xPeaks[i]] - yFiftyRise[i]))
 xNinetyRise[i] <- xTroughs1[i] + which.min(abs(predictCell$y[xTroughs1[i] :
  xPeaks[i]] - yNinetyRise[i]))
}

# Phase and time at half-peak, 10% of peak, and 90% of peak of fall
yTenFall <- predictCell$y[xTroughs2] + (predictCell$y[xPeaks] - predictCell$
 y[xTroughs2])/10
yFiftyFall <- predictCell$y[xTroughs2] + (predictCell$y[xPeaks] - predictCell$
 y[xTroughs2])/2
yNinetyFall <- predictCell$y[xTroughs2] + 9 * (predictCell$y[xPeaks] -
 predictCell$y[xTroughs2])/10
xTenFall <- vector(); xFiftyFall <- vector(); xNinetyFall <- vector()
for (i in 1 : length(xTroughs2)){
 xTenFall[i] <- xPeaks[i] + which.min(abs(predictCell$y[xPeaks[i] :
  xTroughs2[i]] - yTenFall[i]))
 xFiftyFall[i] <- xPeaks[i] + which.min(abs(predictCell$y[xPeaks[i] :
  xTroughs2[i]] - yFiftyFall[i]))
 xNinetyFall[i] <- xPeaks[i] + which.min(abs(predictCell$y[xPeaks[i] :
  xTroughs2[i]] - yNinetyFall[i]))
}

xTenRise <- predictCell$x[xTenRise]
xFiftyRise <- predictCell$x[xFiftyRise]
xNinetyRise <- predictCell$x[xNinetyRise]
xTenFall <- predictCell$x[xTenFall]
xFiftyFall <- predictCell$x[xFiftyFall]
xNinetyFall <- predictCell$x[xNinetyFall]

plot(predictCell$x, predictCell$y, type = 'l', xlab = 'Time (h)',
 ylab = 'Intensity', bty = 'l', main = paste('Session ', session, ' cell ',
 cellNo, sep = ''))
if (sampleTime == 90) points(0 : 89, cell, cex = .75)
if (sampleTime == 117) points(c(0 : 13, seq(14.5, 65.5, by = .5)), cell, cex = .75)
for (i in 1 : length(xPeaks)){
 points(xTenRise, yTenRise, cex = 1.25, pch = 16)
 points(xFiftyRise, yFiftyRise, cex = 1.25, pch = 16)
 points(xNinetyRise, yNinetyRise, cex = 1.25, pch = 16)
 points(xTenFall, yTenFall, cex = 1.25, pch = 16)
 points(xFiftyFall, yFiftyFall, cex = 1.25, pch = 16)
 points(xNinetyFall, yNinetyFall, cex = 1.25, pch = 16)
```

```
 }
 legend('topleft', legend = c('Data', 'Smoothed', 'Values of interest'),
  bty = 'n', lty = c(0, 1, 0), pch = c(1, -1, 16))

 qa <- winDialog(type = 'yesno', message = 'Ok?')
 if (qa == 'NO'){
  graphics.off()
  return(NA)
 }

 graphics.off()

 return(list(predictCell = predictCell, xTenRise = xTenRise, yTenRise =
  yTenRise, xFiftyRise = xFiftyRise, yFiftyRise = yFiftyRise, xNinetyRise =
  xNinetyRise, yNinetyRise = yNinetyRise, xTenFall = xTenFall, yTenFall =
  yTenFall, xFiftyFall = xFiftyFall, yFiftyFall = yFiftyFall, xNinetyFall =
  xNinetyFall, yNinetyFall = yNinetyFall))
}
```

b. "fullAnalysis.r" code

```
#########################################################################
### Run the findValues.r analysis on all cells for a given session ###
###                                                                 ###
### Written by Jeremiah Cohen for Chris Ciarleglio                  ###
### December, 2007                                                  ###
#########################################################################

rm(list = ls())
source('findValues.r'); source('plotData.r'); source('saveData.r')
options(locatorBell = FALSE)

# Organize all sessions into a vector
session <- winDialogString('Enter the session to analyze without quotes.', '')
sampleTime <- as.numeric(winDialogString(paste('Enter the length of the ',
 'recording session.', sep = ''), ''))
path = '../data/excel/'
if (sampleTime == 66) sampleTime <- 117

# Compute values of interest
valsOfInterest <- list()
myData <- read.csv(paste(path, session, '.csv', sep = ''))
for (i in 1 : (dim(myData)[1]/sampleTime)){
 valsOfInterest[[i]] <- findValues(cells = myData, cellNo = i,
  session = session, resolution = 0.1, sampleTime = sampleTime)
 while(is.na(valsOfInterest[[i]])[1]){
  valsOfInterest[[i]] <- findValues(cells = myData, cellNo = i,
   session = session, resolution = 0.1, sampleTime = sampleTime)
 }
}
save(valsOfInterest, file = paste('../data/', session,
 'valsOfInterest.rda', sep = ''))

# Plot
load(paste('../data/', session, 'valsOfInterest.rda', sep = ''))
for (i in 1 : (dim(myData)[1]/sampleTime)){
 plotData(cells = myData, valsOfInterest = valsOfInterest[[i]],
  cellNo = i, path = '../data/pdfs/', outputFile = session,
  sampleTime = sampleTime)
}

# Save to .csv
load(paste('../data/', session, 'valsOfInterest.rda', sep = ''))
```

```
saveData(cells = myData, valsOfInterest = valsOfInterest,
  path = '../data/savedData/', outputFile = session, sampleTime = sampleTime)
```

c. “plotData.r” code

```
#########################################################
### Save data from findValues.r analysis          ###
###                                             ###
### Written by Jeremiah Cohen for Chris Ciarleglio ###
### December, 2007                              ###
#########################################################

plotData <- function(cells, valsOfInterest, cellNo = 1, path = '../data/pdfs/',
  outputFile = '48a', sampleTime)
{
  attach(valsOfInterest, warn.conflicts = FALSE)
  cell <- cells[((cellNo - 1) * sampleTime + 1) : (cellNo * sampleTime), 2]

  # Save plotted data to a .pdf file
  pdf(paste(path, 'cell', outputFile, cellNo, '.pdf', sep = ''))
  plot(predictCell$x, predictCell$y, type = 'l', xlab = 'Time (h)',
    ylab = 'Intensity', bty = 'l', main = paste('Session ', outputFile,
    ' cell ', cellNo, sep = ''))
  if (sampleTime == 90) points(0 : 89, cell, cex = .75)
  if (sampleTime == 117) points(c(0 : 13, seq(14.5, 65.5, by = .5)), cell, cex = .75)
  for (i in 1 : length(xTenRise)){
    points(xTenRise, yTenRise, cex = 1.25, pch = 16)
    points(xFiftyRise, yFiftyRise, cex = 1.25, pch = 16)
    points(xNinetyRise, yNinetyRise, cex = 1.25, pch = 16)
    points(xTenFall, yTenFall, cex = 1.25, pch = 16)
    points(xFiftyFall, yFiftyFall, cex = 1.25, pch = 16)
    points(xNinetyFall, yNinetyFall, cex = 1.25, pch = 16)
  }
  legend('topleft', legend = c('Data', 'Smoothed', 'Values of interest'),
    bty = 'n', lty = c(0, 1, 0), pch = c(1, -1, 16))
  dev.off()
}
```

d. “saveData.r” code

```
#########################################################
### Save data from findValues.r analysis          ###
###                                             ###
### Written by Jeremiah Cohen for Chris Ciarleglio ###
### December, 2007                              ###
#########################################################

saveData <- function(cells, valsOfInterest, path = '../data/savedData/',
  outputFile = '48a', sampleTime)
{
  for (j in 1 : (dim(myData)[1]/sampleTime)){
    attach(valsOfInterest[[j]], warn.conflicts = FALSE)

    mostValues <- sapply(t(cbind(xTenRise, xFiftyRise, xNinetyRise, xTenFall -
      xTenRise, xFiftyFall - xFiftyRise, xNinetyFall - xNinetyRise,
      xNinetyRise - xTenRise)), c)

    periods <- vector()
    for (k in 1 : (length(xFiftyRise) - 1)){
      periods <- c(periods, xFiftyRise[k + 1] - xFiftyRise[k])
    }
```

```
  dataToWrite <- t(data.frame(c(j, length(xTenRise), mostValues, periods)))
  row.names(dataToWrite) <- NULL
  if (j == 1){
    write.table(dataToWrite, file = paste(path, outputFile, '.csv', sep = ''),
      sep = ',', row.names = FALSE, col.names = FALSE)
  } else {
    write.table(dataToWrite, file = paste(path, outputFile, '.csv', sep = ''),
      sep = ',', append = TRUE, row.names = FALSE, col.names = FALSE)
  }
 }
}
```

4. Click the “R” folder shortcut and make sure to start in: \TheCohenProject\r
5. Start R console and type source ("fullAnalysis.r") at the command line. Hit Enter.
6. Type in the *.CSV filename of the session you want to analyze. Hit Enter.
7. Specify how many hours were in the run (usually 90). Hit Enter.
8. Click “OK” at the next prompt.
9. Click around each extremum. See example in Fig. A.3-16.

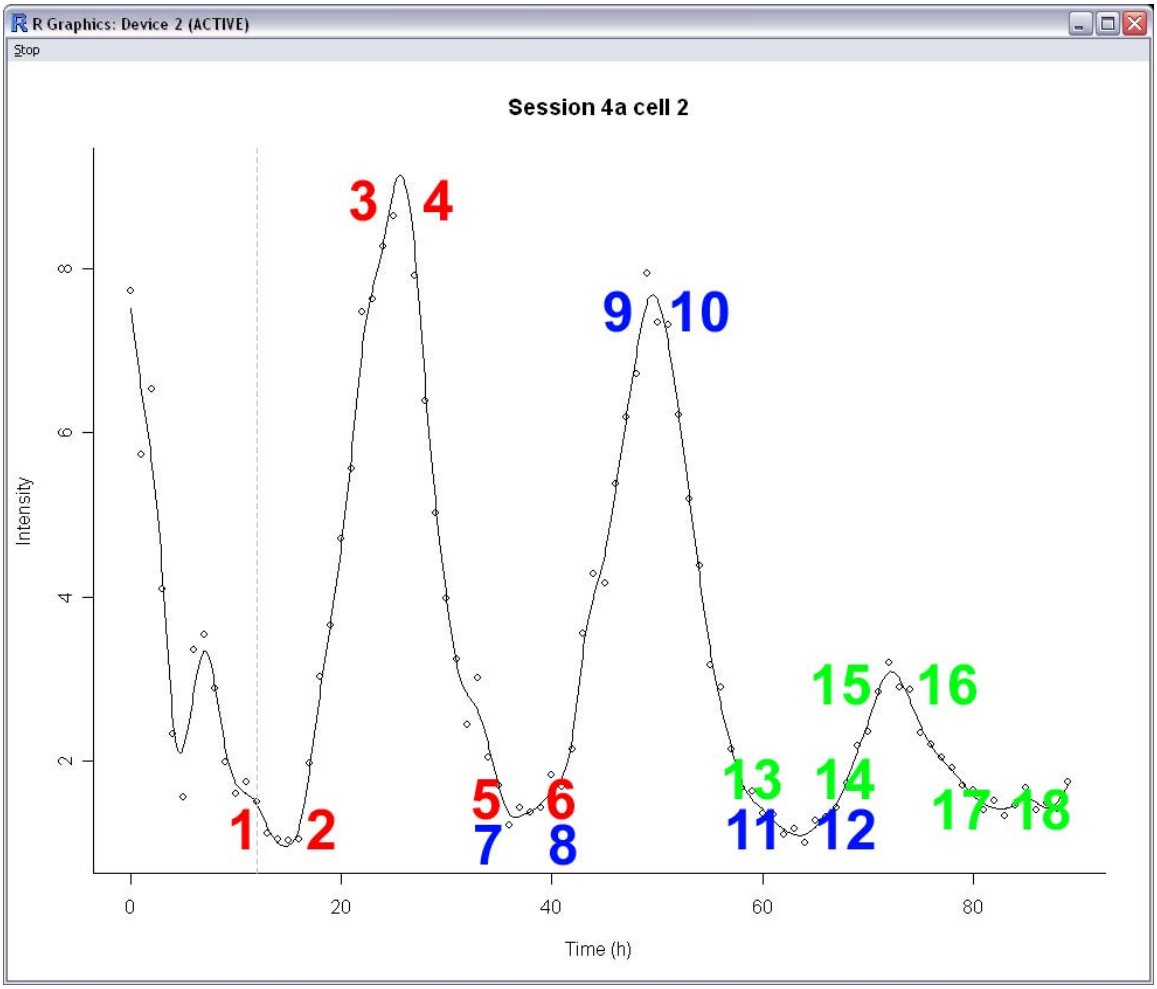

Figure A.3-16. | **TheCohenProject® peak selection.** Clicks are numbered numerically. Font color denotes peak.

10. Right-click anywhere on the screen and select “Stop”.
11. Click “OK” at the prompt if you are satisfied with your picks or “No” if you are not.
12. If you agree with the placement of the extremum lines, click “Yes” at the prompt, or “No” if you are not.
13. Repeat steps 8-12 until done. All files are automatically saved.
14. Compile the PDFs for scoring (\TheCohenProject\data\pdfs\).
15. Compile output files as desired for statistical analyses (\TheCohenProject\data\savedData\)

F. Location Adjustments

1. In the newly compiled output file, adjustments must be made in to phase in order to account for:
    a. Zeitgeber or Circadian Time
    b. the amount of time the Confocal microscope took to get to the slice in question.
2. Using Table A.2-1, adjust for “location time” by adding the amount in the table (hours) to the reported phase.
3. Using your knowledge of what ZT or CT the slice began its run, adjust accordingly.

Table A.2-1 | **Location time adjustments.**

Loading Position				No-Loading Position			
Location	MoveTime	Minutes	Hours	Location	MoveTime	Minutes	Hours
1	35	0.583333333	0.009722222	1	10	0.166666667	0.002777778
2	35	2.75	0.045833333	2	12	1.95	0.0325
3	40	5	0.083333333	3	15	3.783333333	0.063055556
4	35	7.166666667	0.119444444	4	12	5.566666667	0.092777778
5	40	9.416666667	0.156944444	5	15	7.4	0.123333333
6	35	11.58333333	0.193055556	6	12	9.183333333	0.153055556
7	40	13.83333333	0.230555556	7	15	11.01666667	0.183611111
8	35	16	0.266666667	8	12	12.8	0.213333333
9	40	18.25	0.304166667	9	15	14.63333333	0.243888889
10	35	20.41666667	0.340277778	10	12	16.41666667	0.273611111
11	40	22.66666667	0.377777778	11	15	18.25	0.304166667
12	35	24.83333333	0.413888889	12	12	20.03333333	0.333888889
13	40	27.08333333	0.451388889	13	15	21.86666667	0.364444444
14	35	29.25	0.4875	14	12	23.65	0.394166667

Section A.4: Immunocytochemistry (ICC)

i. Materials

4% paraformaldehyde fixative
Phosphate **B**uffered **S**aline or **T**ris **B**uffered **S**aline
35mm culture dishes
Vacuum grease
P1000 pipette
Plastic bulbed pipette
Blocking solution
Bovine **S**erum **A**lbumin
rabbit anti-GFP
guinea pig anti-AVP

guinea pig anti-VIP
Alexa-Fluor 594 Goat α-guinea pig (MP)
Alexa-Fluor 488 Goat α-rabbit (MP)
VectaShield Hardset Medium (Vector)

ii. Recipes

Fixative (8% Stock—1L good 2 weeks)

a. in 1L Erlenmeyer flask, rinse out dust
b. heat 800mL H_2O to 65ºC
c. add 80g paraformaldehyde
d. stir until well mixed (1 min)
e. add 3mL 5N NaOH or 1.5mL 10N NaOH (this clears the liquid)
f. mix until dissolved
g. filter through Whatman #1 paper through a funnel into another clean 1L E. flask
h. add dH_2O to 1L
Keep @ 4ºC

Fixative (4% solution—1L)

a. take 500mL stock solution in 1L E. flask
b. add 500mL 2x PBS
c. pH to ~7.4 with HCL
Prepare when needed, or keep @ 4ºC

1M Tris-Cl

a. 121g Tris base
b. 800 ml dH_2O
c. adjust to pH 7.4 with HCL
d. adjust volume to 1L

Tris-buffered saline (TBS)

a. 0.1M Tris-Cl, pH 7.5
b. 0.9% NaCl (saline)

Keep @ 4ºC

Blocking/Antibody solution, TBX (50mL)

d. 125uL Triton X-100 (0.25%)
e. 1.5mL NGS (3%)
f. fill to 50mL with TBS

or

***P**hosphate **B**uffered **S**aline (10x)*

a. 2 g/L KH_2PO_4
b. 11.5 g/L $Na_2HPO_4 \cdot 7H_2O$
c. 80 g/L NaCl
d. 2 g/L KCl
e. @ pH 7.4 and room T

Keep @ 4ºC until needed

Blocking/Antibody solution, PBX (50mL)

a. 150uL Triton X-100 (0.3%)
b. 0.5g BSA (1%)
c. fill to 50mL with PBS

GFP/AVP 1º antibody solution

a. antibody buffer
b. 1:20,000 rabbit anti-GFP
    a. 0.5uL in 10mL PBX
c. 1:500 guinea pig anti-AVP
    a. 2uL in 1mL of anti-GFP buffer (above)

GFP/VIP 1º antibody solution

d. antibody buffer
e. 1:20,000 rabbit anti-GFP
f. 1:500 guinea pig anti-VIP
    a. 2uL in 1mL of anti-GFP buffer (above)

2º antibody cocktail

a. antibody buffer
b. 1:500 Alexa-Fluor 488 Goat α-rabbit (MP)
c. 1:500 Alexa-Fluor 594 Goat α-guinea pig (MP)

1. At peak fluorescence under live culture microscopy, open dish and place membrane insert with tissue on it into another dish with 1mL 4% paraformaldehyde.
2. Add another 1mL fixative to the top of the insert to submerge the tissue and float it off the membrane.
3. Grease the lid and cover the dish. Keep in 4ºC for at least 2 hours.

Antibody Staining

4. rinse 3x5 minutes in PBS
5. incubate sections in PBX 2 hours
    a. no rinse needed
6. incubate select tissue in 1º anti-GFP/anti-AVP mixture overnight at 4ºC **or** incubate select tissue in 1º anti-GFP/anti-VIP mixture overnight at 4ºC
7. rinse 5x5 minutes in PBS
8. rinse 5x10 minutes in PBS
9. incubate 3 hours in 2º antibodies
10. rinse 5x5 minutes in PBS
11. rinse 5x10 minutes in PBS
12. Mount in 1 drop VectaShield Hardset Medium (Vector – H1400) on a coverslip
13. apply a second coverslip evenly
14. Dry overnight

For microscopy, see Appendix Section A.2.

Section A.5: Circadian Genes and You: An SSCP SNP Primer (v. 2.2)

C.M. Ciarleglio[1], S.A. Larson[2], K.C. Mahautmr Sharkey[2], S.V. Servick[2]

[1]McMahon Lab, Neuroscience Graduate Program
[2]Johnson Lab, Department of Biological Sciences
Vanderbilt University, Nashville, TN 37235

hBmal1 and hBmal2 PCR Conditions

Ingredient	[Final}	Volume/Rxn (15uL)
10x PCR Buffer II (ABi)	1x	1.5
25mM MgCl2 (ABi)	2.5mM	1.5
*10 mM dNTPs	0.2mM	0.3
primers (Fp/Rp)	0.33uM	1.0
DNA template	4-6uL/rxn	6.0
5M Betaine (if applicable)	1M	3.0 (*if applicable*)
100% DMSO (if applicable)	5%	0.75 (*if applicable*)
5unit/uL AlpliTaq Gold (ABi)	1.25 units	0.075
Sterile Milli-Q water	varies	4.625 or 1.625 (Betaine) 3.875 (DMSO)

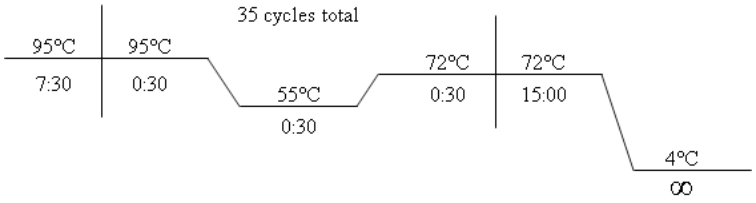

Figure A.5-1. | **PCR thermocycler conditions for *hBmal* (*Arntl*).**

On the following pages, each SNP will be given the top or bottom half of the page to graphically represent what the banding-pattern on an SSCP gel did/would look like.

Gel running time (h):	Min	Max
old	2	12
new		9

Bmal1# 12:
T>G

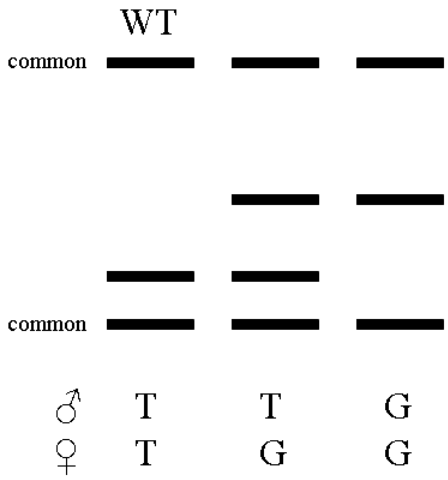

Primers:	Location
12Fp: CTTAAACTGAGGCGGACAC	8246Fp (p4-C7)
12Rp: CATGCTAACAATGCTCAG	8406Rp (p4-D7)

Gel running time (h):	Min	Max
old	6	15
new		13

Bmal1# 2526:
-228A>C

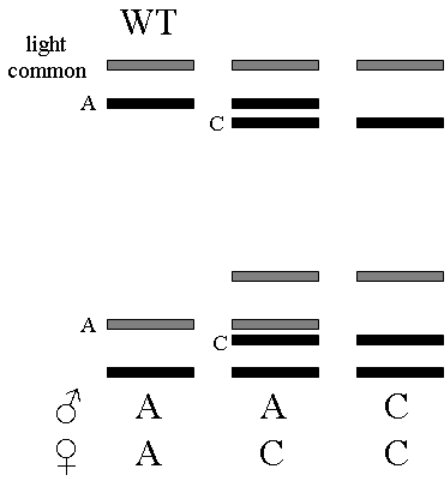

Primers:	Location
25Fp: GTCCAATGGATTTAAAGGAC	9888Fp (p1-A1)
26Rp: CTGGTAACCTCCACAGA	10164Rp (p1-A4)

Bmal1# 4142:
G>A

Gel running time (h):	Min	Max
old	13 only	
new		

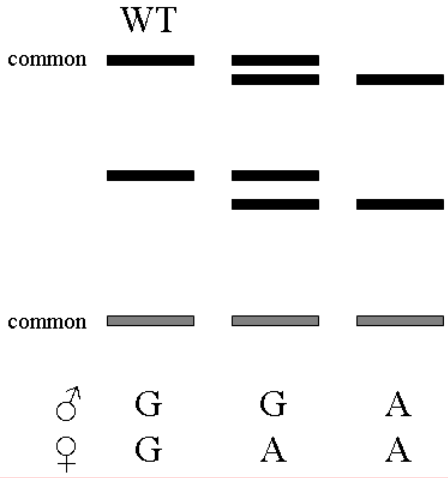

Primers:	**Location**
41Fp: CAGACAAAGATGACCCTC	56766Fp (p1-C9)
41Rp: CAGACACACAAGGGGACT	56931Rp (p1-C10)
42Fp: CAACTGGAGATGAGCAAG	56886Fp (p1-C11)
42Rp: CCTTGGTGTTCTGTATATTC	57055Rp (p1-C12)

Gel running time (h):	Min	Max
old	4	15
new		11

Bmal2# 5 (rs5797225):
GTT (VNTR)

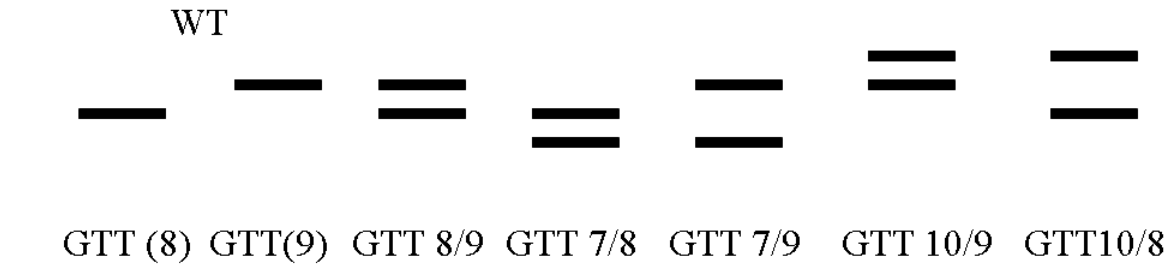

Primers:	**Location**
5Fp: CCTGGCTTCTGTGTTATTTA	86837Fp (p3-A2)
5Rp: GTCCTTTTAGCATTCTGCT	87037Rp (p3-B2)

Gel running time (h):	Min	Max
old	6	10
new		7.5

Bmal2 #6:

#1 G>C (rs137588); #2 A>G (rs11048972); #3 A>G (new)

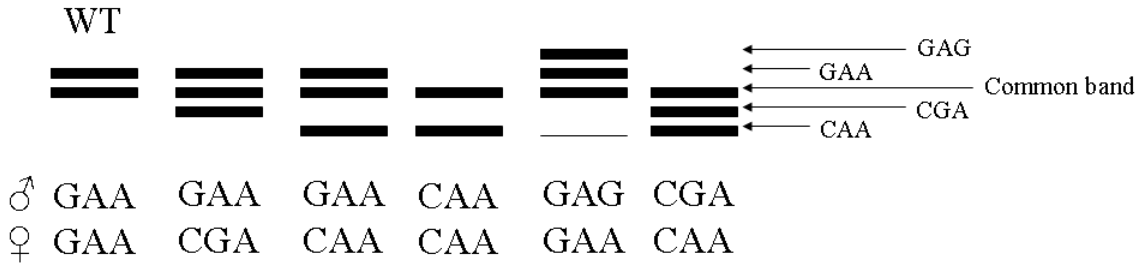

Primers:	**Location**
6Fp: ATCTAAGTGGCTTTAGGG	87000Fp (p3-C2)
6Rp: TCATTGCTAAGTACTCAGG	87141Rp (p3-D2)

Gel running time (h):	Min	Max
old	4	12
new		8

Bmal2 #13 (rs10548381):

TAG insertion/deletion

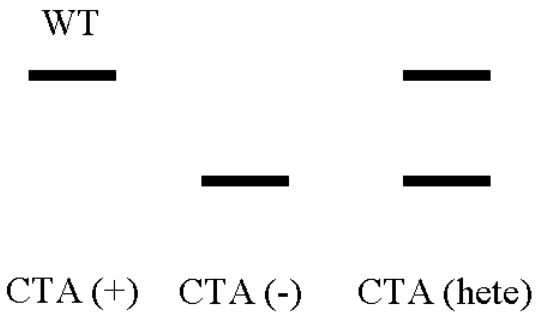

Primers:	**Location**
13Fp: CATCTCTGAACTTCTGTTTC	87852Fp (p3-A4)
13Rp: CTTGGCTTTCCAGACAAG	88032Rp (p3-B4)

Gel running time (h):	Min	Max
old	4	16
new		11

Bmal2 #29:

A>C (rs4964059); T>C

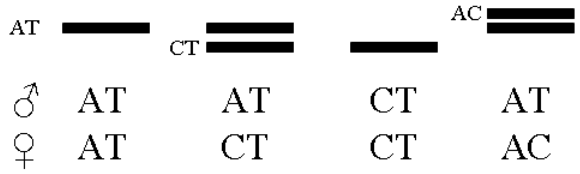

♂	AT	AT	CT	AT
♀	AT	CT	CT	AC

Primers:	**Location**
29Fp: GGAGAATGGTTCATGTAGAC	132371Fp (p3-A8)
29Rp: ACTCACCATGTACCATCTC	132596Rp (p3-B8)

Gel running time (h):	Min	Max
old		
new		

Bmal2 #55:

A C T G

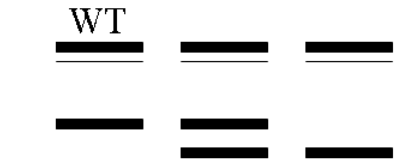

♂	X	X	X
♀	X	X	X

Genotype is unidentified. Change lies near the beginning of primer initiation. No identifiable sequence change using 55F and 55R, no change using 54 F and 55R. Primers 56R and 55F failed. Needs to be tried again. -SS

Primers:	**Location**
55Fp: CAGTCTTCTTCATACCTTG	172083Fp (p4-E2)
55Rp: CTTCCAGCAACTTCATT	172304Rp (p4-F2)

Gel running time (h):	Min	Max
old	2	12
new		7

Bmal2 #62:
A>G

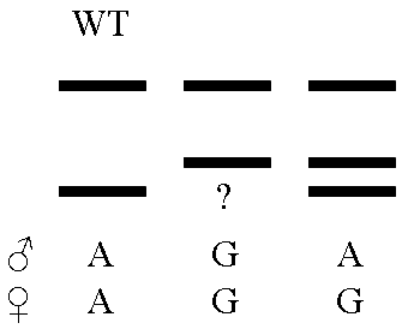

We should consider continuing running looking for this SNP for this study. It has only shown up one time in all the cohorts.

Primers:	**Location**
62Fp: CTTCCTGTCACAGGGATG	176881Fp (p4-C4)
62Rp: GCCAAAACAATATGTAAG	177004Rp (p4-D4)

Clock, P2e17, P3, Ck1ε, AA-NAT(p) PCR Conditions

Ingredient /Rxn (15uL)
9ul Platinum Supermix
DNA
1ul DNA (4-10ng/ul)
or
4ul DNA (1ng/ul)
1ul 10uM Fp
1ul 10uM Rp

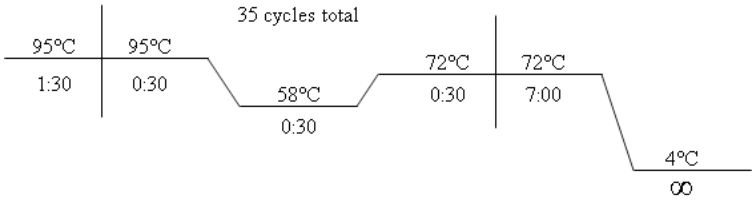

Figure A.5-2. | **PCR thermocycler conditions for Supermix group of genes.**

On the following pages, each SNP will be given the top or bottom half of the page to graphically represent what the banding-pattern on an SSCP gel did/would look like.

Gel running time (h):	Min	Max
old	4	12
new		9

Clock:

T>C (3111; rs1801260), A>G (3125)

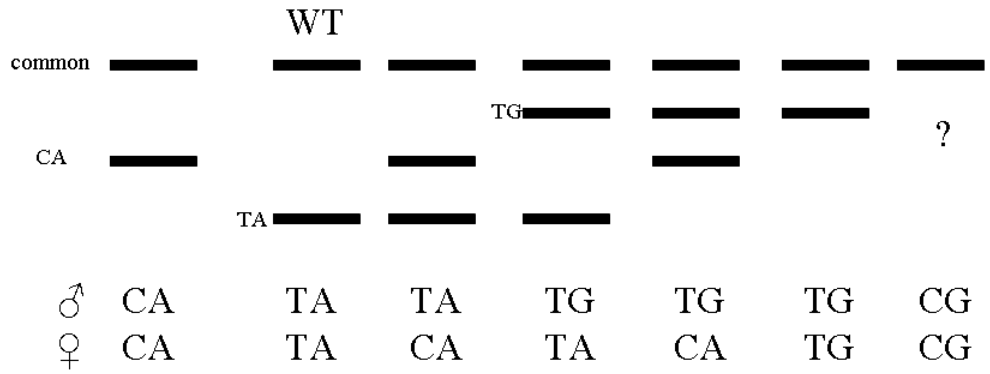

Primers:	**Location**
Fp: TCCAGCAGTTTCATGAGATGC	-20° chest
Rp: GAGGTCATTTCATAGCTGAGC	-20° chest
FpX: CCTTCCAAGGTTCAACCACAG	-20° chest
RpX: TCTACTGGACTGTCTTCATGG	-20° chest

Gel running time (h):	Min	Max
old		
new		

P2e17:

A>G (2087; rs2304669), A>G (2106), C>T (2113; Ala>Val), G>A (2114; rs2304670), G>A (2117; rs2304671)

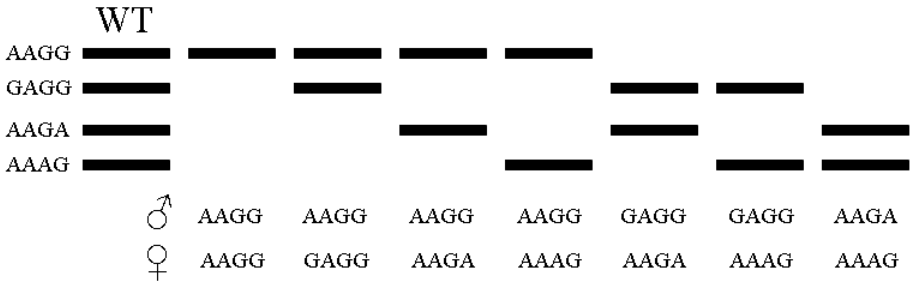

Unnoticed alleles: GAGA, GAAG, AAAA, GGGG

Primers:	**Location**
Fp: GGCACTTGGGTGTCGGTTTCTC	-20° chest
Rp: CCCCTATCGGGCTATGGTGGA	-20° chest
FpX: CTGGGCCAGAGCATCTGTGGGA	-20° chest
RpX: CTGGGCCCTGGCTGGCCGCA	-20° chest

Gel running time (h): Min Max
old
new

P3e11:

1258G>A (AB047526), 1338C>T (AB047527)

(never seen)

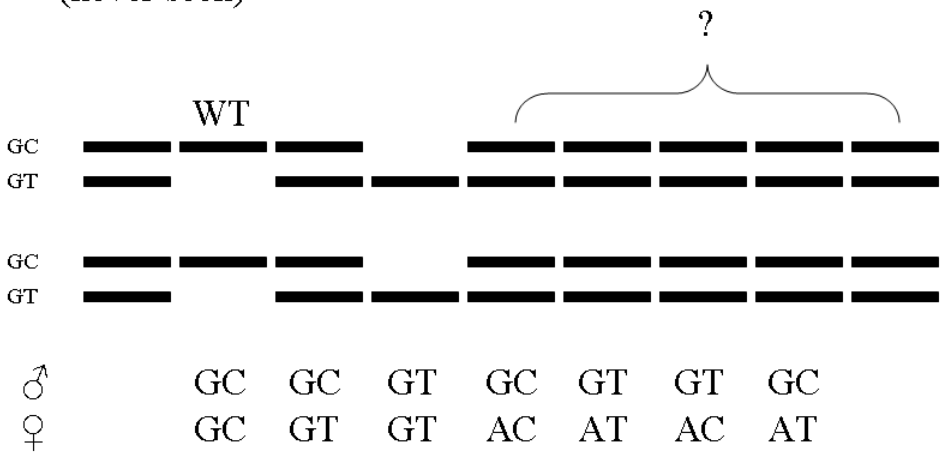

♂		GC	GC	GT	GC	GT	GT	GC
♀		GC	GT	GT	AC	AT	AC	AT

Primers:	**Location**
Fp: ATGATTCTAGATGAGCTCTGCGGTGG	
Rp: GAACCGAGGTAGTACAGAAAACACGATG	
FpX: CTGGAAATACCTACCTAGACTAG	
RpX: ATATCTGTTATCAGTTGAGGTCTTC	

Gel running time (h): Min Max
old
new

P3e15:

A C T G

WT

♂	X	X	X
♀	X	X	X

Primers:	**Location**
Fp: CGTTGGGAATTTTTCTTTTCACTGTCAG	
Rp: TGGTATTCATGACTTTTGTTTTCTCATC	
FpX: ATATTGTTATAAGCATAAAATTCTGGTT	
RpX: TACTAGGTACTGTATTAAGTGCTTTAT	

Gel running time: 11.5 hrs.

P3e15:

T>G (1940), G>A (1969)

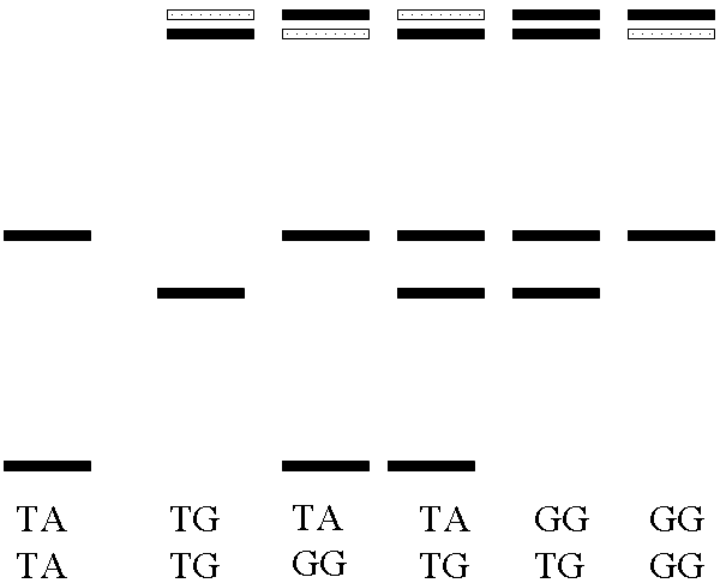

Gel running time (h): Min Max

old

new

P3e17:

2415C>T (AB047531), 2484A>G (AB047532), 2504C>T (new), 2590C>G (AB047533), 2616G>A (AB047534)

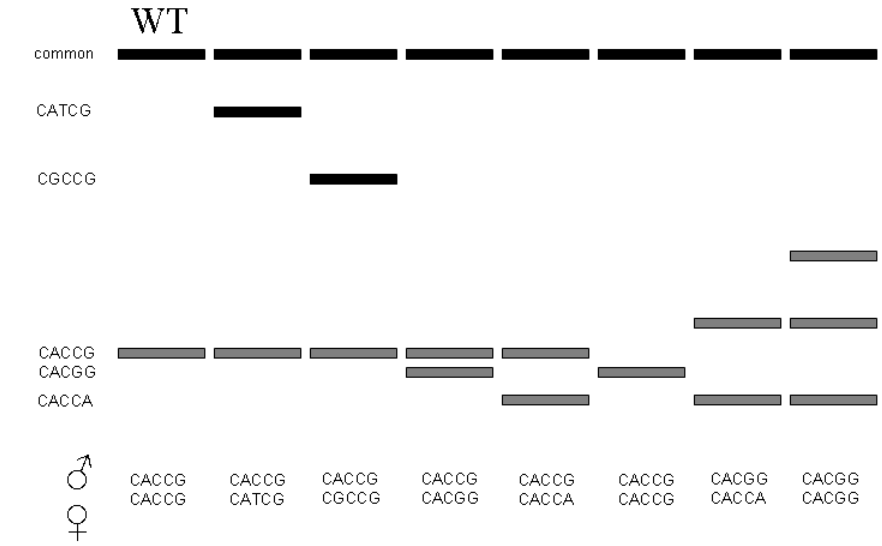

Primers:	**Location**
Fp: ACCTCGAGCCCGACCTTCCCACCTG	
Rp: CAAAAACGATGGCGACAACAGAGGACA	

P3e18 (SSCP):

2934C>T, 3057G>A, 3110T>C, 3121C>G, 3146C>T

Gel running time (h): Min Max
old
new

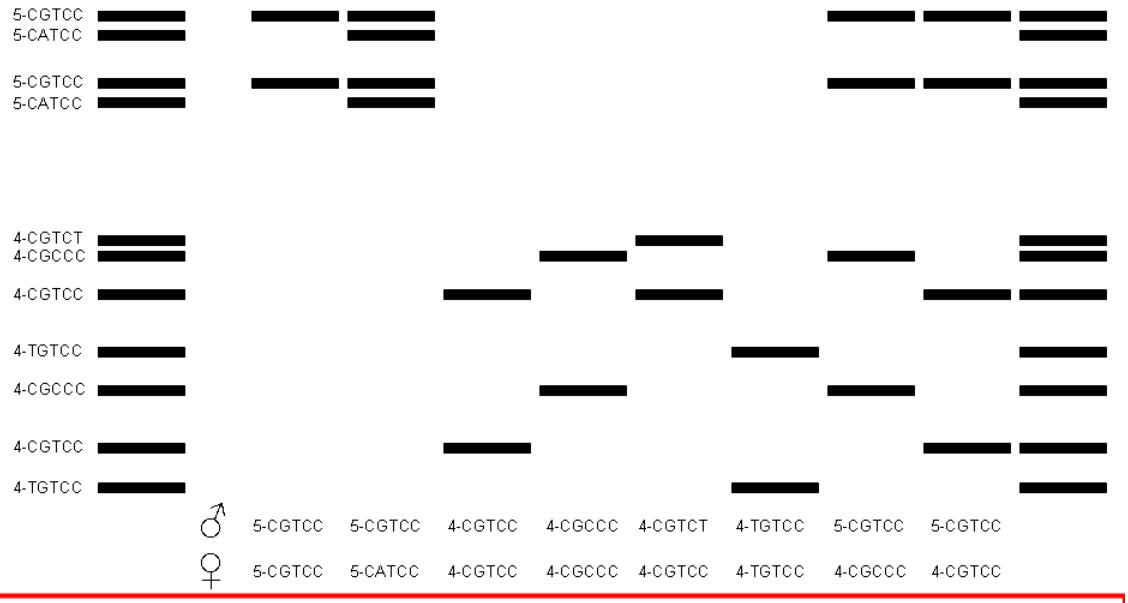

Primers:	**Location**
Fp: GAAGATTAAAGTGTCTTTTCATGTGCCCTTAC	
Rp: AATGTCTGGCATTGGAGTTTGAAACATTAG	

P3e18 (2% agarose):

5 or 4 repeats (54bp VNTR)

Gel running time (h): Min Max
old
new

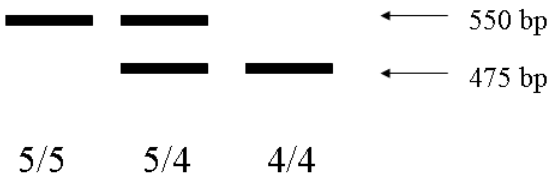

Primers:	**Location**
Fp: GAAGATTAAAGTGTCTTTTCATGTGCCCTTAC	
Rp: AATGTCTGGCATTGGAGTTTGAAACATTAG	

Gel running time (h): Min Max
old
new

P3e20:
3473A>G (rs10462021)

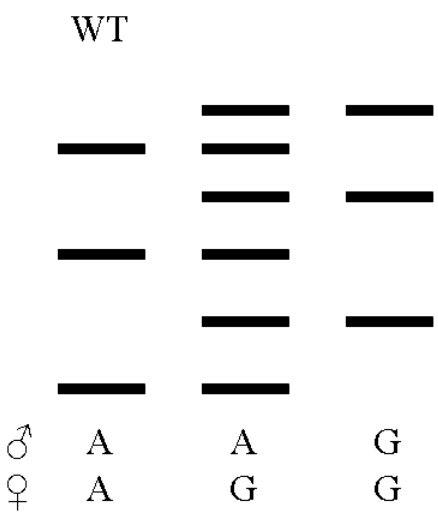

Primers:	**Location**
Fp: CGGGAAAAGAACCCTGTGTCTTATTCAG	
Rp: CTACCTGGCCAAAATACATGAGTATATGAC	

Gel running time (h): Min Max
old
new

CK1ε:
1223G>A

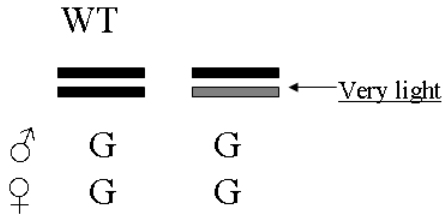

Haven't seen the SNP yet. There seems to be no sequence difference between the above conformation. Some my need to be sequenced: see data set for sample number and corresponding SSCP gel.

Primers:	**Location**
Fp: ATCGCCAGCGGCTAAGGGACTTGAC	
Rp: CCCACCCCTCCACAACACATTGGTC	

Gel running time (h):	Min	Max
old		
new		14

AA-NAT (promoter):
-263G>C (rs3760138), -542T>G (rs4238989)

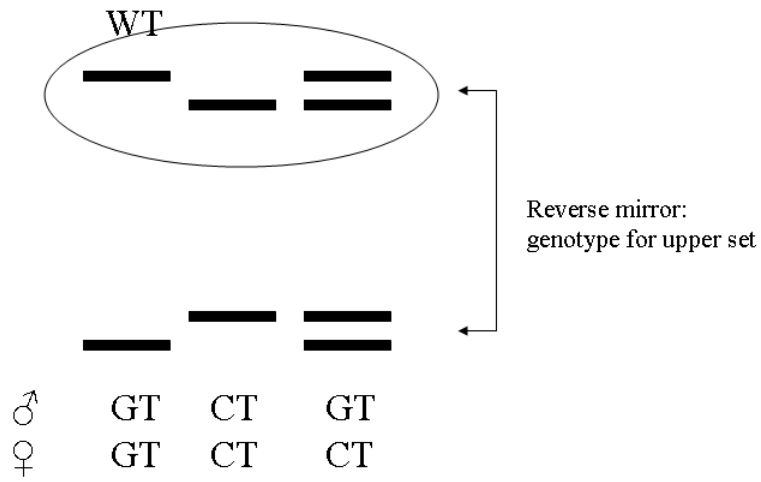

Primers:	**Location**
Fp: CTCTGCAGGGGGTCAAAAG	
Rp: CATCTCTAATCCCTGCTCTGTCAC	

REFERENCES

1. Ciarleglio, C. M., Gamble, K. L., Axley, J. C., Strauss, B. R., Cohen, J. Y., Colwell, C. S. & McMahon, D. G. Population encoding by circadian clock neurons organizes circadian behavior. J Neurosci 29, 1670-6 (2009).

2. Ciarleglio, C. M., Ryckman, K. K., Servick, S. V., Hida, A., Robbins, S., Wells, N., Hicks, J., Larson, S. A., Wiedermann, J. P., Carver, K., Hamilton, N., Kidd, K. K., Kidd, J. R., Smith, J. R., Friedlaender, J., McMahon, D. G., Williams, S. M., Summar, M. L. & Johnson, C. H. Genetic Differences in Human Circadian Clock Genes among Worldwide Populations. J Biol Rhythms 23, 330-40 (2008).

3. Hartmann, W. K. & Davis, D. R. Satellite-Sized Planetesimals and Lunar Origin. Icarus 24, 504-515 (1975).

4. Belbruno, E. & Gott, J. R. Where did the moon come from? Astronomical Journal 129, 1724-1745 (2005).

5. Williams, G. E. Geological constraints on the Precambrian history of earth's rotation and the moon's orbit. Reviews of Geophysics 38, 37-59 (2000).

6. Ouyang, Y., Andersson, C. R., Kondo, T., Golden, S. S. & Johnson, C. H. Resonating circadian clocks enhance fitness in cyanobacteria. Proc Natl Acad Sci U S A 95, 8660-4 (1998).

7. Woelfle, M. A., Ouyang, Y., Phanvijhitsiri, K. & Johnson, C. H. The adaptive value of circadian clocks: an experimental assessment in cyanobacteria. Curr Biol 14, 1481-6 (2004).

8. DeCoursey, P. J. & Krulas, J. R. Behavior of SCN-lesioned chipmunks in natural habitat: a pilot study. J Biol Rhythms 13, 229-44 (1998).

9. DeCoursey, P. J., Krulas, J. R., Mele, G. & Holley, D. C. Circadian performance of suprachiasmatic nuclei (SCN)-lesioned antelope ground squirrels in a desert enclosure. Physiol Behav 62, 1099-108 (1997).

10. DeCoursey, P. J., Walker, J. K. & Smith, S. A. A circadian pacemaker in free-living chipmunks: essential for survival? J Comp Physiol [A] 186, 169-80 (2000).

11. Moore-Ede, M. C., Sulzman, F. M. & Fuller, C. A. The clocks that time us : physiology of the circadian timing system (Harvard University Press, Cambridge, Mass., 1982).

12. Reebs, S. G. & Mrosovsky, N. Large phase-shifts of circadian rhythms caused by induced running in a re-entrainment paradigm: the role of pulse duration and light. J Comp Physiol [A] 165, 819-25 (1989).

13. Wittmann, M., Dinich, J., Merrow, M. & Roenneberg, T. Social jetlag: Misalignment of biological and social time. Chronobiology International 23, 497-509 (2006).

14. Dunlap, J. C., Loros, J. J. & DeCoursey, P. J. Chronobiology : biological timekeeping (Sinauer Associates, Sunderland, Mass., 2004).

15. Pittendrigh, C. & Daan, S. A Functional Analysis of Circadian Pacemakers in Nocturnal Rodents: IV. Entrainment: Pacemaker as Clock. J. Comp. Physiol. A 106, 291-331 (1976).

16. Pittendrigh, C. & Daan, S. A Functional Analysis of Circadian Pacemakers in Nocturnal Rodents: V. Pacemaker Structure: A Clock for All Seasons. J. Comp. Physiol. A 106, 333-355 (1976).

17. Daan, S. & Pittendrigh, C. A Functional Analysis of Circadian Pacemakers in Nocturnal Rodents: II. The Variability of Phase-Response Curves. J. Comp. Physiol. A 106, 253-266 (1976).

18. Daan, S. & Pittendrigh, C. A Functional Analysis of Circadian Pacemakers in Nocturnal Rodents: III. Heavy Water and Constant Light: Homeostasis of Frequency? J. Comp. Physiol. A 106, 267-290 (1976).

19. Pittendrigh, C. & Daan, S. A Functional Analysis of Circadian Pacemakers in Nocturnal Rodents: I. The Stability and Lability of Spontaneous Frequency. J. Comp. Physiol. A 106, 223-252 (1976).

20. Pittendrigh, C. S. Circadian rhythms and the circadian organization of living systems. Cold Spring Harb Symp Quant Biol 25, 159-84 (1960).

21. Pittendrigh, C. S. Temporal organization: reflections of a Darwinian clock-watcher. Annu Rev Physiol 55, 16-54 (1993).

22. Aschoff, J. Circadian Rhythms in Man. Science 148, 1427-32 (1965).

23. Aschoff, J. Human circadian rhythms in activity, body temperature and other functions. Life Sci Space Res 5, 159-73 (1967).

24. Aschoff, J. Desynchronization and resynchronization of human circadian rhythms. Aerosp Med 40, 844-9 (1969).

25. Aschoff, J. Complexity and order of the human circadian system. Boll Soc Ital Biol Sper 52, 1-11 (1976).

26. Aschoff, J. Circadian systems in man and their implications. Hosp Pract 11, 51-97 (1976).

27. Aschoff, J. [Daily periodicity in mice strains under constant environmental conditions.]. Pflugers Arch 262, 51-9 (1955).

28. Aschoff, J. Exogenous and endogenous components in circadian rhythms. Cold Spring Harb Symp Quant Biol 25, 11-28 (1960).

29. Richter, C. P. Sleep and activity: their relation to the 24-hour clock. Res Publ Assoc Res Nerv Ment Dis 45, 8-29 (1967).

30. Moore, R. Y. & Lenn, N. J. A retinohypothalamic projection in the rat. J Comp Neurol 146, 1-14 (1972).

31. Stephan, F. K. & Zucker, I. Circadian rhythms in drinking behavior and locomotor activity of rats are eliminated by hypothalamic lesions. Proc Natl Acad Sci U S A 69, 1583-6 (1972).

32. Inouye, S. T. & Kawamura, H. Persistence of circadian rhythmicity in a mammalian hypothalamic "island" containing the suprachiasmatic nucleus. Proc Natl Acad Sci U S A 76, 5962-6 (1979).

33. Schwartz, W. J. & Gainer, H. Suprachiasmatic nucleus: use of 14C-labeled deoxyglucose uptake as a functional marker. Science 197, 1089-91 (1977).

34. Green, D. J. & Gillette, R. Circadian rhythm of firing rate recorded from single cells in the rat suprachiasmatic brain slice. Brain Res 245, 198-200 (1982).

35. Ralph, M. R., Foster, R. G., Davis, F. C. & Menaker, M. Transplanted suprachiasmatic nucleus determines circadian period. Science 247, 975-8 (1990).

36. van den Pol, A. N. Gamma-aminobutyrate, gastrin releasing peptide, serotonin, somatostatin, and vasopressin: ultrastructural immunocytochemical localization in presynaptic axons in the suprachiasmatic nucleus. Neuroscience 17, 643-59 (1986).

37. van den Pol, A. N. Glutamate and GABA presence and action in the suprachiasmatic nucleus. J Biol Rhythms 8 Suppl, S11-5 (1993).

38. Herzog, E. D., Takahashi, J. S. & Block, G. D. Clock controls circadian period in isolated suprachiasmatic nucleus neurons. Nat Neurosci 1, 708-13 (1998).

39. Liu, C., Weaver, D. R., Strogatz, S. H. & Reppert, S. M. Cellular construction of a circadian clock: period determination in the suprachiasmatic nuclei. Cell 91, 855-60 (1997).

40. Welsh, D. K., Logothetis, D. E., Meister, M. & Reppert, S. M. Individual neurons dissociated from rat suprachiasmatic nucleus express independently phased circadian firing rhythms. Neuron 14, 697-706 (1995).

41. Kuhlman, S. J., Silver, R., Le Sauter, J., Bult-Ito, A. & McMahon, D. G. Phase resetting light pulses induce Per1 and persistent spike activity in a subpopulation of biological clock neurons. J Neurosci 23, 1441-50 (2003).

42. Gamble, K. L., Allen, G. C., Zhou, T. & McMahon, D. G. Gastrin-releasing peptide mediates light-like resetting of the suprachiasmatic nucleus circadian pacemaker through cAMP response element-binding protein and Per1 activation. J Neurosci 27, 12078-87 (2007).

43. Reppert, S. M. & Weaver, D. R. Coordination of circadian timing in mammals. Nature 418, 935-41 (2002).

44. Dunlap, J. C. Molecular bases for circadian clocks. Cell 96, 271-90 (1999).

45. Sato, T. K., Panda, S., Miraglia, L. J., Reyes, T. M., Rudic, R. D., McNamara, P., Naik, K. A., FitzGerald, G. A., Kay, S. A. & Hogenesch, J. B. A functional genomics strategy reveals Rora as a component of the mammalian circadian clock. Neuron 43, 527-37 (2004).

46. Panda, S., Provencio, I., Tu, D. C., Pires, S. S., Rollag, M. D., Castrucci, A. M., Pletcher, M. T., Sato, T. K., Wiltshire, T., Andahazy, M., Kay, S. A., Van Gelder, R. N. & Hogenesch, J. B. Melanopsin is required for non-image-forming photic responses in blind mice. Science 301, 525-7 (2003).

47. Abrahamson, E. E. & Moore, R. Y. Suprachiasmatic nucleus in the mouse: retinal innervation, intrinsic organization and efferent projections. Brain Res 916, 172-91 (2001).

48. Johnson, R. F., Morin, L. P. & Moore, R. Y. Retinohypothalamic projections in the hamster and rat demonstrated using cholera toxin. Brain Res 462, 301-12 (1988).

49. Pickard, G. E. Bifurcating axons of retinal ganglion cells terminate in the hypothalamic suprachiasmatic nucleus and the intergeniculate leaflet of the thalamus. Neurosci Lett 55, 211-7 (1985).

50. Tanaka, M., Ichitani, Y., Okamura, H., Tanaka, Y. & Ibata, Y. The direct retinal projection to VIP neuronal elements in the rat SCN. Brain Res Bull 31, 637-40 (1993).

51. Moore, R. Y. Entrainment pathways and the functional organization of the circadian system. Prog Brain Res 111, 103-19 (1996).

52. Hattar, S., Kumar, M., Park, A., Tong, P., Tung, J., Yau, K. W. & Berson, D. M. Central projections of melanopsin-expressing retinal ganglion cells in the mouse. J Comp Neurol 497, 326-49 (2006).

53. Romijn, H. J., Sluiter, A. A., Pool, C. W., Wortel, J. & Buijs, R. M. Differences in colocalization between Fos and PHI, GRP, VIP and VP in neurons of the rat suprachiasmatic nucleus after a light stimulus during the phase delay versus the phase advance period of the night. J Comp Neurol 372, 1-8 (1996).

54. Ibata, Y., Takahashi, Y., Okamura, H., Kawakami, F., Terubayashi, H., Kubo, T. & Yanaihara, N. Vasoactive intestinal peptide (VIP)-like immunoreactive neurons located in the rat suprachiasmatic nucleus receive a direct retinal projection. Neurosci Lett 97, 1-5 (1989).

55. Earnest, D. J., DiGiorgio, S. & Olschowka, J. A. Light induces expression of fos-related proteins within gastrin-releasing peptide neurons in the rat suprachiasmatic nucleus. Brain Res 627, 205-9 (1993).

56. Earnest, D. J. & Olschowka, J. A. Circadian regulation of c-fos expression in the suprachiasmatic pacemaker by light. J Biol Rhythms 8 Suppl, S65-71 (1993).

57. Moore, R. Y., Speh, J. C. & Leak, R. K. Suprachiasmatic nucleus organization. Cell Tissue Res 309, 89-98 (2002).

58. Speh, J. C. & Moore, R. Y. Retinohypothalamic tract development in the hamster and rat. Brain Res Dev Brain Res 76, 171-81 (1993).

59. Cassone, V. M., Speh, J. C., Card, J. P. & Moore, R. Y. Comparative anatomy of the mammalian hypothalamic suprachiasmatic nucleus. J Biol Rhythms 3, 71-91 (1988).

60. Leak, R. K. & Moore, R. Y. Topographic organization of suprachiasmatic nucleus projection neurons. J Comp Neurol 433, 312-34 (2001).

61. Ban, Y., Shigeyoshi, Y. & Okamura, H. Development of vasoactive intestinal peptide mRNA rhythm in the rat suprachiasmatic nucleus. J Neurosci 17, 3920-31 (1997).

62. Takahashi, Y., Okamura, H., Yanaihara, N., Hamada, S., Fujita, S. & Ibata, Y. Vasoactive intestinal peptide immunoreactive neurons in the rat suprachiasmatic nucleus demonstrate diurnal variation. Brain Res 497, 374-7 (1989).

63. Albers, H. E., Stopa, E. G., Zoeller, R. T., Kauer, J. S., King, J. C., Fink, J. S., Mobtaker, H. & Wolfe, H. Day-night variation in prepro vasoactive intestinal peptide/peptide histidine isoleucine mRNA within the rat suprachiasmatic nucleus. Brain Res Mol Brain Res 7, 85-9 (1990).

64. Shinohara, K., Tominaga, K., Isobe, Y. & Inouye, S. T. Photic regulation of peptides located in the ventrolateral subdivision of the suprachiasmatic nucleus of the rat: daily variations of vasoactive intestinal polypeptide, gastrin-releasing peptide, and neuropeptide Y. J Neurosci 13, 793-800 (1993).

65. Yang, J., Cagampang, F. R., Nakayama, Y. & Inouye, S. I. Vasoactive intestinal polypeptide precursor mRNA exhibits diurnal variation in the rat suprachiasmatic nuclei. Brain Res Mol Brain Res 20, 259-62 (1993).

66. Albers, H. E., Minamitani, N., Stopa, E. & Ferris, C. F. Light selectively alters vasoactive intestinal peptide and peptide histidine isoleucine immunoreactivity within the rat suprachiasmatic nucleus. Brain Res 437, 189-92 (1987).

67. Shinohara, K., Tominaga, K. & Inouye, S. T. Luminance-dependent decrease in vasoactive intestinal polypeptide in the rat suprachiasmatic nucleus. Neurosci Lett 251, 21-4 (1998).

68. Shibata, S., Ono, M., Tominaga, K., Hamada, T., Watanabe, A. & Watanabe, S. Involvement of vasoactive intestinal polypeptide in NMDA-induced phase delay of firing activity rhythm in the suprachiasmatic nucleus in vitro. Neurosci Biobehav Rev 18, 591-5 (1994).

69. Shearman, L. P., Zylka, M. J., Weaver, D. R., Kolakowski, L. F., Jr. & Reppert, S. M. Two period homologs: circadian expression and photic regulation in the suprachiasmatic nuclei. Neuron 19, 1261-9 (1997).

70. Shigeyoshi, Y., Taguchi, K., Yamamoto, S., Takekida, S., Yan, L., Tei, H., Moriya, T., Shibata, S., Loros, J. J., Dunlap, J. C. & Okamura, H. Light-induced resetting of a mammalian circadian clock is associated with rapid induction of the mPer1 transcript. Cell 91, 1043-53 (1997).

71. Yan, L. & Silver, R. Differential induction and localization of mPer1 and mPer2 during advancing and delaying phase shifts. Eur J Neurosci 16, 1531-40 (2002).

72. Piggins, H. D., Antle, M. C. & Rusak, B. Neuropeptides phase shift the mammalian circadian pacemaker. J Neurosci 15, 5612-22 (1995).

73. Cagampang, F. R., Sheward, W. J., Harmar, A. J., Piggins, H. D. & Coen, C. W. Circadian changes in the expression of vasoactive intestinal peptide 2 receptor mRNA in the rat suprachiasmatic nuclei. Brain Res Mol Brain Res 54, 108-12 (1998).

74. Reed, H. E., Meyer-Spasche, A., Cutler, D. J., Coen, C. W. & Piggins, H. D. Vasoactive intestinal polypeptide (VIP) phase-shifts the rat suprachiasmatic nucleus clock in vitro. Eur J Neurosci 13, 839-43 (2001).

75. Meyer-Spasche, A. & Piggins, H. D. Vasoactive intestinal polypeptide phase-advances the rat suprachiasmatic nuclei circadian pacemaker in vitro via protein kinase A and mitogen-activated protein kinase. Neurosci Lett 358, 91-4 (2004).

76. Nielsen, H. S., Hannibal, J. & Fahrenkrug, J. Vasoactive intestinal polypeptide induces per1 and per2 gene expression in the rat suprachiasmatic nucleus late at night. Eur J Neurosci 15, 570-4 (2002).

77. Reed, H. E., Cutler, D. J., Brown, T. M., Brown, J., Coen, C. W. & Piggins, H. D. Effects of vasoactive intestinal polypeptide on neurones of the rat suprachiasmatic nuclei in vitro. J Neuroendocrinol 14, 639-46 (2002).

78. Mrosovsky, N. Locomotor activity and non-photic influences on circadian clocks. Biol Rev Camb Philos Soc 71, 343-72 (1996).

79. Meyer-Bernstein, E. L. & Morin, L. P. Differential serotonergic innervation of the suprachiasmatic nucleus and the intergeniculate leaflet and its role in circadian rhythm modulation. J Neurosci 16, 2097-111 (1996).

80. Yannielli, P. & Harrington, M. E. Let there be "more" light: enhancement of light actions on the circadian system through non-photic pathways. Prog Neurobiol 74, 59-76 (2004).

81. Kawakami, F., Okamura, H., Fukui, K., Yanaihara, C., Yanaihara, N., Nakajima, T. & Ibata, Y. The influence of serotonergic inputs on peptide neurons in the rat suprachiasmatic nucleus: an immunocytochemical study. Neurosci Lett 61, 273-7 (1985).

82. Kawakami, F., Okamura, H., Inatomi, T., Tamada, Y., Nakajima, T. & Ibata, Y. Serotonin depletion by p-chlorophenylalanine decreases VIP mRNA in the suprachiasmatic nucleus. Neurosci Lett 174, 81-4 (1994).

83. Hayashi, S., Ueda, M., Amaya, F., Matusda, T., Tamada, Y., Ibata, Y. & Tanaka, M. Serotonin modulates expression of VIP and GRP mRNA via the 5-HT(1B) receptor in the suprachiasmatic nucleus of the rat. Exp Neurol 171, 285-92 (2001).

84. Okamura, H., Kawakami, F., Tamada, Y., Geffard, M., Nishiwaki, T., Ibata, Y. & Inouye, S. T. Circadian change of VIP mRNA in the rat suprachiasmatic nucleus following p-chlorophenylalanine (PCPA) treatment in constant darkness. Brain Res Mol Brain Res 29, 358-64 (1995).

85. Kawakami, F., Okamura, H., Tamada, Y., Nakajima, T. & Ibata, Y. Changes in vasoactive intestinal peptide mRNA levels in the rat suprachiasmatic nucleus following p-chlorophenylalanine (PCPA) treatment under light/dark conditions. Neurosci Lett 200, 171-4 (1995).

86. Belenky, M. A. & Pickard, G. E. Subcellular distribution of 5-HT(1B) and 5-HT(7) receptors in the mouse suprachiasmatic nucleus. J Comp Neurol 432, 371-88 (2001).

87. Duncan, W. C., Jr., Johnson, K. A. & Wehr, T. A. Increase of 5HT and VIP immunoreactivity within the hamster (Mesocricetus auratus) SCN during chronic MAOI treatment. Neurosci Lett 236, 159-62 (1997).

88. Vacher, C. M., Fretier, P., Creminon, C., Seif, I., De Maeyer, E., Calas, A. & Hardin-Pouzet, H. Monoaminergic control of vasopressin and VIP expression in the mouse suprachiasmatic nucleus. J Neurosci Res 71, 791-801 (2003).

89. Pickard, G. E. & Rea, M. A. Serotonergic innervation of the hypothalamic suprachiasmatic nucleus and photic regulation of circadian rhythms. Biol Cell 89, 513-23 (1997).

90. Quintero, J. E. & McMahon, D. G. Serotonin modulates glutamate responses in isolated suprachiasmatic nucleus neurons. J Neurophysiol 82, 533-9 (1999).

91. American Academy of Sleep Medicine. The international classification of sleep disorders : diagnostic and coding manual (American Academy of Sleep Medicine, Westchester, Ill., 2001).

92. Sack, R. L., Auckley, D., Auger, R. R., Carskadon, M. A., Wright, K. P., Jr., Vitiello, M. V. & Zhdanova, I. V. Circadian rhythm sleep disorders: part II, advanced sleep phase disorder, delayed sleep phase disorder, free-running disorder, and irregular sleep-wake rhythm. An American Academy of Sleep Medicine review. Sleep 30, 1484-501 (2007).

93. Sack, R. L., Auckley, D., Auger, R. R., Carskadon, M. A., Wright, K. P., Jr., Vitiello, M. V. & Zhdanova, I. V. Circadian rhythm sleep disorders: part I, basic principles, shift work and jet lag disorders. An American Academy of Sleep Medicine review. Sleep 30, 1460-83 (2007).

94. Cermakian, N. & Boivin, D. B. A molecular perspective of human circadian rhythm disorders. Brain Res Brain Res Rev 42, 204-20 (2003).

95. Jones, C. R., Campbell, S. S., Zone, S. E., Cooper, F., DeSano, A., Murphy, P. J., Jones, B., Czajkowski, L. & Ptacek, L. J. Familial advanced sleep-phase syndrome: A short-period circadian rhythm variant in humans. Nat Med 5, 1062-5 (1999).

96. Toh, K. L., Jones, C. R., He, Y., Eide, E. J., Hinz, W. A., Virshup, D. M., Ptacek, L. J. & Fu, Y. H. An hPer2 phosphorylation site mutation in familial advanced sleep phase syndrome. Science 291, 1040-3 (2001).

97. Xu, Y., Padiath, Q. S., Shapiro, R. E., Jones, C. R., Wu, S. C., Saigoh, N., Saigoh, K., Ptacek, L. J. & Fu, Y. H. Functional consequences of a CKIdelta mutation causing familial advanced sleep phase syndrome. Nature 434, 640-4 (2005).

98. Ancoli-Israel, S., Schnierow, B., Kelsoe, J. & Fink, R. A pedigree of one family with delayed sleep phase syndrome. Chronobiol Int 18, 831-40 (2001).

99. Archer, S. N., Robilliard, D. L., Skene, D. J., Smits, M., Williams, A., Arendt, J. & von Schantz, M. A length polymorphism in the circadian clock gene Per3 is linked to delayed sleep phase syndrome and extreme diurnal preference. Sleep 26, 413-5 (2003).

100. Ebisawa, T., Uchiyama, M., Kajimura, N., Mishima, K., Kamei, Y., Katoh, M., Watanabe, T., Sekimoto, M., Shibui, K., Kim, K., Kudo, Y., Ozeki, Y., Sugishita, M., Toyoshima, R., Inoue, Y., Yamada, N., Nagase, T., Ozaki, N., Ohara, O., Ishida, N., Okawa, M., Takahashi, K. & Yamauchi, T. Association of structural polymorphisms in the human period3 gene with delayed sleep phase syndrome. EMBO Rep 2, 342-6 (2001).

101. Presser, H. B. Job, family, and gender: determinants of nonstandard work schedules among employed Americans in 1991. Demography 32, 577-98 (1995).

102. McClung, C. A. Circadian genes, rhythms and the biology of mood disorders. Pharmacol Ther 114, 222-32 (2007).

103. Monteleone, P. & Maj, M. The circadian basis of mood disorders: recent developments and treatment implications. Eur Neuropsychopharmacol 18, 701-11 (2008).

104. Laskar, J., Joutel, F. & Robutel, P. Stabilization of the Earth's obliquity by the Moon. Nature 361, 615-617 (1993).

105. Travnickova, Z., Sumova, A., Peters, R., Schwartz, W. J. & Illnerova, H. Photoperiod-dependent correlation between light-induced SCN c-fos expression and resetting of circadian phase. Am J Physiol 271, R825-31 (1996).

106. Sumova, A., Travnickova, Z., Peters, R., Schwartz, W. J. & Illnerova, H. The rat suprachiasmatic nucleus is a clock for all seasons. Proc Natl Acad Sci U S A 92, 7754-8 (1995).

107. Vansteensel, M. J., Michel, S. & Meijer, J. H. Organization of cell and tissue circadian pacemakers: a comparison among species. Brain Res Rev 58, 18-47 (2008).

108. VanderLeest, H. T., Houben, T., Michel, S., Deboer, T., Albus, H., Vansteensel, M. J., Block, G. D. & Meijer, J. H. Seasonal encoding by the circadian pacemaker of the SCN. Curr Biol 17, 468-73 (2007).

109. Rohling, J., Meijer, J. H., VanderLeest, H. T. & Admiraal, J. Phase differences between SCN neurons and their role in photoperiodic encoding; a simulation of ensemble patterns using recorded single unit electrical activity patterns. J Physiol Paris 100, 261-70 (2006).

110. Inagaki, N., Honma, S., Ono, D., Tanahashi, Y. & Honma, K. Separate oscillating cell groups in mouse suprachiasmatic nucleus couple photoperiodically to the onset and end of daily activity. Proc Natl Acad Sci U S A 104, 7664-9 (2007).

111. Naito, E., Watanabe, T., Tei, H., Yoshimura, T. & Ebihara, S. Reorganization of the suprachiasmatic nucleus coding for day length. J Biol Rhythms 23, 140-9 (2008).

112. Mickman, C. T., Stubblefield, J. S., Harrington, M. E. & Nelson, D. E. Photoperiod alters phase difference between activity onset in vivo and mPer2::luc peak in vitro. Am J Physiol Regul Integr Comp Physiol 295, R1688-94 (2008).

113. Molyneux, P. C., Dahlgren, M. K. & Harrington, M. E. Circadian entrainment aftereffects in suprachiasmatic nuclei and peripheral tissues in vitro. Brain Res 1228, 127-34 (2008).

114. Levitt, A. J. & Boyle, M. H. The impact of latitude on the prevalence of seasonal depression. Can J Psychiatry 47, 361-7 (2002).

115. Levitt, A. J., Boyle, M. H., Joffe, R. T. & Baumal, Z. Estimated prevalence of the seasonal subtype of major depression in a Canadian community sample. Can J Psychiatry 45, 650-4 (2000).

116. Murray, G., Michalak, E. E., Levitt, A. J., Levitan, R. D., Enns, M. W., Morehouse, R. & Lam, R. W. O sweet spot where art thou? Light treatment of Seasonal Affective Disorder and the circadian time of sleep. J Affect Disord 90, 227-31 (2006).

117. Castrogiovanni, P., Iapichino, S., Pacchierotti, C. & Pieraccini, F. Season of birth in psychiatry. A review. Neuropsychobiology 37, 175-81 (1998).

118. Torrey, E. F., Miller, J., Rawlings, R. & Yolken, R. H. Seasonality of births in schizophrenia and bipolar disorder: a review of the literature. Schizophr Res 28, 1-38 (1997).

119. Torrey, E. F., Miller, J., Rawlings, R. & Yolken, R. H. Seasonal birth patterns of neurological disorders. Neuroepidemiology 19, 177-85 (2000).

120. Bartlik, B. D. Monthly variation in births of autistic children in North Carolina. J Am Med Womens Assoc 36, 363-8 (1981).

121. Konstantareas, M. M. Early developmental backgrounds of autistic and mentally retarded children. Future research directions. Psychiatr Clin North Am 9, 671-88 (1986).

122. Konstantareas, M. M., Hauser, P., Lennox, C. & Homatidis, S. Season of birth in infantile autism. Child Psychiatry Hum Dev 17, 53-65 (1986).

123. Barry, H., 3rd & Bary, H., Jr. Season of birth. An epidemiological study in psychiatry. Arch Gen Psychiatry 5, 292-300 (1961).

124. Dalen, P. Month of birth and schizophrenia. Acta Psychiatr Scand Suppl 203, 55-60 (1968).

125. Mongrain, V., Paquet, J. & Dumont, M. Contribution of the photoperiod at birth to the association between season of birth and diurnal preference. Neurosci Lett 406, 113-6 (2006).

126. Natale, V., Adan, A. & Chotai, J. Further results on the association between morningness-eveningness preference and the season of birth in human adults. Neuropsychobiology 46, 209-14 (2002).

127. Natale, V., Adan, A. & Chotai, J. Season of birth modulates mood seasonality in humans. Psychiatry Res 153, 199-201 (2007).

128. Kuhlman, S. J., Quintero, J. E. & McMahon, D. G. GFP fluorescence reports Period 1 circadian gene regulation in the mammalian biological clock. Neuroreport 11, 1479-82 (2000).

129. Quintero, J. E., Kuhlman, S. J. & McMahon, D. G. The biological clock nucleus: a multiphasic oscillator network regulated by light. J Neurosci 23, 8070-6 (2003).

130. LeSauter, J., Yan, L., Vishnubhotla, B., Quintero, J. E., Kuhlman, S. J., McMahon, D. G. & Silver, R. A short half-life GFP mouse model for analysis of suprachiasmatic nucleus organization. Brain Res 964, 279-87 (2003).

131. Harmar, A. J., Marston, H. M., Shen, S., Spratt, C., West, K. M., Sheward, W. J., Morrison, C. F., Dorin, J. R., Piggins, H. D., Reubi, J. C., Kelly, J. S., Maywood, E. S. & Hastings, M. H. The VPAC(2) receptor is essential for circadian function in the mouse suprachiasmatic nuclei. Cell 109, 497-508 (2002).

132. Cutler, D. J., Haraura, M., Reed, H. E., Shen, S., Sheward, W. J., Morrison, C. F., Marston, H. M., Harmar, A. J. & Piggins, H. D. The mouse VPAC2 receptor confers suprachiasmatic nuclei cellular rhythmicity and responsiveness to vasoactive intestinal polypeptide in vitro. Eur J Neurosci 17, 197-204 (2003).

133. Aton, S. J., Colwell, C. S., Harmar, A. J., Waschek, J. & Herzog, E. D. Vasoactive intestinal polypeptide mediates circadian rhythmicity and synchrony in mammalian clock neurons. Nat Neurosci 8, 476-83 (2005).

134. Hughes, A. T., Fahey, B., Cutler, D. J., Coogan, A. N. & Piggins, H. D. Aberrant gating of photic input to the suprachiasmatic circadian pacemaker of mice lacking the VPAC2 receptor. J Neurosci 24, 3522-6 (2004).

135. Maywood, E. S., Reddy, A. B., Wong, G. K., O'Neill, J. S., O'Brien, J. A., McMahon, D. G., Harmar, A. J., Okamura, H. & Hastings, M. H. Synchronization and maintenance of timekeeping in suprachiasmatic circadian clock cells by neuropeptidergic signaling. Curr Biol 16, 599-605 (2006).

136. Colwell, C. S., Michel, S., Itri, J., Rodriguez, W., Tam, J., Lelievre, V., Hu, Z., Liu, X. & Waschek, J. A. Disrupted circadian rhythms in VIP- and PHI-deficient mice. Am J Physiol Regul Integr Comp Physiol 285, R939-49 (2003).

137. Weaver, D. R. The suprachiasmatic nucleus: a 25-year retrospective. J Biol Rhythms 13, 100-12 (1998).

138. Rusak, B. Role of Suprachiasmatic Nuclei in Generation of Circadian-Rhythms in Golden-Hamster, Mesocricetus-Auratus. Journal of Comparative Physiology 118, 145-164 (1977).

139. Moore, R. Y. & Eichler, V. B. Central neural mechanisms in diurnal rhythm regulation and neuroendocrine responses to light. Psychoneuroendocrinology 1, 265-79 (1976).

140. Lehman, M. N., Silver, R., Gladstone, W. R., Kahn, R. M., Gibson, M. & Bittman, E. L. Circadian rhythmicity restored by neural transplant. Immunocytochemical characterization of the graft and its integration with the host brain. J Neurosci 7, 1626-38 (1987).

141. Ohta, H., Mitchell, A. C. & McMahon, D. G. Constant light disrupts the developing mouse biological clock. Pediatr Res 60, 304-8 (2006).

142. Ohta, H., Yamazaki, S. & McMahon, D. G. Constant light desynchronizes mammalian clock neurons. Nat Neurosci 8, 267-9 (2005).

143. Brown, T. M., Colwell, C. S., Waschek, J. A. & Piggins, H. D. Disrupted neuronal activity rhythms in the suprachiasmatic nuclei of vasoactive intestinal polypeptide-deficient mice. J Neurophysiol 97, 2553-8 (2007).

144. Hughes, A. T., Guilding, C., Lennox, L., Samuels, R. E., McMahon, D. G. & Piggins, H. D. Live Imaging of Altered Period1 Expression in the Suprachiasmatic Nuclei of Vipr2(-/-) Mice. J Neurochem (2008).

145. Low-Zeddies, S. S. & Takahashi, J. S. Chimera analysis of the Clock mutation in mice shows that complex cellular integration determines circadian behavior. Cell 105, 25-42 (2001).

146. Georgopoulos, A. P., Schwartz, A. B. & Kettner, R. E. Neuronal population coding of movement direction. Science 233, 1416-9 (1986).

147. de la Iglesia, H. O., Meyer, J., Carpino, A., Jr. & Schwartz, W. J. Antiphase oscillation of the left and right suprachiasmatic nuclei. Science 290, 799-801 (2000).

148. Albers, H. E., Liou, S. Y., Stopa, E. G. & Zoeller, R. T. Interaction of colocalized neuropeptides: functional significance in the circadian timing system. J Neurosci 11, 846-51 (1991).

149. Ciarleglio, C. M., Gamble, K. L., Axley, J. C., Strauss, B. R., Cohen, J. Y., Colwell, C. S. & McMahon, D. G. Population encoding by circadian clock neurons organizes circadian behavior. J Neurosci 29, 1670-1676 (2009).

150. Mrosovsky, N. & Salmon, P. A. A behavioural method for accelerating re-entrainment of rhythms to new light-dark cycles. Nature 330, 372-3 (1987).

151. Mistlberger, R. E., Bossert, J. M., Holmes, M. M. & Marchant, E. G. Serotonin and feedback effects of behavioral activity on circadian rhythms in mice. Behav Brain Res 96, 93-9 (1998).

152. Sokal, R. R. & Rohlf, F. J. Biometry : the principles and practice of statistics in biological research (W.H. Freeman, New York, 1995).

153. Shioiri, T., Takahashi, K., Yamada, N. & Takahashi, S. Motor activity correlates negatively with free-running period, while positively with serotonin contents in SCN in free-running rats. Physiol Behav 49, 779-86 (1991).

154. Yamada, N., Shimoda, K., Ohi, K., Takahashi, S. & Takahashi, K. Free-access to a running wheel shortens the period of free-running rhythm in blinded rats. Physiol Behav 42, 87-91 (1988).

155. Edgar, D. M., Martin, C. E. & Dement, W. C. Activity feedback to the mammalian circadian pacemaker: influence on observed measures of rhythm period length. J Biol Rhythms 6, 185-99 (1991).

156. Hughes, A. T. & Piggins, H. D. Behavioral responses of Vipr2-/- mice to light. J Biol Rhythms 23, 211-9 (2008).

157. Rosenwasser, A. M. & Dwyer, S. M. Circadian phase shifting: Relationships between photic and nonphotic phase-response curves. Physiol Behav 73, 175-83 (2001).

158. Albers, H. E., Gerall, A. A. & Axelson, J. F. Circadian rhythm dissociation in the rat: effects of long-term constant illumination. Neurosci Lett 25, 89-94 (1981).

159. Eastman, C. & Rechtschaffen, A. Circadian temperature and wake rhythms of rats exposed to prolonged continuous illumination. Physiol Behav 31, 417-27 (1983).

160. Honma, K. I. & Hiroshige, T. Endogenous ultradian rhythms in rats exposed to prolonged continuous light. Am J Physiol 235, R250-6 (1978).

161. Honma, K. I. & Hiroshige, T. Internal synchronization among several circadian rhythms in rats under constant light. Am J Physiol 235, R243-9 (1978).

162. Yamazaki, S., Kerbeshian, M. C., Hocker, C. G., Block, G. D. & Menaker, M. Rhythmic properties of the hamster suprachiasmatic nucleus in vivo. J Neurosci 18, 10709-23 (1998).

163. Dulcis, D. & Spitzer, N. C. Illumination controls differentiation of dopamine neurons regulating behaviour. Nature 456, 195-201 (2008).

164. Hubel, D. H. & Wiesel, T. N. The period of susceptibility to the physiological effects of unilateral eye closure in kittens. J Physiol 206, 419-36 (1970).

165. Pyter, L. M. & Nelson, R. J. Enduring effects of photoperiod on affective behaviors in Siberian hamsters (Phodopus sungorus). Behav Neurosci 120, 125-34 (2006).

166. Provencio, I., Rodriguez, I. R., Jiang, G., Hayes, W. P., Moreira, E. F. & Rollag, M. D. A novel human opsin in the inner retina. J Neurosci 20, 600-5 (2000).

167. Gooley, J. J., Lu, J., Chou, T. C., Scammell, T. E. & Saper, C. B. Melanopsin in cells of origin of the retinohypothalamic tract. Nat Neurosci 4, 1165 (2001).

168. Sekaran, S., Lupi, D., Jones, S. L., Sheely, C. J., Hattar, S., Yau, K. W., Lucas, R. J., Foster, R. G. & Hankins, M. W. Melanopsin-dependent photoreception provides earliest light detection in the mammalian retina. Curr Biol 15, 1099-107 (2005).

169. Hannibal, J. & Fahrenkrug, J. Melanopsin containing retinal ganglion cells are light responsive from birth. Neuroreport 15, 2317-20 (2004).

170. Fahrenkrug, J., Nielsen, H. S. & Hannibal, J. Expression of melanopsin during development of the rat retina. Neuroreport 15, 781-4 (2004).

171. Gooley, J. J., Lu, J., Fischer, D. & Saper, C. B. A broad role for melanopsin in nonvisual photoreception. J Neurosci 23, 7093-106 (2003).

172. Hattar, S., Lucas, R. J., Mrosovsky, N., Thompson, S., Douglas, R. H., Hankins, M. W., Lem, J., Biel, M., Hofmann, F., Foster, R. G. & Yau, K. W. Melanopsin and rod-cone photoreceptive systems account for all major accessory visual functions in mice. Nature 424, 76-81 (2003).

173. Lucas, R. J., Hattar, S., Takao, M., Berson, D. M., Foster, R. G. & Yau, K. W. Diminished pupillary light reflex at high irradiances in melanopsin-knockout mice. Science 299, 245-7 (2003).

174. Brainard, G. C., Hanifin, J. P., Greeson, J. M., Byrne, B., Glickman, G., Gerner, E. & Rollag, M. D. Action spectrum for melatonin regulation in humans: evidence for a novel circadian photoreceptor. J Neurosci 21, 6405-12 (2001).

175. Thapan, K., Arendt, J. & Skene, D. J. An action spectrum for melatonin suppression: evidence for a novel non-rod, non-cone photoreceptor system in humans. J Physiol 535, 261-7 (2001).

176. Munch, M., Kobialka, S., Steiner, R., Oelhafen, P., Wirz-Justice, A. & Cajochen, C. Wavelength-dependent effects of evening light exposure on sleep architecture and sleep EEG power density in men. Am J Physiol Regul Integr Comp Physiol 290, R1421-8 (2006).

177. Wiesel, T. N. & Hubel, D. H. Effects of Visual Deprivation on Morphology and Physiology of Cells in the Cats Lateral Geniculate Body. J Neurophysiol 26, 978-93 (1963).

178. Wiesel, T. N. & Hubel, D. H. Single-Cell Responses in Striate Cortex of Kittens Deprived of Vision in One Eye. J Neurophysiol 26, 1003-17 (1963).

179. Hubel, D. H. & Wiesel, T. N. Effects of Monocular Deprivation in Kittens. Naunyn Schmiedebergs Arch Exp Pathol Pharmakol 248, 492-7 (1964).

180. Wiesel, T. N. & Hubel, D. H. Comparison of the effects of unilateral and bilateral eye closure on cortical unit responses in kittens. J Neurophysiol 28, 1029-40 (1965).

181. Hubel, D. H., Wiesel, T. N. & LeVay, S. Functional architecture of area 17 in normal and monocularly deprived macaque monkeys. Cold Spring Harb Symp Quant Biol 40, 581-9 (1976).

182. LeVay, S., Wiesel, T. N. & Hubel, D. H. The development of ocular dominance columns in normal and visually deprived monkeys. J Comp Neurol 191, 1-51 (1980).

183. Prendergast, B. J. & Nelson, R. J. Affective responses to changes in day length in Siberian hamsters (Phodopus sungorus). Psychoneuroendocrinology 30, 438-52 (2005).

184. Geiser, F., McAllan, B. M., Kenagy, G. J. & Hiebert, S. M. Photoperiod affects daily torpor and tissue fatty acid composition in deer mice. Naturwissenschaften 94, 319-25 (2007).

185. Weil, Z. M., Pyter, L. M., Martin, L. B., 2nd & Nelson, R. J. Perinatal photoperiod organizes adult immune responses in Siberian hamsters (Phodopus sungorus). Am J Physiol Regul Integr Comp Physiol 290, R1714-9 (2006).

186. Pyter, L. M., Samuelsson, A. R., Quan, N. & Nelson, R. J. Photoperiod alters hypothalamic cytokine gene expression and sickness responses following immune challenge in female Siberian hamsters (Phodopus sungorus). Neuroscience 131, 779-84 (2005).

187. Pyter, L. M., Adelson, J. D. & Nelson, R. J. Short days increase hypothalamic-pituitary-adrenal axis responsiveness. Endocrinology 148, 3402-9 (2007).

188. Foster, R. G. & Roenneberg, T. Human responses to the geophysical daily, annual and lunar cycles. Curr Biol 18, R784-R794 (2008).

189. Lowrey, P. L. & Takahashi, J. S. Mammalian circadian biology: elucidating genome-wide levels of temporal organization. Annu Rev Genomics Hum Genet 5, 407-41 (2004).

190. Lewy, A. J., Emens, J., Jackman, A. & Yuhas, K. Circadian uses of melatonin in humans. Chronobiol Int 23, 403-12 (2006).

191. Bunger, M. K., Wilsbacher, L. D., Moran, S. M., Clendenin, C., Radcliffe, L. A., Hogenesch, J. B., Simon, M. C., Takahashi, J. S. & Bradfield, C. A. Mop3 is an essential component of the master circadian pacemaker in mammals. Cell 103, 1009-17 (2000).

192. van der Horst, G. T., Muijtjens, M., Kobayashi, K., Takano, R., Kanno, S., Takao, M., de Wit, J., Verkerk, A., Eker, A. P., van Leenen, D., Buijs, R., Bootsma, D., Hoeijmakers, J. H. & Yasui, A. Mammalian Cry1 and Cry2 are essential for maintenance of circadian rhythms. Nature 398, 627-30 (1999).

193. Vitaterna, M. H., King, D. P., Chang, A. M., Kornhauser, J. M., Lowrey, P. L., McDonald, J. D., Dove, W. F., Pinto, L. H., Turek, F. W. & Takahashi, J. S. Mutagenesis and mapping of a mouse gene, Clock, essential for circadian behavior. Science 264, 719-25 (1994).

194. Staels, B. When the Clock stops ticking, metabolic syndrome explodes. Nat Med 12, 54-5; discussion 55 (2006).

195. Rudic, R. D., McNamara, P., Curtis, A. M., Boston, R. C., Panda, S., Hogenesch, J. B. & Fitzgerald, G. A. BMAL1 and CLOCK, two essential components of the circadian clock, are involved in glucose homeostasis. PLoS Biol 2, e377 (2004).

196. Fu, L., Pelicano, H., Liu, J., Huang, P. & Lee, C. The circadian gene Period2 plays an important role in tumor suppression and DNA damage response in vivo. Cell 111, 41-50 (2002).

197. Kryger, M. H., Roth, T. & Dement, W. C. Principles and practice of sleep medicine (Elsevier/Saunders, Philadelphia, PA, 2005).

198. Viola, A. U., Archer, S. N., James, L. M., Groeger, J. A., Lo, J. C., Skene, D. J., von Schantz, M. & Dijk, D. J. PER3 polymorphism predicts sleep structure and waking performance. Curr Biol 17, 613-8 (2007).

199. Wang, G. Y., Lee, C. G. & Lee, E. J. Genetic variability of arylalkylamine-N-acetyl-transferase (AA-NAT) gene and human sleep/wake pattern. Chronobiol Int 21, 229-37 (2004).

200. Katzenberg, D., Young, T., Finn, L., Lin, L., King, D. P., Takahashi, J. S. & Mignot, E. A CLOCK polymorphism associated with human diurnal preference. Sleep 21, 569-76 (1998).

201. Serretti, A., Cusin, C., Benedetti, F., Mandelli, L., Pirovano, A., Zanardi, R., Colombo, C. & Smeraldi, E. Insomnia improvement during antidepressant treatment and CLOCK gene polymorphism. Am J Med Genet B Neuropsychiatr Genet 137, 36-9 (2005).

202. Nadkarni, N. A., Weale, M. E., von Schantz, M. & Thomas, M. G. Evolution of a length polymorphism in the human PER3 gene, a component of the circadian system. J Biol Rhythms 20, 490-9 (2005).

203. Hogenesch, J. B., Gu, Y. Z., Jain, S. & Bradfield, C. A. The basic-helix-loop-helix-PAS orphan MOP3 forms transcriptionally active complexes with circadian and hypoxia factors. Proc Natl Acad Sci U S A 95, 5474-9 (1998).

204. Hogenesch, J. B., Gu, Y. Z., Moran, S. M., Shimomura, K., Radcliffe, L. A., Takahashi, J. S. & Bradfield, C. A. The basic helix-loop-helix-PAS protein MOP9 is a brain-specific heterodimeric partner of circadian and hypoxia factors. J Neurosci 20, RC83 (2000).

205. Williams, S. M., Addy, J. H., Phillips, J. A., 3rd, Dai, M., Kpodonu, J., Afful, J., Jackson, H., Joseph, K., Eason, F., Murray, M. M., Epperson, P., Aduonum, A., Wong, L. J., Jose, P. A. & Felder, R. A. Combinations of variations in multiple genes are associated with hypertension. Hypertension 36, 2-6 (2000).

206. Nataraj, A. J., Olivos-Glander, I., Kusukawa, N. & Highsmith, W. E., Jr. Single-strand conformation polymorphism and heteroduplex analysis for gel-based mutation detection. Electrophoresis 20, 1177-85 (1999).

207. Excoffier, L. & Slatkin, M. Maximum-likelihood estimation of molecular haplotype frequencies in a diploid population. Mol Biol Evol 12, 921-7 (1995).

208. Hawley, M. E. & Kidd, K. K. HAPLO: a program using the EM algorithm to estimate the frequencies of multi-site haplotypes. J Hered 86, 409-11 (1995).

209. Zaykin, D. V., Westfall, P. H., Young, S. S., Karnoub, M. A., Wagner, M. J. & Ehm, M. G. Testing association of statistically inferred haplotypes with discrete and continuous traits in samples of unrelated individuals. Hum Hered 53, 79-91 (2002).

210. Weir, B. S. & Cockerham, C. C. Estimating F-Statistics for the Analysis of Population Structure. Evolution 38, 1358-1370 (1984).

211. Liu, K. & Muse, S. V. PowerMarker: an integrated analysis environment for genetic marker analysis. Bioinformatics 21, 2128-9 (2005).

212. Friedlaender, J. S., Friedlaender, F. R., Reed, F. A., Kidd, K. K., Kidd, J. R., Chambers, G. K., Lea, R. A., Loo, J. H., Koki, G., Hodgson, J. A., Merriwether, D. A. & Weber, J. L. The genetic structure of Pacific Islanders. PLoS Genet 4, e19 (2008).

213. den Dunnen, J. T. & Antonarakis, S. E. Mutation nomenclature. Curr Protoc Hum Genet Chapter 7, Unit 7 13 (2003).

214. Sawyer, L. A., Sandrelli, F., Pasetto, C., Peixoto, A. A., Rosato, E., Costa, R. & Kyriacou, C. P. The period gene Thr-Gly polymorphism in Australian and African Drosophila melanogaster populations: implications for selection. Genetics 174, 465-80 (2006).

215. Tauber, E., Zordan, M., Sandrelli, F., Pegoraro, M., Osterwalder, N., Breda, C., Daga, A., Selmin, A., Monger, K., Benna, C., Rosato, E., Kyriacou, C. P. & Costa, R. Natural selection favors a newly derived timeless allele in Drosophila melanogaster. Science 316, 1895-8 (2007).

216. Tishkoff, S. A. & Kidd, K. K. Implications of biogeography of human populations for 'race' and medicine. Nat Genet 36, S21-7 (2004).

217. Silver, R., LeSauter, J., Tresco, P. A. & Lehman, M. N. A diffusible coupling signal from the transplanted suprachiasmatic nucleus controlling circadian locomotor rhythms. Nature 382, 810-3 (1996).

218. Harmar, A. J. An essential role for peptidergic signalling in the control of circadian rhythms in the suprachiasmatic nuclei. J Neuroendocrinol 15, 335-8 (2003).

219. Morin, L. P. & Blanchard, J. Depletion of brain serotonin by 5,7-DHT modifies hamster circadian rhythm response to light. Brain Res 566, 173-85 (1991).

220. Smale, L., Michels, K. M., Moore, R. Y. & Morin, L. P. Destruction of the hamster serotonergic system by 5,7-DHT: effects on circadian rhythm phase, entrainment and response to triazolam. Brain Res 515, 9-19 (1990).

221. Wheeler, J. A. & Zurek, W. H. Quantum theory and measurement (Princeton University Press, Princeton, N.J., 1983).

222. Navara, K. J. & Nelson, R. J. The dark side of light at night: physiological, epidemiological, and ecological consequences. J Pineal Res 43, 215-24 (2007).

223. Wehr, T. A., Duncan, W. C., Jr., Sher, L., Aeschbach, D., Schwartz, P. J., Turner, E. H., Postolache, T. T. & Rosenthal, N. E. A circadian signal of change of season in patients with seasonal affective disorder. Arch Gen Psychiatry 58, 1108-14 (2001).

224. Hendricks, T., Francis, N., Fyodorov, D. & Deneris, E. S. The ETS domain factor Pet-1 is an early and precise marker of central serotonin neurons and interacts with a conserved element in serotonergic genes. J Neurosci 19, 10348-56 (1999).

225. Hendricks, T. J., Fyodorov, D. V., Wegman, L. J., Lelutiu, N. B., Pehek, E. A., Yamamoto, B., Silver, J., Weeber, E. J., Sweatt, J. D. & Deneris, E. S. Pet-1 ETS gene plays a critical role in 5-HT neuron development and is required for normal anxiety-like and aggressive behavior. Neuron 37, 233-47 (2003).